Benzodiazepines: structural mechanisms underlying their actions at $GABA_A$ receptors

By

Elaine V. Morlock

A dissertation submitted in partial fulfillment of
the requirements for the degree of

Doctor of Philosophy
(Molecular and Cellular Pharmacology)

University of Wisconsin-Madison
2012

Date of final oral examination: June 7th, 2012

The dissertation is approved by the following members of the final oral committee:
Cynthia Czajkowski, Professor, Neuroscience
Gail Robertson, Professor, Neuroscience
Baron Chanda, Associate Professor, Neuroscience
Meyer Jackson, Professor, Neuroscience
Mathew Jones, Professor, Neuroscience

Table of Contents

List of Figures

List of Tables

List of Abbreviations

GPCR: g-protein coupled receptor

LGIC: ligand gated ion channel

pLGIC: pentameric ligand gated ion channel

nAChR: nicotinic acetylcholine receptor

5-HT_3: serotonin type 3

BZD: benzodiazepine

GABA: γ-aminobutyric acid

$GABA_A$: γ-aminobutyric acid type A

LBD: ligand binding domain

ECD: extracellular domain

TMD: transmembrane domain

IPSC: inhibitory post synaptic current

SCAM: substituted cysteine accessibility method

P4S: piperidine-4-sulfate

ITC: isothermal titration calorimetry

ZPM: zolpidem

ESZ: eszopiclone

WT: wild-type

i-BZD: imidazobenzodiazepine

GABA: γ amino butyric acid

FZM: flurazepam

DMCM: 3-carbomethoxy-4-ethyl-6,7-dimethoxy-β-carboline

I_{GABA}: GABA mediated current

EPR: electron paramagnetic resonance

Benzodiazepines: structural mechanisms underlying their actions at $GABA_A$ receptors

Elaine V. Morlock
Graduate Program in Molecular and Cellular Pharmacology
University of Wisconsin - Madison

Benzodiazepines (BZDs) are clinically important drugs that exert their CNS actions by binding to the $GABA_A$ receptor and allosterically modulating GABA-activated chloride currents (I_{GABA}). Their actions depend on residues in the BZD binding site that mediate their high-affinity binding as well as residues that mediate local movements in the site important for coupling BZD binding to modulation of I_{GABA} (efficacy). To identify and distinguish residues involved in each of these functions, we made 22 mutations in and surrounding the BZD binding pocket. To assess BZD binding, mutant $\alpha_1\beta_2\gamma_2$ $GABA_A$ receptors were expressed in HEK293T cells and radioligand binding assays used to measure BZD affinity. To identify residues that contribute to drug efficacy, mutant receptors were expressed in *Xenopus laevis* oocytes, characterized using two-electrode voltage clamp and BZD maximal potentiation of I_{GABA} was measured. We identified six residues whose mutation altered BZD efficacy without altering BZD binding affinity, three residues whose mutation altered binding but had no effect on efficacy, and four residues whose mutation affected both binding and efficacy. These data advance our understanding of allosteric modulation and will aid in future rational drug design.

Seven of the mutations assessed for their effects on BZD efficacy exhibit altered GABA kinetic effects apparent in two electrode voltage clamp experiments. This method is not as well suited to assess macroscopic kinetics and excised patch clamp recordings with rapid solution exchange were employed to evaluate these mutant receptors kinetically. αS205C and αG157C containing receptors both exhibited a decreased extent

of desensitization after 1 sec in 10mM GABA and αG157C containing receptors have a significantly reduce 10-90% rise time.

Taken together this data improves our knowledge of atypical BZDs interactions at the BZD binding site, but also provides some insight into how structural perturbations at subunit interfaces affect $GABA_A$ receptor functioning. These perturbations come from ligand occupancy, such as BZD presence in the BZD binding site, or by mutation, such as the cysteine mutations engineered into the BZD binding site. Also, this data paves the way for further experimentation to explore the effects of ligand orientation on channel function or for *in silico* modeling or drug screens.

CHAPTER 1. Introduction

Signaling in the brain controls movement, sleep patterns, thoughts and perceptions. Communication at the neuronal level is both electrical and chemical. Electrical signals travel down neurons aided by voltage-gated receptors. As this electrical impulse reaches an axon terminal, voltage gated calcium channels open causing an influx of calcium ions. Calcium binding to SNARE proteins on docked vesicles at the presynaptic membrane causes fusion of vesicular membrane with the cellular membrane and a release of neurotransmitter into the synaptic cleft. When neurotransmitter is released from a presynaptic neuron it diffuses across the synaptic cleft where it can bind receptors on the postsynaptic neuron (Fig. 1.1).

Receptors at the postsynaptic receptor can be ligand gated ion channels (LGICs) or G protein coupled receptors (GPCRs). Neurotransmitter binding to GPCRs, such as the muscarinic acetylcholine receptor, γ-amino butyric acid (GABA) type B receptor, or metabotropic glutamate receptor triggers the uncoupling of the G-protein α subunit from its associated β and γ subunits. The uncoupled subunits trigger signaling cascades that have far reaching effects in cellular activity. Changes in the activity of a cell caused by these receptors is slow. Alternatively, activation of LGICs is fast. Ligand binding to the LGIC opens an intrinsic ion-conducting channel on a millisecond time scale. These ionotropic receptors are of two structural classes: glutamate receptors and pentameric ligand gated ion channels (pLGICs).

Glutamate receptors include kainate, NMDA and AMPA receptors. They are activated by the neurotransmitter glutamate and vary in their pharmacology. Glutamate receptors consist of four subunits arranged around a nonselective cation pore, fluxing

mainly sodium and potassium ions. pLGICs include the nicotinic acetylcholine receptor (nAChR), GABA type A ($GABA_A$) receptor, glycine receptor and serotonin type 3 (5-HT_3) receptor. These receptors are composed of five homologous subunits arranged pseudo symmetrically around a central ion conducting pore. nAChR and 5-HT_3 receptors are cationic ion channels whereas glycine and $GABA_A$ receptors are anionic, fluxing chloride.

The focus of my thesis is $GABA_A$ receptors. When GABA, the endogenous neurotransmitter, binds to the receptor the typical result is an influx of chloride into the cell, driving the membrane potential toward the chloride reversal potential (Bormann, 1987). This generally results in a hyperpolarization of the cell membrane, driving the membrane potential away from threshold potential, which inhibits action potential firing. $GABA_A$ receptors are responsible for the majority of fast synaptic inhibition in the brain.

The $GABA_A$ receptor is made of five homologous subunits. Many subunits have been cloned including: α, β, γ, δ, ε, π, ρ, and θ, with multiple subtypes (Schofield, 1989, Whiting et al., 1999, Simon et al., 2004). The substituent subunits of the $GABA_A$ receptor dictate their distribution throughout the brain and their cellular location (synaptic, and extrasynaptic) as well as their pharmacology and kinetics.

GABA binding at the $\beta-\alpha$ subunit interfaces triggers rapid opening of the intrinsic chloride-conducting channel (activation). In the continued presence of GABA, receptors can maintain bound GABA but the channel closes, in a process called desensitization. Current deactivation results from GABA unbinding resulting in channel closure. The receptor exists in at least three different states: the unbound-closed channel state, bound-active open channel state, and bound-desensitized closed channel state.

Hypotheses as to connectivity of these states and the existence of additional kinetics states vary.

$GABA_A$ receptor function is modulated by a wide variety of clinically relevant drugs that are used in the treatment of sleep, seizure and anxiety disorders. Among these drugs are commonly prescribed benzodiazepines (BZDs), barbiturates and anesthetics. Ligands that bind to the $GABA_A$ receptor bind either at the orthosteric site or at several allosteric sites around the receptor. Many clinically relevant drugs bind the $GABA_A$ receptor at these other binding sites and act allosterically to modulate GABA activated current responses (I_{GABA}).

1.1 The role of $GABA_A$ receptors in neuronal signaling.

GABAergic synapses mediate two types of inhibition, phasic and tonic (Farrant and Nusser, 2005). Phasic inhibition results from GABA release following the fusion of synaptic vesicles at the presynaptic membrane. $GABA_A$ receptors located at synapses are exposed to high concentrations (mM) of GABA released into the synaptic cleft. These receptors are most commonly composed of the α, β, and γ subunits. Phasic inhibition results in inhibitory post-synaptic currents (IPSCs). GABA exposure is transient as GABA is readily taken up by GABA transporters (GATs) on the presynaptic neuron or astrocytes (Roth and Draguhn, 2012, Rowley et al., 2012).

The time course of IPSCs is shaped by $GABA_A$ receptor subtype combinations, endogenous allosteric modulators, exogenous pharmaceuticals, phosphorylation and associated proteins. All of these factors affect the microscopic rates into various kinetic states visited by the receptor that in turn shape the timecourse of IPSCs (Jones and

Westbrook, 1995, 1997, Nusser et al., 1999, Eyre et al., 2012). IPSCs regulate neuronal firing as they hyperpolarize the membrane and are a major regulator of network oscillations (Whittington et al., 1995, Whittington et al., 2000, Whittington and Traub, 2003). In the cortex, connectivity between GABAergic interneurons and glutamatergic cells sets up rhythmic and synchronous firing of populations of neurons that produce β and γ oscillations (Isaacson and Scanziani, 2011, Mendez and Bacci, 2011). In the hippocampus, θ and γ oscillations have been shown to be involved in learning and memory (Mohler, 2007). Aberrations in $GABA_A$ receptor signaling can alter frequency or rhythmicity and result in pathology, including epilepsy (Traub et al., 1999) and psychiatric disorders (Benes and Berretta, 2001, Levitt et al., 2004, Lewis et al., 2005). A number of familial mutations in the $GABA_A$ receptor have been found to cause epilepsy in humans (Baulac et al., 2001, Harkin et al., 2002, Marini et al., 2003, Dibbens et al., 2009).

Tonic inhibition is mediated by extrasynaptic $GABA_A$ receptors, that usually contain $\alpha_{4,6}$ or δ subunits (Wei et al., 2003, Caraiscos et al., 2004, Jia et al., 2005, Scimemi et al., 2006, Mortensen et al., 2010, Brickley and Mody, 2012). $GABA_A$ receptors containing these subunits have higher GABA potency (Mortensen, 2012) and slower desensitization (Saxena and Macdonald, 1994) causing greater sensitivity to the lower ambient levels of GABA that spillover into the extrasynaptic space (Rossi and Hamann, 1998). This constitutive current acts to hyperpolarize the membrane and decreases the likelihood of reaching threshold potential for action potential firing. Depending on the cell type and brain region, tonic inhibition can differ in current amplitudes and kinetics largely dependent on substituent subunits (Belelli et al., 2009).

Additionally, the extrasynaptic environment can vary by the reuptake transporters present as well as the possible presence of allosteric modulators such as neurosteroids (Semyanov et al., 2004). Aberrant tonic inhibition is involved in stress, sleep and mood disorders and drugs targeting extrasynaptic $GABA_A$ receptors are important therapies for these ailments (Brickley and Mody, 2012).

1.2 $GABA_A$ receptor structure

$GABA_A$ receptors are comprised of five subunits arranged pseudo symmetrically around a central ion-conducting pore. Each subunit of the receptor contains a large N-terminal extracellular domain (ECD), a transmembrane domain (TMD) consisting of four α helical segments, termed M1-M4, and a short extracellular C-terminus. The M2 helix of each subunit contributes to the channel pore (Leonard et al., 1988, Xu and Akabas, 1993, 1996, Zhang and Karlin, 1998) (Fig. 1.2). The ECD of each subunit consist of 10 beta strands and a single alpha helix and constitutes the ligand binding domain (LBD). The beta strands are folded into a beta sandwich configuration with an inner and outer beta sheet surrounding a hydrophobic core (Brejc et al., 2001, Cromer et al., 2002, Dellisanti et al., 2011) (Fig 1.3).

1.2.1 $GABA_A$ receptor subunit subtypes

The $GABA_A$ receptor is made of five homologous subunits all with the basic structure outlined above. However, the subunit composition of the receptors can vary. Nineteen subunits of the $GABA_A$ receptor have been cloned: α_{1-6}, β_{1-3}, γ_{1-3}, δ, ε, π, ρ_{1-3}, and θ (Schofield, 1989, Whiting et al., 1999, Simon et al., 2004). The various subtypes

are expressed differently in different brain regions (Hevers and Luddens, 1998, Akinci and Schofield, 1999, Sieghart et al., 1999, Sieghart, 2006). Additionally, different subtype combinations combine preferentially (Olsen and Sieghart, 2009). For example, the δ subunit is found extrasynaptically (Nusser et al., 1998) and typically combines with the α_4 subunit in the thalamus, striatum and outer layers of the cortex, yet is found in conjunction with the α_6 subunit in the cerebellum (Pirker et al., 2000). The localization of various subunit subtypes has been shown by *in situ* hybridization (Persohn et al., 1992, Wisden et al., 1992) and immunohistochemistry (Fritschy et al., 1992, Pirker et al., 2000). The most common receptor in the brain is $\alpha_1\beta_2\gamma_2$ (Benke et al., 1991, Sieghart et al., 1999, Pirker et al., 2000). This is the subunit combination used in experiments throughout this thesis. These receptors contain 2α, 2β and a single γ subunit arranged αβαβγ clockwise when looking down onto the ECD from outside the cell (Chang et al., 1996, Baumann et al., 2001, 2002) (Fig. 1.3A).

1.2.2 The GABA binding site

Photoaffinity labeling identified the GABA binding sites at the interface of the β (principal subunit, + side) and α (minor subunit, - side) subunits in the ECD (Casalotti et al., 1986, Smith and Olsen, 1994). There are two GABA binding sites per pentameric receptor (Fig. 1.2). In general, for heteropentameric receptors two GABA molecules are bound to open the receptor (Macdonald and Young, 1981). However, use of concatameric receptors indicates that a single bound GABA molecule can open the channel (Sigel et al., 1992) and recent kinetic modeling suggests a singly bound open state contributes to shaping IPSCs (Petrini et al., 2011). In addition to photoaffinity

labeling, the substituted cysteine accessibility method (SCAM) has been used to identify and characterize the GABA binding site (Boileau et al., 1999, Holden and Czajkowski, 2002, Wagner et al., 2004). There are six regions that contribute to the binding site that have historically been called loops A, B, and C in the β subunit and D, E, and F in the α subunit. Agonist binds under loop C, which is believed to close over the ligand (Hansen et al., 2005). Loop C capping is thought to trigger a series of conformational movements that are translated through residues at the ECD-TMD interface and ultimately to an outward twist of M2 that results in channel opening (Unwin, 2005, Cheng et al., 2006).

1.2.3 Structural information based on homologous proteins

Much of what is know about the overall structure of the $GABA_A$ receptor is based on crystal structures of homologous proteins. Based on the various crystal structures, homology models of the $GABA_A$ receptor have been made. *Lymnae stagnalis* acetylcholine binding protein (AChBP) has five identical subunits and is homologous to the N-terminal extracellular ligand binding domain (LBD) of the pLGICs. The crystal structures of this protein in apo, agonist and antagonist bound states have been refined to 2.7Å (Brejc et al., 2001, Celie et al., 2005a, Hansen et al., 2005). A 4Å resolution structure of the nAChR in the resting state has been solved from cryo-electron microscopy (Unwin, 2005). An isolated ECD from the nAChR was crystallized at higher (1.94Å) resolution providing detailed information on side chain locations not possible with lower resolution structures (Dellisanti et al., 2007). A crystal structure of a nAChR/AChBP chimera has also provided important structural information (Li et al.,

2011). Most recently, a glutamate activated chloride channel from *C. elegans* was crystallized at 3.3Å (Hibbs and Gouaux, 2011).

Two prokaryotic pLGICs from *G. violaceus* (GLIC) and *E. chyrsanthemi* (ELIC) pentameric ion channels have been identified and crystallized. The x-ray structure of ELIC in a presumed closed channel state was solved at 3.3Å resolution (Hilf and Dutzler, 2008) (Fig. 1.4). Recently, ELIC was crystallized with acetylcholine docked in the agonist binding site (analogous to the neurotransmitter binding site in eukaryotic pLGICs) and a contraction of loop C was observed (Pan et al., 2012). Additionally, electron paramagnetic resonance (EPR) spectroscopy studies on GLIC indicated loop C is less mobile in an open to desensitized transition (Velisetty and Chakrapani, 2012) similar to what is known about these movements in AChBP and eukaryotic pLGICs (Celie et al., 2004b, Celie et al., 2005b, Hansen et al., 2005, Venkatachalan and Czajkowski, 2008, Mukhtasimova et al., 2009). More recently a crystal structure of ELIC, which contained a mutation that rendered the channel with an open probability (P_o) >0.9 was crystallized in an attempt to capture the receptor in an open conformation (Gonzalez-Gutierrez et al., 2012). In the mutant crystal structure, the channel still appeared closed, resembling that of the native, apo crystal. This highlights some of the weaknesses of crystallography in that the protein crystals represent a single, static state captured in a highly artificial environment and cannot tell us very much about protein movements, especially in physiological conditions. In addition, it is difficult to assign functional states to crystal structures.

The other prokaryotic channel, GLIC, was resolved at 2.9Å in an apparently open confirmation (Bocquet et al., 2009). It has also been crystalized in the presence of

propofol and desflurane (Nury et al., 2011) and the open channel blockers, lidocaine and quaternary ammonium compounds (Hilf et al., 2010). Additionally, an isolated extracellular domain of GLIC was solved at 2.3Å resolution but this protein crystallized as a hexamer (Nury et al., 2010). Electrophysiological characterization of mutant containing GLIC receptors combined with molecular docking studies suggest a site for alcohol modulation within the "linking tunnel", a cavity within the TMD helices that spans from plasma membrane into the channel pore (Alqazzaz et al., 2011). Co-crystaliization studies indicate propofol binds in an intrasubunit transmembrane pocket between M1, M2, M3 and M4 helices. Additionally, functional chimeras of GLIC with glycine receptor have been made and shown to be potentiatied by ivermectin, anasthetics and propofol and alcohol, each of these drugs inhibits GLIC. This chimera allows for the study of glycine receptor pharmacology in a purified protein (Duret et al., 2011).

The recent availability of homologous prokaryotic channels that can be readily purified in large quatities makes available a wide variety of techniques for the study of pLGIC structure and function. High resolution structures allow for the visualization of a wide variety of ligands and pharmacological agents in complex with the protein (Corringer et al., 2010). Additionally, the ability to purify protein makes available a number of techniques including: electron paramagnetic resonance (EPR) spectroscopy, isothermal calorimetry (ITC), patch clamp of liposomes etc… These techniques are useful to assess the biophysical properties of the proteins in a lipid environment under non-static conditions.

1.3 $GABA_A$ receptor kinetics

LGICs do not simply transition from a closed to open state and back again. Early work suggests that LGICs can exist in an agonist bound, inactive transition state that exists between the closed-unbound state and bound-active state. (Del Castillo and Katz, 1957). This idea stemmed from antagonists that can bind a receptor, but do not result in channel opening. Since this early work, additional states have been hypothesized. It is thought that $GABA_A$ receptors exist in at least three interconvertible, conformational states: an unliganded, closed channel, non-conducting state (U); a ligand-bound, open channel, ion-conducting state (O); and a ligand-bound, closed channel desensitized state (Fig. 1.5A). Upon agonist binding, the channel rapidly opens (activation). In the continued presence of agonist, $GABA_A$ receptors undergo a conformational transition that closes the channel even though agonist is still bound with high affinity, a process called desensitization. When agonist unbinds (e.g. when agonist is removed), the channel closes and the receptor adopts a non-conducting, unliganded closed resting state. Models suggest open and desensitized states can exist with one or two bound GABA molecules. However, the probability of channel opening is greatest with two bound agonist molecules (Monod et al., 1965, Changeux, 2011).

The transitions and microscopic rates between various kinetic states determines $GABA_A$ receptor macroscopic current responses. Multiple models have been developed that describe kinetic states (i.e. closed, open, and desensitized) and how they are inter-connected. Depending on the model, connectivity between the states varies, some have desensitized states branching from closed channel states (Jones and Westbrook, 1995, Bianchi et al., 2007, Mozrzymas et al., 2007), whereas others have the desensitized state connected to the open channel state (Burkat et al., 2001, Corradi et al., 2009). More

recently, a model has emerged with a "flip state" as an additional, higher agonist affinity, closed state that precedes channel opening. This model has been used to explain partial agonism. (Burzomato et al., 2004, Lape et al., 2008, Sivilotti, 2010). More complicated kinetic models include additional states to account for allosteric modulation of GABA actions by various drugs (Gielen et al., 2012) (Fig. 1.5).

The microscopic transitions between kinetics states determine the time course of macroscopic current responses and can be modulated by many things. Desensitization prolongs IPSCs by maintaining receptors in a GABA-bound, non-conducting state which can later re-sensitize to an open channel, conducting state before releasing GABA and converting back to a closed channel, resting state (Jones and Westbrook, 1995, Dominguez-Perrot et al., 1996, Tia et al., 1996, Haas and Macdonald, 1999, Bianchi et al., 2001). Desensitization influences IPSC duration and decay and thus, regulates neuronal firing patterns. Moreover, $GABA_A$ receptor desensitization and recovery from desensitization influences a cell response to repeated high frequency stimuli (Jones and Westbrook, 1996). Receptor deactivation and desensitization kinetics are dependent on ligand affinity, ligand concentration, and subunit composition (Tia et al., 1996, Bianchi et al., 2002a) and can be modulated by phosphorylation (Jones and Westbrook, 1997, Hinkle and Macdonald, 2003), proton concentration (Feng and Macdonald, 2004), and neurosteroid binding (Zhu and Vicini, 1997). $GABA_A$ receptor desensitization is multiphasic, featuring fast, medium and slow components (Celentano and Wong, 1994, Puia et al., 1994, Jones and Westbrook, 1995).

Little is known about the structural elements that regulate $GABA_A$ receptor kinetic state transitions. Receptor subtype composition clearly affects receptor kinetics,

including desensitization. In comparing $\alpha_1\beta_3\gamma_{2L}$ and $\alpha_4\beta_3\gamma_{2L}$ receptors, receptors that contained the α_4 subunit exhibit more rapid and extensive desensitization (Lagrange et al., 2007). Animal models of epilepsy show upregulation of α_4 subunit containing receptors (Schwarzer et al., 1997, Brooks-Kayal et al., 1998, Sperk et al., 1998). The γ and δ subunits also confer distinct kinetics. δ subunit containing receptors exhibit very little desensitization (Haas and Macdonald, 1999). Our lab has shown that desensitization is slower in $\alpha_1\beta_2\gamma_2$ receptors compared to receptors that lack the γ subunit (Boileau et al., 2003, Boileau et al., 2005). Distinct regions within subunits have also been implicated in desensitization, specifically the M1 region. Mutations of conserved hydrophobic residues in the extracellular end of M1 in the α, β, γ and ρ subunits alter desensitization (Amin and Weiss, 1994, Bianchi et al., 2001).

Determination of macroscopic kinetics and microscopic rates requires specific experimental methods. IPSCs reach maximal amplitude on a time scale of hundreds of microseconds (Edwards et al., 1990). Techniques that can reliably apply agonist faster than the activation rate are necessary to accurately resolve kinetics, as slower solution exchange results in receptors being in multiple kinetic states (i.e. unbound-resting, bound-open, bound, desensitized). Excised patch clamp recordings with rapid solution exchange allow for resolution of kinetics (Jones et al., 1998). Determining the microscopic kinetics rates is complicated and depends on *in silico* modeling. However, specific rates and parameters to constrain kinetic models can be measured experimentally to further refine the estimate of kinetic rates. Channel open probabilities (P_o) can be measured by single channel recordings, or a technique called nonstationary variance analysis can be utilized (Sigworth, 1980). Single channel recordings can also be used to

assess channel open and closing rates. To measure binding rates, co application of agonist and competitive antagonist can be used in a "race" experiment. The peak current of the co-application is smaller than that of agonist alone as some binding sites will be occupied by antagonist. The ratio of the relative currents can be used to calculate agonist and antagonist binding rates (k_{on}) (Jones et al., 1998). These parameters are useful in conjunction with various agonist application protocols to constrain *in silico* kinetic models to estimate microscopic rates. The use of kinetic modeling will be further discussed in chapter 4.

Transitions amongst kinetic states determine current responses and thus dictate the time course of IPSCs. The precise timing of IPSCs is crucial for proper brain function and mutations that alter pLGIC kinetics are seen in disease states. $GABA_A$ receptors containing the γ_2K289M mutation, seen in some epileptic patients, exhibit increased current deactivation rate (Bianchi et al., 2002b). In glycine receptors, homomeric receptors containing the α_1K276E mutation that causes hyperekplexia, produce currents with slower rise times and faster decay rates (Lape et al., 2012). Additionally, macroscopic kinetics can be altered by various pharmacological agents as well as by endogenous modulators. Thorough characterization of these effects will provide a better understanding of the mechanisms underlying the actions of commonly used therapeutics.

1.4 Pharmacology of $GABA_A$ receptors

$GABA_A$ receptors bind a variety of different ligands, which have different actions. Among these are many clinically relevant pharmaceuticals as well as numerous reagents

that are of experimental use. There are a number of ligands that bind at the orthosteric site, as well as a wide variety of allosteric effectors, that bind in a variety of places within the protein. Among ligands at the orthosteric site, some are agonists (that fully activate the receptor), partial agonists (that activate the channel submaximally), and antagonists (that bind but exert little to no effect on I_{GABA}). Allosteric ligands also come in several varieties. This thesis focuses on the BZD binding site. BZDs come in three varieties, termed: agonists (positive modulators), antagonists (zero modulators) and inverse agonists (negative modulators). Allosteric agonists potentiate $I_{GABA,}$ allosteric inverse agonists inhibit I_{GABA}, and allosteric antagonists bind, but have little to no effect on I_{GABA}.

The diverse pharmacology of the $GABA_A$ receptor is invaluable in the study of protein structure as it relates to function. Utilizing ligands that bind at the same binding site, such a GABA and gabazine (at the orthosteric site) or diazepam and Ro15-788 (at the BZD binding site) can be used in competitive binding experiments. Additionally, ligands that bind at the same binding site yet have different efficacies (i.e. diazepam is a BZD agonist, DMCM is a BZD inverse agonist) can be used to study different conformation movements within the receptors originating from ligand binding at the same site. For example, these types of experiments were used to implicate movements within the loop F region (spanning from near the BZD binding site toward the TMD/ECD interface) of the γ_2 subunit in the action of BZD agonists, but not inverse agonists (Hanson and Czajkowski, 2008). Alternatively, ligands that bind at different sites but have similar actions, i.e. both etomidate and GABA open the channel but bind in different regions, can be used to monitor actions that are not binding site specific, but

specific to an action, such as channel activation. Experiments in appendix one used this approach to suggest that, regardless of where the activating ligand is bound, opposing, twisting movements between the ECD and TMD are universal to channel activation. Furthering the complexity of the pharmacology of the $GABA_A$ receptor, some ligands have differing properties at different concentrations; pentobarbital can potentiate the actions of GABA at low concentrations, and at high concentrations activate the channel in the absence of GABA. It is thought that these two activities require different structural regions of the $GABA_A$ receptor (Dalziel et al., 1999, Greenfield et al., 2002).

Therapeutically, ligands of the GABA receptor are used to treat many conditions. To name a few clinical uses for $GABA_A$ receptor modulators, anesthetics such at pentobarbital and etomidate, are used for surgery and sedation; benzodiazepines, such as diazepam and midazolam, are used to treat epileptic, sleep and anxiety disorders. There is growing evidence that drugs that target $GABA_A$ receptors could be used to treat Alzheimer's disease and other cognitive impairments (Lanctot et al., 2004, Rissman and Mobley, 2011). Neuronal death in Alzheimer's patients alters the balance of inhibition and excitation, with GABAergic neurons being largely spared (Lowe et al., 1988, Reinikainen et al., 1988). Drugs that modulate $GABA_A$ receptor function could restore that balance, especially inverse agonists at the α_5 subunit, which is abundant in the hippocampus, a brain region important for learning and memory (Klausberger, 2009, Olsen and Sieghart, 2009).

1.4.1 GABA and the orthosteric binding site

Many ligands bind at the orthosteric binding site. These ligands are agonists: GABA, muscimol and β-alanine; partial agonists: piperidine-4-sulfate (P4S), THIP; and competitive antagonists: bicuculine and SR-95531 (gabazine). These additional ligands are experimentally useful as they induce different conformational movements in the receptor (Boileau et al., 2002b). Also, ^{3}H-muscimol has been used for competitive radioligand binding assays and photoaffinity studies (Casalotti et al., 1986, Smith and Olsen, 1994).

1.4.2 Pentobarbitol and anaesthetics

Multiple drugs used in sedation and anesthesia target the $GABA_A$ receptor. Volatile anesthetics, such as isoflurane and halothane as well as intravenous anesthetics pentobarbital, etomidate and propofol potentiate $GABA_A$ receptor activity. General anesthetics are thought to bind in the TMD (Jenkins et al., 2001). Volatile anesthetic actions require residues within the M2 and M3 helices (Mihic et al., 1997). Photoaffinity labeling with etomidate analogs has identified a binding site at the β–α subunit interface, the same interface as GABA binding, yet within the TMD helices, specifically α_1M236 (in M1) ($\alpha_{1,2,3,5}$ also have an M in the analogous position) and β_3M286 (in M3) (β_1 and β_2 also have aligned M) (Li et al., 2006). Etomidate and pentobarbital bind to sites that are different from the GABA and BZD binding sites and allosterically enhance GABA and BZD binding (Leeb-Lundberg et al., 1980, 1981a, b, Olsen and Snowman, 1982, Olsen et al., 1986). In single channels, propofol modulation of I_{GABA} results in increased open time (Hales and Lambert, 1991). At the synapse, IPSCs are prolonged by anesthetics (Tanelian and MacIver, 1991). Additionally, it is known that specific

subunits are responsible for different activities of anesthetics. For example, β_2 subunit is involved in sedative effects of etomidate whereas β_3 accounts for anesthetic effects (Reynolds et al., 2003).

1.4.3 Neurosteroids: endogenous modulators of $GABA_A$ receptor function

Neurosteroids, such as allopregnanalone, are endogenously produced in the mammalian brain (Majewska et al., 1986) and bind within the TMD to modulate $GABA_A$ receptor function (Ueno et al., 1997). Neurosteroids alter the effects of many $GABA_A$ receptors *in vitro* but δ subunit containing receptors are particularly sensitive and react to physiology relevant concentrations (Belelli et al., 2002). In neurons, the response of $GABA_A$ receptors to neurosteroids is highly varied dependent on brain structures and receptor subunit composition (Belelli et al., 2009). Neurosteroids also modulate the activity of administered pharmaceuticals, including BZDs (Dhir and Rogawski, 2012).

1.5 Benzodiazepines

A main focus of this thesis is the actions of BZDs on the $GABA_A$ receptor. BZDs are generally constructed of a benzene ring fused to a diazepine ring. Classical benzodiazepines such as valium, flurazepam and midazolam have this chemical structure (Fig. 1.6). However, structurally diverse ligands bind at the BZD binding site which have similar actions as classical BZDs. Some examples of atypical BZDs are shown in Fig. 1.6. In this thesis, the term BZD is used to describe ligands that bind at the BZD binding site even if they are structurally distinct from classical BZDs.

BZDs act at $GABA_A$ receptors and allosterically modulate the actions of GABA. Three functional types of BZDs exist: agonists (positive modulators), antagonists (zero modulators) and inverse agonists (negative modulators). BZD agonists, such as diazepam or zolpidem, potentiate I_{GABA} and have a clinical effect of inducing sleep, reducing anxiety and slowing seizure activity. BZD antagonists, such as Ro15-1788 (flumazenil), bind at the BZD binding site with high affinity but have little to no effect on GABA activated current (I_{GABA}). Flumazenil is the only FDA approved BZD antagonist, it is used clinically to treat BZD overdose and works by displacing other BZDs. BZD inverse-agonists, such as DMCM (3-carbomethoxy-4-ethyl-6,7-dimethoxy-β-carboline) and Ro15-4513 inhibit I_{GABA}. DMCM is used experimentally to induce anxiety (Cole et al., 1995). As described above, the use of inverse agonists at the α_5 subunit have been recently suggested as a potential treatment for Alzheimer's disease (Atack, 2010, Gabriella and Giovanna, 2010). It is not well understood what makes a BZD a positive, negative or zero modulator. In fact, a single $GABA_A$ receptor point mutation can switch the modulator type of a BZD (Mihic et al., 1994, Benson et al., 1998, Morlock and Czajkowski, 2011). For example, eszopiclone (ESZ) is a positive modulator of the WT receptor whereas at αF99Cβγ receptors, it is a negative modulator (see chapter 3 of this thesis).

1.5.1 Clinical use of benzodiazepines

Clinical actions of BZDs are related to the subtype selectivity of the various drugs and the distribution of different $GABA_A$ receptor subtypes in various brain regions. The α_4 and α_6 subunits do not bind classical BZDs. Classical BZDs such as diazepam are not

selective amongst $\alpha_{1\text{-}3,5}$ subunits. However, newer drugs have been developed that are less promiscuous and target specific subtypes and thus brain regions. For example, the atypical BZD zolpidem (Ambien) is highly selective for α_1 containing $GABA_A$ receptors.

BZDs have many actions including: anxiolysis, myorelaxation, sedation and amnesia and have anticonvulsant properties. When BZDs are administered for long periods tolerance can be developed to BZDs (Weerts et al., 1998). Knock in mice have been used to determine which α subunit contributes to the diverse effects of these drugs. BZD sensitive subunits, $\alpha_{1\text{-}3,5}$ contain a histidine at position 101, the classical BZD insensitive α_4 and α_6 subunits have an arginine at the corresponding position. H101 has shown to be crucial for the binding of classical BZDs (Wieland et al., 1992, Kleingoor et al., 1993, Benson et al., 1998). Knock-in mice containing the α_1H101R mutations and the corresponding mutations in other α subunits were used to tease apart the roles of the various α subunit containing $GABA_A$ receptors in mediating the diverse actions of BZDs.

α_1H101R mice are phenotypically normal, except when administered diazepam. Compared to WT mice, the α_1H101R mice do not exhibit the amnestic or sedative reaction to the drug (Rudolph et al., 1999, McKernan et al., 2000). In α_2H101R knock-in mice the anxiolytic effects of diazepam are abolished, indicating the role of the α_2 subunit in anxiety (Low et al., 2000). This effect is not seen in α_3H126R mutant knock-in mice (Low et al., 2000). In slice work from α_3H126R knock-in mice, α_3 subunits in the thalamus were implicated in the anti-epileptic effects of clonazepam (Sohal et al., 2003). In the analogous α_5H105R mice the sedative, anticonvulsant and anxiolytic activities of diazepam are not impaired and myorelaxation is only modestly affected

suggesting the α_5 containing $GABA_A$ receptors do not mediate these actions (Crestani et al., 2002) Studies employing these diazepam insensitive knock in mice also implicate the α_5 subunit in BZD tolerance (van Rijnsoever et al., 2004).

1.5.2 Benzodiazepine mechanisms of action

BZDs bind at a binding site homologous to the GABA binding site, but located at the $\alpha-\gamma$ ECD subunit interface. BZD binding site residues have been identified by photoaffinity labeling with [^{3}H]-Flunitrazepam and [^{3}H]Ro15-4513 (Davies et al., 1996, Duncalfe and Dunn, 1996, Sawyer et al., 2002) and substituted cysteine accessibility method (SCAM) (Amin et al., 1997, Boileau et al., 1998, Renard et al., 1999, Kucken et al., 2000, Teissere and Czajkowski, 2001, Kucken et al., 2003) (Fig 1.3). Detailed information about specific residues involved in BZD binding is provided in Chapter 2 (Hanson et al., 2008). A recent study suggests that a low affinity BZD site exists at the $\alpha-\beta$ subunit interface as well, an idea that will be discussed further in chapter 5 (Ramerstorfer et al., Sieghart et al., 2012).

Binding at a site distant from the GABA binding site, BZD agonists left shift the GABA concentration response curve, i.e in the presence of BZDs, GABA EC_{50} is decreased. BZDs, however, do not increase maximal GABA activation (Fig. 1.7A). The effects of BZDs are thought to be caused either by shifting the $GABA_AR$ closed to open state channel equilibrium (altering channel gating) (Downing et al., 2005, Rusch and Forman, 2005, Campo-Soria et al., 2006) or by altering the receptor's microscopic binding affinity for GABA (Twyman et al., 1989, Rogers et al., 1994b, Lavoie and Twyman, 1996, Mellor and Randall, 1997, Thompson et al., 1999, Goldschen-Ohm et al.,

2010). It is believed that GABA affinity is increased specifically by a decrease in the microscopic rate of GABA unbinding (Bianchi et al., 2009, Goldschen-Ohm et al., 2010). Recent work has also suggested that BZDs may increase formation of a pre-open bound 'flip' state of the receptor (Gielen et al., 2012).

At the single channel level, diazepam acts to increase P_0 by increasing burst frequency (Rogers et al., 1994a). This is in contrast to barbiturates that increase channel open duration (MacDonald et al., 1989, Twyman et al., 1989). In whole cells, with rapid solution exchange into saturating (mM) concentrations of GABA, diazepam acts to prolong current deactivation (Bianchi et al., 2009). This mimics what happens at the synapse, as release of GABA into the synaptic cleft results in mM concentrations of neurotransmitter (Kleinle et al., 1996). Resultantly, IPSCs recorded from neurons are prolonged in the presence of BZDs (Strecker et al., 1999) (Fig. 1.7).

1.6 Overview and significance of this work

Much is known about $GABA_A$ receptors and their interactions with BZDs. Many BZDs are available for clinical use and many more are useful experimentally. Where these drugs bind and the actions they have on $GABA_A$ receptor current responses are well documented. However, the structural mechanisms that mediate BZD binding and the mechanisms underlying BZD effects on I_{GABA} are relatively unknown. What dictates whether a BZD is an agonist, antagonist, or inverse agonist is unknown. Related to this, what contributes to differing efficacies amongst modulators of the same type has not been elucidated (i.e. high efficacy positive modulators vs low efficacy positive modulators). I hypothesize that different types of modulators cause different conformational movements

within the BZD binding site that dictate their potentiating or inhibiting abilities and these movements are not well characterized. Concerning the actions of BZDs on I_{GABA} kinetics, there is disagreement in the field as to how BZDs affect $GABA_A$ receptor kinetics. Some experiments indicate BZDs increase receptor microscopic affinity for GABA, while others suggest that BZDs effect channel gating. Additionally, detailed information about what dictates specificity for different subunit subtypes is not available. Addressing these holes in our understanding of BZD actions at the $GABA_A$ receptor will be valuable clinically as more detailed information about BZD subunit selectivity and causes for varied BZD efficacy and type of modulation will allow for focused drug screens and more specific therapeutic indications for future BZDs that could alleviate side effects.

Using subunit selective BZDs could provide a way to design in or out certain drug actions (i.e. non-sedative anxiolysis). The more that is known about BZD interactions with the $GABA_A$ receptor the more feasible the development of subunit selective drugs will be (Rudolph and Knoflach, 2011). For example, L-838,417 is a positive modulator of the $\alpha_{2,3}$ and α_5 subunits and has anticonvulsant and anxiolytic effects in mice and primates, but does not exhibit the sedative and motor performance effects of diazepam (McKernan et al., 2000, Rowlett et al., 2005). Further utilizing subunit selectivity and BZDs of differing modulator type (from the standard positive modulators like diazepam), inverse agonists at α_5 subunit have been implicated in cognitive enhancement. RO4938581, a imidazo[1,5-a][1,2,4]-triazolo[1,5-d][1,4]benzodiazepine (Achermann et al., 2009) has been shown to reduce memory impairment induced by scopolamine, a muscarinic antagonist, (Ballard et al., 2009) and cognitive defects caused by PCP

(Redrobe et al., 2011). Additionally, these drugs may be useful in treating cognitive defects caused by Alzheimer's disease (Atack, 2010).

This thesis aims at teasing apart which amino acid residues within the benzodiazepine binding site affect the high affinity binding (chapter 2) and efficacy (chapter 3) with a focus on the commonly prescribed sleep aids eszopiclone (Lunesta) and zolpidem (Ambien). Additionally, receptors containing mutant residues within this binding site exhibit altered kinetic effects. Characterization of the macroscopic kinetic effects resulting from these mutations in chapter 4 increase our understanding of the role of structural perturbations at subunit interfaces and provides insight into the mechanisms by which BZDs may exert their effects on I_{GABA} kinetics. Additional work in the appendix of this thesis explores structural perturbations of non-binding subunit interfaces in the $GABA_A$ receptor and demonstrate the importance of these protein interfaces and their role in the conformational movements that dictate $GABA_A$ receptor function.

Overall, my work expands our understanding of how typical and atypical BZDs interact with the BZD binding site. This information can be paired with information from other BZD binding site ligands and used to refine *in silico* docking for use in computational drug screens or to help explain experimental data. Additionally, this data, collected from $\alpha_1\beta_2\gamma_2$ receptors can be used in concert with homology models and sequence alignments as a starting point for experiments exploring BZD actions at other $GABA_A$ subunit subtypes. Data in this thesis also leads to hypotheses on the role of ligand orientation in BZD binding and efficacy. This information is critical for understanding BZDs and their actions at the $GABA_A$ receptor. The basic principles underlying protein-ligand interactions that I have resolved in this thesis extend beyond

$GABA_A$ receptors and have implications in the structural mechanisms underlying allosteric drug action for many types of proteins.

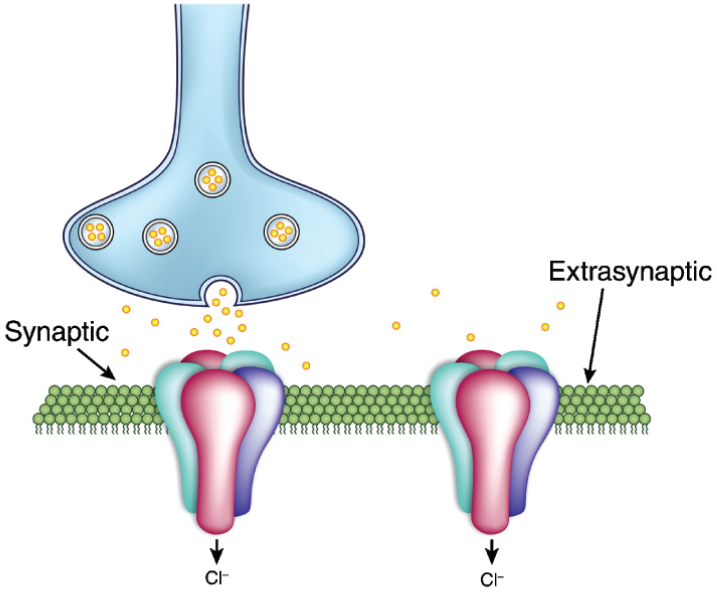
Synaptic
Extrasynaptic
Cl⁻
Cl⁻

Figure 1.1. $GABA_A$ receptors at the synapse. Fusion of vesicles containing GABA result from action potential propagation down a presynaptic neuron. $GABA_A$ receptors in the synaptic density react to high concentrations of GABA while extrasynaptic $GABA_A$ receptors respond to lower GABA concentrations that diffuse out from the synaptic cleft. Figure adapted from (Avoli and de Curtis, 2011).

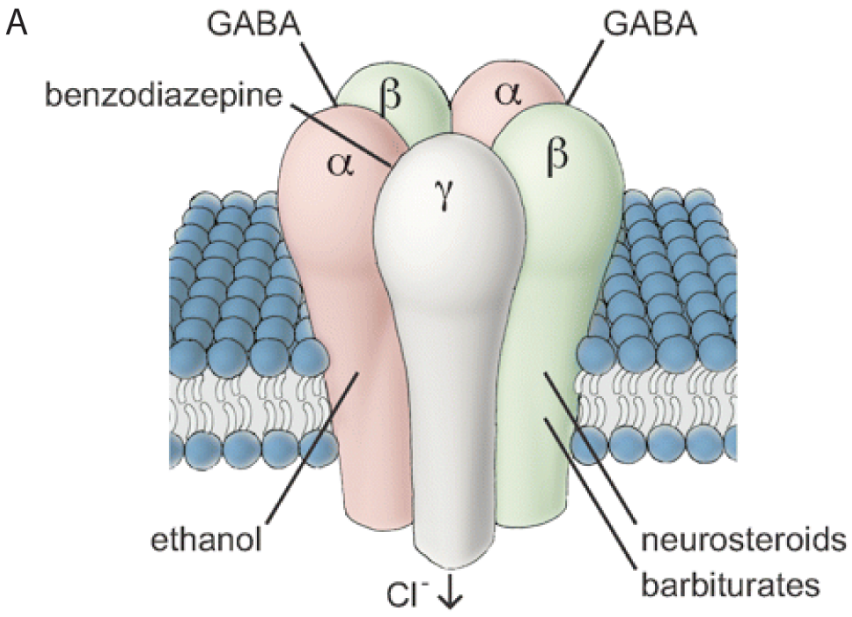
A
GABA
GABA
benzodiazepine
β
α
α
γ
β
ethanol
neurosteroids
barbiturates
Cl⁻

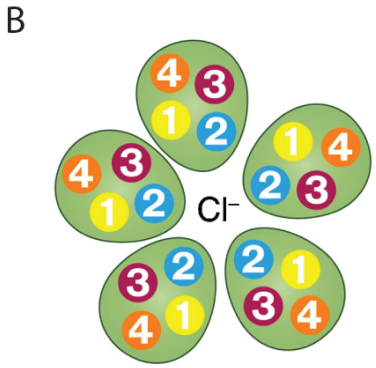
B
Cl⁻


C
NH3+
COO⁻
1
2
3
4

Figure 1.2. Basic structure of $GABA_A$ receptors. A) Five subunits are arranged around a central chloride conduction pore. GABA binds at the two β−α interfaces and BZDs bind at the α−γ interface. Other ligands such as barbiturates bind within the TMD. Image adapted from (Uusi-Oukari and Korpi, 2010). B) Top down view of the receptor showing the TMD helices surrounding a chloride conducting pore. The M2 helix lines the channel pore. C) Membrane topology of a single subunit. Each subunit consists of a large extracellular n-terminus that constitutes the LBD and 4 transmembrane helices. B) and C) adapted from (Avoli and de Curtis, 2011).

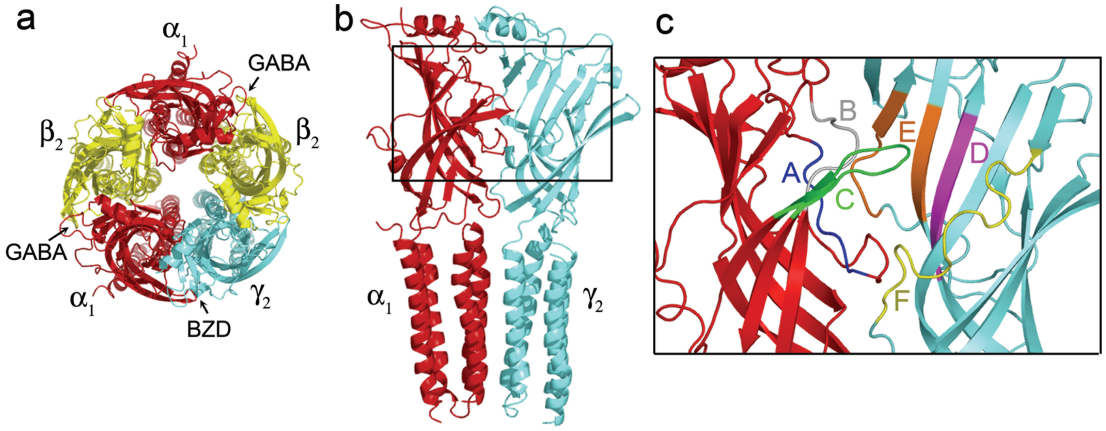
a
α1
GABA
β2
β2
GABA
α1
γ2
BZD
b
α1
γ2
c
B
E
D
A
C
F

Figure 1.3. $GABA_A$ receptor structure and detailed view of the BZD binding site. A) Homology model of the $\alpha_1\beta_2\gamma_2$ $GABA_A$ receptor pentamer (Mercado and Czajkowski, 2006) as seen from the extracellular membrane surface. The α_1, β_2, and γ_2 subunits are highlighted in red, yellow, and blue, respectively. Arrows indicate that GABA binds at the β_2-α_1 interfaces whereas benzodiazepines (BZDs) bind at the α_1-γ_2 interface of the receptor. B) Side view of the α_1 (red) and γ_2 (blue) subunits. The region of the interface encompassing the BZD binding site is boxed and highlighted in C), where BZD binding site Loops A-F are individually color-coded. Figure adapted from (Hanson et al., 2008).

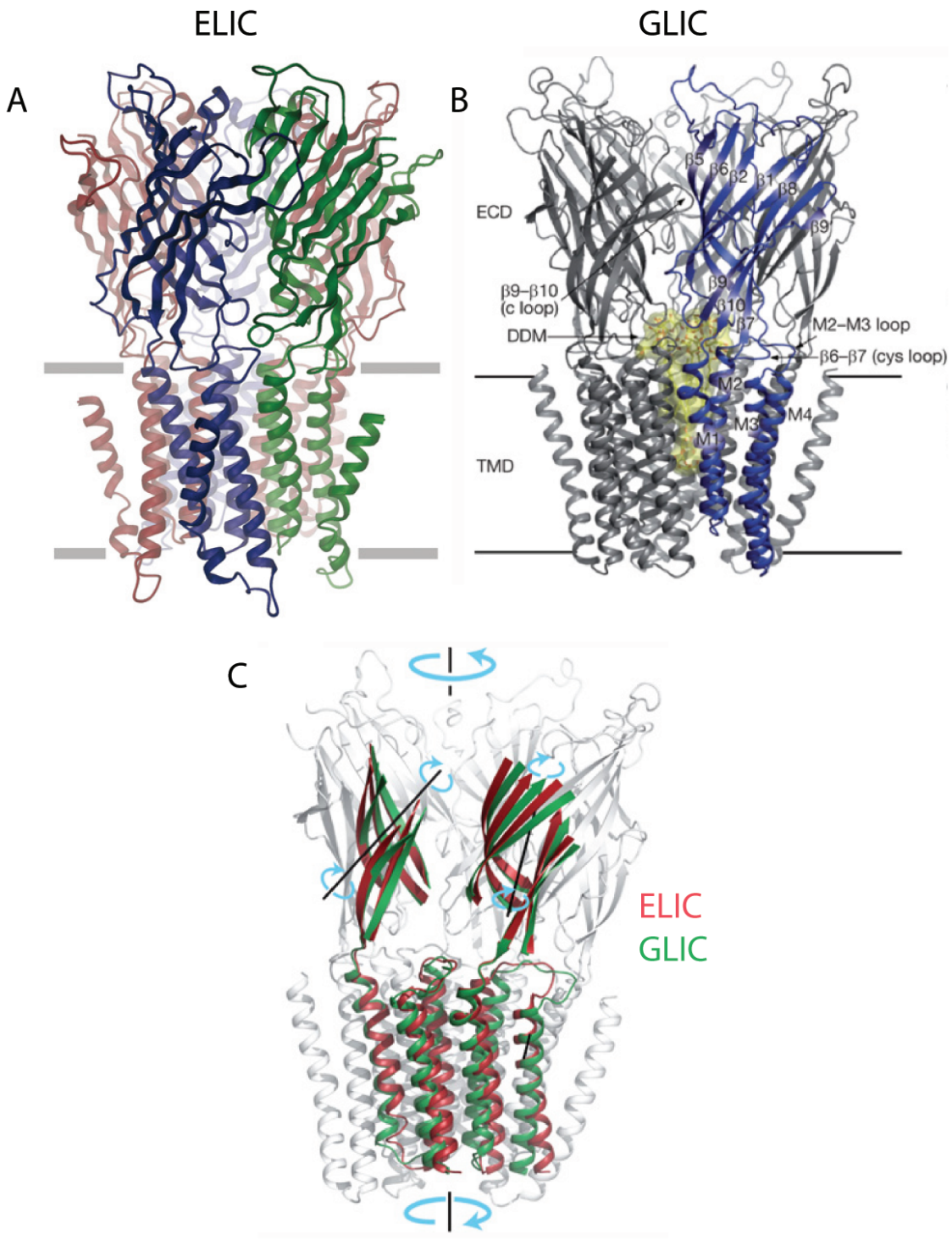
ELIC
GLIC
A
B
C
ECD
β9–β10
(c loop)
DDM
TMD
β5
β6
β2
β1
β8
β9'
β9
β10
β7
M2–M3 loop
β6–β7 (cys loop)
M2
M3
M4
M1
ELIC
GLIC

Figure 1.4. Recent crystal structures of homologous prokaryotic pLGICs. A) ELIC was crystallized in a closed conformation (Hilf and Dutzler, 2008). B) GLIC was crystallized in an apparently open conformation (Bocquet et al., 2009). C) Comparisons of the two structures provide information about the movements involved in channel opening. GLIC is in green, ELIC in red (Bocquet et al., 2009).

A

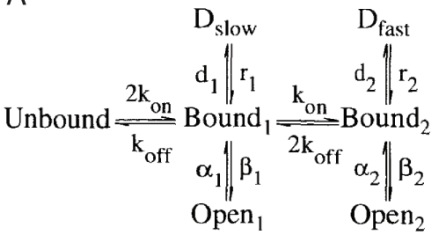
D_slow
D_fast
d_1
r_1
d_2
r_2
Unbound
2k_on
k_off
Bound_1
k_on
2k_off
Bound_2
α_1
β_1
α_2
β_2
Open_1
Open_2

B

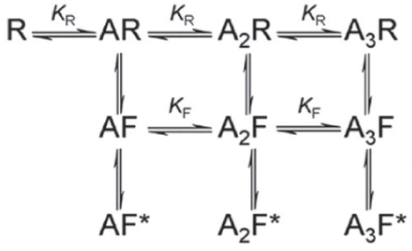
R
K_R
AR
A_2R
A_3R
AF
K_F
A_2F
A_3F
AF*
A_2F*
A_3F*

C

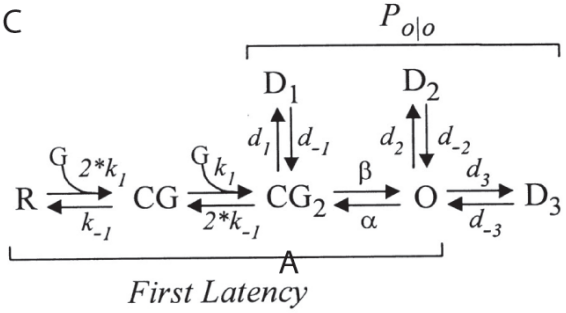
P_o|o
D_1
D_2
d_1
d_-1
d_2
d_-2
G
2*k_1
k_-1
G
k_1
2*k_-1
CG
CG_2
β
α
O
d_3
d_-3
D_3
R
A
First Latency

D

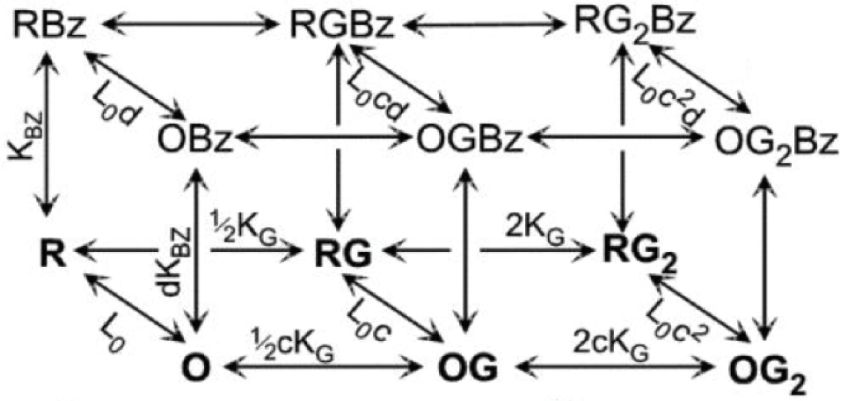
RBz
RGBz
RG_2Bz
K_BZ
L_od
L_ocd
L_oc2d
OBz
OGBz
OG_2Bz
R
dK_BZ
½K_G
RG
2K_G
RG_2
L_o
L_oc
L_oc2
O
½cK_G
OG
2cK_G
OG_2

Figure 1.5. Kinetic models showing hypothesized pLGIC receptor states and interconnectedness. A) Standard model showing unbound, closed state, single and double bound open, closed and desensitized states from (Jones and Westbrook, 1995). B) Model of glycine receptor activity incorporating singly, doubly or triply bound "flipped" states (AF) as transitions between the closed states (AR) and open states (AF*) (Burzomato et al., 2004). C) An alternative kinetic model for $GABA_A$ receptors where two binding of two GABA molecules (G) produces two bound, closed states (CG and CG_2) precedes the open state (O). There are three desensitized states (D_1, D_2 and D_3) that are connected only to the doubly bound closed state and open states (Burkat et al., 2001). D) Models that include many more kinetics states are often used to describe allosteric effects of drugs. This model features and unbound, closed state (R) as well as closed states bound by GABA (RG and RG_2), benzodiazepine alone (RBz), and both GABA and benzodiazepine (RGBz and RG_2BZ). Additionally there are separate states accounting for spontaneous opening (O), opening with only benzodiazepine bound (OBz), singly and doubly bound GABA opening with benzodiazines (OGBZ and OG_2BZ) and without (OG and OG_2). This particular model does not account for a desensitized state independent from the bound, closed state (Rusch and Forman, 2005).

Flunitrazepam
Classical BZD

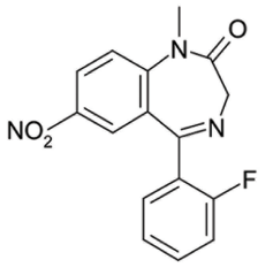

Diazepam
Classical BZD

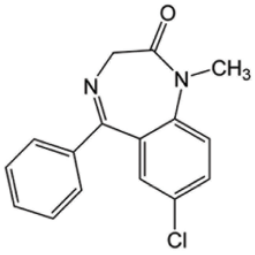

DMCM
Beta-carboline

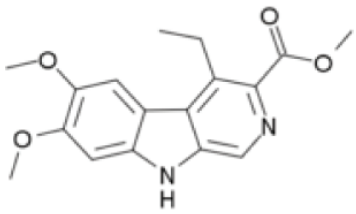

Eszopiclone (ESZ)
Cyclopyrrolone

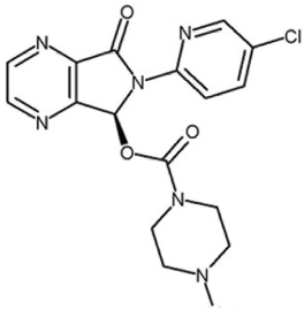

Zolpidem (ZPM)
Imidazopyridine

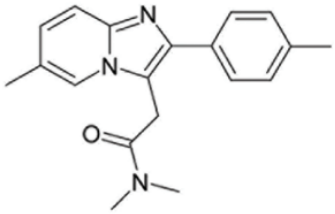

Ro15-1788/Flumazenil
Imidazobenzodiazepine

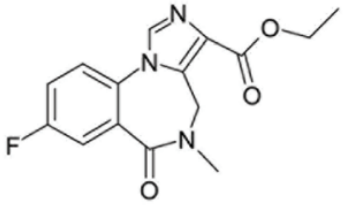

Figure 1.6. Chemical Structures of BZD binding site ligands. Classical BZD agonists flunitrazepam and diazepam show the core BZD structure. DMCM is a BZD inverse agonist of the beta-carboline family. Eszopiclone and Zolpidem are atypical benzodiazepine agonists, that are commonly used sleep aids. Ro15-1788 is a BZD antagonist.

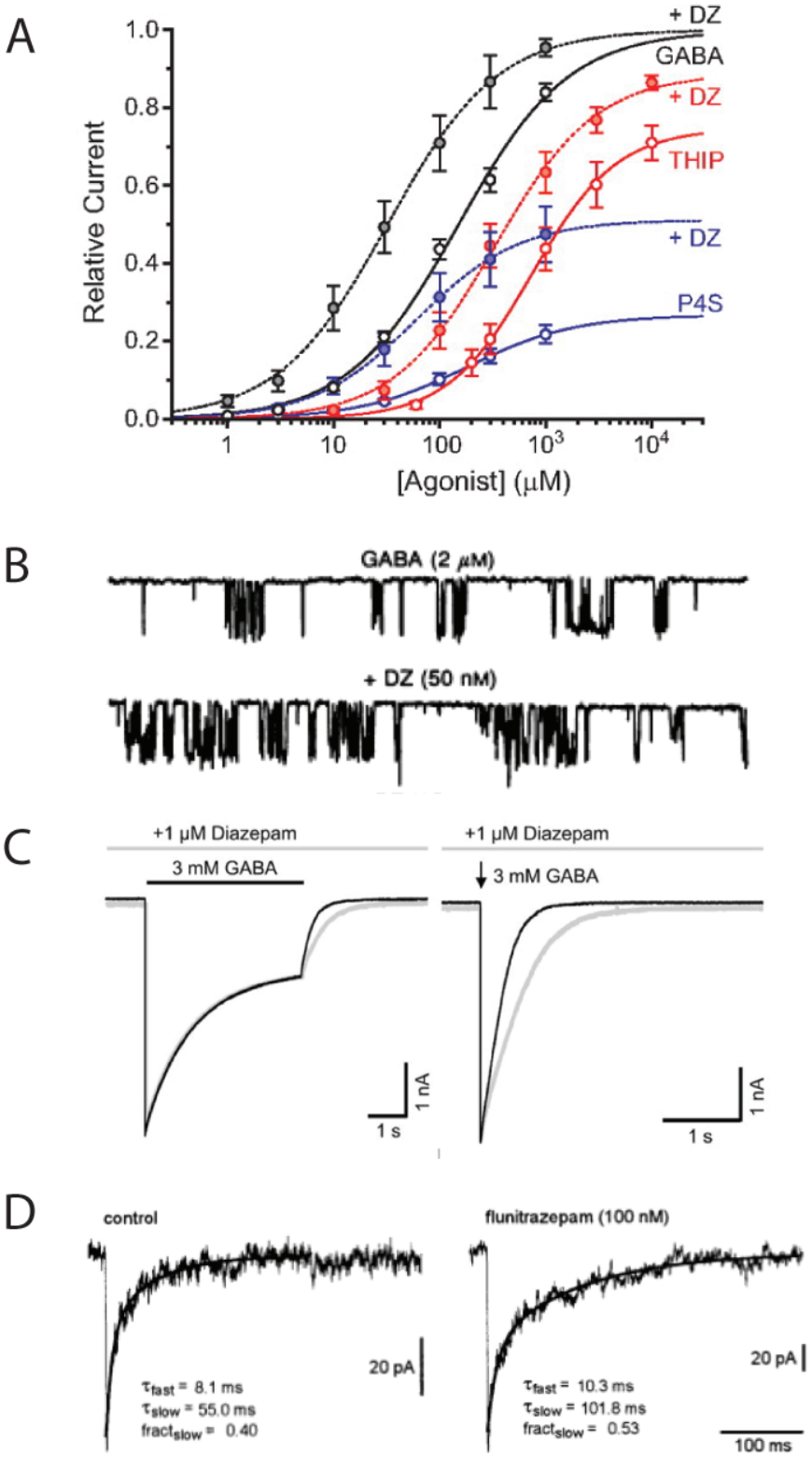
A
Relative Current
1.0
0.8
0.6
0.4
0.2
0.0
1
10
100
10^3
10^4
[Agonist] (μM)
+ DZ
GABA
+ DZ
THIP
+ DZ
P4S
B
GABA (2 μM)
+ DZ (50 nM)
C
+1 μM Diazepam
3 mM GABA
+1 μM Diazepam
3 mM GABA
1 nA
1 s
1 nA
1 s
D
control
20 pA
τfast = 8.1 ms
τslow = 55.0 ms
fractslow = 0.40
flunitrazepam (100 nM)
20 pA
τfast = 10.3 ms
τslow = 101.8 ms
fractslow = 0.53
100 ms

Figure 1.7. Benzodiazepine mechanisms of actions. A) Concentration response curves demonstrate potentiating affects of the BZD agonist, diazepam (DZ). BZDs do not increase the effect of the full agonist GABA, but effectively left shift the concentration response curve. For partial agonists, THIP and P4S there is both a left shift and increase in max current with the addition of diazepam. Figure adapted from (Gielen et al., 2012). B) At the single channel level diazepam increases burst frequency. Figure adapted from (Rogers et al., 1994a). C) In whole cell recordings from HEK cells, diazepam (gray) prolongs deactivation when compared to the current from GABA alone (black) both after a long and brief GABA pulse. Figure adapted from (Bianchi et al., 2009). D) In neurons, the BZD agonist flunitrazepam prolongs deactivation of IPSCs similar to what is seen with recombinant receptors. Figure adapted from (Strecker et al., 1999).

CHAPTER 2: Structural requirements for eszopiclone and zolpidem binding to the $GABA_A$ receptor are different[1]

2.1 Contributions

This work was completed in conjunction with Dr. Susan Hanson and Dr. Kenneth Satyshur. Dr. Kenneth Satyshur constructed the homology models as well as performed the molecular docking studies. Dr. Susan Hanson and I constructed GABA receptor mutants as well as performed radioligand binding experiments. I specifically constructed the αS204C, αS205C, αV211C, γT81C, γR132C, γL140C mutant containing subunits. I contributed to analyzing the data, figure preparation and writing the paper.

2.2 Abstract

The sleep-aids, zolpidem and eszopiclone, exert their effects by binding to and modulating $GABA_A$ receptors ($GABA_A$Rs), but little is known about the structural requirements for their actions. We made 24 cysteine mutations in the benzodiazepine (BZD) binding site of $\alpha_1\beta_2\gamma_2$ $GABA_A$Rs, and measured zolpidem, eszopiclone, and BZD-site antagonist binding. Mutations in γ_2Loop D and α_1Loops A and B altered the affinity of all ligands tested, indicating that these loops are important for BZD pocket structural integrity. In contrast, γ_2Loop E and α_1Loop C mutations differentially affected ligand affinity, suggesting that these loops are important for ligand selectivity. In agreement

[1] Published as Hanson SM, Morlock EV, Satyshur KA, Czajkowski C (2008) Structural requirements for eszopiclone and zolpidem binding to the gamma-aminobutyric acid type-A (GABAA) receptor are different. J Med Chem 51:7243-7252.

[2] Published as Morlock EV, Czajkowski C (2011) Different residues in the GABAA

with our mutagenesis data, eszopiclone docking yielded a single model stabilized by several hydrogen bonds. Zolpidem docking yielded three equally populated orientations with few polar interactions, suggesting that unlike eszopiclone, zolpidem relies more on shape recognition of the binding pocket than on specific residue interactions and may explain why zolpidem is highly α_1- and γ_2-subunit selective.

2.2 Introduction

Insomnia is associated with increased morbidity and mortality resulting from accidents, cardiovascular disease, and psychiatric disorders (Balter and Uhlenhuth, 1992). Approximately 10% of the population suffers from insomnia (Ohayon, 2002). with an estimated 2.5% using medications to aid sleep each year (Balter and Uhlenhuth, 1992). Past pharmacological treatments have included barbiturates and benzodiazepines (BZDs), both of which promote sleep by binding to and allosterically modulating $GABA_A$ receptors ($GABA_ARs$) in the CNS. These drugs however, have several unwanted side effects including alteration of sleep architecture, nightmares, agitation, confusion, lethargy, withdrawal, and a risk of dependence and abuse (Ramakrishnan and Scheid, 2007). The newest generation of sleep-aid drugs, the non-BZD hypnotics, were developed to overcome some of these disadvantages. These drugs, which include zolpidem (ZPM) and eszopiclone (ESZ) (Fig. 2.1), act through a similar neural mechanism as classical BZDs in that they bind to the same site in the $GABA_AR$, but differ significantly in their chemical structures and neuropharmacological profiles. Unlike classical BZDs, the non-BZDs have minimal impact on cognitive function and psychomotor performance while facilitating more restorative sleep stages, thus inducing a

pattern and quality of sleep similar to that of natural sleep (Scharf et al., 1994, Darcourt et al., 1999). Moreover, patients taking non-BZDs are less likely to exhibit tolerance, physical dependence, or withdrawal (Scharf et al., 1994, Darcourt et al., 1999, Krystal et al., 2003, Sanger, 2004).

Unlike classical BZDs, the sedative/hypnotic effect of ZPM occurs at much lower doses than the other pharmacological effects attributed to BZD-site action such as muscle relaxation and anti-convulsant activity (Sanger, 2004). This likely results from its selective binding to a specific $GABA_AR$ subtype. The $GABA_AR$ is a pentameric ligand-gated ion channel that can be formed by several different subunits (e.g. α, β, γ, etc.) and subunit isoforms (e.g. α_1, α_2, α_3, etc.). Receptors composed of different subunits have different kinetics, cellular distributions, and pharmacological profiles. Classical BZDs bind equally well to $GABA_ARs$ containing all of the α subunit isoforms except α_4 and α_6 (Pritchett and Seeburg, 1990, Wieland and Luddens, 1994). In contrast, ZPM has high affinity for receptors containing the α_1 subunit, low affinity for α_2- and α_3-containing receptors, and no significant affinity for α_5-containing receptors (Table 1) (Pritchett and Seeburg, 1990, Benavides et al., 1992, Wieland and Luddens, 1994). The sedative actions of BZDs have been shown to be mediated by α_1-containing $GABA_ARs$, whereas BZD effects such as anxiolysis, are mediated by other α subunit isoforms (Rudolph and Mohler, 2006). This helps explain why ZPM is useful as a sedative/hypnotic but is not a clinically efficacious anxiolytic, whereas classical BZDs such as diazepam are effective at treating anxiety but their use is accompanied by a myriad of adverse side effects. Interestingly, the non-BZD ESZ (and its racemate zopiclone) has similar affinity for $GABA_ARs$ containing α_1, α_2, α_3, and α_5 subunits (Table 1) (Benavides et al., 1992,

Graham et al., 1996), yet when taken for extended periods does not induce the adverse side effects associated with classical BZD treatment (Krystal et al., 2003). Thus, the neuropharmacological properties of ESZ must stem from more than just α-subunit selectivity.

The BZD binding site is located on the extracellular surface of the $GABA_AR$ at the interface of the α and γ subunits and is formed by residues located in at least six noncontiguous regions (historically designated Loops A-F) (Fig. 2.1) (Sigel, 2002). Although several studies have made significant strides in uncovering the specific amino acid residues that contribute to the binding of classical BZDs (e.g. flunitrazepam and diazepam; (Fig. 2.1)) (Sigel, 2002) complete descriptions of the residues that preferentially contribute to the binding of non-BZD ligands and the orientation of these ligands within the BZD site are relatively unknown.

In this study, we used site-directed mutagenesis, radioligand binding, and molecular docking to compare the structural requirements for ZPM and ESZ binding to α_1-containing $GABA_ARs$. We found that residues in γ_2Loop D, and α_1Loops A and B are important for maintaining the overall structural integrity of the binding pocket whereas residues in γ_2Loop E and α_1Loop C are important for ligand selectivity. Molecular docking is in good agreement with the binding data and suggests that unlike ESZ, ZPM binding relies more on the overall shape of the binding pocket than on specific residue interactions within the BZD site.

2.4 Materials and Methods

2.4.1 Site-directed mutagenesis

Cysteine mutants of γ_{2L} and α_1 receptor subunits were made by recombinant PCR in the pUNIV vector (Venkatachalan et al., 2007) and verified by double-stranded DNA sequencing.

2.4.2 Radioligand binding

HEK293T cells were grown in Minimum Essential Medium with Earle's salts (Invitrogen, Grand Island, NY) containing 10% fetal bovine serum in a 37^{o}C incubator under 5% CO_2 atmosphere. Cells were plated on 100mm dishes at ~40% confluency(Venkatachalan et al., 2007) for transient transfection using a standard $CaHPO_4$ precipitation method (Graham and van der Eb, 1973). Cells were transfected with equal ratios of α, β, and γ subunit DNA in the same vector (4 μg/subunit). For experiments involving cysteine mutants and WT $\alpha_1\beta_2\gamma_2$ receptors, cells were co-transfected with WT pUNIV-α_1, pUNIV-β_2, pUNIV-γ_{2L}, or mutant subunit cDNA. For expression of $\alpha_2\beta_2\gamma_2$, $\alpha_3\beta_2\gamma_2$, and $\alpha_6\beta_2\gamma_2$ receptors, cells were co-transfected with β_2-pRK5 and γ_2-pRK5 and either α_2-pRK5, α_3-pRK5, or α_6-pRK5 (constructs kindly provided by S. Dunn (Department of Pharmacology, University of Alberta, Edmonton, Canada)). For expression of $\alpha_4\beta_2\gamma_2$ and $\alpha_5\beta_2\gamma_2$ receptors, cells were co-transfected with α_4-pUNIV, β_2-pUNIV, and γ_2-pUNIV or α_5-pCEP4, β_2-pCEP4, and γ_2-pCEP4 cDNA, respectively. Cells were harvested and membrane homogenates prepared 48 hours post-transfection as described.(Boileau et al., 1998) Briefly, membrane homogenates (50 μg) were incubated at room temperature for 40 min with a sub-K_d concentration of radioligand ([^{3}H] Ro15-1788, 70.7Ci/mmol; [^{3}H] flunitrazepam, 85.2 Ci/mmol; [^{3}H] Ro15-4513, 35.7 Ci/mmol; PerkinElmer Life and Analytical Sciences, Boston, MA) in the absence or presence of seven different concentrations of unlabeled ligand in a final

volume of 250 μL. Data were fit by non-linear regression to a one-site competition curve defined by the equation $y=B_{max}/[1+(x/IC_{50})]$, where y is bound [^{3}H] ligand in disintegrations per minute, B_{max} is maximal binding, x is the concentration of displacing ligand, and IC_{50} is the concentration of unlabeled ligand that inhibits 50% of [^{3}H] ligand binding (Prism; GraphPad Software). Equilibrium dissociation constant values for the unlabeled ligand (K_i) were calculated using the Cheng-Prusoff/Chou equation: $K_i=IC_{50}/[1+L/K_d]$, where K_d is the equilibrium dissociation constant of the radioligand, and L is the concentration of the radioligand.

2.4.3 Statistical analysis

Binding data represent mean ± SD from three experiments performed in triplicate. The data were analyzed by one-way ANOVA with Dunnett's post-test for significance of differences (StatView v.5.0.1, SAS Institute Inc, Cary, NC).

2.4.4 Automated ligand docking

The homology model of the $GABA_AR$ used in this study was constructed as described (Mercado and Czajkowski, 2006). ESZ and ZPM were built using Sybyl Modeling software (Tripos Corp., St. Louis, MO). Each of the drug structures were energy minimized using the Tripos force field, then a random search was performed for the lowest energy conformations. The single lowest energy form was placed in the $GABA_AR$ α_1/γ_2 interface using Sybyl and a 15 Å sphere of residues around the ligand was chosen as the starting active site. The active site was setup for docking using AutoDock 4.0 Tools, placing Gatseiger charges and desolvation parameters on the chosen 15 Å receptor sphere. Autodock 4 (Morris et al., 1998, Huey et al., 2007) parameters were chosen for the Genetic Algorithm (GA) to examine 150 individuals in a population with a maximum

of 5 million energy evaluations, followed by 300 iterations of Solis & Wets local search (Lakmarkian algorithm). A total of 10 to 30 of these hybrid dockings were performed on each drug. The binding results were clustered based upon lowest energy, visual similarities, and the orientation in the active site. The reported binding energies in kcal/mol is the sum of the final intermolecular energy, the internal energy of the ligand, and the torsional free energy minus the unbound systems energy. The orientation with stronger binding has the lower total energy and the cluster of highest number of bindings represents a higher probability of binding. The drug was allowed to flexibly dock, but the receptor's backbone and side chains remained rigid during docking. Each docking gave an ensemble of docking modes, with many orientations nearly identical and only differing by less than 0.1 kcal/mol.

2.5 Results

2.5.1 Effects of BZD-site mutations on [^{3}H] Ro15-1788 binding affinity

Several residues that contribute to the binding of BZD ligands have previously been identified (Fig. 2.1e). On the α subunit these residues include: **H101** (Loop A) (Wieland et al., 1992, Wieland and Luddens, 1994, Duncalfe et al., 1996, Davies et al., 1998, Davies et al., 2000, Berezhnoy et al., 2004, Tan et al., 2007b), **G157**, **Y159**, **T162** (Loop B) (Wieland and Luddens, 1994, Amin et al., 1997, Renard et al., 1999, Tan et al., 2007b), and **G200**, **V202**, **S204**, **S205**, **T206**, **Y209**, and **V211** (Loop C) (Pritchett and Seeburg, 1991, Wieland and Luddens, 1994, Amin et al., 1997, Buhr et al., 1997a, Schaerer et al., 1998, Sigel et al., 1998, Renard et al., 1999, Strakhova et al., 2000, Sawyer et al., 2002, Derry et al., 2004, Tan et al., 2007b); on the γ subunit these include:

F77, **A79**, **T81** (Loop D) (Buhr and Sigel, 1997, Wingrove et al., 1997, Sigel et al., 1998, Kucken et al., 2000, Teissere and Czajkowski, 2001, Kucken et al., 2003, Berezhnoy et al., 2004) and **M130** (Loop E) (Buhr et al., 1997b, Sigel et al., 1998).

To help elucidate the unique structural requirements for ESZ and ZPM binding, 24 single cysteine mutations (12 each in the α_1 and γ_2 subunits) were made in or near the BZD binding site in the $GABA_AR$ (Fig 2.1e). These included all of the sites mentioned above with the exception of two residues and some new sites. We did not mutate α_1H101, as it has already been shown to contribute to the high affinity binding of both zopiclone and ZPM (Wieland et al., 1992, Wieland and Luddens, 1994, Davies et al., 2000), and α_1Y159, because serine and cysteine substitutions at this site abolish [^{3}H] Ro15-1788 and [^{3}H] flunitrazepam binding thereby precluding further BZD affinity measurements (Amin et al., 1997, Tan et al., 2007b).

The mutant subunits were co-expressed with wild-type (WT) subunits in HEK293T cells to form $\alpha_1\beta_2\gamma_2$ $GABA_ARs$ and the binding of the BZD-site antagonist, [^{3}H] Ro15-1788 (Fig. 2.1d) was measured. The majority of mutant receptors bound Ro15-1788 with similar affinity as WT receptors ($K_i = 3.3 \pm 1.3$ nM) (Table 2.2). Seven mutations caused small but significant decreases (2.0 - 4.5 fold) in Ro15-1788 affinity, whereas one mutation, α_1G157C, increased the affinity over 17-fold (Table 2.2). For three mutant receptors ($\alpha_1\beta_2\gamma_2$F77C, α_1D97C$\beta_2\gamma_2$, and α_1Y209C$\beta_2\gamma_2$) specific binding of [^{3}H] Ro15-1788 or the BZD-site agonist [^{3}H] flunitrazepam (Fig. 2.1d) was not measurable (data not shown), precluding any further examination.

2.5.2 Effects of γ_2 subunit mutations on ESZ and ZPM binding affinity

ESZ and ZPM binding affinities were determined by their ability to competitively displace [^{3}H] Ro15-1788. In the γ_2 subunit, one mutation in Loop D (β-strand 2), A79C, significantly reduced both ESZ and ZPM affinity (~8-9 fold) compared to WT receptors ($K_{i\ ESZ}$ = 50.1 $\pm$ 10.1 nM; $K_{i\ ZPM}$ = 61.9 $\pm$ 7.3 nM), whereas γ_2T81C located adjacent to γ_2A79, had a small but significant effect on ZPM but not ESZ binding (Fig. 2.2, 2.3a; Table 2). γ_2D56C on the neighboring β-strand (Fig. 2.3a) had no effect on the binding of either drug (Fig. 2; Table 2.2).

γ_2Loop E of the BZD binding site is composed of two adjacent β-strands (5/6) that form the back and side of the BZD binding pocket (Fig 2.1c). Several mutations in the middle of these β-strands differentially affected ESZ and ZPM binding (Fig. 2.2, 2.3b; Table 2). Whereas cysteine substitution of γ_2M130 and γ_2R132 each *decreased* ESZ affinity ~2-fold, these mutations *increased* ZPM affinity ~2-4 fold. While γ_2T142C significantly reduced the affinity of both ligands, it had a larger effect on ZPM binding compared to ESZ (21-fold vs. 10-fold change). Moreover, $\alpha_1\beta_2\gamma_2$R144C receptors showed a significant reduction in ESZ affinity (3.5-fold) but no change in ZPM binding. γ_2T126C and γ_2L140C, located at the periphery of the BZD-site (Fig. 2.3b) did not affect the binding of ESZ or ZPM. Overall, the data suggest that Loop E plays an important role in determining ligand selectivity of the BZD binding site.

Loop F of the γ_2 subunit (~residues 182-197) is a dynamic region of the receptor located between the BZD binding site and the transmembrane channel domain (Fig. 2.1). Through the use of γ_2/α_1 chimeras, a portion of Loop F ($\gamma_2$186-192) was shown to be important for high affinity ZPM binding (Sancar et al., 2007). A chimeric subunit, χ161 (containing γ_2 residues up to and including amino acid 161 and α_1 residues C-terminal to

161), when expressed with WT α_1 and β_2 subunits retained WT binding affinity for flunitrazepam, but the binding affinity for ZPM decreased 8-fold. Here, we used the same chimera to test whether residues C-terminal to 161 were also important for ESZ binding. We found that χ161 slightly increased (~2-fold) the affinity of the receptor for ESZ (Fig. 2.2, 2.3c; Table 2.2).

We noticed that in our homology model of the $GABA_AR$ (Mercado and Czajkowski, 2006) two arginine residues and a glutamate from Loop F (γ_2R185, γ_2R194, and γ_2E189) point toward the ligand binding pocket (Fig. 2.3c). We individually mutated the arginine residues to cysteine and found the binding of Ro15-1788, ESZ, and ZPM to γ_2R185C- and γ_2R194C-containing receptors was indistinguishable from WT (Fig. 2.2; Table 2). These data are consistent with our previous study of γ_2Loop F where we demonstrated mutations in this region (γ_2W183C, γ_2E189C, and γ_2R197C) affect modulation of GABA current by BZD agonists without affecting binding affinity of various BZD ligands including ZPM, Ro15-1788, the classical BZD, flurazepam, and the inverse agonist, DMCM (Hanson and Czajkowski, 2008). Overall, these results strongly suggest no one residue in γ_2Loop F is critical for binding classical or non-BZDs.

2.5.3 Effects of α_1 subunit mutations on ESZ and ZPM binding affinity

In α_1 Loops A and B, cysteine substitution of two residues, α_1A160 and α_1T162, had no significant effect on either ESZ or ZPM binding affinity (Fig. 2.2; Table 2.2). In contrast, cysteine substitution of α_1F99 and α_1G157, caused significant changes in the affinity of both ligands. α_1F99C reduced ESZ and ZPM affinity by ~8- and 3-fold, respectively, compared to WT receptors. α_1G157C had a larger effect, with 42- and 20-fold changes in ESZ and ZPM binding affinity, respectively (Fig. 2.2, 2.4a; Table 2.2).

Cysteine substitution of several residues in α_1Loop C also significantly altered the binding affinity of both ligands. α_1G200C and α_1V202C reduced ESZ affinity by 2.4- and 5.0-fold, respectively, and reduced ZPM affinity 9.7- and 9.0-fold, respectively (Fig. 2.2, 2.4b; Table 2.2). Other mutations differentially affected ZPM and ESZ affinity. α_1S204C reduced ZPM affinity by 7-fold, but had no effect on ESZ binding, whereas α_1T206C increased ESZ affinity over 60-fold while having no effect on ZPM binding (Fig. 2.2, 2.4b; Table 2.2). Receptors containing α_1S205C and α_1V211C bound both ligands with WT affinity. These results suggest that together with γ_2Loop E, α_1Loop C is an important determinant for BZD-site ligand selectivity.

2.5.4 Molecular docking of eszopiclone and zolpidem

Independent of the radioligand binding experiments described above, we used our homology model of the $GABA_AR$ to dock ESZ and ZPM into the BZD binding site. ESZ docking yielded a single most populated pose with low energy (-6.61 kcal/mol). In this pose (termed ESZ-dock), the free carbonyl of ESZ is pointed up toward Loop C and the ring carbonyl is near γ_2R144 (Loop E) and α_1H101 (Loop A) near the base of the pocket (Fig. 2.5a, 2.6a). In contrast, ZPM docking yielded three equally populated poses with similar energies (between -7.0 and -6.7 kcal/mol), one with the imidazopyridine ring under α_1Loop C, the carbonyl pointed up toward the tip of α_1Loop C and the dimethyl amide pointed towards γ_2Loop D (ZPM-up-dock) (Fig. 2.5b), one with the imidazopyridine ring under α_1Loop C and the dimethyl amide pointed down in the pocket toward α_1H101 (ZPM-down-dock) (Fig. 2.5c, 2.6b), and one where the imidazopyridine ring pointed toward the back wall of the pocket, the carbonyl pointed down away from

α_1Loop C and the dimethyl amide positioned under the tip of α_1Loop C (ZPM-out-dock) (Fig. 2.5d).

To gain insight into the potential interactions between ESZ or ZPM and the $GABA_AR$ in our docked ligand-receptor complexes, we measured the distance between atoms in each ligand and atoms in the protein, with the idea that functional groups separated by less than 7 Å have the potential to interact (Schreiber and Fersht, 1995) and those within 4 Å may form salt bridges or hydrogen bonds (Kumar and Nussinov, 1999). In ESZ-dock, residues γ_2F77, γ_2A79, γ_2T142, γ_2R144, α_1H101, α_1Y159, α_1T206, and α_1Y209 all come within 4 Å of the ligand (Fig. 2.5a, 2.6a), and when mutated alter ESZ binding (Table 2.2) and/or BZD binding in general. In this docking, potential polar contacts exist between ESZ and γ_2R144, α_1Y159, α_1S204, α_1Y209, and the backbone of α_1Loop C (shown as dashed lines in Fig. 2.5a, 2.6a). In addition, residues α_1F99, α_1V202, γ_2M130, and γ_2R132, which when mutated all adversely affect ESZ binding (Table 2.2), are all within 7 Å of ESZ in our model.

For ZPM, the three poses are similar in that residues including γ_2F77, γ_2M130, γ_2T142, α_1H101, α_1Y159, α_1S204, and α_1Y209, all come within 5 Å of the ligand in each case (Fig. 2.5, 2.6b). Likewise, residues α_1F99, α_1V202, γ_2A79, and γ_2R132 are within ~7 Å or less from ZPM in each model. Thus, even though the free carbonyl of ZPM is oriented differently in each pose, the space occupied by ZPM within the binding pocket is similar. The major difference between the three models lies in the potential for hydrogen bonding. In ZPM-up-dock, potential hydrogen bonds exist between ZPM and the backbone of Loop C near α_1T206/G207, in ZPM-down-dock, the free carbonyl may form

a hydrogen bond with α_1S204 in Loop C, and in ZPM-out-dock the carbonyl may interact with γ_2R194 in Loop F (dashed lines, Fig. 2.5, 2.6b).

2.6 Discussion

Although several studies have revealed important information on the amino acid side chains that contribute to classical BZD binding in the $GABA_AR$, a complete description of the residues that participate in non-BZD binding has been lacking. Residues previously shown to participate in ZPM binding include: γ_2F77, γ_2M130, α_1H101, α_1T162, α_1G200, α_1S204, α_1T206, α_1Y209, and α_1V211 (Pritchett and Seeburg, 1991, Wieland et al., 1992, Wieland and Luddens, 1994, Buhr et al., 1997a, Buhr et al., 1997b, Buhr and Sigel, 1997, Wingrove et al., 1997, Schaerer et al., 1998, Sigel et al., 1998, Renard et al., 1999, Strakhova et al., 2000). To our knowledge, only one site, α_1H101, has been identified that is important for zopiclone (the racemate of ESZ) binding (Davies et al., 2000). Here, we define receptor models for how ESZ and ZPM are oriented in the binding site, evaluate how specific residues in the binding site interact with ESZ and ZPM, and provide new insight into the pharmacophores for these drugs.

2.6.1 Residues in Loops A, B, and D are critical for the overall structure of the BZD site

Several lines of evidence suggest that residues in γ_2Loop D and α_1Loops A and B are critical to the binding of BZDs in general and thus are important for the overall structure of the BZD binding site. Mutations in these areas affect the binding affinities of a variety of structurally diverse BZD-site ligands. In γ_2Loop D, we were unable to detect specific binding of BZD antagonist, [^{3}H] Ro15-1788 or the BZD agonist [^{3}H]

flunitrazepam to F77C-containing receptors, suggesting that the native phenylalanine at this position is a key structural element in the BZD binding pocket. This is consistent with previous findings that showed a variety of substitutions at γ_2F77 dramatically alter the affinity of various BZDs including Ro15-1788, diazepam, flunitrazepam, and ZPM (Buhr and Sigel, 1997, Wingrove et al., 1997, Sigel et al., 1998), and where γ_2F77C was shown to completely abolish flurazepam potentiation (Teissere and Czajkowski, 2001).

Moreover, we found mutation γ_2A79C reduced the binding of ESZ and ZPM to a similar extent (~8-9-fold) (Fig. 2.2) and the affinity of the receptor for Ro15-1788 was also significantly decreased (Table 2.2). Previous studies found mutation of γ_2A79 was also detrimental to flunitrazepam, Ro15-4513, Ro15-1788, and diazepam binding (Kucken et al., 2000, Kucken et al., 2003, Berezhnoy et al., 2004). These results are in good agreement with cysteine accessibility studies that showed γ_2A79 is part of the BZD binding pocket (Teissere and Czajkowski, 2001, Kucken et al., 2003).

Cysteine substitution of γ_2T81 had no effect on ESZ or Ro15-1788 and only a minor effect on ZPM affinity (<2-fold) (Table 2). However, larger volume BZD-site ligands such as Ro15-4513, Ro40-6129, and Ro41-3380 are affected by mutations at this site (Kucken et al., 2003). Thus, even though γ_2T81 may not contribute significantly to ESZ or ZPM binding, it likely forms part of the binding site for other BZDs.

In α_1Loop A, we observed no specific binding of [^{3}H] Ro15-1788 or [^{3}H] flunitrazepam to α_1D97C$\beta_2\gamma_2$ receptors. Functional α_1D97C$\beta_2\gamma_2$ receptors that respond to GABA can be expressed in Xenopus oocytes (Sharkey and Czajkowski, 2008a). Thus, it is unlikely that cysteine substitution at this location impairs proper folding or expression of the receptor. Molecular docking indicates that α_1D97 is within 8 Å of ESZ and ZPM.

In our model, α_1D97 appears part of an electrostatic network of residues that bridges the α_1/γ_2 subunit interface. We speculate that the lack of specific binding for this mutant is because α_1D97 is important for maintaining the structural integrity of the BZD pocket.

Mutation of α_1F99 in Loop A significantly reduces $GABA_AR$ affinity for ESZ, ZPM, and Ro15-1788. This may be because α_1F99 participates in hydrophobic interactions with bound drug, or because mutation of α_1F99 to cysteine alters the position of α_1H101 (Loop A) and α_1Y159 (Loop B) which lie on either side of it in the binding pocket (Fig. 2.5). Indeed, the necessity of α_1H101 in binding ZPM (Wieland et al., 1992, Wieland and Luddens, 1994), zopiclone (Davies et al., 2000), and several other BZDs (Duncalfe et al., 1996, Davies et al., 1998, Berezhnoy et al., 2004) has been established. The importance of α_1Y159 is underscored by its potential to hydrogen bond directly with ESZ in the binding pocket (Fig. 2.5) and the inability of [^{3}H] Ro15-1788 or [^{3}H] flunitrazepam to bind α_1Y159C- or α_1Y159S-containing receptors (Amin et al., 1997, Tan et al., 2007b).

One of the most dramatic shifts in BZD binding affinity was measured for the α_1Loop B mutant, G157C. This residue appears to be at the side wall of the ESZ and ZPM binding pocket (Fig. 2.5). In our homology model of the $GABA_AR$, a larger cysteine side chain would decrease the volume of the binding site. This may hinder occupation of the site by ZPM and ESZ and/or affect the positioning of nearby residues including α_1H101 (Loop A) and α_1Y209 (Loop C) (Fig. 2.5). The fact that G157C drastically reduces ZPM and ESZ binding (Fig. 2.2; Table 2.2) but increases Ro15-1788 affinity 17-fold supports the idea that G157C alters the shape of the BZD binding pocket and that imidazobenzodiazepines (i-BZDs) such as Ro15-1788, have different structural

requirements than the non-BZDs. Indeed, a recent study showed that a sulfhydryl-reactive derivative of the i-BZD, Ro15-4513, was able to covalently attach to a cysteine at α_1G157 (Tan et al., 2007b).

Since mutation of residues in γ_2LoopD and α_1Loops A and B alter the binding affinity of a variety of structurally diverse BZD-site ligands (our work and others), we envision that these regions define the core of the binding site for BZD-site ligands. Thus, a question remains as to what defines ligand specificity at the BZD binding site.

2.6.2 Residues in Loops C and E determine ligand selectivity at the BZD site

Unlike residues in Loops A, B, and D, γ_2Loop E residues are located at the back of the binding pocket where extra space exists for ligand placement/movement (Fig. 2.6c, *right panel*). The large unfilled volume bordered by Loop E is likely ideal for accommodating ligands of different size and chemical composition. Indeed, we found mutations M130C, R132C, and R144C in γ_2Loop E differentially affect ESZ, ZPM, and Ro15-1788 affinity (Table 2.2; Fig. 2.2). In addition, the magnitude of the effect of the T142C mutation was different for all three ligands tested. Interestingly, previous studies have shown mutation of γ_2M130 to leucine reduces ZPM affinity while having very small or no effects on the binding of several other BZDs (Buhr et al., 1997b, Sigel et al., 1998). Thus, substitution of native Loop E residues may cause a change in the volume of the binding site that results in altered positioning of the ligand in the pocket, thereby affecting affinity. For example, molecular docking shows the native arginine at position 144 stabilizes the ring carbonyl of ESZ in the binding pocket via a hydrogen bond (Fig. 2.5), thus removal of this H-bond via cysteine substitution likely causes the observed

reduction in ESZ affinity. In contrast, ZPM dockings show no interaction with γ_2R144, explaining the lack of effect of γ_2R144C on ZPM binding.

Mutations in α_1Loop C also differentially affect ligand binding to the BZD-site of the $GABA_AR$ (Fig. 2.2) suggesting that these residues also play a role in determining ligand selectivity. We found that three mutations, G200C, V202C, and S204C, had a much greater effect on ZPM affinity than ESZ or Ro15-1788, whereas T206C dramatically increased ESZ affinity without affecting ZPM or Ro15-1788 (Fig. 2.2; Table 2.2). In addition, previous studies have shown mutations T206V and T206A selectively alter the affinity of diazepam, flunitrazepam, and ZPM but not that of several other BZDs (Buhr et al., 1997a, Sigel et al., 1998).

Based on the low sequence homology of α_1Loop C to other α subunit isoforms (Fig. 2.1e), Loop C is likely a significant determinant in the α_1-subunit selectivity of ZPM. This is supported by previous studies. First, replacement of α_1G200 with the aligned glutamate residue present in all other α subunit isoforms reduces ZPM binding (Schaerer et al., 1998), whereas replacement of the glutamate in α_3, α_5, and α_6 with glycine increases the affinity of these receptors for ZPM (Pritchett and Seeburg, 1991, Wieland and Luddens, 1994, Renard et al., 1999). Second, replacement of the threonine in α_5 with the aligned serine at 204 in α_1 increases the affinity of α_5 for ZPM (Renard et al., 1999). Lastly, mutation of α_1V211 to the aligned isoleucine in α_5 and α_6 decreases flunitrazepam and ZPM affinity, while increasing the affinity of α_5-selective ligands (Strakhova et al., 2000). All of these substitutions show that α_1Loop C residues promote ZPM binding whereas Loop C residues from other α subunit isoforms reduce ZPM affinity, supporting the idea that α_1Loop C contributes to ZPM selectivity.

Loop C residues α_1Val211, α_1Val202, and α_1Ser205 also appear to be especially important for i-BZD binding. A sulfhydryl-reactive derivative of Ro15-4513 has been shown to covalently attach to α_1V202C and α_1V211C (Tan et al., 2007b), whereas α_1S205C reduced the affinity for Ro15-1788 (Table 2), and replacement of α_1S205 with the aligned asparagine in α_6 was shown to decrease the affinity of i-BZDs and β-carbolines (Derry et al., 2004). Of the cysteine substitutions at these sites, only α_1V202C had an effect on ESZ and ZPM binding (Fig. 2.2; Table 2.2). Overall, mutations in γ_2Loop E and α_1Loop C differentially affect binding of structurally diverse classes of BZD-site ligands supporting the idea that these regions define specificity.

2.6.3 Zolpidem interaction with the BZD site is less specific than eszopiclone

The orientation of ESZ in the BZD binding pocket as presented in Fig. 2.5 and 2.6 is supported by our mutagenesis data. This docking was the lowest energy, most highly populated pose obtained using AutoDock 4.0. A similar orientation of ESZ was observed using AutoDock 3.0 and SureFlex Dock (data not shown) and the docking is consistent with the recently described unified pharmacophore/receptor model of the BZD site (Clayton et al., 2007). Essential functional groups defining the ESZ pharmacophore and its orientation in the site are its two carbonyls, which hydrogen bond with the backbone of Loop C and γ_2R144 (Loop E), respectively, and two ring nitrogens, which hydrogen bond with α_1S204 (Loop C) and α_1Y159 (Loop B), respectively (Fig. 2.6).

In contrast, ZPM may bind in multiple orientations in the BZD site. Our molecular docking revealed three equally populated poses with equivalent energies that occupy a similar space within the BZD site (Fig. 2.5 and 2.6), but with few potential polar contacts in any orientation. Thus, the essential descriptor of the ZPM

pharmacophore is likely its size and shape. ZPM has only a single carbonyl, which appears capable of interacting with several different residues in the BZD binding site (Fig. 2.5). We found that this carbonyl could hydrogen bond with α_1Loop C (at α_1S204 or the backbone near α_1T206/G207) or with γ_2Loop F (Arg194) (Fig. 2.5). Similar orientations were observed with Autodock 3.0 and SureFlex Dock software (data not shown). Our ZPM-up-dock pose is similar to that reported by Sancar et al, which allowed flexible movement of the side chains during docking (Sancar et al., 2007). While our mutagenesis data would favor hydrogen bonding with α_1S204, we cannot exclude any of the poses presented here. Overall, we believe that unlike ESZ, ZPM binding relies more on shape recognition of the binding pocket than on specific interactions in the BZD site. This would explain several observations:

First, this would account for the α_1 subunit selectivity of ZPM (Table 2.1) (Pritchett and Seeburg, 1990, Puia et al., 1991, Benavides et al., 1992, Herb et al., 1992, Wieland and Luddens, 1994). The included volume of the BZD binding pocket for α_1-containing receptors has a slightly different shape, polarity, and lipophilicity compared to α_2- and α_3-containing receptors (Clayton et al., 2007), explaining the reduced but still measurable affinity of ZPM for α_2 and α_3 (Table 2.1). Furthermore, the included volume of α_1-containing receptors is much larger than α_4-, α_5-, and α_6-containing receptors (Clayton et al., 2007), thus explaining the lack of ZPM binding at these α subtypes (Table 2.1). It follows that differences in the included volumes of the BZD-site for γ_2-versus γ_1- and γ_3-containing receptors also likely play a role in ZPM selectivity.

Second, this clarifies why χ161, but not specific mutations in Loop F, specifically reduce ZPM binding (Table 2.2). The replacement of the entire γ_2Loop F, which is poorly

conserved, with the α_1Loop F that is also two amino acids longer, likely changes the size of the binding pocket to the detriment of ZPM binding.

Third, shape recognition by ZPM would explain why minor mutations in Loop C like α_1G200C, α_1V202C, and α_1S204C, affect ZPM binding to a much greater extent than ESZ (Fig. 2.2). Loop C, which comprises the entire lid over of the BZD site (Fig. 2.6c) is highly flexible, and is believed to move upon ligand binding (Celie et al., 2004a, Gao et al., 2005a, Hansen et al., 2005). Thus, it stands to reason that mutation of α_1G200, located at the hinge of Loop C (Fig. 2.5), would change the overall flexibility of the Loop, perhaps preventing its full closure on the binding site, resulting in an altered shape of the binding pocket, which in turn precludes high affinity ZPM binding. In contrast, ESZ, which is anchored to the BZD site by multiple interactions (e.g. Arg144, Tyr209, Tyr159, etc.)(Fig. 2.6a), is less affected by any single mutation.

Overall, this evidence suggests that ZPM binding depends largely on the size and shape of the BZD binding pocket rather than specific polar interactions.

2.6.4 Summary and Conclusions

In summary, our data provide new insights toward defining the pharmacophore for non-BZD hypnotics as well as the structure of the BZD binding site (Fig. 2.6). We provide a comprehensive description of the amino acid residues that contribute to the binding of these ligands and present molecular models for their orientation in the BZD binding site. We show that residues in γ_2Loop D and α_1Loops A and B provide the necessary framework for ligand binding in the pocket, while specific residues in γ_2Loop E and α_1Loop C play a key role in determining ligand selectivity. We conclude that γ_2Loop F does not directly contribute to BZD binding but may serve indirectly to

maintain the structural integrity of the region. We also provide evidence that the subunit selectivity of ZPM results mainly from the overall shape of the binding pocket and is based largely on its interaction with Loop C.

Thus, their footprint within the BZD binding pocket of the $GABA_AR$ may in part determine the pharmacological properties of the non-BZDs. Further experiments will be necessary to determine if specific residues in Loops C and E differentiate the efficacies of the classical and non-BZD ligands. The identification of the structural elements important for the high affinity binding and efficacy of these drugs provides insight into the unique neuropharmacological profile of ESZ and ZPM in the CNS and will be beneficial in the design and development of more pharmacologically and behaviorally selective BZD site ligands.

2.7 Acknowledgments

This work was supported by a research grant from Sepracor Inc. to C.C. and NIH grants F32 MH082504 to S.M.H and NS34727 to C.C. E.V.M. is supported by NIH training grant GM008688. We thank Susan Dunn for $GABA_AR$ cDNA constructs and Joseph Esquibel and James Raspanti for technical assistance.

2.8 Supporting Information

pdb files containing eszopiclone and zolpidem docked at the BZD site of the $GABA_AR$ are provided. This material is available free of charge via the Internet at http://pubs.acs.org.

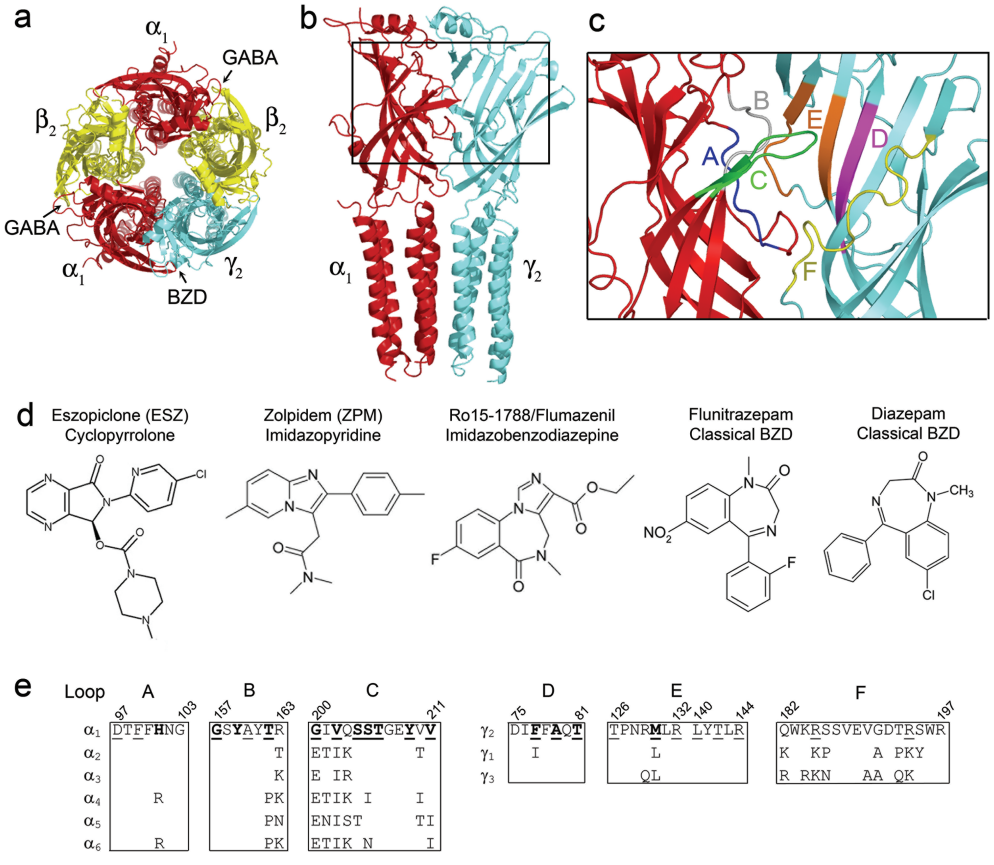
a
α1
GABA
β2
β2
GABA
α1
γ2
BZD
b
α1
γ2
c
A
B
C
D
E
F
d
Eszopiclone (ESZ)
Cyclopyrrolone
Zolpidem (ZPM)
Imidazopyridine
Ro15-1788/Flumazenil
Imidazobenzodiazepine
Flunitrazepam
Classical BZD
Diazepam
Classical BZD
e
Loop A B C D E F
α1 DTFFHNG GSYAYTR GIVQSSTGEYVV
α2 T ETIK T
α3 K E IR
α4 R PK ETIK I I
α5 PN ENIST TI
α6 R PK ETIK N I
γ2 DIFFAQT TPNRMLR LYTLR QWKRSSVEVGDTRSWR
γ1 I L K KP A PKY
γ3 QL R RKN AA QK

Figure 2.1 The $GABA_A$ receptor α_1/γ_2 interface and structures of benzodiazepine binding site ligands. (a) Homology model of the $\alpha_1\beta_2\gamma_2$ $GABA_A$ receptor pentamer (Mercado and Czajkowski, 2006) as seen from the extracellular membrane surface. The α_1, β_2, and γ_2 subunits are highlighted in red, yellow, and blue, respectively. Arrows indicate that GABA binds at the β_2/α_1 interfaces whereas benzodiazepines (BZDs) bind at the α_1/γ_2 interface of the receptor. **(b)** Side view of the α_1 (red) and γ_2 (blue) subunits. The region of the interface encompassing the BZD binding site is boxed and highlighted in **(c)**, where BZD binding site Loops A-F are individually color-coded. **(d)** Structures of the BZD binding site ligands eszopiclone, zolpidem, Ro15-1788, flunitrazepam, and diazepam. **(e)** Rat $GABA_AR$ sequence alignment of Loops A, B, and C of $\alpha_{1\text{-}6}$ subunits and Loops D, E, and F of $\gamma_{1\text{-}3}$ subunits, where only differences from α_1 and γ_2 are shown. Amino acid residues shown previously to be important for BZD binding are bold, residues examined in this study are underlined.

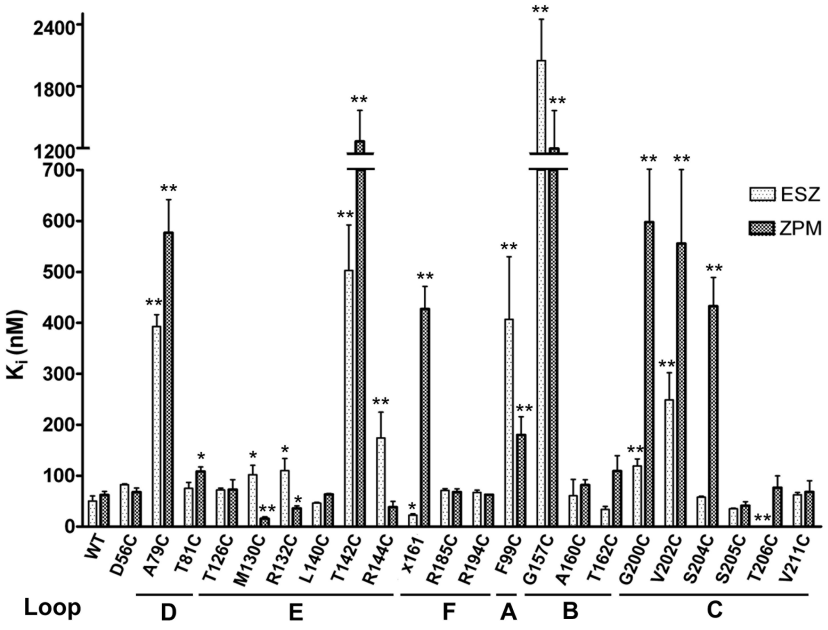
2400
1800
1200
700
600
500
400
300
200
100
0
Ki (nM)
ESZ
ZPM
WT
D56C
A79C
T81C
T126C
M130C
R132C
L140C
T142C
R144C
x161
R185C
R194C
F99C
G157C
A160C
T162C
G200C
V202C
S204C
S205C
T206C
V211C
Loop
D
E
F
A
B
C

Figure 2.2 Cysteine mutations in the benzodiazepine binding site differentially affect eszopiclone and zolpidem affinity for the $GABA_A$ receptor. The apparent affinity (K_i) of WT, γ_2-mutant (Loops D-F) and α_1-mutant (Loops A-C) receptors for ESZ (light bars) and ZPM (dark bars) is graphed and was measured as described in the Methods. x161 is the γ/α chimera where residues N-terminal to 161 are γ_2 sequence and residues C-terminal to 161 are α_1 sequence. Bars represent mean $\pm$ SD of at least three independent experiments. Values significantly different from WT are indicated (*$p<0.05$; **$p<0.01$).

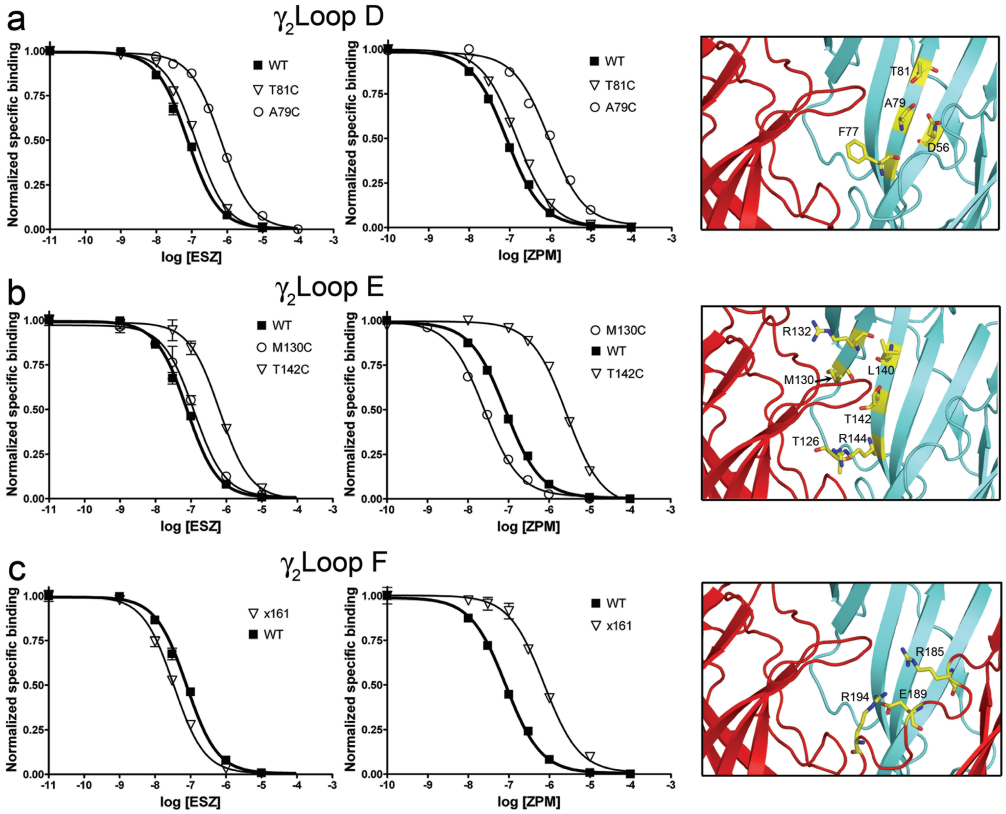
a
γ2Loop D
Normalized specific binding
log [ESZ]
log [ZPM]
WT
T81C
A79C
T81
A79
F77
D56
b
γ2Loop E
WT
M130C
T142C
R132
L140
M130
T142
T126
R144
c
γ2Loop F
x161
WT
R185
R194
E189

Figure 2.3 Mutations in the γ_2 subunit differentially affect eszopiclone and zolpidem binding to the $GABA_A$ receptor. (a-c) Representative radioligand binding curves depict the displacement of [^{3}H] Ro15-1788 binding by ESZ (*left panels*) and ZPM (*middle panels*) for WT $\alpha_1\beta_2\gamma_2$ receptors (filled squares) and the indicated γ_2 mutant receptors (open symbols) in Loop D **(a)**, Loop E **(b)**, and Loop F **(c)**, respectively. Representative binding curves are shown for a selected group of mutants. Each data point is the mean $\pm$ SEM of triplicate measurements. Data were fit by nonlinear regression as described in the Methods and K_i values are reported in Table 2. A close-up view of the benzodiazepine binding site (*right panels*), with the α_1 subunit in red and the γ_2 subunit in blue, highlights all sites where individual cysteine substitutions were introduced (yellow). For x161, residues 1-161 are γ_2 sequence (blue), and residues C-terminal to 161 are α_1 sequence (red). The localization of residues γ_2R185, γ_2E189, and γ_2R194 is based on their position in the WT γ_2 sequence.

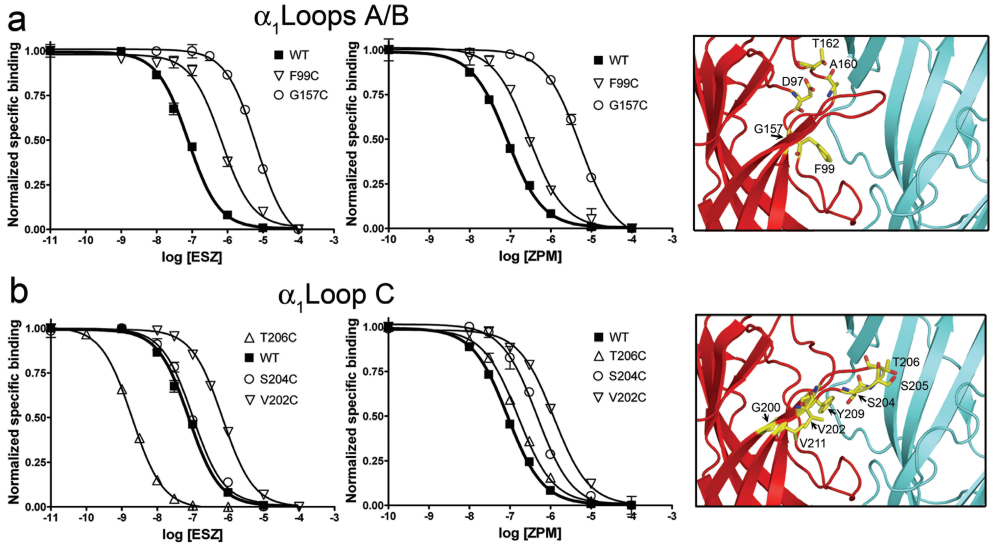
a
α1Loops A/B
Normalized specific binding
log [ESZ]
WT
F99C
G157C
log [ZPM]
T162
A160
D97
G157
F99
b
α1Loop C
T206C
WT
S204C
V202C
T206
S205
S204
G200
Y209
V202
V211

Figure 2.4 Mutations in the α_1 subunit differentially affect eszopiclone and zolpidem binding to the $GABA_A$ receptor. (a-b) Representative radioligand binding curves depict the displacement of [^{3}H] Ro15-1788 binding by ESZ (*left panels*) and ZPM (*middle panels*) for WT $\alpha_1\beta_2\gamma_2$ receptors (filled squares) and the indicated α_1 cysteine mutant receptors (open symbols) in Loops A and B **(a)** and Loop C **(b)**, respectively. Representative binding curves are shown for a selected group of mutants. Each data point is the mean $\pm$ SEM of triplicate measurements. Data were fit by nonlinear regression as described in the Methods and K_i values are reported in Table 2. A close-up view of the benzodiazepine binding site (*right panels*), with the α_1 subunit in red and the γ_2 subunit in blue, highlights all sites where individual cysteine substitutions were introduced (yellow).

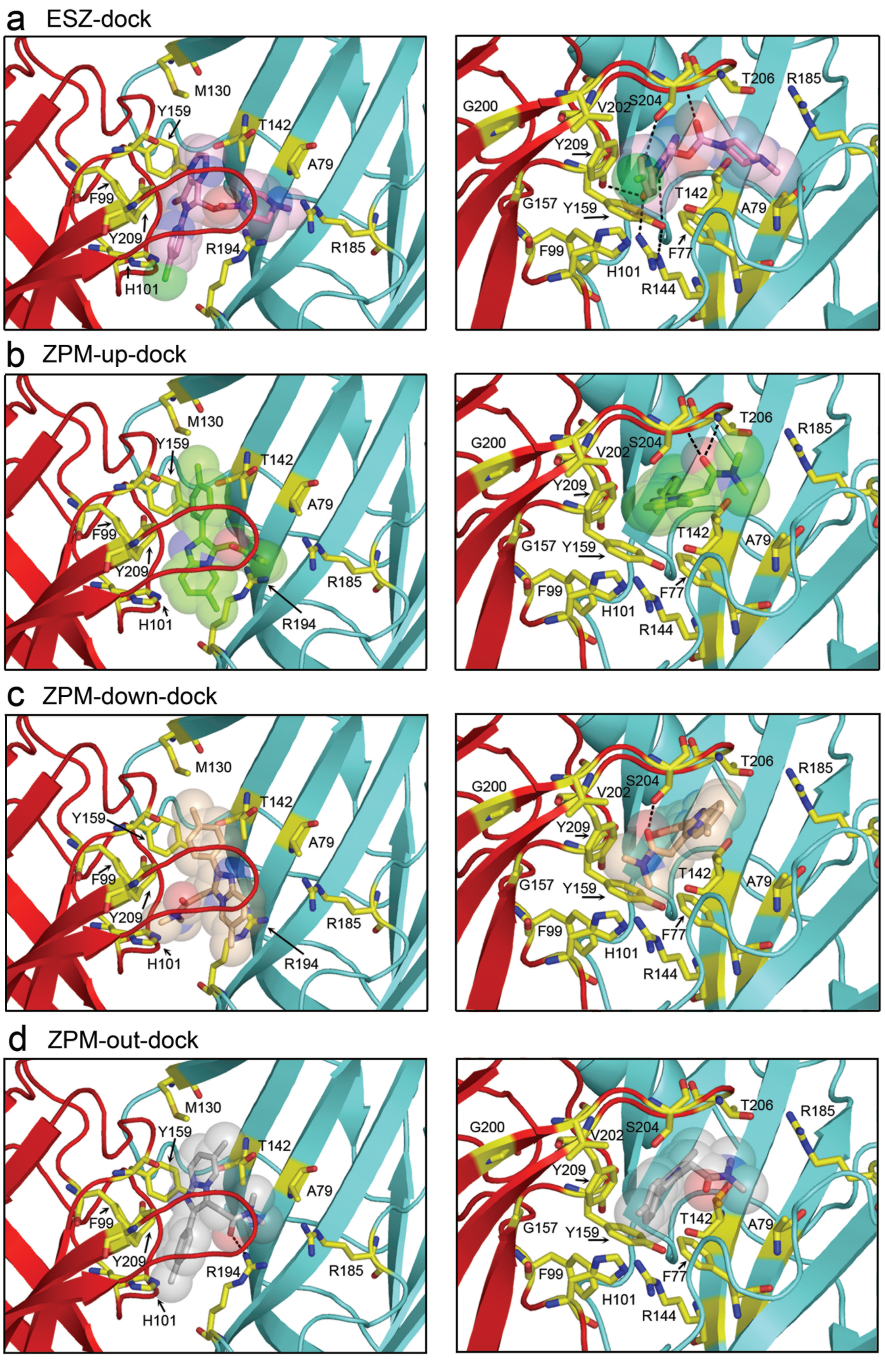
a ESZ-dock
M130
Y159
T142
A79
F99
Y209
R194
R185
H101
G200
V202
S204
T206
R185
Y209
G157
Y159
T142
A79
F99
H101
F77
R144
b ZPM-up-dock
M130
Y159
T142
A79
F99
Y209
R185
H101
R194
G200
V202
S204
T206
R185
Y209
G157
Y159
T142
A79
F99
H101
F77
R144
c ZPM-down-dock
M130
Y159
T142
A79
F99
Y209
R185
H101
R194
G200
V202
S204
T206
R185
Y209
G157
Y159
T142
A79
F99
H101
F77
R144
d ZPM-out-dock
M130
Y159
T142
A79
F99
Y209
R194
R185
H101
G200
V202
S204
T206
R185
Y209
G157
Y159
T142
A79
F99
H101
F77
R144

Figure 2.5 Molecular docking of eszopiclone and zolpidem.

View looking down on α_1Loop C (*left panels*) and underneath α_1Loop C (*right panels*) of **(a)** ESZ and **(b,c,d)** ZPM docked into the benzodiazepine binding site of the $GABA_AR$ using AutoDock 4.0 software as described in the Methods. The α_1 subunit is red, the γ_2 subunit is blue, and residues of interest are highlighted in yellow. Docked ligands are represented as sticks with transparent space-fill. Atoms are color coded as follows: oxygen, red; nitrogen, blue; sulfur, yellow; chloride (ESZ), green. Potential hydrogen bonds are represented by dashed lines. Pdb files containing eszopiclone and zolpidem docked at the BZD site of the $GABA_AR$ are provided in the supplementary material.

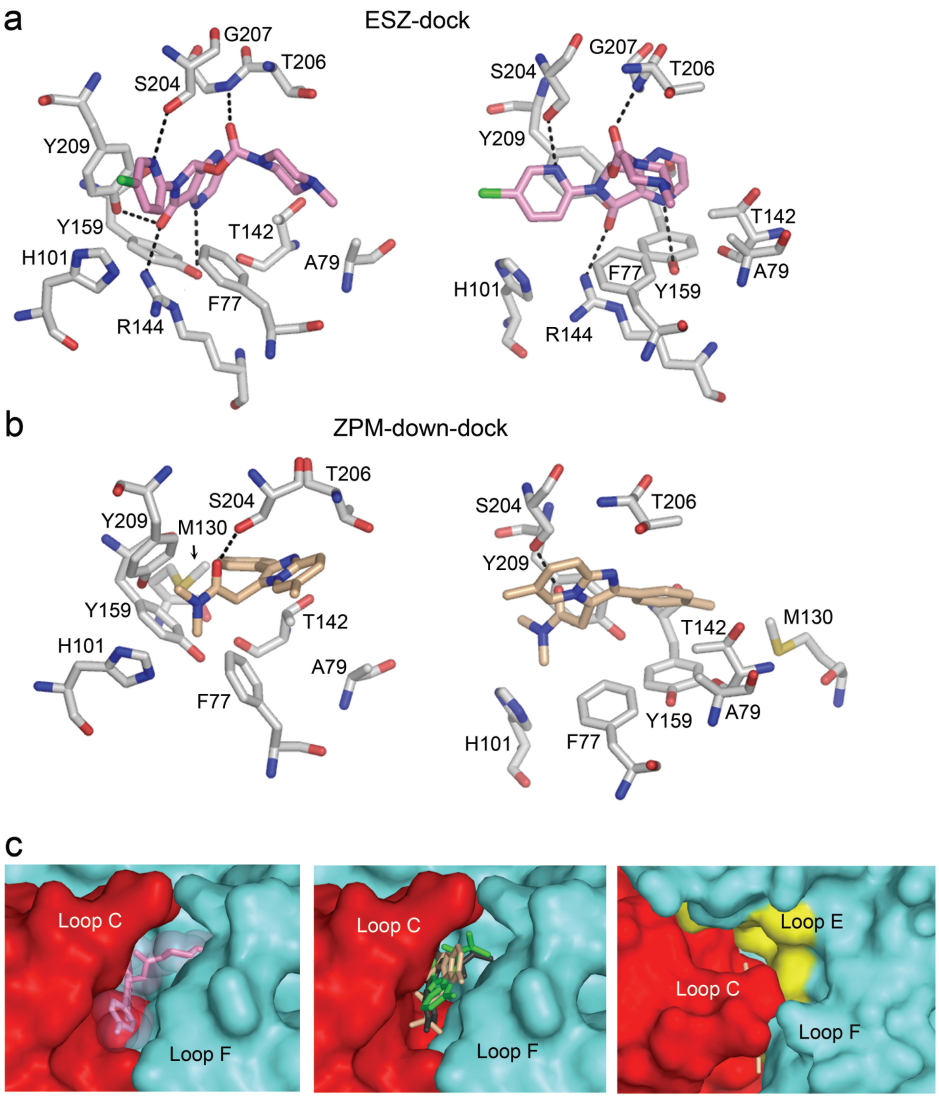
a
ESZ-dock
G207
T206
S204
Y209
Y159
T142
H101
A79
F77
R144
G207
S204
T206
Y209
T142
F77
A79
H101
Y159
R144
b
ZPM-down-dock
T206
S204
Y209
M130
Y159
T142
H101
A79
F77
S204
T206
Y209
T142
M130
Y159
A79
H101
F77
c
Loop C
Loop F
Loop C
Loop F
Loop E
Loop C
Loop F

Figure 2.6 Eszopiclone and zolpidem in the BZD binding pocket.

Two views of ESZ-dock **(a)** and ZPM-down-dock **(b)** showing the relative orientation of ligand and residues of interest in the BZD-site. Potential hydrogen bonds are represented by dashed lines. Atoms are color coded as follows: oxygen, red; nitrogen, blue; sulfur, yellow; chloride (ESZ), green. **(c)** The surface of the α_1 (red) and γ_2 (blue) subunits near the BZD-site is shown to highlight the size of the binding pocket. *Left panel*: ESZ (pink) is represented as sticks with transparent space-fill. *Middle panel*: The three orientations of ZPM (green, tan, gray) are represented as sticks. *Right panel*: Surface view of ZPM-down-dock (tan, sticks) as seen looking down on α_1Loop C. (Note: most of the molecule is occluded by Loop C). The surface of Loop E residues examined in this study is highlighted in yellow. Observe the large unfilled volume of space bordered by Loop E residues.

Table 2.1 Binding affinities of Ro15-1788, Ro15-4513, eszopiclone and zolpidem for $\alpha_x\beta_2\gamma_2$ receptors.

Receptor	Ro15-1788 Ki (nM)	Eszopiclone Ki (nM)	Zolpidem Ki (nM)	Ro15-4513 Ki (nM)
α1	3.3 ± 1.3	50.1 ± 10.1	61.9 ± 7.3	N.D.
α2	5.7 ± 0.1	114 ± 40.8	408 ± 35	N.D.
α3	8.1 ± 0.1	162 ± 29.5	975 ± 132	N.D.
α5	2.0 ± 0.1	102 ± 17.9	>15000	N.D.
α4	N.D.	>15000	>15000	3.1 ± 0.1
α6	N.D.	>15000	>15000	5.1 ± 0.1

K_i values were determined by displacement of [^{3}H] ethyl 8-fluoro-5,6-dihydro-5-methyl-6-oxo-4*H*-imidazo[1,5-*a*][1,4]benzodiazepine-3-carboxylate (Ro15-1788)(Codding and Muir, 1985) binding (for α_1, α_2, α_3, and α_5) or [^{3}H] ethyl-8-azido-5,6-dihydro-5-methyl-6-oxo-4H-imidazo-1,4-benzodiazepine-3-carboxylate (Ro15-4513)(Wong and Skolnick, 1992) binding (for α_4 and α_6) and represent the equilibrium dissociation constant (apparent affinity) of the unlabeled ligand. Data represent mean +/- SD from at least 3 separate experiments; N.D.= not determined.

Table 2.2 Binding affinities of Ro15-1788, eszopiclone and zolpidem for WT and mutant $\alpha_1\beta_2\gamma_2$ receptors.

		Ro15-1788		Eszopiclone		Zolpidem	
Loop	Receptor	Ki (nM)	mut/wt	Ki (nM)	mut/wt	Ki (nM)	mut/wt
	WT	3.3 ± 1.3	1.0	50.1 ± 10.1	1.0	61.9 ± 7.3	1.0
	αβγD56C	3.1 ± 0.2	0.9	82.4 ± 16.1	1.6	67.6 ± 8.0	1.1
D	αβγF77C	N.B.		N.D.		N.D.	
D	αβγA79C	9.2 ± 1.6 *	2.8	393 ± 23.3 **	7.9	577 ± 64.7 **	9.3
D	αβγT81C	4.4 ± 1.4	1.3	75.2 ± 11.6	1.5	108 ± 9.2 *	1.7
E	αβγT126C	4.4 ± 0.3	1.3	71.9 ± 3.5	1.4	72.7 ± 19.2	1.2
E	αβγM130C	13.8 ± 4.7 *	4.1	102 ± 18.4 *	2.0	15.5 ± 3.7 **	0.3
E	αβγR132C	13.0 ± 4.7 *	3.9	110 ± 23.7 *	2.2	35.8 ± 4.8 *	0.6
E	αβγL140C	3.8 ± 0.1	1.2	46.3 ± 1.4	0.9	63.1 ± 1.9	1.0
E	αβγT142C	9.2 ± 2.0 *	2.8	503 ± 89.1 **	10	1321 ± 300 **	21
E	αβγR144C	3.7 ± 1.1	1.1	174 ± 50.6 **	3.5	38.0 ± 11.5	0.6
F	αβχ161	9.6 ± 1.5 *	2.9	22.4 ± 2.6 *	0.4	427 ± 44.8 **	6.9
F	αβγR185C	3.3 ± 0.0	1.0	70.9 ± 3.5	1.4	67.4 ± 6.8	1.1
F	αβγR194C	4.1 ± 0.0	1.2	67.0 ± 4.6	1.3	62.6 ± 0.7	1.0
A	αD97Cβγ	N.B.		N.D.		N.D.	
A	αF99Cβγ	15.0 ± 0.8 **	4.5	407 ± 123 **	8.1	180 ± 35.6 *	2.9
B	αG157Cβγ	0.19 ± 0.06 **	0.06	2103 ± 400 **	42	1252 ± 367 **	20
B	αA160Cβγ	4.0 ± 0.6	1.2	60.4 ± 32.2	1.2	81.4 ± 10.7	1.3
B	αT162Cβγ	2.2 ± 0.1	0.7	33.8 ± 5.6	0.7	109 ± 30.4	1.8
C	αG200Cβγ	3.0 ± 0.3	0.9	119 ± 13.8 **	2.4	598 ± 104 **	9.7
C	αV202Cβγ	1.5 ± 0.1	0.4	249 ± 52.9 **	5.0	556 ± 153 **	9.0
C	αS204Cβγ	8.8 ± 0.6 **	2.7	57.9 ± 1.6	1.2	433 ± 56.4 **	7.0
C	αS205Cβγ	6.5 ± 1.0 *	2.0	34.9 ± 1.1	0.7	41.2 ± 7.6	0.7
C	αT206Cβγ	2.1 ± 0.5	0.6	0.83 ± 0.23 **	0.02	76.4 ± 23.2	1.2
C	αY209Cβγ	N.B.		N.D.		N.D.	
C	αV211Cβγ	4.1 ± 1.4	1.2	62.4 ± 4.4	1.2	67.8 ± 22.2	1.1

K_i values were determined by displacement of [^{3}H] Ro15-1788 binding and represent the equilibrium dissociation constant (apparent affinity) of the unlabeled ligand. The loop where each mutation is located inside the BZD binding pocket is indicated. The ratio of mutant to WT binding is shown and was calculated by dividing the K_i value for the mutant by the K_i value for WT. Data represent mean +/- SD from at least three separate experiments; N.B.= no binding detected; N.D.=not determined. Values significantly different from WT are indicated (* $p<0.05$; ** $p<0.01$).

CHAPTER 3: Different residues in the $GABA_A$ receptor benzodiazepine binding pocket mediate benzodiazepine efficacy and binding[2]

3.1 Abstract

Benzodiazepines (BZDs) exert their therapeutic actions by binding to the γ-aminobutyric acid type A receptor ($GABA_AR$) and allosterically modulating GABA-activated chloride currents (I_{GABA}). A variety of ligands with divergent structures bind to the BZD site and the structural mechanisms that couple their binding to potentiation of I_{GABA} are not well understood. Here, we measured the effects of individually mutating twenty-two residues throughout the BZD binding pocket on the abilities of eszopiclone, zolpidem and flurazepam to potentiate I_{GABA}. Wild-type and mutant $\alpha_1\beta_2\gamma_2$ $GABA_ARs$ were expressed in *Xenopus* oocytes and analyzed using two-electrode voltage clamp. GABA EC_{50}, BZD EC_{50} and BZD maximal potentiation were measured. This data, combined with previous radioligand binding data describing the mutations' effects on BZD apparent binding affinities (Hanson and Czajkowski, 2008, Hanson et al., 2008), were used to distinguish residues within the BZD pocket that contribute to BZD efficacy and BZD binding. We identified six residues whose mutation altered BZD maximal potentiation of I_{GABA} (BZD efficacy) without altering BZD binding apparent affinity, three residues whose mutation altered binding but had no effect on BZD efficacy, and four residues whose mutation affected both binding and efficacy. Moreover, depending on the BZD ligand, the effects

[2] Published as Morlock EV, Czajkowski C (2011) Different residues in the GABAA receptor benzodiazepine binding pocket mediate benzodiazepine efficacy and binding. Mol Pharmacol 80:14-22.

of some mutations were different indicating that the structural mechanisms underlying the ability of BZD ligands with divergent structures to potentiate I_{GABA} are distinct.

3.2 Introduction

Benzodiazepines (BZDs) are commonly used in the treatment of sleep disorders, anxiety, muscle spasms, seizure disorders, and some forms of depression (Mohler et al., 2002). They exert their therapeutic actions by binding to the γ-aminobutyric acid type A receptor ($GABA_AR$) and modulating GABA-induced chloride current (I_{GABA}). The $GABA_AR$ is a heteropentameric, ligand-gated ion channel and belongs to the cys-loop superfamily of receptors that includes the $5HT_3$ receptor, glycine receptor and nicotinic acetylcholine receptor (nAChR) (Ortells and Lunt, 1995). The most common $GABA_A$ receptor subtype found in the brain is comprised of α_1, β_2, and γ_2 subunits in a ratio of 2α:2β:γ (Chang et al., 1996, Farrar et al., 1999, Baumann et al., 2002, Sieghart and Sperk, 2002). The BZD binding site is located in the extracellular domain of the receptor at the interface of the α and γ subunits (Fig. 3.1A), and is formed by six noncontiguous regions historically designated loops A-F (Fig. 3.1B) (Sigel and Buhr, 1997, Boileau et al., 1998, Boileau et al., 2002a).

Ligands that bind to the BZD site can act as negative modulators that inhibit I_{GABA} (BZD inverse agonists), as positive modulators that potentiate I_{GABA} (BZD agonists) or as zero modulators that bind yet have no effect on I_{GABA} (BZD antagonists). While multiple studies have identified residues that are involved in mediating the apparent binding affinity (K_d) of BZD-site ligands including classical, [1,4]benzodiazepines (Wieland and Luddens, 1994, Kucken et al., 2000, Boileau et al., 2002a, Derry et al., 2004), cyclopyrrolones (e.g. eszopiclone) (Davies et al., 2000, Hanson and Czajkowski, 2008)

and imidazopyridines (e.g. zolpidem) (Buhr et al., 1996, Buhr et al., 1997b, Buhr and Sigel, 1997, Schaerer et al., 1998, Hanson et al., 2008), much less is known about the structural determinants that couple their binding to modulation of I_{GABA} and govern whether a BZD-site ligand is a positive modulator, zero modulator or negative modulator (i.e. BZD efficacy).

In general, it is believed that BZDs exert their allosteric effects by either shifting the $GABA_AR$ closed to open state channel equilibrium (Downing et al., 2005, Rusch and Forman, 2005, Campo-Soria et al., 2006) or by altering the receptor's microscopic binding affinity for GABA (Twyman et al., 1989, Rogers et al., 1994b, Lavoie and Twyman, 1996, Mellor and Randall, 1997, Thompson et al., 1999, Goldschen-Ohm et al., 2010). Regardless of the mechanism, BZD binding to the receptor is the initial perturbation that triggers structural rearrangements in the protein that result in modulation of $GABA_AR$ function. Residues that line the BZD binding site pocket likely have different roles in this process. Some residues may directly interact with the ligand and contribute to its binding affinity, some may stabilize binding site structure, whereas others may mediate local conformational movements important for coupling BZD binding to modulation of I_{GABA}. Identifying the residues that are involved in these actions is critical for elucidating the structural mechanisms that govern the pharmacological effects of these drugs and will help predict the therapeutic effects of new drugs.

Previously, we identified residues within the BZD binding site that were important for high-affinity binding of flumazenil (Ro15-1788), eszopiclone (ESZ) and zolpidem (ZPM) (Hanson and Czajkowski, 2008, Hanson et al., 2008). Here, we tested

the hypothesis that residues in the BZD binding site are also crucial for determining BZD efficacy. We measured the effects that 22 single cysteine mutations (Fig. 3.1D), made throughout the BZD binding site, had on the abilities of flurazepam (FZM), ESZ and ZPM to potentiate I_{GABA} (BZD EC_{50} values and maximum potentiations were measured). We focused on residues that have not been extensively examined previously and for which the effects of mutating the residue on BZD apparent binding affinities were known. We identified six residues whose mutation solely altered BZD efficacy suggesting that they are part of the allosteric pathway involved in coupling BZD binding to modulation of $GABA_AR$ function. We identified three residues that when mutated only altered BZD binding affinity suggesting that they are important for ligand docking. Four additional residues, in the α subunit, when mutated, decreased both the binding affinity and efficacy of the BZD ligands suggesting that they play roles in mediating high affinity BZD binding and the initial structural rearrangements in the site that help couple binding to modulation of I_{GABA} and likely contribute to the structural integrity of the binding site. Moreover, we provide evidence that the structural mechanisms underlying the ability of BZD ligands of diverse structure to modulate I_{GABA} are distinct.

3.3 Materials and Methods

3.3.1 Site directed mutagenesis.

Rat cDNAs encoding the GABAR α_1, β_2 and γ_{2L} subunits in the pUNIV vector (Venkatachalan et al., 2007) were used. Cysteine mutations in the α_1 and γ_{2L} subunits were made previously (Hanson and Czajkowski, 2008, Hanson et al., 2008) using recombinant PCR and verified by double stranded DNA sequencing.

3.3.2 Expression in *Xenopus laevis* oocytes.

Expression of WT and mutant GABARs was performed as described previously (Hanson and Czajkowski, 2008). Capped cRNA from *Not*I- digested cDNA was *in vitro* transcribed using the mMessage mMachine T7 kit (Ambion, Austin, TX). *X. Laevis* oocytes were harvested and prepared as described previously (Boileau et al., 1998). Oocytes were injected within 24h of treatment with 27nl cRNA (1-15pg/nl/subunit) in the ratio 1:1:10 (α:β:γ) (Boileau et al., 2002a) and stored at 16ºC in ND96 buffer (in mM: 96 NaCl, 2KCl, 1$MgCl_2$, 1.8$CaCl_2$, 5 HEPES, pH 7.2) supplemented with 100μg/ml BSA until used for electrophysiological recordings.

3.3.3 Two-electrode voltage clamp.

Electrophysiological recordings were performed as described previously (Hanson and Czajkowski, 2008). Oocytes were held at –80mV under two-electrode voltage clamp while being continuously perfused with ND96 at a rate of 5ml/min in a bath volume of 200μl. Borosilicate glass electrodes (0.4-1.0 mΩ) (Warner Instruments, Hamden, CT) were filled with 3M KCl. Electrophysiological data were collected using GeneClamp 500 (Molecular Devices, Sunnyvale, CA) interfaced to a computer with a Digidata 1200 A.D device (Molecular Devices). Recordings were made using the Whole Cell Program, v.3.6.7 (kindly provided by J. Dempster, University of Strathclyde, Glasgow, UK). Stock solutions of FZM (RBI, Natick, MA*)* were dissolved in ND96 and diluted in ND96 for working concentrations. GABA (Sigma, St. Louis, MO) solutions were prepared fresh daily with ND96. Stock solutions of DMCM (3-carbomethoxy-4-ethyl-6,7-dimethoxy-β-carboline) (RBI, Natick, MA), ZPM (Sigma, St. Louis, MO) and ESZ (kindly provided by Sepracor, Inc.) were prepared in DMSO and subsequently diluted in ND96 for

working concentrations where the final [DMSO] (≤ 2%) did not affect $GABA_AR$ function.

3.3.4 Concentration-response analysis.

GABA concentration-response curves were determined as described previously (Hanson and Czajkowski, 2008). Six to twelve concentrations of GABA were used for each GABA EC_{50} value determination. Each current response was scaled to a low, non-desensitizing concentration of GABA (EC_{1-5}) applied just before the test concentration to correct for any drift in I_{GABA} responsiveness over the course of the experiment. Concentration-response data were fit by the following equation: $I = I_{max}/[1+EC_{50}/[A]^n)]$, where I is the peak response to a given drug concentration, I_{max} is the maximum amplitude of current, EC_{50} is the drug concentration that produces that half-maximal response, [A] is drug concentration, and n is the Hill coefficient using Prism V.4.0 (GraphPad Software, San Diego, CA). The EC_{50} values in Table 1 for four mutants (γR185C, γE189C, γR194C and γR197C) are from Hanson and Czajkowski, 2008 with the associated errors in SEM, as opposed to SD reported in the 2008 publication. Two values that were significantly different from wild-type (WT) values in the 2008 publication (γR185C and γR194C) are no longer significant in the present study because the GABA EC_{50} value for WT receptors in this study is slightly lower than in the previous report and the full data sets that was used for the ANOVAs in both studies are different.

BZD concentration responses (6-8 different concentrations) were measured at GABA EC_{15}. BZD modulation was defined as follows: $[(I_{GABA+BZD}/I_{GABA})-1]$, where $I_{GABA+BZD}$ is the current response in the presence of GABA and BZD, and I_{GABA} is the

current evoked by GABA alone (GABA EC_{15}). When measuring BZD concentration responses, each application of GABA + BZD is preceded by a brief pulse of EC_{15} GABA alone. Wash times between application of GABA + BZD and the following application of GABA alone were increased with every increase in BZD concentration. During the experiment, the magnitude of the currents elicited by the GABA EC_{15} pulses alone did not change (< 3%) even following high concentrations of BZD, indicating complete washout of the BZDs. BZD concentration response curves were fit with the equation $P = P_{max} /(1+(EC_{50} /A)^n)$, where A is the BZD concentration, EC_{50} is the concentration of BZD eliciting half maximal current potentiation, P_{max} is the maximal BZD potentiation of I_{GABA}, P is the potentiation amplitude and n the Hill coefficient. The reported values for maximum potentiation were determined from curve fitting the data.

3.3.5 Statistical analysis.

All data are from at least three different oocytes from at least two different frogs. Data represent mean ± SEM. Significant differences in EC_{50} values and maximal BZD modulation values were determined by one-way ANOVA, followed by a post hoc Dunnett's test using Prism v.4.0 (GraphPad Software Inc., San Diego, CA). Log (EC_{50}) values were used for statistical analyses.

3.4 Results

We previously made 22 single cysteine mutations throughout the BZD binding site in loops A (D97C, F99C), B (G157C, A160C, T162C), and C (G200C, V202C, S204C, S205C, T206C, Y209C, V211C) of the α_1 subunit and loops E (T126C, M130C, R132C, L140C, T142C, R144C) and F (R185C, E189C, R194C, R197C) of the γ_2

subunit (Fig. 3.1) and examined the effects of these mutations on BZD binding using competitive radioligand binding experiments (see Table 2 for mut/WT K_i values) (Hanson and Czajkowski, 2008, Hanson et al., 2008). The mutations in the γ Loop F region had no effect on BZD apparent binding affinity, whereas at least one mutation in each of the α loops A and B and γ loop D altered the affinities of all of the ligands tested (Ro15-1788, ZPM and ESZ) suggesting that these regions are critical for the binding of a variety of structurally-diverse BZD-site ligands (Hanson et al., 2008). In contrast, a number of the mutations in α loop C and γ loop E altered the binding of some BZDs but not others suggesting that residues in these regions help define BZD selectivity (Hanson et al., 2008). Here, we tested the hypothesis that residues in the BZD binding site are not only important for BZD binding but also play a role in defining BZD efficacy. Cysteine mutant subunits were co-expressed with wild type (WT) subunits in *Xenopus laevis* oocytes to form $\alpha_1\beta_2\gamma_2$ $GABA_A$ receptors and analyzed using two-electrode voltage clamp. We examined the effects the mutations had on GABA-activated currents (I_{GABA}) and on FZM, ESZ and ZPM modulation of EC_{15} I_{GABA}.

3.4.1 Effects of cysteine substitutions on I_{GABA}

All of the mutant subunits assembled into functional $GABA_A$Rs (Table 1). Seven out of the twelve cysteine substitutions in the α_1 subunit significantly increased GABA EC_{50} values (13-31 fold) as compared to WT receptors (18.1± 4.4μM; Table 1). In general, the mutations in the γ_2 subunit had smaller effects. γT126C and γM130C increased GABA EC_{50} approximately 3-fold, whereas γR144C decreased GABA EC_{50} 6-fold compared to WT receptors (Table 1).

3.4.2 Effects of cysteine substitutions on FZM modulation of I_{GABA}

We measured the effects the mutations had on the abilities of three structurally different BZD-site positive modulators, FZM (1,4 benzodiazepine), ESZ (cyclopyrrolone) and ZPM (imidazopyridine) to potentiate GABA (EC_{15}) currents. Current traces and dose response curves for BZD potentiation of I_{GABA} are depicted in Figures 3.2 and 3.3, respectively. At saturating BZD concentrations (i.e. when the BZD binding site is fully occupied), the effects of the mutations on BZD efficacy are being monitored. Eight out of the 22 mutations significantly decreased FZM maximal potentiation of I_{GABA} compared to WT receptors (pot = 2.3 ± 0.2; Fig. 3.4, Table 3.2). In the α_1 subunit, cysteine substitution of D97 and F99 in loop A; G157 and A160 in loop B; and Y209 in loop C significantly decreased FZM maximal potentiation. In the γ_2 subunit, cysteine substitution of T142 and R144 in loop E, and R197 in loop F also significantly decreased FZM maximal potentiation. Note, that αF99C and γR144C almost completely eliminated FZM potentiation of I_{GABA} and thus FZM EC_{50} values could not be determined.

3.4.3 Effects of cysteine substitutions on ESZ modulation of I_{GABA}

The effects of the mutations on ESZ were also measured. Eight of the 22 mutations altered ESZ max potentiation of I_{GABA} as compared to WT receptors (pot = 2.8 ± 0.3) (Figs. 3.2, 3.3, 3.4; Table 3.2). In the α_1 subunit, D97C in loop A; G157C and A160C in loop B; and T206C and Y209C in loop C significantly decreased ESZ maximal potentiation. ESZ inhibited I_{GABA} and became a negative modulator at αF99C containing receptors (Figs. 3.2B, 3.3B). As reported in Hanson et al. (2008), the specific binding of [^{3}H]Ro15-1788, [^{3}H]flunitrazepam or [^{3}H]Ro15-4513 to alpha D97C- and Y209C-mutant receptors was not detectable using a filtration-based radioligand binding assay (Table 2).

The inability to detect radioligand binding is likely due to inherent limitations of filtration binding assays, which preclude measuring binding when the affinity of the radioligand is much above 100nM. Given that we can measure BZD modulation of I_{GABA} for these mutant receptors, these drugs bind to the mutant receptors, likely with lower apparent affinity. The rightward shifts in the BZD concentration responses are consistent with this idea. In the γ_2 subunit, mutations at R144 in loop E and R197 in loop F significantly reduced ESZ maximal potentiation. While αA160C significantly reduced ESZ potentiation of I_{GABA} (i.e. ESZ efficacy), this mutation had little to no effect on ESZ apparent binding affinity (K_i, Table 2).

3.4.4 Effects of cysteine substitutions on ZPM modulation of I_{GABA}

The effects of the mutations on ZPM modulation of I_{GABA} were also examined. Nine out of the 22 mutations altered ZPM max potentiation of I_{GABA} (Figs 3.2, 3.3, 3.4, Table 3.2). αF99C in loop A, αG157C and αA160C in loop B, αT206C and αY209C in loop C, γR144C in loop E, and γR197C in loop F significantly decreased ZPM potentiation when compared to WT receptors (pot = 2.8 ± 0.3). Interestingly, αV211C (loop C) and γE189C (loop F) significantly increased ZPM potentiation of I_{GABA} (1.8 and 2.3 fold, respectively; Figs. 3.3C and 3.4C). Previously, we reported that γE189C had no effect on ZPM potentiation (Hanson and Czajkowski, 2008, Hanson et al., 2008). The differences in results are likely due to using higher concentrations of ZPM used in this study. While αA160C, αT206C, αV211C, γR144C, γE189C and γR197C significantly altered ZPM potentiation of I_{GABA} (efficacy), the mutations had little to no effect on ZPM apparent binding affinity (K_i, Table 2).

3.4.5 Effects of cysteine substitutions on DMCM modulation of I_{GABA}

For a subset of mutations (αF99C, αG157C, αA160C, αT206C, αY209C and γR144C), we also examined the ability of DMCM (3-carbomethoxy-4-ethyl-6,7-dimethoxy-β-carboline) to inhibit GABA (EC_{15}) currents. DMCM is a BZD site inverse agonist. None of the mutations tested significantly altered DMCM inhibition of I_{GABA} (WT, DMCM inh = 0.55 ± 0.04, n = 3, Fig. 3.5) indicating that the effects of the mutations on BZD positive modulator actions are specific. DMCM inhibition of one mutant, γR144C, was decreased compared to WT but this did not reach significance. Since only γ-containing $GABA_A$Rs are modulated by DMCM, the near WT inhibition of I_{GABA} by DMCM also indicates that the mutations do not impair subunit assembly or incorporation into functional αβγ $GABA_A$Rs.

3.4.6 Changes in BZD modulation of I_{GABA} are not correlated to changes in GABA EC_{50}

Some mutations caused significant changes in GABA EC_{50} raising the possibility that the changes in BZD potentiation observed are linked to the GABA EC_{50} alterations. BZD positive modulators enhance $GABA_A$R current by decreasing GABA EC_{50} and shifting the GABA dose response curve to the left. If a mutation only shifted the GABA dose response curve to the right, one would expect that the mutation would increase FZM, ESZ and ZPM potentiation and that inhibition by a negative modulator, such as DMCM, would decrease if a fixed GABA concentration was being used to elicit the responses. In our experiments, BZD modulation of I_{GABA} was measured at the same effective GABA concentration (EC_{15}) for each of the mutant and wild-type receptors, which should mitigate GABA EC_{50} effects on BZD modulation. Moreover, for many of the mutations, their effects on GABA EC_{50} and BZD potentiation were not correlated

(Fig. 3.6). Some mutations significantly altered BZD potentiation without affecting GABA EC_{50} (γT142, γE189 and γR197) whereas others affected GABA EC_{50} without changing BZD potentiation (γT126C, γM130C, αS205C, αV211C). Additionally, while the αF99C, αAG157C, αA160C, αT06C, αY209C, γR144C mutations altered GABA EC_{50}, inhibition of I_{GABA} by DMCM was not significantly altered (Fig. 3.5). Taken together, these data indicate that the observed changes in GABA EC_{50} are not causative for the observed alterations in the efficacies of BZD site positive modulators (Fig. 3.4).

3.5 Discussion

We identified four residues in the BZD binding pocket that specifically contribute to BZD-site agonist efficacy: in loop B, A160; in loop C, T206; in loop E, R144; and in loop F, R197 (Fig. 3.7, Top row). Mutating these residues significantly disrupted the abilities of ZPM, ESZ and FZM to potentiate I_{GABA} but had little to no effect on high affinity binding (Table 3.2) (Hanson et al., 2008). Consistent with the mutations having little effect on binding, these residues are largely localized at the periphery of the binding pocket (Fig. 3.7C) and thus, are in an ideal position to propagate local movements in the BZD binding pocket outward to more distant regions of the protein involved in modulating I_{GABA}. We also identified two residues (αV211 and γE189) that when mutated significantly increased ZPM potentiation of I_{GABA} without affecting FZM or ESZ potentiation indicating that the residues involved in coupling high affinity BZD binding to potentiation of I_{GABA} can be different depending upon the type of BZD-site ligand bound. This is consistent with our previous data, where we demonstrated that structural determinants for high affinity binding of ESZ and ZPM are different (Hanson and

Czajkowski, 2008, Hanson et al., 2008). One can envision that depending on the orientation of the BZD in the binding pocket and its contact residues that some of the residues involved in the initial coupling of binding to potentiation of I_{GABA} may differ. ZPM binding is largely dependent on shape recognition and *in silico* docking has revealed that ZPM can adopt multiple orientations in the site (Hanson et al., 2008). Mutating γE189 or αV211 may cause ZPM to preferentially adopt a position that has a higher efficacy.

We also identified three residues (αG200, γM130 and γR132) that specifically mediate high affinity BZD agonist binding. In contrast to the residues discussed above, mutating these residues had no significant effects on BZD agonist efficacy but significantly altered their binding (Fig. 3.7, middle row). Consistent with the mutations affecting binding and not efficacy, αG200, γM130 and γR132 are located on β strands (Fig. 3.7F) that line the core of the BZD binding pocket. Previous mutagenesis studies have demonstrated the importance of αG200 and γM130 in BZD binding. The glycine at position 200 is only found in the $GABA_AR$ α_1 subunit isoform, $\alpha_{2\text{-}6}$ subunits have a glutamate at aligned positions (Fig. 3.1D). Schaerer et al. showed that replacing α_1G200 with glutamate decreases ZPM binding affinity (Schaerer et al., 1998). Mutating α_6E200 to its α_1 counterpart in a background of 3 other point mutations confers ZPM binding to the BZD insensitive α_6 subunit (Wieland and Luddens, 1994). Mutating γ_2M130 to a variety of different residues also alters ZPM binding (Buhr and Sigel, 1997) and replacement of the aligned lysine in the γ_1 subunit (Fig. 3.1D) with a methionine increases the binding affinity of a variety of classical BZDs (Wingrove et al., 1997).

Here, we also identified residues that are important for both high affinity BZD agonist binding and BZD efficacy: αD97and αF99 in loop A, αG157 in loop B and αY209 in loop C. Introducing cysteines at these positions decreased ZPM and ESZ binding and decreased the efficacy of FZM, ZPM and ESZ potentiation of I_{GABA} (Fig. 3.7, bottom row, Table 3.2). The binding of ZPM and ESZ to αD97C and αY209C containing receptors was so disrupted, their binding affinities could not be reliably measured (Hanson et al., 2008). These residues are located in the back of the BZD binding pocket in loop A (D97 and F99), the side of the pocket in loop B (G157) and at the base of loop C facing directly into the binding site (Y209) (Fig. 3.7I). αD97and αF99 in loop A are located near αH101. αH101 has been previously shown to be important for binding of ZPM (Wieland et al., 1992, Wieland and Luddens, 1994), zopiclone (the racemate of ESZ) (Davies et al., 1998), flunitrazepam (Berezhnoy et al., 2004), and diazepam (Davies et al., 2000, Berezhnoy et al., 2004). Mutation of αH101 to arginine has also been shown to alter BZD efficacy (Benson et al., 1998). Previous studies have also identified αG157 in loop B and αY209 in loop C as important determinants for BZD binding (Amin et al., 1997, Tan et al., 2007b)**.** Interestingly, all of the residues we have identified that are important for both high affinity BZD agonist binding and BZD efficacy are located in the α subunit and are conserved in all α subunit isoforms (Fig. 3.1D). Residues in the α subunit are likely to play critical roles in BZD efficacy since a single α subunit contributes to forming both a GABA and BZD binding site at the β-α and α-γ interfaces, respectively. Thus, BZD induced movements may be directly propagated through the α subunit from the BZD site to the GABA binding site. Previous studies

have demonstrated that BZDs cause movements at the GABA binding site interface (Kloda and Czajkowski, 2007).

Interestingly, mutating αF99 to cysteine caused ESZ to switch from a potent positive modulator to a negative modulator (Fig. 3.2B) and had similar effects on the BZD agonist diazepam, making it a weak negative modulator (Tan et al., 2007a). It is not unprecedented that a single mutation can alter a BZD's action from enhancement to inhibition of I_{GABA}. The γT142S mutation, as well as mutations of αH101, cause the inverse agonist Ro15-4513 and the antagonist flumazenil to become BZD agonists and potentiate I_{GABA} (Mihic et al., 1994, Benson et al., 1998). How these mutations result in switches in a BZD's actions is not clear. Many structurally diverse ligands bind to the BZD binding site indicating the site can accommodate a variety of ligands. We speculate that the mutations may alter the positioning of the drug in the site and/or positioning of nearby residues, which then induces different downstream allosteric rearrangements.

Previously, we identified residues and regions in the γ_2 subunit, outside of the BZD binding pocket, that were critical for coupling BZD agonist binding to potentiation of I_{GABA} actions but were not involved in coupling DMCM binding to inhibition of I_{GABA} (Boileau and Czajkowski, 1999, Kloda and Czajkowski, 2007, Hanson and Czajkowski, 2008). Here, none of the mutations we tested significantly altered the inhibitory abilities of DMCM (Fig. 3.5) demonstrating, even at the level of the BZD binding site, that the structural mechanisms underlying the coupling of DMCM binding to inhibition of I_{GABA} are different than those underlying BZD agonist modulation.

The benzodiazepine (BZD) binding site of the $GABA_A$ receptor is pharmacologically complex. Structurally diverse ligands can bind to it and elicit a range

of actions from potentiation of I_{GABA} to inhibition. Residues that line the BZD binding site pocket likely play different roles in mediating these actions. Here, we have identified specific residues that contribute to BZD binding affinity, other residues that contribute to BZD efficacy and others that mediate both binding and efficacy. Moreover, we show that local structural elements important for coupling BZD binding to modulation I_{GABA} are not only different for BZD positive modulators versus negative modulators but are also different for structurally diverse BZD positive modulators indicating that, at the level of the binding site, there is not a single common set of BZD induced movements that underlies BZD positive modulation. We envision that depending on how a BZD occupies the site (e.g. the orientation of the BZD in the site and its interactions with the receptor), its binding elicits distinct motions within the site, which then can induce different downstream allosteric rearrangements. It has been demonstrated for G-protein coupled receptors that even structurally similar agonists interacting with the same orthosteric site can bind to and activate the receptor via different structural mechanisms. (Ghanouni et al., 2001, Swaminath et al., 2004, Swaminath et al., 2005). In summary, the data in this study provide substantial new insights into the structural determinants important for BZD allosteric modulation of $GABA_A$ receptor function. Our results, which identify residues within the BZD binding site that encode BZD efficacy versus affinity, will aid in the design of more efficacious and selective drugs.

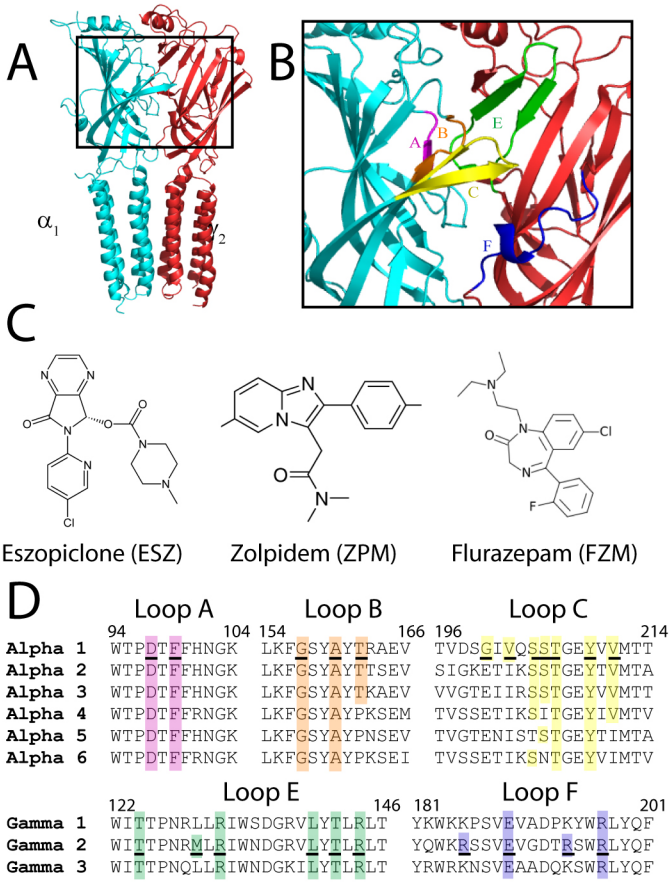
A
B
C
D
α1
γ2
A
B
C
E
F
Eszopiclone (ESZ)
Zolpidem (ZPM)
Flurazepam (FZM)
Loop A
Loop B
Loop C
Loop E
Loop F
94
104
154
166
196
214
122
146
181
201
Alpha 1 WTPDTFFHNGK LKFGSYAYTRAEV TVDSGIVQSSTGEYVVMTT
Alpha 2 WTPDTFFHNGK LKFGSYAYTTSEV SIGKETIKSSTGEYTVMTA
Alpha 3 WTPDTFFHNGK LKFGSYAYTKAEV VVGTEIIRSSTGEYVVMTT
Alpha 4 WTPDTFFRNGK LKFGSYAYPKSEM TVSSETIKSITGEYIVMTV
Alpha 5 WTPDTFFHNGK LKFGSYAYPNSEV TVGTENISTSTGEYTIMTA
Alpha 6 WTPDTFFRNGK LKFGSYAYPKSEI TVSSETIKSNTGEYVIMTV
Gamma 1 WITTPNRLLRIWSDGRVLYTLRLT YKWKKPSVEVADPKYWRLYQF
Gamma 2 WITTPNRMLRIWNDGRVLYTLRLT YQWKRSSVEVGDTRSWRLYQF
Gamma 3 WITTPNQLLRIWNDGKILYTLRLT YRWRKNSVEAADQKSWRLYQF

Figure 3.1 The BZD binding site at the α_1/γ_2 interface of the $GABA_AR$ and structures of BZD site ligands. (A) Homology model of the α_1/γ_2 interface perpendicular to the plane of the membrane. The α_1 subunit is in blue and the γ_2 subunit is in red. (B) The region of the α_1/γ_2 interface that contains the BZD binding site is expanded and BZD binding site loop regions A-F are each highlighted in a different color. (C) Structures of BZD ligands ESZ, ZPM and FZM. (D) Sequence alignments of the extracellular domain of $\alpha_{1\text{-}6}$ and $\gamma_{1\text{-}3}$ rat $GABA_AR$ subunit isoforms with BZD binding site loops are shown. Loop regions are colored as in (B). Residues mutated in this study are underlined and residues highlighted in color are identical. Numbering refers to α_1 and γ_2 residues.

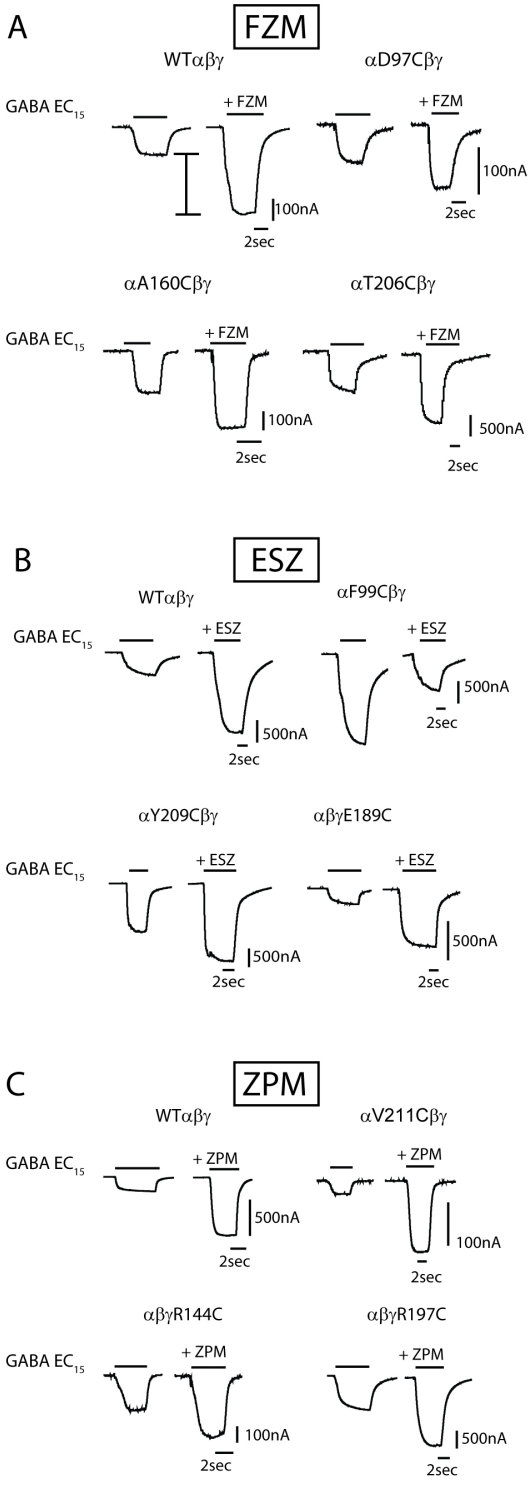
A
FZM
WTαβγ
αD97Cβγ
GABA EC15
+ FZM
100nA
2sec
αA160Cβγ
αT206Cβγ
500nA
B
ESZ
WTαβγ
αF99Cβγ
+ ESZ
500nA
2sec
αY209Cβγ
αβγE189C
C
ZPM
WTαβγ
αV211Cβγ
+ ZPM
αβγR144C
αβγR197C

Figure 3.2 Effects of the mutations on BZD maximal potentiation. Representative current traces showing maximal potentiation of GABA EC_{15} current from oocytes expressing WT and mutant receptors by (A) FZM, (B) ESZ or (C) ZPM. In all cases, BZDs were at concentrations that elicited maximal responses. I bar in panel A indicates potentiation of I_{GABA}. Note, in panel B, for αF99Cβγ receptors, ESZ inhibited I_{GABA}.

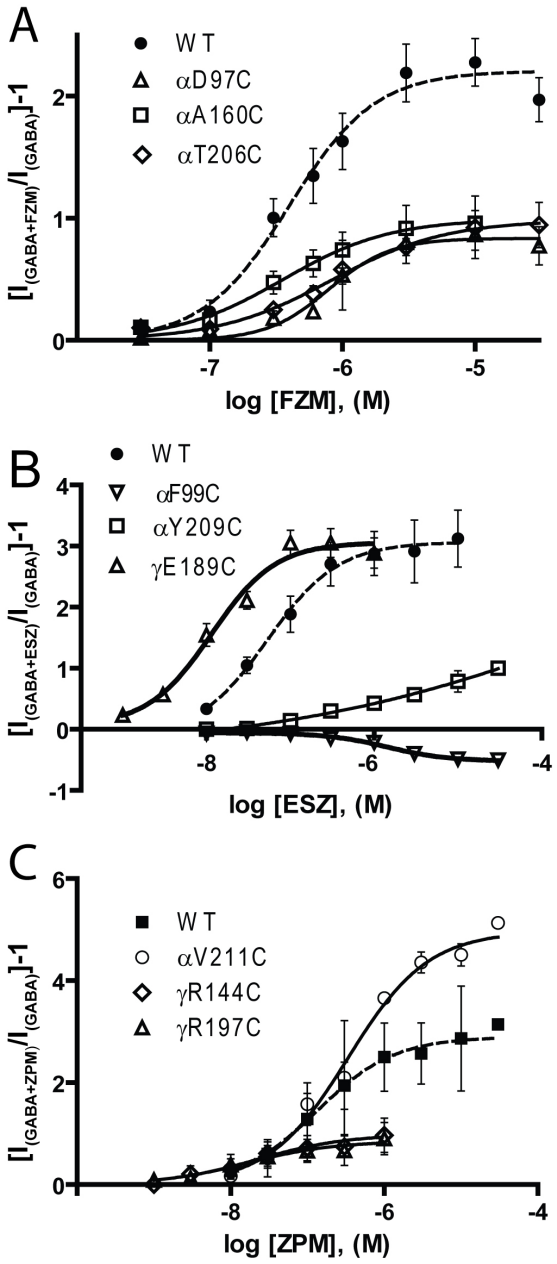
A
WT
αD97C
αA160C
αT206C
[I(GABA+FZM)/I(GABA)]-1
log [FZM], (M)
B
WT
αF99C
αY209C
γE189C
[I(GABA+ESZ)/I(GABA)]-1
log [ESZ], (M)
C
WT
αV211C
γR144C
γR197C
[I(GABA+ZPM)/I(GABA)]-1
log [ZPM], (M)

Figure 3.3 BZD concentration response curves from WT and mutant $GABA_ARs$ for (A) FZM, (B) ESZ and (C) ZPM. BZD potentiation was calculated as $[(I_{GABA+BZD}/I_{GABA})-1]$. Data represent mean ± SEM. Data were fit by nonlinear regression as described in Materials and Methods. Dashed lines are curve fits from WT receptors. BZD EC_{50} values and BZD maximal potentiation values are reported in Table 2.

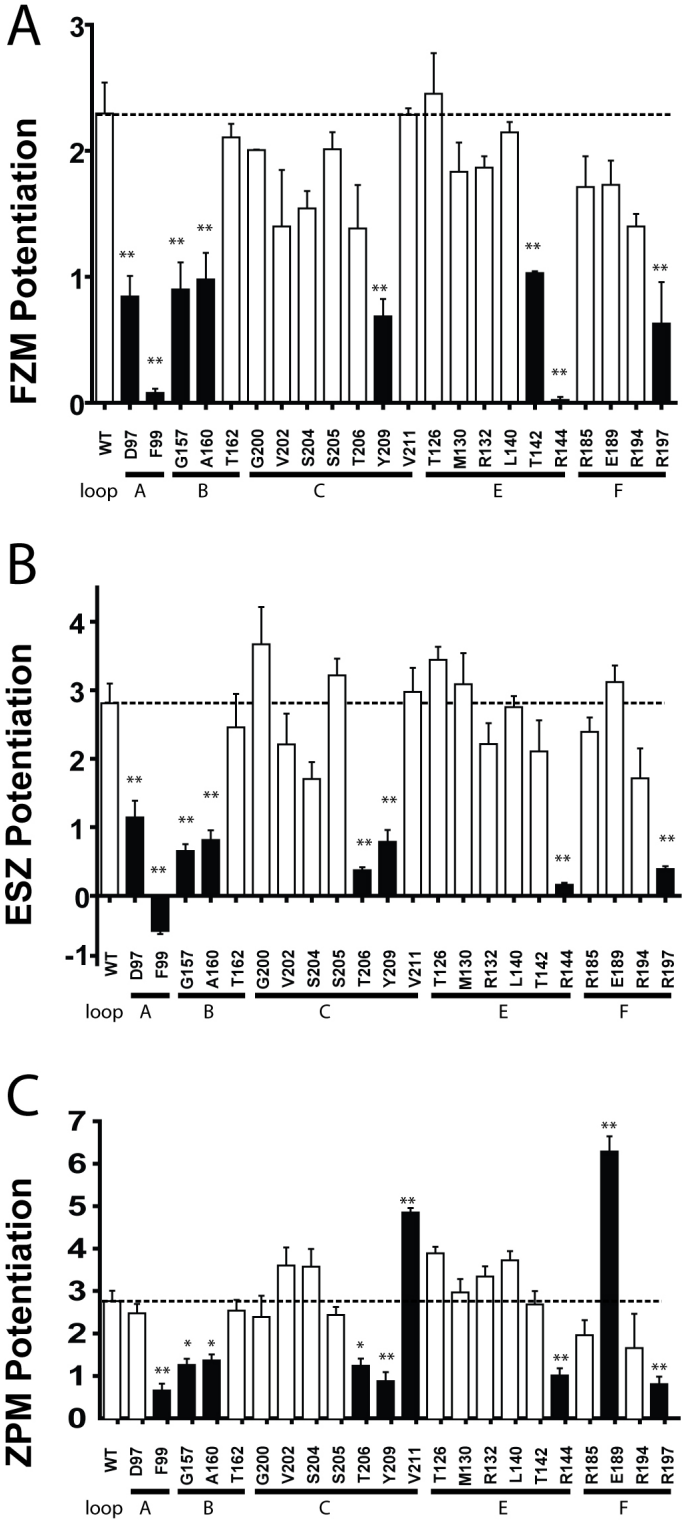
A
FZM Potentiation
B
ESZ Potentiation
C
ZPM Potentiation
WT
D97
F99
G157
A160
T162
G200
V202
S204
S205
T206
Y209
V211
T126
M130
R132
L140
T142
R144
R185
E189
R194
R197
loop
A
B
C
E
F

Figure 3.4 Mutations throughout the BZD binding site affect BZD efficacy. Maximal potentiation of GABA EC_{15} current from WT and mutant receptors by (A) FZM, (B) ESZ or (C) ZPM is plotted. BZD potentiation was calculated as $[(I_{GABA+BZD}/I_{GABA})-1]$. Data are mean ± SEM from at least three oocytes from two or more batches. Dashed lines indicate WT levels of potentiation. Black bars indicate values that are significantly different from WT (*, $p < 0.05$; **, $p < 0.01$).

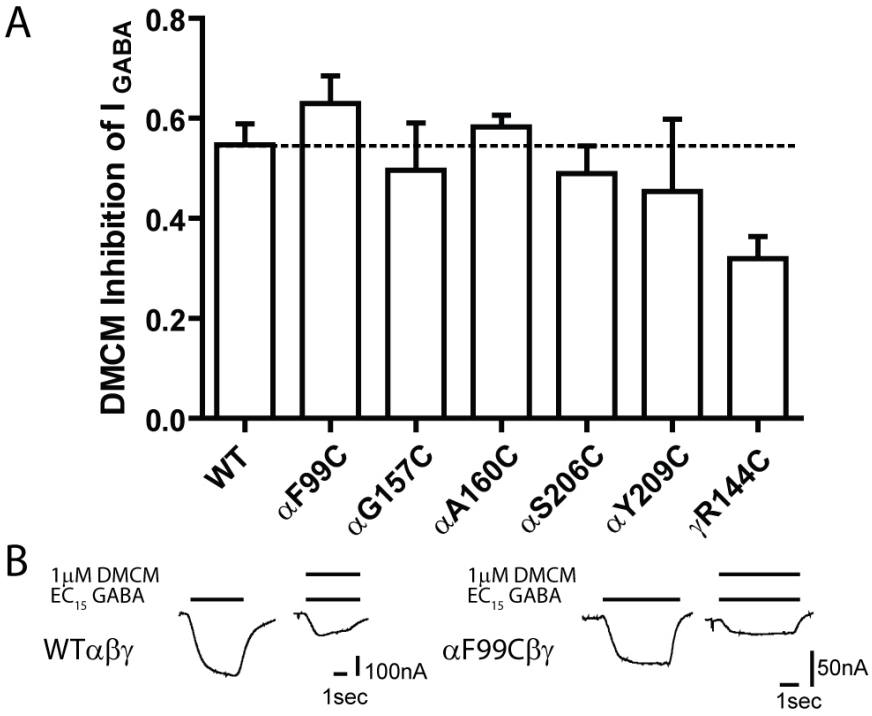
A
DMCM Inhibition of I GABA
0.8
0.6
0.4
0.2
0.0
WT
αF99C
αG157C
αA160C
αS206C
αY209C
γR144C
B
1μM DMCM
EC15 GABA
WTαβγ
100nA
1sec
1μM DMCM
EC15 GABA
αF99Cβγ
50nA
1sec

Figure 3.5 DMCM modulation of WT and mutant $GABA_A$ receptors. Inhibition of EC_{15} GABA by 1μM DMCM for WT and mutant receptors is plotted. Inhibition of GABA current was calculated as $[(I_{GABA+DMCM}/I_{GABA})-1]$. Data are mean ± SEM from at least three oocytes from two or more batches. The dashed line indicates the level of WT inhibition. None of the mutations significantly altered DMCM inhibition of I_{GABA}. (B) Representative current traces from oocytes expressing WT αβγ and αF99Cβγ receptors in response to EC_{15} GABA and EC_{15} GABA + 1μM DMCM.

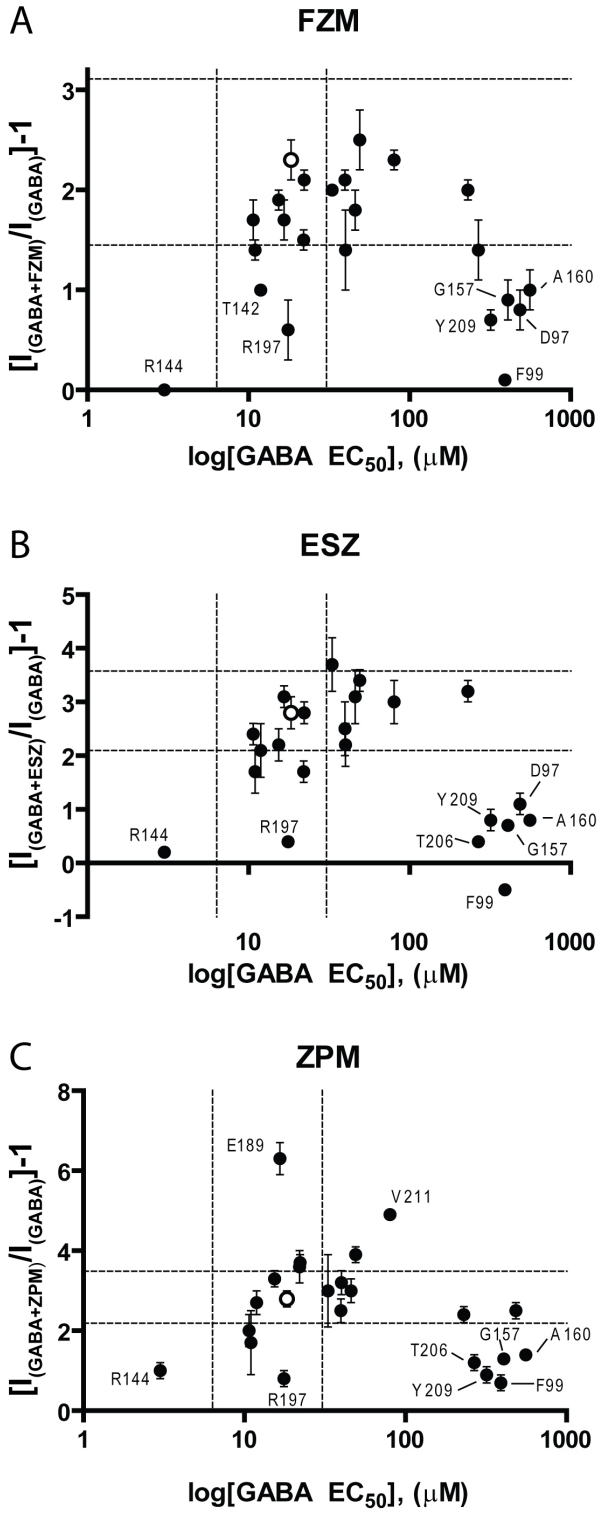
A
FZM
[I(GABA+FZM)/I(GABA)]-1
log[GABA EC50], (μM)
R144
T142
R197
G157
A160
Y209
D97
F99
B
ESZ
[I(GABA+ESZ)/I(GABA)]-1
log[GABA EC50], (μM)
R144
R197
D97
Y209
A160
T206
G157
F99
C
ZPM
[I(GABA+ZPM)/I(GABA)]-1
log[GABA EC50], (μM)
E189
V211
R144
R197
G157
A160
T206
Y209
F99

Figure 3.6 GABA EC_{50} is not correlated with BZD maximal potentiation. For WT and each mutant receptor, the maximal BZD potentiation of EC15 GABA current is plotted versus log[GABA EC_{50}] for A) FZM, B) ESZ and C) ZPM. Data are mean values. Error bars are SEM of BZD potentiation. Open circles represent WT values. Dashed lines represent 95% confidence intervals for WT GABA EC_{50} (vertical lines) and BZD maximal potentiation (horizontal lines). Residues whose mutation significantly altered BZD potentiation compared to WT are labeled.

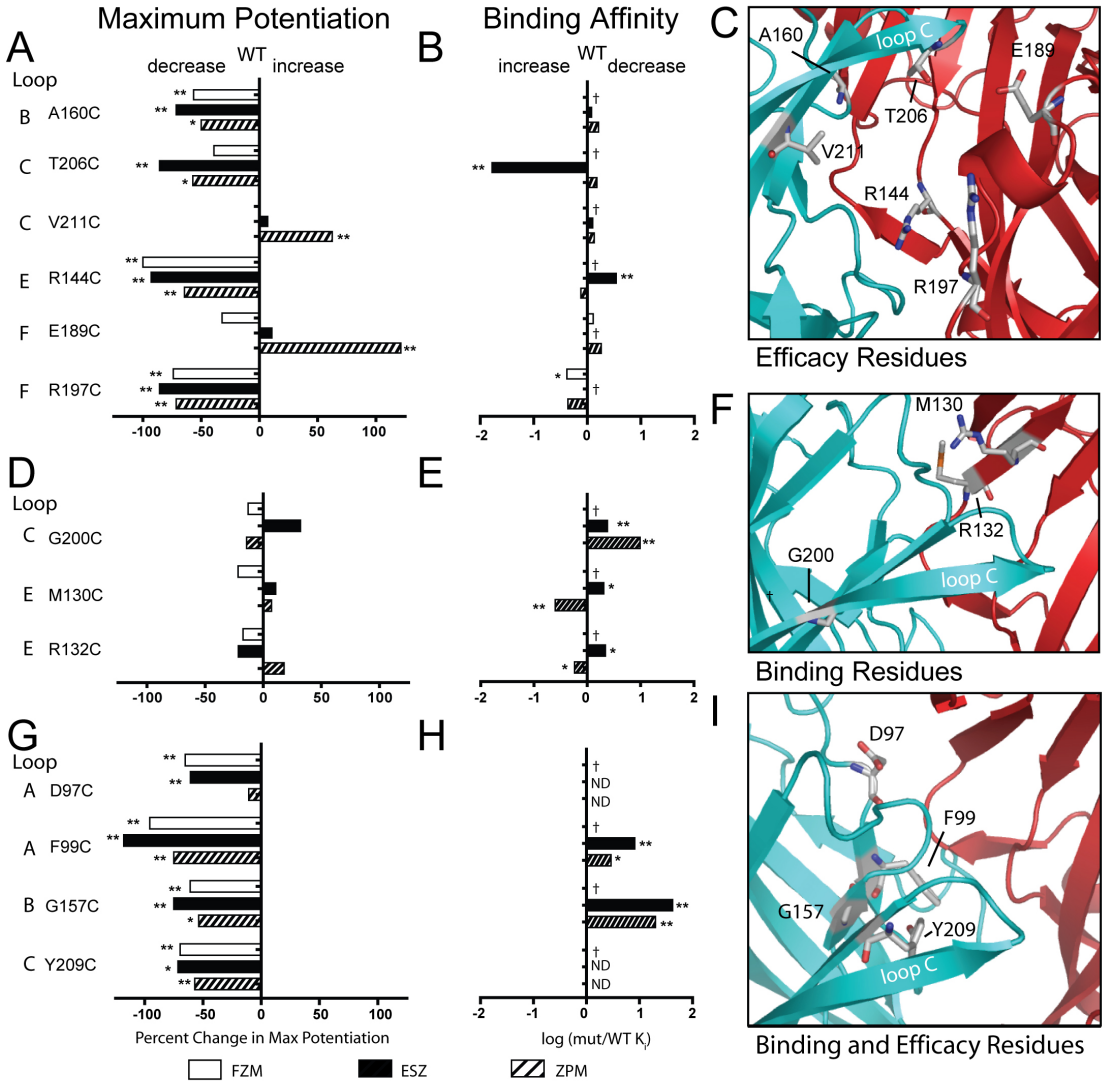
A
Maximum Potentiation
decrease
WT
increase
Loop
B A160C
C T206C
C V211C
E R144C
F E189C
F R197C
-100
-50
0
50
100
B
Binding Affinity
increase
WT
decrease
-2
-1
0
1
2
C
A160
loop C
E189
T206
V211
R144
R197
Efficacy Residues
D
Loop
C G200C
E M130C
E R132C
E
F
M130
R132
G200
loop C
Binding Residues
G
Loop
A D97C
A F99C
B G157C
C Y209C
Percent Change in Max Potentiation
FZM
ESZ
H
ND
log (mut/WT K$_i$)
ZPM
I
D97
F99
G157
Y209
loop C
Binding and Efficacy Residues

Figure 3.7 Summary of data highlighting residues important for BZD efficacy (A, B, C), BZD binding (D, E, F), and BZD binding and efficacy (G, H, I). Panels A, D and G plot the percent change in maximum potentiation for FZM , ESZ and ZPM [((mutant max potentiation-WT max potentiation)/WT max potentiation)(100)], respectively. Negative values represent a decrease in potentiation, while positive values indicate an increase. Panels B, E, and H plot changes in binding affinity [log (mut K_i/WT K_i)]. K_i values for FZM, ESZ and ZPM are from (Hanson and Czajkowski, 2008, Hanson et al., 2008) and were determined by displacement of [^{3}H]Ro15-1788 binding. Negative values indicate increased affinity, positive values indicate decreased affinity. Panels C, F and I are homology models with residues involved in BZD efficacy (C), BZD binding (F) or BZD binding and efficacy (I) shown in sticks. α subunit is blue, γ is red. Loop C is labeled. Values statistically different from WT are indicated (*, $p < 0.05$; **, $p < 0.01$). ND, binding of [^{3}H]Ro15-1788 was not detectable thus K_i values for FZM, ESZ and ZPM were not determined. †, no binding data available

Table 3.1. Summary of GABA dose-response data for WT and mutant $\alpha_1\beta_2\gamma_2$ $GABA_A$Rs

	receptor	EC_{50} (μM)	n_H	n	I_{max} range (μA)
	WT αβγ	18.4 ± 4.4	1.50 ± 0.09	5	8.4 - 11.6
Loop A	αD97Cβγ	485 ± 67**	0.66 ± 0.10**	5	2.3 - 4.0
	αF99Cβγ	391 ± 94*	0.75 ± 0.06**	7	2.7 - 3.1
B	αG157Cβγ	408 ± 93*	0.65 ± 0.03**	8	1.4 - 4.1
	αA160Cβγ	560 ± 138**	0.60 ± 0.04**	6	3.3 - 5.0
	αT162Cβγ	39.8 ± 13.2	0.89 ± 0.12**	4	7.6 - 9.3
C	αG200Cβγ	33.0 ± 11.0	1.03 ± 0.02**	3	4.4 - 8.0
	αV202Cβγ	40.0 ± 22.5	0.99 ± 0.06**	3	6.0 - 7.2
	αS204Cβγ	22.0 ±4.7	1.04 ± 0.03**	3	2.7 - 8.8
	αS205Cβγ	230 ± 126*	1.08 ± 0.20*	3	2.6 - 7.7
	αT206Cβγ	268 ± 58.0*	0.59 ± 0.05**	3	1.9 - 2.8
	αY209Cβγ	319 ± 170*	0.68 ± 0.13**	3	3.5 - 8.8
	αV211Cβγ	80.3 ± 27.5	1.11 ± 0.19*	3	3.2 - 11.4
E	αβγT126C	49.1 ± 7.8**	1.13 ± 0.26	4	4.3 - 8.2
	αβγM130C	45.9 ± 7.5*	1.43 ± 0.02	3	2.6 - 3.5
	αβγR132C	15.4 ± 3.1	1.64 ± 0.04	3	5.8 - 9.2
	αβγL140C	22.2 ± 7.1	1.28 ± 0.21	3	4.4 - 11.0
	αβγT142C	11.9 ± 0.2	1.61 ± 0.12	4	10.6 - 13.7
	αβγR144C	3.0 ± 0.7*	1.55 ± 0.13	3	7.6 - 16.4
F	αβγR185C[a]	10.7 ± 2.0	1.52 ± 0.16	3	11.2-16.0
	αβγE189C[a]	16.6 ± 3.1	1.50 ± 0.03	4	5.2-11.2
	αβγR194C[a]	11.0 ± 2.4	1.41 ± 0.10	3	12.4-17.2
	αβγR197C[a]	17.4 ± 2.3	1.17 ± 0.04	4	9.7-12.0

Data are mean ± SEM for n experiments. n_H values are calculated Hill coefficients. I_{max} range is the lowest and highest maximal GABA current amplitude measured for each of the receptors. [a] Values are from (Hanson and Czajkowski, 2008) with errors in SEM not SD as previously reported. Values significantly different from wild type $\alpha_1\beta_2\gamma_2$ are indicated (*, $p < 0.05$, **, $p < 0.01$). In Hanson and Czajkowski (2008), GABA EC_{50} values for γR185C and γR194C were decreased 2.5-fold compared to WT and were statistically different. Here, these values are no longer significant due to a slight decrease in the WT EC_{50} value reported here and due to differences in the data sets analyzed by ANOVA.

Table 3.2. Summary of BZD concentration response data and binding data for WT and mutant $\alpha_1\beta_2\gamma_2$ $GABA_A$Rs.

		Flurazepam				Eszopiclone				Zolpidem			
	receptor	Max potentiation	EC_{50} (nM)	n	mut/WT K_i[a]	Max potentiation	EC_{50} (nM)	n	mut/WT K_i[b]	Max potentiation	EC_{50} (nM)	n	mut/WT K_i[b]
	WT αβγ	2.3 ± 0.2	442 ± 34	3	1.0	2.8 ± 0.3	55 ± 8.5	8	1.0	2.8 ± 0.2	76.9 ± 27.4	6	1.0
Loop A	αD97Cβγ	0.8 ± 0.2**	941 ± 140	3		1.1 ± 0.2**	166 ± 49	3	ND	2.5 ± 0.2	331 ± 18	3	ND
	αF99Cβγ	0.1 ± 0.0**		3		-0.5 ± 0.0**	1400 ± 290**	3	8.1**	0.7 ± 0.2**	3670 ± 1900**	3	2.9*
B	αG157Cβγ	0.9 ± 0.2**	1620 ± 760	4		0.7 ± 0.1**	1230 ± 140**	3	42**	1.3 ± 0.1*	2820 ± 610**	3	20**
	αA160Cβγ	1.0 ± 0.2**	368 ± 14	3		0.8 ± 0.1**	140 ± 47	3	1.2	1.4 ± 0.1*	118 ± 13	3	1.3
	αT162Cβγ	2.1 ± 0.1	500 ± 53	3		2.5 ± 0.5	131 ± 20	3	0.7	2.5 ± 0.3	410 ± 84	3	1.8
C	αG200Cβγ	2.0 ± 0.0	454 ± 83	3		3.7 ± 0.5	230 ± 8.1	4	2.4**	2.4 ± 0.5	996 ± 481**	3	9.7**
	αV202Cβγ	1.4 ± 0.4*	922 ±165	3		2.2 ± 0.4	522 ± 130**	3	5.0**	3.2 ± 0.3	2490 ± 250**	3	9.0**
	αS204Cβγ	1.5 ± 0.1	305 ± 43	3		1.7 ± 0.2	139 ± 39	3	1.2	3.6 ± 0.4	2100 ± 280**	3	7.0**
	αS205Cβγ	2.0 ± 0.1	366 ± 68	3		3.2 ± 0.2	75 ± 21	3	0.7	2.4 ± 0.2	143 ± 63.4	3	0.7
	αT206Cβγ	1.4 ± 0.3	946 ± 188	3		0.4 ± 0.0**	50.9 ± 19.1	3	0.02**	1.2 ± 0.2*	245 ± 42	3	1.2
	αY209Cβγ	0.7 ± 0.1**	2770 ± 649**	3		0.8 ± 0.2*	766 ± 250**	3	ND	0.9 ± 0.2**	14300 ± 2300**	3	ND
	αV211Cβγ	2.3 ± 0.1	511 ± 93	3		3.0 ± 0.4	115 ± 21	3	1.2	4.9 ± 0.1**	356 ± 117	3	1.1
E	αβγT126C	2.5 ± 0.3	280 ± 35.7	3		3.4 ± 0.2	14.4 ± 4.1	3	1.4	3.9 ± 0.2	9.6 ± 1.7	3	1.2
	αβγM130C	1.8 ± 0.2	305 ± 90	3		3.1 ± 0.5	24.5 ± 7.7	3	2.0*	3.0 ± 0.3	4.4 ± 0.4	3	0.3**
	αβγR132C	1.9 ± 0.1	264 ± 76.7	3		2.2 ± 0.3	12.5 ± 3.1	3	2.2*	3.3 ± 0.2	7.03 ± 1.28	3	0.6*
	αβγL140C	2.1 ± 0.1	330 ± 65	3		2.8 ± 0.2	12.6 ± 1.4*	4	0.9	3.7 ± 0.2	12.1 ± 2.7	3	1.0
	αβγT142C	1.0 ± 0.0**	561 ± 58	3		2.1 ± 0.5	148 ± 39**	3	10*	2.7 ± 0.3	980 ± 260**	3	21**
	αβγR144C	0.0 ± 0.0**		3		0.2 ± 0.0**		3	3.5**	1.0 ± 0.2**	22.5 ± 9.4	3	0.6
F	αβγR185C	1.7 ± 0.2	317 ± 82	3		2.4 ± 0.2	10.4 ± 1.5*	3	1.4	2.0 ± 0.4	10.0 ± 2.2	3	1.1
	αβγE189C	1.7 ± 0.2	645 ± 78	3	1.3	3.1 ± 0.2	12.2 ± 3.0*	4		6.3 ± 0.4**	1838 ± 636**	5	1.8[a]
	αβγR194C	1.4 ± 0.1	332 ± 53	3		1.7 ± 0.4	12.8 ± 3.4	3	1.3	1.7 ± 0.8	21.2 ± 8.3	3	1.0
	αβγR197C	0.6 ± 0.3**	494 ± 48	3	0.4*	0.4 ± 0.0**	6.0 ± 2.1*	3		0.8 ± 0.2**	13.8 ± 2.3	4	0.4[a]

Data are mean ± SEM for n experiments. Maximal potentiation is calculated as $[(I_{GABA+BZD}/I_{GABA})-1]$. The values for BZD binding affinities (K_i) were determined previously and the ratio of mutant to WT binding affinity is shown. [a] Values from (Hanson and Czajkowski, 2008). [b] Values from (Hanson et al., 2008). ND, not detectable. Values significantly different from wild type $\alpha_1\beta_2\gamma_2$ are indicated (*, $p < 0.05$, **, $p < 0.01$).

CHAPTER 4. Alterations to GABA macroscopic kinetics caused by mutations at non GABA binding site interfaces.

4.1 Introduction

The γ amino butyric acid type A receptor ($GABA_AR$) is a pentameric ligand gated ion channel that is a member of the cys-loop family of receptors that includes the nicotinic acetylcholine receptor, serotonin type 3 ($5\text{-}HT_3$ receptor) and glycine receptors. $GABA_ARs$ are the major source of fast synaptic inhibition in the brain. These neurotransmitter receptors also bind a variety of clinically relevant drugs used as sedatives, antiepileptics, anxiolytics and general anesthetics.

The most common subunit subtype combination in the brain is two α_1, two β_2 and a single γ_2 subunit (McKernan and Whiting, 1996). The five subunits are arranged in βαβαγ order around a central chloride conducting channel (Baumann et al., 2002). Binding of the endogenous neurotransmitter GABA, in the extracellular domain at the β−α subunit interface opens this channel. Drugs such as benzodiazepines, anesthetics and barbiturates allosterically modulate channel properties, in most cases potentiating GABA-induced currents (I_{GABA}). Benzodiazepines, such as diazepam, bind at the α−γ subunit interface at a binding site homologous to that of the GABA binding site.

$GABA_ARs$ exist in at least three interconvertible, conformational states: an unliganded, closed channel, non-conducting state (Unbound); a ligand-bound, open channel, ion-conducting state (Open); and a ligand-bound, closed channel desensitized state. Upon agonist binding, the channel rapidly opens (activation). In the continued

presence of agonist, $GABA_A$Rs undergo a conformational transition that closes the channel even though agonist is still bound, a process called desensitization. When agonist is removed, the channel closes and the receptor adopts a non-conducting, unliganded closed resting state.

$GABA_A$R desensitization is multiphasic (Celentano and Wong, 1994, Puia et al., 1994, Jones and Westbrook, 1995). Desensitization prolongs IPSCs by maintaining receptors in a GABA-bound, non-conducting state which can again convert to an open channel, conducting state before releasing GABA and converting to the resting state (Jones and Westbrook, 1995, Dominguez-Perrot et al., 1996, Tia et al., 1996, Haas and Macdonald, 1999, Bianchi et al., 2001). Desensitization influences IPSC duration and decay and thus, contributes to neuronal firing patterns. Moreover, $GABA_A$R desensitization and recovery from desensitization influences a cell's response to repeated high frequency stimuli (Jones and Westbrook, 1996).

Receptor deactivation and macroscopic desensitization kinetics are dependent on ligand affinity, ligand concentration, and subunit composition (Tia et al., 1996, Haas and Macdonald, 1999, Bianchi et al., 2002a, Boileau et al., 2003, Boileau et al., 2005, Eyre et al., 2012) and can be modulated by phosphorylation (Jones and Westbrook, 1997, Hinkle and Macdonald, 2003), proton concentration (Feng and Macdonald, 2004), and neurosteroid binding (Zhu and Vicini, 1997). In comparing $\alpha_1\beta_3\gamma_{2L}$ and $\alpha_4\beta_3\gamma_{2L}$ receptors, receptors that contained the α_4 subunit exhibit more rapid and extensive desensitization (Lagrange et al., 2007). Upregulation of α_4 subunit containing receptors is seen in rats after epileptogenic injection with pilocarpine or kainic acid (Schwarzer et al., 1997, Brooks-Kayal et al., 1998, Sperk et al., 1998). Little is known about the structural

elements that regulate GABAR kinetics, especially desensitization. Receptor subtype composition clearly affects receptor kinetics. Distinct regions within subunits have been implicated in desensitization, specifically the M1 region. Mutations of conserved hydrophobic residues in the extracellular end of M1 in the α, β, and γ subunits alter desensitization (Amin and Weiss, 1994, Bianchi et al., 2001). A recent study indicated that a residue within the GABA binding site, α_1R120 significantly decreases the extent of desensitization (Laha and Wagner, 2011).

In my previous work, using receptor expression in *Xenopus laevis* oocytes and two electrode voltage clamp, apparent alterations in macroscopic current kinetics were seen for several mutant containing receptors. Overall, the mutations αD97C, αF99C, αG157C, αA160C, αS205C, αT206C, and αY209C, located in loops A, B and C of the α_1 subunit, appeared to slow current activation, decrease the extent of desensitization and increased the rate of current deactivation compared to WT receptors (Fig. 4.1). These mutations are located within the BZD binding site and at a second, non-binding interface. Because of the large size of oocytes the rate of solution exchange in two electrode voltage clamp recordings is too slow to accurately resolve kinetics. The slow solution exchange rates of two electrode voltage clamp results in the receptors occupying a mixture of states with some receptors open, some desensitized and others not open. Assessing a mixed population of receptors does not accurately reflect fast activation and maximal current amplitude (Jones and Westbrook, 1996). For the experiments in this chapter, mutations exhibiting altered macroscopic kinetics in Xenopus oocytes were expressed in HEK293 cells. I used excised outside-out patch clamp recordings and ultra-rapid solution exchange. The solution exchange rates, measured by open tip potential,

were ~300-500μs. This rate approaches that of channel opening and thus allows for resolution of macroscopic activation rates. Though expression was low or not detectable for several of the mutations, an effort was made to assess at least a single mutation from each of the affected loops for which BZD binding data was available (Hanson and Czajkowski, 2008, Hanson et al., 2008). The goal of these experiments was to test the hypothesis that structural perturbations at non-GABA binding site subunit interfaces can influence $GABA_A$ receptor kinetics.

4.2 Materials and Methods

4.2.1 Mutagenesis

Mutants were constructed previously (Hanson et al., 2008). Cysteine mutants of α_1 receptor subunits were made by recombinant PCR in the pUNIV vector (Venkatachalan et al., 2007) and verified by double-stranded DNA sequencing.

4.2.2 Cell Culture and Transfection

Human Embryonic Kidney (HEK) 293 cells (American Type Culture Collection CRL 1573) were cultured in minimal essential media with Earle's salts (Mediatech, Manassas, VA) containing 10% fetal bovine serum (Hyclone, Logan, UT) in a 37°C incubator under 5% CO_2 atmosphere. Cells were plated in 60 mM culture dishes 24 hrs prior to transfection with Lipofectamine2000 reagent (Invitrogen, Carlsbad, CA) as indicated. Cells were transfected with 500 ng α_1, 500 ng β_2 and 5 μg γ_2 cDNA and 300 ng eGFP. For low expressing mutant receptors, I tried two protocols to increase expression: maintaining cells at 31°C post transfection and the addition of the pAdVAntage vector

(Promega, Madison, WI) but neither approach noticeably increased expression.. Recordings were performed 48-80 hrs after transfection.

4.2.3 Excised Outside-out Patch Clamp Recordings

Outside-out patches excised from HEK293 cells were made using borosilicate glass pipettes filled with 140 mM KCL, 10 mM EGTA, 2 mM MgATP, 20 mM phosphocreatine, and 10 mM HEPES, pH 7.3, osmolarity 320 mOsm. Patches were voltage clamped at -60mV and placed in the stream of a multi-barreled flowpipe. Position of the flowpipe was controlled by a piezeoelectric bimorph (Dagan Corporation, Minneapolis, MN). Rapid solution exchange was accomplished by a computer controlled constant current source which drove the flowpipes to move, relative to the patch electrode achieving 10-90% rise times for open tip solution exchange of ~300-500 μsec. 10 mM GABA was dissolved in the perfusion solution which contained 145 mM NaCl, 2.5 mM KCl, 2 mM $CaCl_2$, 1 mM $MgCl_2$, 10 mM HEPES and 4 mM glucose, pH 7.4. Solution exchange rates were monitored by a junction current produced by altering the ionic strength of solutions with an additional 5 mM NaCl. Currents were low-pass filtered with a four-pole Bessel filter and digitized at a rate no less than twice the filter frequency. Data were collected at 20 kHz using an Axopatch 200B amplifier (Molecular Devices, Sunnyvale, CA) and a digidata 1322A digitizer (Molecular Devices, Sunnyvale, CA) controlled by Axograph X software (Axograph Scientific, Sydney, Australia).

4.2.4 Data Fitting and Statistical Analysis

Curve fitting was also performed using Axograph X software. Deactivation phases were fit with a biexponential function and desensitization was fit with bi-exponential or single exponential functions. Traces fit by a single exponential were not fit by a bi-exponential

function with two positive time constants (τ_1 and τ_2) with corresponding negative amplitudes (A_1 and A_2). For deactivation, the time of GABA removal was set to zero and the remaining current fit with the equation $Y = A_1 * e^{(-t/\tau_1)} + A_2 * e^{(-t/\tau_2)}$. % Contribution of each τ is calculated as $\%\tau_1 = A_1/(A_1 + A_2)$ and $\%\tau_2 = A_2/(A_1 + A_2)$ respectively. For desensitization, the onset of desensitization was set to zero, and the region of desensitization was fit with the equation $Y = A_1 * e^{(-t/\tau_1)} + A_2 * e^{(-t/\tau_2)} + C$. $A_2 = 0$ for cases where the current trace was best fit by a single exponential function. A weighted time constant ($\tau_{weighted}$) was calculated for those traces fit best by a bi-exponential function. $\tau_{weighted} = (A_1/(A_1 + A_2)) * \tau_1 + (A_2/(A_1 + A_2)) * \tau_2$. For those traces best fit by a single exponential function $\tau_{weighted} = \tau_1$. Percent remaining is calculated as % remaining $= C/(A_1 + A_2 + C)$. % Contribution of each τ of desensitization is calculated as $\%\tau_1 = A_1/(A_1 + A_2 + C)$ and $\%\tau_2 = A_2/(A_1 + A_2 + C)$. Figures of raw data represent ensemble averages that have been decimated. Significant differences from WT were determined by one-way ANOVA with a post hoc Dunnett's test (Prism 5; GraphPad Software, Inc., San Diego, CA). Outlier in kinetic rates were removed using a Grubb's test with a significance level of $P < 0.05$.

4.2.5 Kinetic Modeling

Kinetic modeling was performed using custom software from the lab of Matt Jones (University of Wisconsin-Madison) using the Q-matrix method (Colquhoun and Hawkes, 1995). A 7 state model was used which included two ligand binding steps, channel opening and desensitization (Fig. 4.7A and 4.8B). This model has been described previously (Jones et al., 1998, Wagner et al., 2004, Goldschen-Ohm et al., 2010, Laha and Wagner, 2011). During optimization k_{on} was constrained to 1.9×10^6 molar^{-1} sec^{-1} as

determined in (Goldschen-Ohm et al., 2010). α_1 and α_2 were also constrained, α_1 to 3300 sec^{-1} and α_2 to 380 sec^{-1} as described previously (Goldschen-Ohm et al., 2010). These rates are based on prior single channel recordings (Fisher and Macdonald, 1997). For WT modeling other values were initially set to published values (Goldschen-Ohm et al., 2010). For modeling of αS205Cβγ receptors other values (except k_{on}, α_1 and α_2) were initially set to WT values determined in this study. Current responses from 3 msec and 1 sec pulses of 10 mM GABA were simultaneously fit for each patch. Optimization used a simplex algorithm to minimize the amplitude-weight sum of square errors between actual and simulated currents.

4.3 Results

4.3.1 Mutations altered cell surface expression of functional receptors in HEK293 cells.

In my previous studies, I noticed that expression of αD97Cβγ, αF99Cβγ, αG157Cβγ, αA160Cβγ, αS205Cβγ, αT206Cβγ, and αY209Cβγ receptors was decreased in oocytes compared to WTαβγ receptors based on decreases in I_{max} range (Table 1). However, each of the mutant containing receptors reliably expressed in oocytes. This was not the case for HEK293 cells. For each of the above mutant receptors, expression in HEK293 cells and and patch clamp recordings were attempted at least three times. For αD97Cβγ, αA160Cβγ and αT206Cβγ receptors, I could never record GABA activated currents above the +/- 5 pA noise level. For the other mutations, measurable currents above noise were less common than with WT receptors and only currents with amplitudes of 20 pA above noise or greater were included in my analyses. Current

amplitudes for the αF99Cβγ, αG157Cβγ, S205Cβγ, and αY209Cβγ receptors were generally decreased compared to WT receptors. αG157Cβγ receptors were the most affected, never producing a current above 38pA and only rarely producing measurable currents, hence the low number of patches, n, in Table 2.

4.3.2. Current deactivation is not significantly altered in mutant containing receptors.

Exponential functions were used to fit the current traces and examined by eye for goodness of fit. In all cases (WT and mutant receptors), the current deactivation phase after a 1 sec pulse or a ~3 msec pulse of 10mM GABA were well fit by a bi-exponential function (Fig. 4.2B,C and 4.. 4.4A). No significant differences in deactivation rates were found using a 1sec pulse of GABA or an ~3 msec pulse of GABA and the data were pooled. No short pulse traces are available for αG157Cβγ receptors. None of the mutations significantly altered current deactivation kinetics as compared to WT (τ_{slow} ,WT = 189 ± 16.3, n= 14; τ_{fast}, WT = 25.5 ± 3.4, n= 14, and $\tau_{weighted}$,WT = 96.3 ± 9.6, n= 14). Percent contribution of each of the time constants was also unaltered (Fig. 4.4 and Table 4.2).

4.3.3 Components of desensitization in the continued presence of 10 mM GABA are altered in αF99Cβγ, αG157Cβγ, S205Cβγ, and αY209Cβγ receptors.

All of the curve fits of current desensitization in the presence of a 1sec pulse of 10mM GABA were examined by eye and assessed for minimal sum of squared errors. All of the WT and αY209Cβγ desensitization traces were well fit using a bi-exponential functions

(4.2A). Some αF99Cβγ (1 out of 8), S205Cβγ (5 out of 7) and all αG157Cβγ receptor current desensitization traces were best fit by single exponential functions. (Fig. 4.5A). The single time constants from these current traces were statistically indistinguishable from the τ_{slow} of their biexponential counter parts and no significant differences were found when comparing these to the WT τ_{slow} (653 ± 59 msec, n = 15) (Fig. 4.5B, Table 4.3). In receptor traces that were best fit using a bi-exponential function, τ_{fast} did not differ from WT (32.5 ± 4.2, n = 15) (Fig. 4.5C, Table 4.3). For αG157Cβγ receptors, the fast component of desensitization was missing (Fig. 4.5C). For αY209Cβγ receptors, there was a significant decrease in the % of current contributing to τ_{fast} as compared to WT (WT, $\%\tau_1$ = 47.8 ± 1.9, $\%\tau_2$ = 23.7 ± 2.5, n = 15; αY209Cβγ, $\%\tau_1$ = 54.8 ± 6.9, $\%\tau_2$ = 10.2 ± 1.7, n = 4) (Table 3). Desensitization time constants were altered when comparing the single exponential fits of αG157Cβγ (607 ± 108, n = 5) and αS205Cβγ (577 ± 75, n = 5) current traces to WT weighted τ (Fig. 4.5E) The time constant from the single exponential fit from αF99Cβγ receptors (666, n = 1) appeared increased compared to WT, but an ANOVA cannot assess differences with n = 1.

Current remaining after 1 sec in 10 mM GABA is calculated from the asymptote of the exponential fit. This value was increased (total desensitization was decreased) compared to WT receptors (28.5% ± 2.9, n = 15) in αG157Cβγ receptors (60.4% ± 2.1, n = 5), and αS205Cβγ receptors (single exponential fits: 54.1% ± 4.0, n = 5; biexponential fits: 42.4% ± 2.7, n =7; all combined: 47.3% ± 2.8, n = 12). Current remaining after 1 sec is increased in the one αF99Cβγ receptor current trace with a single exponential fit, but ANOVA cannot assess differences with n = 1 (Fig. 4.3, 4.5 and Table 4.3).

4.3.4 Activation rate at 10 mM GABA is altered only in αG157Cβγ receptors.

Activation rate was determined by measuring the 10-90% current rise time in the presence of 10 mM GABA. Rise times were measured from long pulse traces (1 sec in 10 mM GABA). Traces with small signal to noise (average noise of +/- 5 pA) ratio were excluded from these analyses as measurement to peak was unreliable. The 10-90% rise times for αF99Cβγ (1.26 ± 0.13 msec, n =8), αS205Cβγ (0.86 ± 0.08 msec, n =8) and αY209Cβγ (1.31 ± 0.26 msec, n = 4) receptors did not differ from WT (1.05 ± 0.11 msec, n = 11) (4.6). Rise times that are unaltered from WT receptor suggest that 10mM GABA is saturating for these receptors. Rise times decrease (i.e. activation get fasters) with increasing concentrations of GABA until it reaches a plateau at GABA concentrations that saturate the binding site (Bianchi et al., 2007). 10mM GABA is above saturating for WTαβγ receptors. The 10-90% current rise time was significantly slower for αG157Cβγ receptors (2.92 ± 0.31 msec, n =5) compared to WT receptors for 10mM GABA (Fig. 4.6). Despite multiple attempts, I was not able to collect additional patch clamp data from αG157Cβγ receptors at higher GABA concentrations due to abrogated expression. For each of the mutations in this study, GABA EC_{50} is right shifted compared to WT when I measured it using two electrode voltage clamp recordings from *X. laevis* oocytes expressing WT and mutant receptors.

4.3.5 Kinetic Modeling provides insights into microscopic rates contributing to alterations in αS205Cβγ receptor macroscopic kinetics.

Using a previously described 7 state Markov model (Jones et al., 1998, Barberis et al., 2007, Goldschen-Ohm et al., 2010, Laha and Wagner, 2011) some insight into the

microscopic rates between kinetics states can be gained. Comparisons between WT and αS205Cβγ were examined as this mutant receptor had the most reliable and robust expression as well as displayed a significant decrease in the extent of desensitization after 1 sec in 10mM GABA. Simulations increasing specific rates 3 fold from the published values (Laha and Wagner, 2011) were performed (Fig. 4.7). Simulations increasing the rates of channel opening (β_1 and β_2) (Fig. 4.7E) as well as the rate of resensitization (r_1 and r_2) (Fig. 4.7D) both decrease the extent of desensitization. However, deactivation appears slower with increased rate of channel opening and no significant changes were seen in the deactivation rate of S205Cβγ receptors. Simulations were used as a starting point for kinetic modeling of mutant receptor traces.

Two kinetic models were fit to the WT and αS205Cβγ receptor current traces. Traces were best fit by the previously describe model in Fig. 4.8B (Jones et al., 1998, Wagner et al., 2004, Goldschen-Ohm et al., 2010, Laha and Wagner, 2011). Current traces from a single patch from 1sec and ~3ms 10mM GABA pulses were fit simultaneously. Data from a single patch was fit for both WT and αS205Cβγ receptors to assess which microscopic rates could possibly be altered to produce the macroscopic kinetics of αS205Cβγ receptors. Due to the lack of additional, high quality paired long and short pulse data statistical significance cannot be assigned to modeling data. Modeling is provided as an example. WT currents were modeled starting with published rates (Goldschen-Ohm et al., 2010) and all values except k_{on}, α_1 and α_2 were allowed to float. When modeling αS205Cβγ, the starting rates were set to that of WT values from this study and k_{on}, α_1 and α_2 constrained as above.

Microscopic rates estimated by kinetic modeling for 1 sec and ~3ms pulses of 10mM GABA for αS205Cβγ receptors differed by more than 2 fold from WT estimated rates in the rate of unbinding the second bound GABA molecule (k_{off2}, increased 2.2 fold), the rate of entering the singly bound desensitized state (d_1, decreased 2.5 fold), the rate of resensitizing from the doubly bound desensitized state (r_2, increased 2.8 fold), and the rate of the singly bound desensitized state binding an additional GABA molecule (q, decreased 3.3 fold) (Fig. 4.8D). Overall, these changes shift the equilibrium away from the desensitized states. Equilibria are shifted in both desensitized states, favoring the bound-inactive states (d_1 is decreased, while r_1 is near WT and d_2 is near WT while r_2 is increased). These specific changes in rates and shifts in equilibria may explain the decrease in the extent of desensitization seen in αS205Cβγ receptors compared to WT. Changes in binding rates, both between the desensitized states (q) and bound-inactive states (k_{off2}) may be the result of nuances in the particular traces that were fit as these rates would have minimal impact on the decreased extent of desensitization observed between WT and αS205Cβγ receptor traces. Additional experimental protocols would help to further constrain kinetic models. Modeling of data from multiple patches is necessary to make finite conclusions as to the specific microscopic rates contributing to observed macroscopic behavior.

4.4 Discussion

4.4.1 Further mutant characterization required and potential alternative methods to address decreased mutant containing receptor expression.

Patches from HEK cells expressing mutant containing $GABA_A$ receptors that produced great than 20pA currents were pulled less frequently than those cells expressing WT receptors. Additionally, some mutant containing receptors produced no discernable currents. It is possible that these receptors did traffic to the cell surface and were not functional and thus produced no currents. However, each of the mutant containing receptors reliably expressed functional receptors in *X. laevis* oocytes and each of the mutant containing receptors, with the exception of αD97Cβγ and αY209Cβγ also produced receptors on the cell surface capable of binding BZDs (Hanson and Czajkowski, 2008). Binding could not be determined for αD97Cβγ and αY209Cβγ receptors indicating these receptors did not express in HEK293 cells or that binding of [^{3}H] Ro15-1788 and [^{3}H] Ro15-4513 was so severely abrogated as to be below the level of detection.

To study these mutant receptors further one would need to explore different expression systems or methods of transfection to help alleviate issues of low expression. Perhaps the simplest thing to try is a wholly different transfection method, such as calcium phosphate, which has been used for excised patches in HEK293 cells previously (Goldschen-Ohm et al., 2010). Alternatively, the receptors may express better in a different cell line, such as Cos-7 cells. Additionally, use of a different vector may improve expression. Experiments using $GABA_A$Rs for excised outside-out patch clamp recordings have used DNA constructs in a pcDNA3.1 vector (Goldschen-Ohm et al., 2010, Laha and Wagner, 2011). Also, excised patches can be pulled from the membrane of *X. laevis* oocytes (Stuhmer, 1998) as these receptors were reliably expressed in oocytes previously (Morlock and Czajkowski, 2011).

With more reliably expressing mutants a larger sample size could be assayed. This is crucial for understanding the effects these mutation have on GABAA receptor kinetics as there is wide degree of variability from patch to patch in many of the metrics assayed. It is particularly puzzling that a decrease in the extent of desensitization occurred with no alteration in the desensitization time constants. However, due to the large degree of variability in both the WT and mutant receptor time constants, no significant differences were apparent. Also, it would appear that for αS205Cβγ and possibly for αF99Cβγ containing receptors there were two kinetically distinct populations. Those traces from patches that were best fit with a single exponential appeared to have no fast phase of desensitization. These seemingly different populations could not be attributed to specific transfections or recordings days and could not be correlated to low signal to noise ratios. Increased sample size from reliably expressing receptors would allow for a more accurate assessment of any differences in receptor populations.

Additional experimentation to ensure incorporation of each subunit should also be included. However, of the mutant containing receptors described in the present study, all but αY209Cβγ bound either Ro15-1788, eszopiclone or zolpidem with near WT, or higher, binding affinity when expressed in HEK293 cells, indicative of accurate incorporation of the γ subunit, which is required to bind BZDs (Hanson et al., 2008). However, assaying the functionality of these BZD ligands, which require a γ subunit to function, or Zn^{2+} block, which is disrupted at low concentrations by the presence of the γ subunit, (Hosie et al., 2003) using patch clamp recordings would assure the incorporation of all subunits in this experimental set up.

Additional experimentation to more accurately describe the kinetics could be performed. Concentration response of mutant containing receptors is needed to address whether 10mM GABA is saturating. Kinetic properties of $GABA_AR$, including activation rate, desensitization and deactivation vary with GABA EC (Bianchi et al., 2007). Also, race experiments to assess the microscopic binding rate for GABA (Jones et al., 1998) and non-stationary variance analysis that would provide a measure of $P_{o\text{-}max}$ (Sigworth, 1980). These measurements would allow for more constraints on kinetic modeling and provide more detailed information as to the effects of the mutations. Additional constraints and data for modeling are necessary to draw specific conclusions as to microscopic rates affecting macroscopic kinetic alterations seen in αS205Cβγ receptors.

4.4.2 Despite caveats to the data, there is an indication that GABA macroscopic kinetics are altered by mutations at a non GABA binding site.

Despite difficulty collecting these data, the low expression of mutant containing receptors and large variability within the data, significant decreases in extent of desensitization in αG157Cβγ and αS205Cβγ receptors and increased rise time of αG157Cβγ receptors support a more thorough characterization of these mutant receptors. The difference in extent of desensitization seen in αS205Cβγ receptors is robust and exists in both data populations, those fit by one or two exponential functions. Additionally, the activation rate of αG157Cβγ is significantly slowed and the extent of desensitization decreased compared to WT receptors. This warrants further experimentation to resolve the concentration dependence of these phenomena.

These differences in macroscopic kinetics of I_{GABA} caused by mutations in loops A, B and C of the $GABA_AR$ are of particular interest as these mutations are distant from the GABA binding site, yet located in a site homologous to the GABA binding site. These mutations are crucial to the binding and efficacy of multiple BZD ligands at the α–γ interface (Hanson et al., 2008, Morlock and Czajkowski, 2011) and are also located at the α–β interface. Using concatameric receptors, it would be possible to isolate mutations discussed in this chapter to a single α subunit at either the α–γ interface or α–β interface to assess individual contributions of these mutant locations (for review see (Ericksen and Boileau, 2007)).

Pharmacological agents that allosterically modulate I_{GABA}, such at BZDS which bind at the α–γ interface, do so by altering macroscopic GABA kinetics. BZDs have been shown to speed desensitization (Mellor and Randall, 1997), prolong deactivation (Mellor and Randall, 1997, Strecker et al., 1999, Bianchi et al., 2009), and increase rates of activation (Lavoie and Twyman, 1996). It is enticing to think that there is a relationship between the kinetic aberrations resulting from two types of structural perturbations at these binding sites: those caused by ligand occupancy and those from engineered mutations.

Additionally, recent work suggests the α–β interface may be a site of action for BZDs. A recent screen of BZD actions at $\alpha_1\beta_3$ receptors, that do not contain an α–γ interface, indicate that the α–β interface contains a low affinity binding site (Ramerstorfer et al., 2011, Sieghart et al., 2011). Experiments in concatameric receptors limited an αH101C mutation (or analogous mutations in other α subunits) to the α–β interface. The diazepam insensitive α_6 subunit was inserted at the α–γ interface.

Covalently linking a diazepam analog to the αH101C mutation in a single alpha subunit at the α–β interface indicates the activity of BZDs at this site (Baur et al., 2008). This data provides further impetus to assess the individual contribution to macroscopic kinetic effects of mutations at either the α–β or α–γ interface. These ideas will be further discussed in Chapter 5.

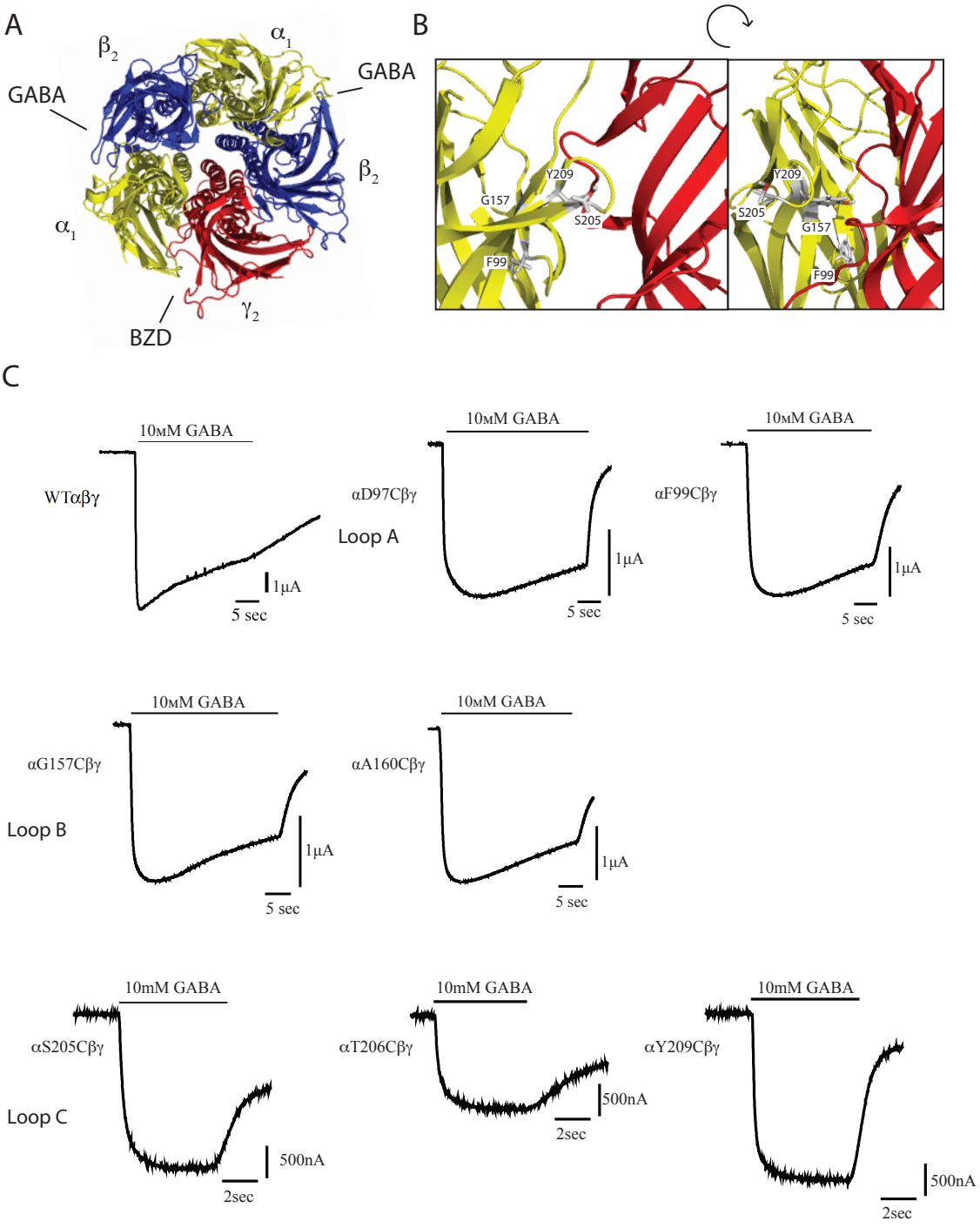
A
β2
α1
GABA
GABA
β2
α1
γ2
BZD
B
Y209
G157
S205
F99
Y209
S205
G157
F99
C
10мM GABA
WTαβγ
1μA
5 sec
10мM GABA
αD97Cβγ
Loop A
1μA
5 sec
10мM GABA
αF99Cβγ
1μA
5 sec
10мM GABA
αG157Cβγ
Loop B
1μA
5 sec
10мM GABA
αA160Cβγ
1μA
5 sec
10mM GABA
αS205Cβγ
Loop C
500nA
2sec
10mM GABA
αT206Cβγ
500nA
2sec
10mM GABA
αY209Cβγ
500nA
2sec

Figure 4.1. Two electrode voltage clamp recordings from *X. laevis* oocytes expressing BZD binding site mutations are indicative of differences in macroscopic kinetics of I_{GABA}. (A) top down view of the $GABA_A$ receptor homology model indicating GABA and BZD binding sites. Mutations of interest are located in the α subunit at the BZD binding site at α–γ interface and at the nonbinding β–α interface. (B) A close up view of the BZD binding site at the α–γ interface with residues F99, G157, S250 and Y209 shown in sticks and labeled. (C) Recordings from oocytes expressing αD97Cβγ, αF99Cβγ, αG157Cβγ, αA160Cβγ, αS205Cβγ, αT206Cβγ, and αY209Cβγ receptors produced traces at max GABA concentrations that appeared to have slower current activation, a lesser extent of desensitization and faster deactivation than WTαβγ receptors. These affects were not observed from many other mutations within the BZD binding site as well as elsewhere in the $GABA_A$ receptor, including the GABA binding site and provided the impetus for more thorough kinetic analysis with excised outside-out patch clamp recordings.

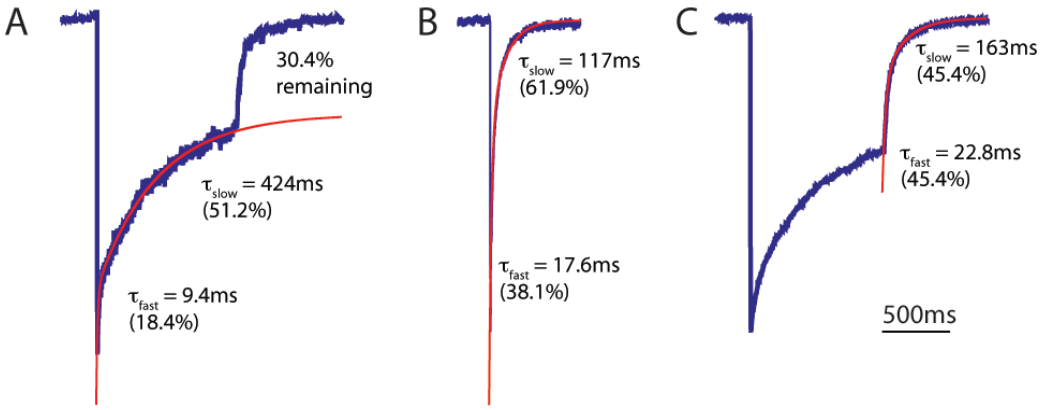
A
30.4%
remaining
τslow = 424ms
(51.2%)
τfast = 9.4ms
(18.4%)
B
τslow = 117ms
(61.9%)
τfast = 17.6ms
(38.1%)
C
τslow = 163ms
(45.4%)
τfast = 22.8ms
(45.4%)
500ms

Figure 4.2. WTαβγ deactivation and desensitization are well fit exponential functions. Axograph software was used to fit exponential functions to desensitization during a 1 sec pulse of 10mM GABA (A) and deactivation after 3ms in 10mM GABA (B) or at the end of a 1sec pulse (C). Deactivation and desensitization from all WTαβγ receptors were well fit by two exponentials. Time constants and % contribution are labeled for the individual fits. % Remaining is the current remaining after a 1sec exposure to 10mM GABA.

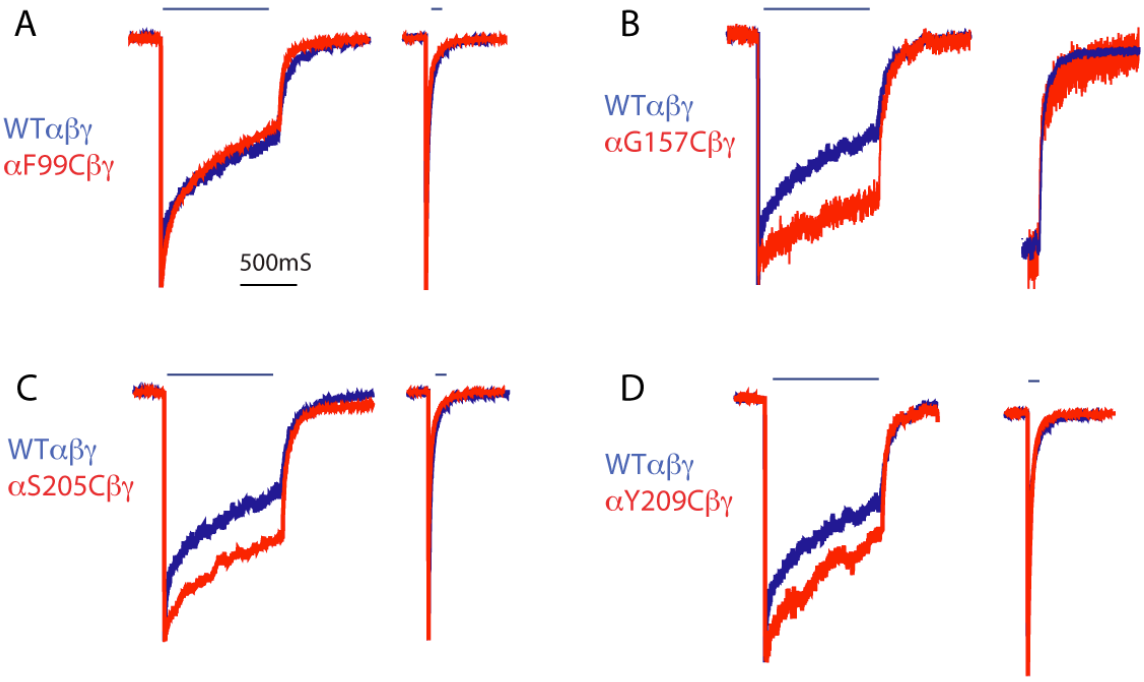
A
WTαβγ
αF99Cβγ
500mS
B
WTαβγ
αG157Cβγ
C
WTαβγ
αS205Cβγ
D
WTαβγ
αY209Cβγ

Figure 4.3. Traces from αF99Cβγ, αG157Cβγ, αS205Cβγ, and αY209Cβγ receptors elicited by 10mM GABA for 1sec or ~3ms are shown overlaid with corresponding current traces from WTαβγ receptors. (A) αF99Cβγ, (B) αG157Cβγ, (C) αS205Cβγ and (D) αY209Cβγ receptor current traces are overlaid with WTαβγ normalized for current amplitude to illustrate some differences in macroscopic kinetics such as reduced extent of desensitization for αG157Cβγ and αS205Cβγ receptors. Minimal differences are seen in deactivation kinetics. For αG157Cβγ (C), no current trace from a 3ms exposure is available, a zoomed in image of deactivation after 1 sec exposure to GABA is shown instead.

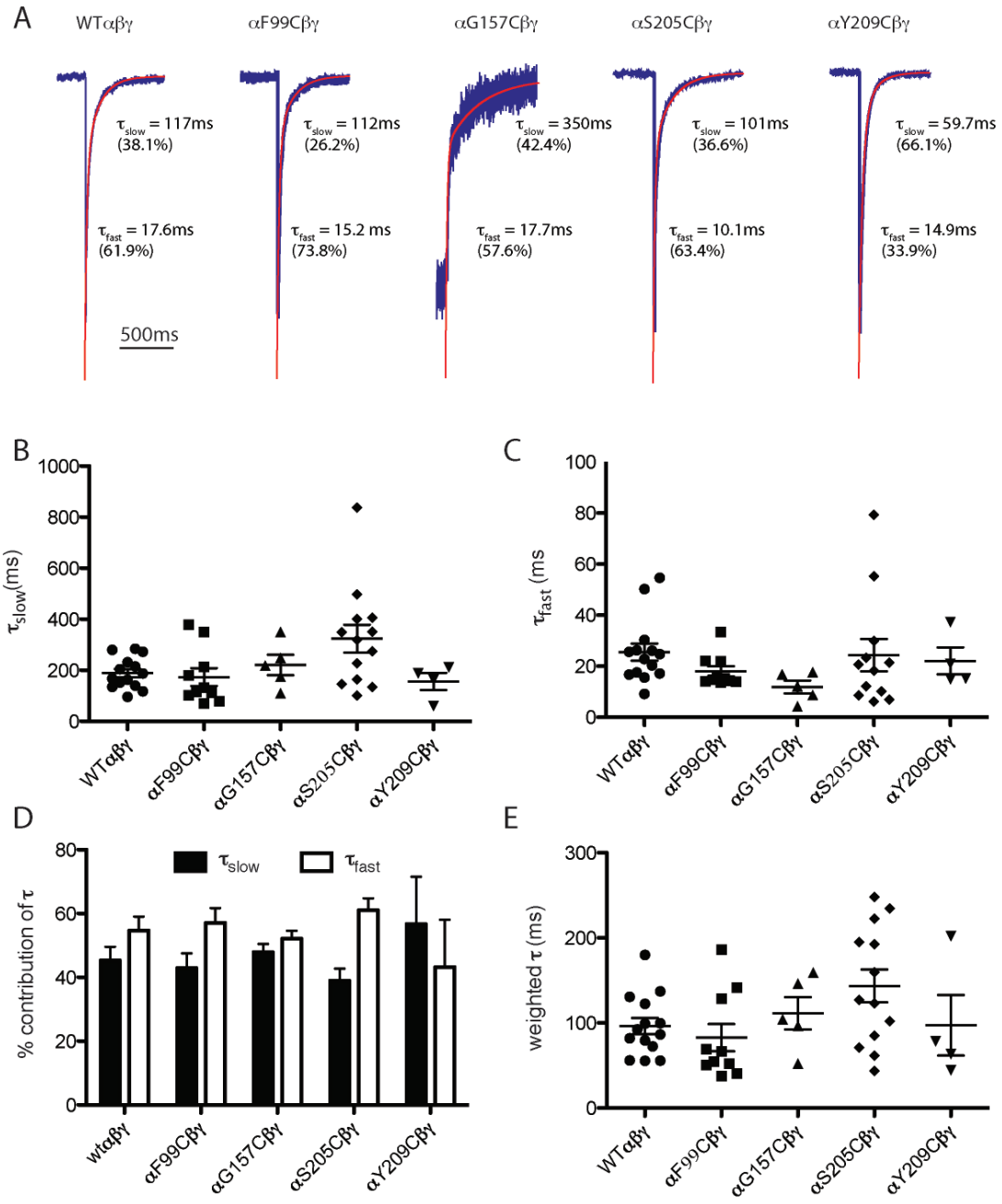
A
WTαβγ
αF99Cβγ
αG157Cβγ
αS205Cβγ
αY209Cβγ
τslow = 117ms (38.1%)
τfast = 17.6ms (61.9%)
τslow = 112ms (26.2%)
τfast = 15.2 ms (73.8%)
τslow = 350ms (42.4%)
τfast = 17.7ms (57.6%)
τslow = 101ms (36.6%)
τfast = 10.1ms (63.4%)
τslow = 59.7ms (66.1%)
τfast = 14.9ms (33.9%)
500ms
B
τslow(ms)
C
τfast (ms
D
% contribution of τ
τslow
τfast
E
weighted τ (ms)
WTαβγ
αF99Cβγ
αG157Cβγ
αS205Cβγ
αY209Cβγ
wtαβγ

Figure 4.4. Deactivation kinetics of mutant containing receptors are not different from WTαβγ receptors. (A) Deactivation of all current traces was well fit by two exponential functions. (B) τ_{slow}, (C) τ_{fast} and (E) $\tau_{weighted}$ for αF99Cβγ, αG157Cβγ, αS205Cβγ, αY209Cβγ receptors did not differ from WTαβγ kinetics. (D) The relative contributions of τ_{fast} and τ_{slow} were also unaltered from the WT receptor.

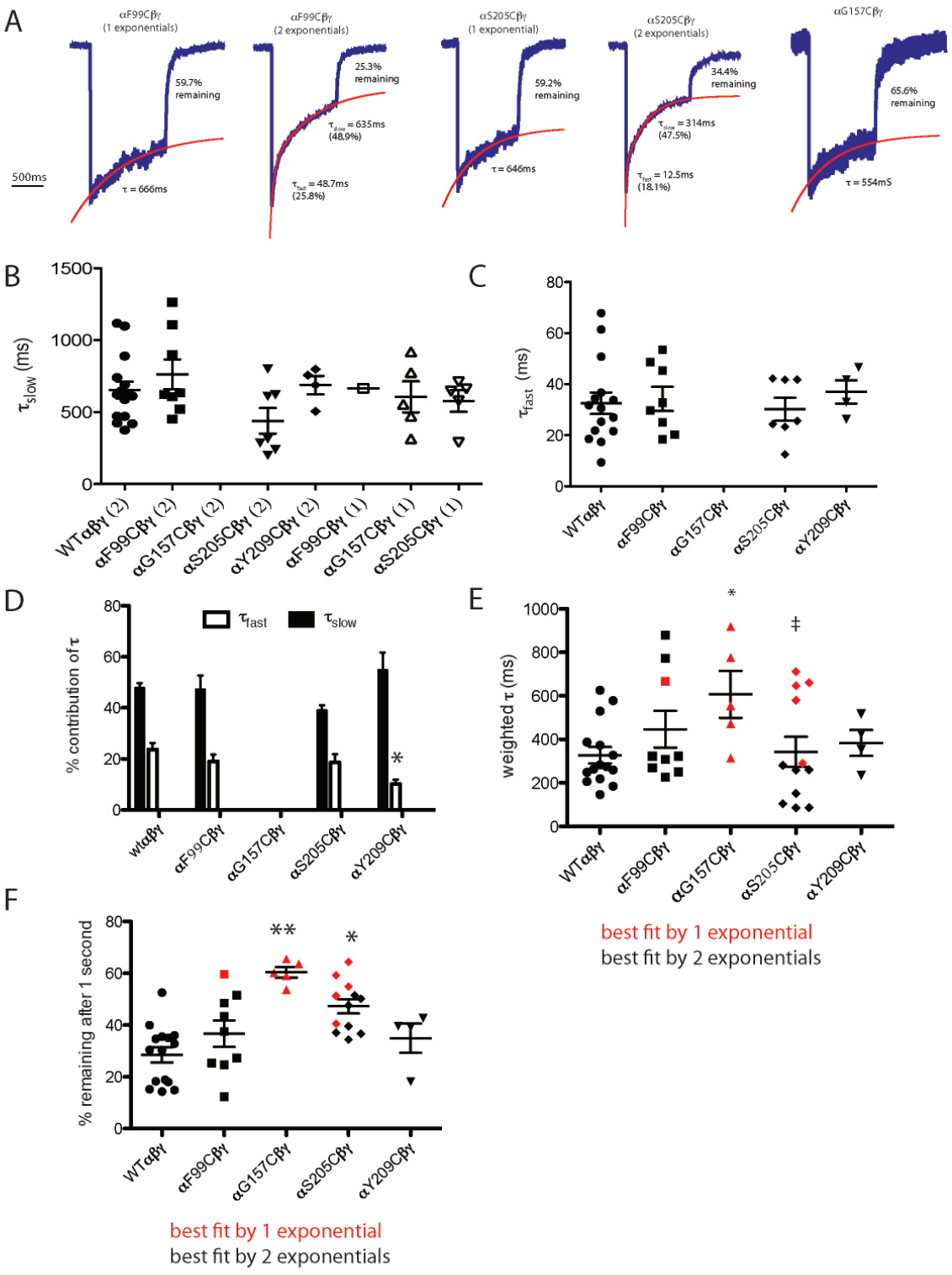
A
αF99Cβγ (1 exponentials)
59.7% remaining
τ = 666ms
500ms
αF99Cβγ (2 exponentials)
25.3% remaining
τslow = 635ms (48.9%)
τfast = 48.7ms (25.8%)
αS205Cβγ (1 exponential)
59.2% remaining
τ = 646ms
αS205Cβγ (2 exponentials)
34.4% remaining
τslow = 314ms (47.5%)
τfast = 12.5ms (18.1%)
αG157Cβγ
65.6% remaining
τ = 554mS
B
τslow (ms)
1500
1000
500
0
WTαβγ (2)
αF99Cβγ (2)
αG157Cβγ (2)
αS205Cβγ (2)
αY209Cβγ (2)
αF99Cβγ (1)
αG157Cβγ (1)
αS205Cβγ (1)
C
τfast (ms)
80
60
40
20
0
WTαβγ
αF99Cβγ
αG157Cβγ
αS205Cβγ
αY209Cβγ
D
τfast
τslow
% contribution of τ
80
60
40
20
0
*
wtαβγ
αF99Cβγ
αG157Cβγ
αS205Cβγ
αY209Cβγ
E
weighted τ (ms)
1000
800
600
400
200
0
*
‡
WTαβγ
αF99Cβγ
αG157Cβγ
αS205Cβγ
αY209Cβγ
best fit by 1 exponential
best fit by 2 exponentials
F
% remaining after 1 second
80
60
40
20
0
**
*
WTαβγ
αF99Cβγ
αG157Cβγ
αS205Cβγ
αY209Cβγ
best fit by 1 exponential
best fit by 2 exponentials

Figure 4.5. Desensitization of mutant containing receptors vary in several kinetic measurements from WTαβγ receptors. (A) Some αF99Cβγ, S205Cβγ and all αG157Cβγ receptor current traces were best fit by a single exponential function. Time constants from single exponential fits were similar to those of the τ_{slow} from current traces fit by two exponentials and are included in chart (B) with the number of receptor and number exponential fits labeled in parenthesis. (C) τ_{fast} is shown for those current traces fit best by two exponentials. (D) The relative contributions of τ_{fast} and τ_{slow} for those current traces fit by two exponentials differed from the WT receptor only in the τ_{slow} for αY209Cβγ. (D) Average and SEM of $\tau_{weighted}$ from all data are indicated by the box and whiskers. Individual $\tau_{weighted}$ are indicated by each point, those in black from traces fit by two exponential functions, those in red fit by a single exponential function. $\tau_{weighted}$ differs from WT only for αG157Cβγ receptors and for αS205Cβγ if considering only those receptors fit best by a single exponential function ($\tau_{weighted}$ = 577 ± 75, Table 3). Despite minimal differences in time constants, percent of current remaining after 1sec exposure to 10mM GABA is significantly increased in αG157Cβγ and S205Cβγ receptors fit by both one and two exponential functions. *$p<0.05$, **$p<0.01$ by one-way ANOVA. In some cases data from single exponential fits differs from WT for αS205Cβγ receptors where average data from αS205Cβγ receptors does not, ‡ $p<0.05$.

A

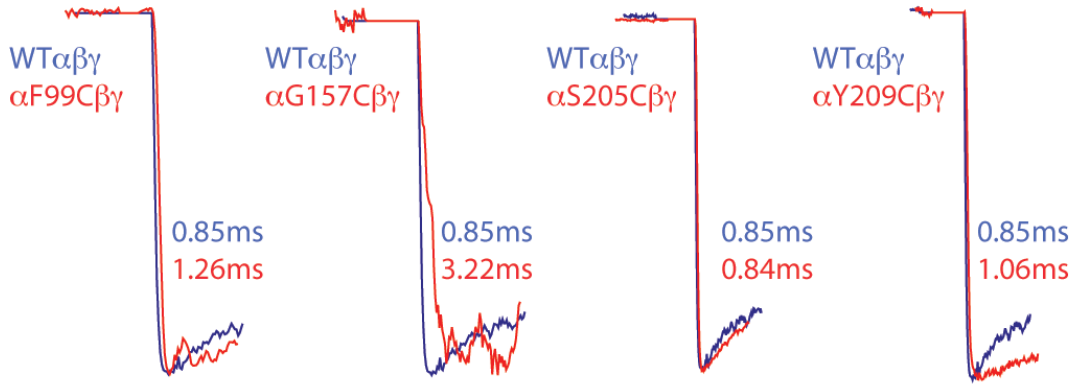

B

receptor	10-90% rise time (ms)	n
WTαβγ	1.05 ± 0.11	11
αF99Cβγ	1.26 ± 0.13	8
αG157Cβγ	2.92 ± 0.31**	5
αS205Cβγ	0.86 ± 0.08	8
αY209Cβγ	1.31 ± 0.26	4

C

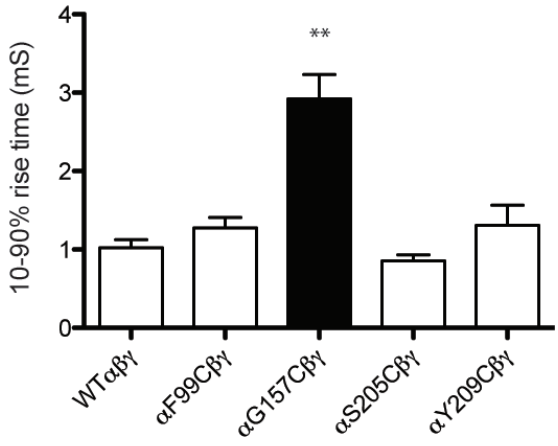

Figure 4.6. At 10mM GABA 10-90% rise time is slowed in αG157Cβγ receptors.

(A) Close up images of current onset of WTαβγ (blue) and mutant containing receptors (red) are overlaid normalized for current amplitude. (B) Mean current rise times ± SEM are tabulated. (C) Rise times are shown graphically, 10-90% rise time for αG157Cβγ is significantly different from WT. ** $p<0.01$.

A

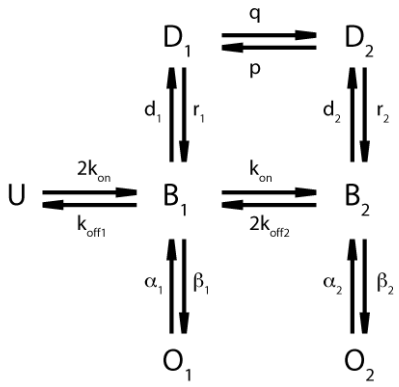

B

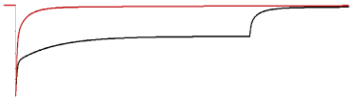

C

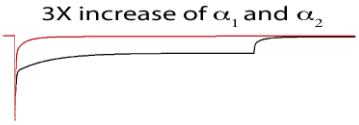

↑ extent of desensitization
↑ rate of desensitization
↑ rate of deactivation

D

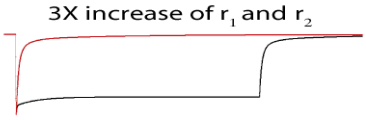

↓ extent of desensitization
↓ rate of desensitization
↑ rate of deactivation

E

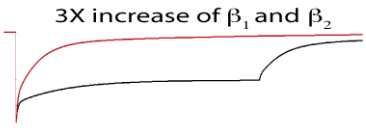

↓ extent of desensitization
↓ rate of desensitization
↓ rate of deactivation

F

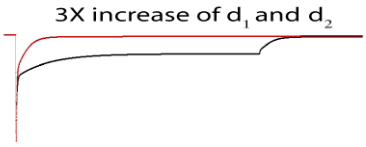

↑ extent of desensitization
↑ rate of desensitization
↓ rate of deactivation

G

	B	C	D	E	F
k_{on}	7.4×10^6	-	-	-	-
k_{off1}	8	-	-	-	-
k_{off2}	271	-	-	-	-
β_1	400	-	-	1200	-
α_1	2800	8400	-	-	-
β_2	2500	-	-	7500	-
α_2	1000	3000	-	-	-
d_1	12	-	-	-	36
r_1	3.2	-	9.6	-	-
d_2	371	-	-	-	1113
r_2	115	-	345	-	-
p	0.03	-	-	-	-
q	5.7	-	-	-	-

Figure 4.7. Simulation of macroscopic kinetics from 1sec and 3ms GABA pulse. Simulations based on microscopic kinetic rates publish in (Laha and Wagner, 2011) using the kinetic scheme show in (A) were run to demonstrate the effects of specific microscopic rates. (B) The simulation run with the microsopic rates as published closely resembles data from WT$\alpha\beta\gamma$ receptors. Increasing the rate of channel closing (α_1 and α_1) (C), the rate of resensitizing (r_1 and r_2) (D), the rate of channel opening (β_1 and β_2) (E), or the rate of entering the desensized state (d_1 and d_2) (F) alters macroscopic kinetics. Traces (D) and (E) show reduced extent of desensitization, with deactivation affected to a lesser extent in (D). These data more closely resemble macroscopic kinetics seen in αS205C$\beta\gamma$ receptors and provide some insight into kinetic modeling that may indicate microscopic rates affected by this mutation. (G) Table of rates used in simulations.

A

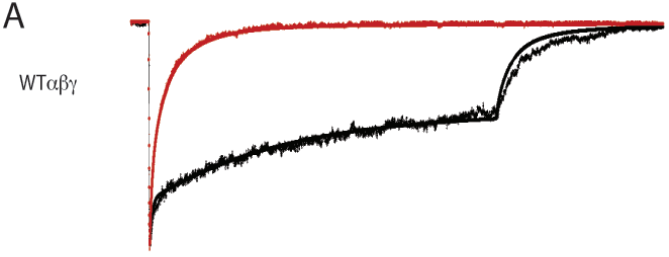

B

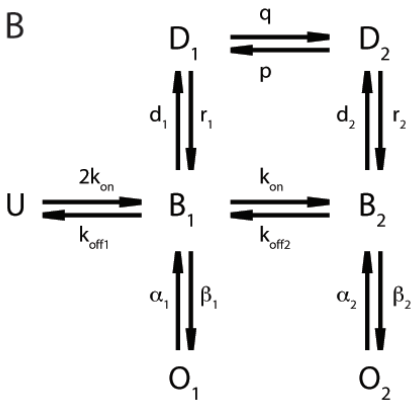

C

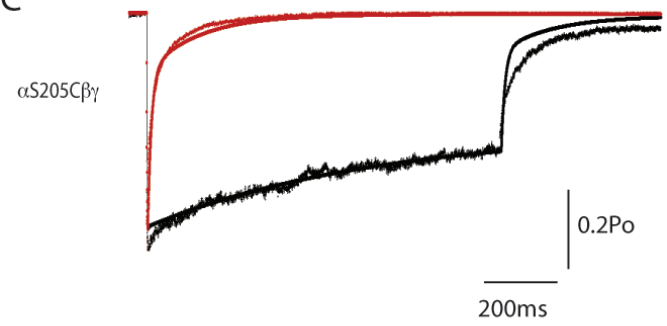

D

	WTαβγ	αS205Cβγ
k_{on}	1.9×10^6	1.9×10^6
k_{off1}	4.9	5.8
k_{off2}	270	**600**
β_1	510	530
α_1	3300	3300
β_2	1600	1000
α_2	380	380
d_1	4.9	**2.0**
r_1	1.3	0.9
d_2	410	430
r_2	120	**340**
p	3.1	2.7
q	0.1	**0.03**

Figure 4.8. Kinetic Modeling of WTαβγ and αS205Cβγ illustrate possible rates that could influence altered kinetics. The 7 state markov models that best fits WTαβγ and (A) αS205Cβγ (C) is shown (B) (U, unbound; B, bound; O, open; D, desensitized). Rates are tabulated (D), units are sec^{-1} except for GABA binding steps, which are $molar^{-1}$ sec^{-1}. Rates for αS205Cβγ that are altered more than two-fold from WT are shown in bold. Black traces are 1 sec pulse overlaid with model fit, and red pulse is 3ms pulse overlaid with model fit. Both pulses were fit simultaneously.

Table 4.1. Concentration Response data from two electrode voltage clamp recordings in *Xenopus laevis* oocytes.

Loop	receptor	EC_{50} (μM)	n_H	n	I_{max} range (μA)
	WTαβγ	18.4 ± 4.4	1.50 ± 0.09	5	8.4 - 11.6
A	αD97Cβγ	485 ± 67**	0.66 ± 0.10**	5	2.3 - 4.0
	αF99Cβγ	391 ± 94*	0.75 ± 0.06**	7	2.7 - 3.1
B	αG157Cβγ	408 ± 93*	0.65 ± 0.03**	8	1.4 - 4.1
	αA160Cβγ	560 ± 138**	0.60 ± 0.04**	6	3.3 - 5.0
C	αS205Cβγ	230 ± 126*	1.08 ± 0.20*	3	2.6 - 7.7
	αT206Cβγ	268 ± 58.0*	0.59 ± 0.05**	3	1.9 - 2.8
	αY209Cβγ	319 ± 170*	0.68 ± 0.13**	3	3.5 - 8.8

Data are mean ± SEM for n experiments. n_H values are calculated Hill coefficients. I_{max} range is the lowest and highest maximal GABA current amplitude measured for each of the receptors. Values significantly different from wild type $\alpha_1\beta_2\gamma_2$ are indicated (*, $p < 0.05$, **, $p < 0.01$)

Table 4.2. Deactivation kinetic measurements for WT and mutant containing receptors

receptor	τ_{slow} (ms)	$\%\tau_{slow}$	τ_{fast} (ms)	$\%\tau_{fast}$	$\tau_{weighted}$ (ms)	I_{max} range (pA)	n
WTαβγ	189 ± 16.3	45.3 ± 4.3	25.5 ± 3.4	54.7 ± 4.3	96.3 ± 9.6	53-973	14
αF99Cβγ	169 ± 32.9	42.9 ± 4.6	17.3 ± 2.3	57.1 ± 4.6	82.6 ± 16.1	32-785	10
αG157Cβγ	248 ± 37.2	49.1 ± 2.9	12.7 ± 3.1	50.9 ± 2.9	126 ± 15.1	25-38	4
αS205Cβγ	324 ± 54.4	39.0 ± 3.7	36.6 ± 17.7	61.0 ± 3.7	143 ± 19.4	23-765	13
αY209Cβγ	156 ± 3.3	56.8 ± 14.8	22.1 ± 5.3	43.2 ± 14.8	97.2 ± 35.6	56-304	4

Data are mean ± SEM for n experiments. Deactivation after 3ms and 1sec pulse of 10mM GABA are grouped. All current traces were well fit by biexponential functions. I_{max} range is the range of max current amplitudes for recorded traces.

Table 4.3. Desensitization kinetic measurements for WT and mutant containing receptors

receptor (exponentials fit)	τ_{slow} (ms)	$\%\tau_{slow}$	τ_{fast} (ms)	$\%\tau_{fast}$	$\tau_{weighted}$ (ms)	current remaining after 1 sec (%)	n
WTαβγ (2)	653 ± 59	47.8 ± 1.9	32.5 ± 4.2	23.7 ± 2.5	327 ± 38	28.5 ± 2.9	15
αF99Cβγ (1)	666	-	-	-	666[a]	59.7[a]	1
αF99Cβγ (2)	763 ± 104	47.2 ± 5.5	34.2 ± 4.7	19.0 ± 2.7	419 ± 90	33.8 ± 4.8	8
αF99Cβγ (all)					435 ± 88	36.7 ± 5.1	9
αG157Cβγ (1)	607 ± 108	-	-	-	607 ± 108*	60.4 ± 2.1**	5
αS205Cβγ (1)	577 ± 75				577 ± 75*	54.1 ± 4.0**	5
αS205Cβγ (2)	439 ± 88	39.0 ± 2.0	30.2 ± 4.4	18.6 ± 3.2	175 ± 33	42.4 ± 2.7*	7
αS205Cβγ (all)					343 ± 31	47.3 ± 2.8*	12
αY209Cβγ (2)	688 ± 65	54.8 ± 6.9	37.0 ± 4.6	10.2 ± 1.7*	383 ± 60	35.0 ± 5.6	4

Data are mean ± SEM for n experiments. Desensitization is in the continued presence of 1sec pulse of 10mM GABA. All WTαβγ and αY209Cβγ current traces were all well fit by biexponential functions and αG157Cβγ current traces were best fit by a single exponential. αF99Cβγ and αS205Cβγ had receptors fit best by both one and two exponential functions. For these receptors mean of current remaining and $\tau_{weighted}$ are shown for grouped populations (all) those traces fit by a single exponential (1) and those fit best by two exponentials (2). In the case of current traces fit best by a single exponential that exponential is tabulated as τ_{slow} as it is statistically indistinguishable from the WT τ_{slow}. Values significantly different from WTαβγ are indicated (*, $p < 0.05$, **, $p < 0.01$). [a]These values are apparently different from WT but differences cannot be assessed by ANOVA as n = 1.

CHAPTER 5. Discussion and Future Directions

$GABA_A$ receptors are crucial for neuronal signaling. The myriad pharmaceuticals that target these receptors are invaluable to human health. Diazepam, lorazepam and phenobarbital are all on the World Health Organization essential medicines list, indicating the "minimum medicine needs for a basic health-care system" (WHO, 2011). Diazepam, trade name Valium, is widely used today and at its peak sales in 1978 sold 2.3 billion pills (Sullivan, 2005). Valium is so pervasive in our healthcare and culture it is even widely credited as the inspiration for the Rolling Stones song "Mother's Little Helper." Current usage of BZDs is widespread, zolpidem was the 15th most prescribed drug in 2010 at approximately 38 million prescriptions (IMS, 2011). Despite the large variety of BZD site ligands available and their widespread use and value in the treatment of anxiety, seizure disorders, and sleep disorders there is much to still learn about these drugs and their actions. More detailed information about how these drugs interact with the $GABA_A$ receptor to exert their effects will aid in the design of drugs with reduced side effects and abuse potential as well as allow for targeted design of drugs for specific uses. For example, this information could lead to the development of α_5 selective inverse agonists that can be used to treat cognitive dysfunction, an ever-expanding issue with an increasing elderly population, or to explore the mechanisms by which zolpidem can increase responsiveness of patients in vegetative states (Shames and Ring, 2008, Whyte and Myers, 2009).

5.1 Benzodiazepine binding site residues: roles in binding and efficacy

Like any drug, the utility of BZDs relies on two basic components: the ability of the drugs to bind with adequate affinity, and the ability of a drug to exert an effect while occupying the binding site (efficacy). These basal elements of protein-ligand interaction are affected by protein structure not only in a limited, regional sense but also by the protein as a whole, its substituent components or domains, and even other interacting proteins. At the local level there are amino acids that make up the immediate binding site, these are structures within close proximity to the bound ligand that interact with the ligand. The interactions can be hydrophobic and/or electrostatic. For example, nonpolar residues that interact with a nonpolar ligand, amino acids that hydrogen bond to the ligand or residues that contribute to cation-pi interactions. In addition, some residues may dictate the physical shape of the site and could contribute to repulsive forces such as steric hindrance.

Residues within the binding pocket contribute to both drug binding and efficacy. Some residues affect drug binding directly or can influence movements within the binding site that are the origin of conformational movements caused by ligand interactions. These local movements cause downstream actions that ultimately shape the efficacy of a drug. At the agonist binding site of pentameric ligand gated ion channels (pLGICs) local structural rearrangements caused by orthosteric agonists and antagonists have been proposed. Using AChBP as an analog of the extracellular ligand binding domain, it has been shown that agonists induce a closure of loop C over docked ligands, whereas antagonist binding either causes an outward movement or does not affect loop C mobility (Hansen et al., 2005). More recently a crystral structure of GLIC in the presence of ligands supports movement of loop C (Pan et al., 2012). Beyond the binding

site ligand binding also elicits long range conformational movements. Work from Nigel Unwin on the nAChR suggests that binding of agonist sets in motion a twisting of the β sandwich ECD that is propagated through interactions at the ECD-TMD interface to a rotation of the M2 helix resulting in channel opening (Unwin, 2005). These movements are thought to be triggered by loop C closure (Cheng et al., 2006). Recent work suggests that loop C closure is indicative of the "flipped state", a pre-activated bound state (Mukhtasimova et al., 2009). Comparisons of the GLIC and ELIC structure indicate a twisting movement in the ECD, with a coordinated, opposing twist in the TMD that leads to channel opening (Bocquet et al., 2009). My data in Appendix 1 of this thesis support this idea. Disulfide crosslinking loop 9 of one subunit to the M2-M3 loop of an adjacent subunit results in inhibition of I_{GABA}, consistent with this hypothesis as this crosslink would inhibit an opposing twisting motion.

The conformation motions underlying BZD actions are less well known. Several groups have described conformational movements that are induced by BZD positive modulation. Experiments from our lab implicate γ_2 loop F in the actions of BZD positive modulators, but not in the effects of the negative modulator DMCM (Hanson et al., 2008). In addition, preventing movement of the γ_2 loop 9 by disulfide trapping decreased zolpidem (ZPM) and flurazepam potentiation of I_{GABA} consistent with a role in positive modulation. The crosslinking did not affect negative modulation by DMCM further implicating the γ_2 loop F/ loop 9 region in BZD positive modulation (Hanson and Czajkowski, 2011). Additional studies show that BZD binding causes movements at the GABA binding site as well as in the transmembrane M3 segment (Williams and Akabas, 2000, Kloda and Czajkowski, 2007, Sancar and Czajkowski, 2011). These studies

indicate structures distant from the BZD binding site can be altered by BZDs and that these movements differ by the type of BZD modulator. Little is known about the local movements at the BZD binding site where these long range movements originate and what dictates if a BZD is a positive, negative or zero modulator. My studies in chapters 2 and 3 of this thesis address this knowledge gap and identified residues within the BZD binding site that contribute to binding and efficacy. The data provide framework for understanding the local origins of conformational pathways that dictate BZD efficacy.

Residues that form the BZD binding site have been identified by photoaffinity labeling, the substituted cysteine accessibility method (SCAM), and chimeragenesis (Davies et al., 1996, Duncalfe and Dunn, 1996, Sigel and Buhr, 1997, Boileau and Czajkowski, 1999, Kucken et al., 2000, Sawyer et al., 2002, Kucken et al., 2003). More recently, homology modeling combined with *in silico* docking studies have also been instrumental in developing a structural picture of the BZD binding site (Richter et al., 2012).

Radioligand binding studies described in chapter 2 greatly expanded our understanding of specific residues involved in the high affinity binding of the atypical BZDs, eszopiclone (ESZ) and ZPM. The molecular docking results in that chapter agreed with the binding results. Mutations that caused significant disruption to drug binding correlate with those residues that had direct interactions (hydrogen bonds) with the drug *in silico*. In chapter 3, I expanded on this study and assessed the effects of specific mutation on the efficacy of these drugs. Data from both studies allowed me to distinguish which residues were important for drug binding, drug efficacy or both. This work is crucial for understanding how atypical benzodiazepines interact with the BZD

binding site. Teasing apart the participation of each of the residues in binding versus efficacy paves the way for *in silico* drug screens or rational drug design.

Molecular docking in chapter 2 suggests that some ligands can dock in a variety of orientations. I envision that point mutations that cause altered efficacy in chapter 3 may be the result of a disturbed binding site forcing a different ligand orientation. Distinct orientation of ligands within the binding site can result in interactions with different residues of the binding site that contribute to altered binding affinity, or efficacy (maximal potentiation). I further hypothesize that BZDs that elicit different modulation (i.e. agonism, antagonism, or inverse agonism) induce distinct local conformational movements within the BZD binding site that trigger different long range conformational movements. Moreover, BZD positive modulators with varying degrees of efficacy (i.e. FZM has maximal potentiation of 2.3, whereas ESZ has a maximal potentiation of 2.8) have an overall potentiation that is the net result of a multiple local conformational movements triggered by distinct interactions within the binding site. Further characterization of mutations at the BZD binding site may provide evidence into the individual conformational movements resulting in altered I_{GABA} kinetics. These same residues may be the trigger points through which bound BZDs exert their effects on the kinetics of I_{GABA} and thus dictate their modulator type or degree of efficacy.

5.2 Effects of mutations at the benzodiazepine binding site on $GABA_A$ receptor kinetics

Ultimately the efficacy of a BZD is due to the conformational movements induced by BZD binding and how these perturbations to protein structure affect the macroscopic

kinetics of I_{GABA}. Allosteric modulation by BZDs has distinct effects on $GABA_A$ receptor kinetics. At the single channel level, diazepam act to increase P_0 by increasing burst frequency (Rogers et al., 1994a). In whole cells, with rapid solution exchange into saturating GABA, diazepam acts to prolong GABA deactivation (Bianchi et al., 2009). This mimics what happens at the synapse, as release of GABA into the synaptic cleft results in mM concentrations of neurotransmitter within hundreds of microseconds (Kleinle et al., 1996). Resultantly, IPSCs are prolonged as a result of slowed deactivation in the presence of BZDs (Strecker et al., 1999). BZDs been shown to speed desensitization (Mellor and Randall, 1997), prolong deactivation (Mellor and Randall, 1997, Strecker et al., 1999, Bianchi et al., 2009), and decrease 10-90% rise time (Lavoie and Twyman, 1996).

There is some disagreement as to the microscopic kinetic alterations caused by BZDs that result in these macroscopic phenomena. Studies examining the ability of BZDs to potentiate currents elicited by saturating concentrations of partial agonists and, at high concentrations, to directly gate mutant $GABA_A$ receptors with a gain of function suggest BZDs shift the $GABA_A$ receptor closed to open state equilibrium (alter channel gating) (Downing et al., 2005, Rusch and Forman, 2005, Campo-Soria et al., 2006). Other studies suggest BZDs alter the receptor's microscopic binding affinity for GABA (Twyman et al., 1989, Rogers et al., 1994b, Lavoie and Twyman, 1996, Mellor and Randall, 1997, Thompson et al., 1999, Goldschen-Ohm et al., 2010). In a recent study, BZDs have been proposed to increase the probability of receptors transitioning into a "flipped" pre-gating state (Gielen et al., 2012). Overall, experiments showing BZDs alter $GABA_A$ receptor affinity for GABA are convincing. However, BZDs acting solely as a

modulator of GABA binding affinity does not explain the ability of BZDs to directly gate a mutant receptor or to increase partial agonist efficacy. I believe BZDs work through a mechanism that can alter both GABA binding and channel gating. This belief is based on experiments supportive of both hypotheses and an understanding that protein behavior is highly nuanced and heavily amenable to many forms of modulation. Structural perturbations caused by ligand binding or mutation often have long range structural repercussions and broad ranging effects on $GABA_A$ receptor functioning, it is not hard to imagine BZD binding could impact many aspects of $GABA_A$ receptor functioning.

My two electrode voltage data presented in chapter 4 indicates point mutations (another type of structural perturbation) in the BZD binding site cause changes in the macroscopic kinetics of GABA activation. These mutations in the α subunit increase GABA EC_{50} and alter current responses. Overall, these mutations appear to have slower activation, decreased extent of desensitization, and increased rate of deactivation when examined using two electrode voltage clamp. These mutations are in the α subunit and are located at both α–β and α–γ interfaces distant from the GABA binding sites. Two electrode voltage clamp is not suitable to accurately resolve macroscopic kinetics as slow solution exchange rates blur kinetic transitions. Therefore, the kinetic affects of these mutations were further assessed by excised patch clamp recordings with rapid solution exchange. Patch clamp data presented in Chapter 4 describe the kinetic effects of several point mutations in the BZD binding site. αS205C and αG157C decrease the extent of desensitization after 1 sec in 10mM GABA, and αG157C increased the 10-90% rise time. The mutations at the BZD binding site caused nearly opposite kinetic effects than BZD positive modulators. The mutations had relatively minimal effects on deactivation, they

decreased extents of desensitization and slowed current activation rate compared to the WT receptor. It is not surprising that a single cysteine mutation would not mimic the effects on kinetics as occupation of a binding site by a small molecule. In addition, the mutations I made are located at two interfaces, whereas BZDs bind at a single α–γ interface (though recent work suggests a low affinity site at the α–β interface as well (Ramerstorfer et al., Baur et al., 2008, Sieghart et al., 2012)). Concatameric receptors composed of tethered concatameric subunits could be used to isolate mutations to either the α–γ or α–β interface to independently evaluate their effects on macroscopic kinetics.

5.3 Subunit interface rearrangements: A common mechanism underlying GABA induced channel activation and BZD modulation of $GABA_A$ receptor current responses

Interactions at subunit interfaces are of clear importance to the functioning of $GABA_A$ receptors. Photoaffinity labeling has shown that many ligands bind at subunit interfaces, such as GABA (Casalotti et al., 1986, Smith and Olsen, 1994), BZDs (Davies et al., 1996, Duncalfe and Dunn, 1996, Sawyer et al., 2002), and anesthetics (Li et al., 2006, McCracken et al., 2010). Perturbations at various interfaces are capable of causing structural changes in the receptor, both in the channel region but also in effects at other subunit-subunit interfaces in the ECD as well. BZD binding has been shown to cause alterations at the distant GABA binding site (Boileau et al., 1998, Holden and Czajkowski, 2002, Sharkey and Czajkowski, 2008b, Goldschen-Ohm et al., 2010, Sancar

and Czajkowski, 2011). Of course BZDs can also cause alterations to the kinetics of I_{GABA} as stated above.

These types of long range perturbations can be caused, not only by ligand binding, but by mutations. Naturally occurring mutations at subunit interfaces have profound affects on $GABA_A$ receptor functioning. The γ_2R43Q mutation at the γ_2–β_2 interface was discovered in patients with epileptic disorders (Wallace et al., 2001). From modeling studies, γR43 appears to be involved in a network of inter subunit electrostatic interactions with βR117 and γE178 (Cromer et al., 2002). The γR43Q mutation breaks these interactions and has profound affects on both GABA and BZD kinetics (Goldschen-Ohm et al., 2010).

Additional evidence of long range structural perturbations come from engineered mutations in the $GABA_A$ receptor. The appendix of this thesis describes mutations in loop 9 of the β subunit. Loop 9 spans a region near the GABA binding site to the ECD-TMD interface at the non-binding α–β and γ–β interfaces. Mutations in this region had significant effects on GABA $EC_{50,}$ and modification of the introduced cysteines by MTS reagents decreased I_{GABA}. Most notable of these mutations is Q185C. This mutation caused a significant left shift in GABA EC_{50}. Previous work suggested that Q185 is involved in stabilizing the closed state of the receptor (Williams et al., 2010). I used disulfide trapping to examine the proximity of Q185C and loop 9 of the β subunit to the M2-M3 loops of the adjacent α or γ subunit. Using disulfide trapping to inhibit movements between these domains I tested the hypothesis that movements in these non-binding site interfaces were important for $GABA_A$ receptor activation. My experiments demonstrate that Q185C can form spontaneous crosslinks across subunits at both the α–β

and γ−β interface to mutant cysteine residues in the M2-M3 loop of opposing subunits. The data were important for determining that homology models of the $GABA_A$ receptor should resemble the GLIC and ELIC structures, not the cryo-EM structure of the nAChR in this region. These crosslinks significantly decreased the amplitude of current elicited by GABA (binding in the ECD at the β−α interface), or by etomidate (binding in the TMD at the β−α interface). The data suggested that, regardless of the ligand, channel activation is accompanied by structural rearrangements at non-binding site subunit interfaces near the border of the TMD and ECD.

My data in combination with data from ligands and mutations at other $GABA_A$ receptor interfaces conveys the importance of subunit interfaces in the communication of conformational movements contributing to channel activity. This concept pertains not just to pLGIC function but to the utility of many protein-protein interfaces as druggable targets. In fact, benzodiazepine derivatives are among the drugs that have been found to block the interaction of P53 and MDM2, an interaction that inhibits the check point activities of P53 and is found in 50% of cancers (Zhu et al., 2011). Such protein-protein interfaces are an appealing target of drug discovery (Winter et al., 2012).

5.4 Future experimentation

Much is known about benzodiazepine interactions with the $GABA_A$ receptor as described in earlier chapters. There are many known ligands at the BZD binding site that have varying efficacy and selectivity. However, what chemical moieties of a BZD dictate its efficacy or selectivity are unknown and increased information about how BZDs fit into the binding site might make this level of specificity possible through more

focused drug screens and, eventually, through rational drug design. Ultimately, a true understanding of how BZDS interact with the $GABA_A$ receptor requires atomic level structures.

With the recent availability of readily purified homologous proteins and the expanded experimental methods available with purified proteins it is enticing to utilize these proteins for the study of BZDs. Data from the Uhlens lab recently presented at the Society for Neuroscience meeting has shown that ELIC current can be inhibited by BZDs. Additionally, protein crystals of ELIC grown in the presence of BZDs show BZDs docked at the ECD subunit interfaces and reveal a novel BZD binding site located along the ECD channel vestibule. Though this information will be beneficial, it may be more informative to engineer in specific residues seen within the BZD binding site of the $GABA_A$ receptor to more accurately mimic BZD binding in its native site.

Using previous data describing residues that contribute to BZD binding as well as data from chapters 2 and 3 of this thesis it would be possible to select residues to construct a putative BZD binding site in both GLIC and ELIC. Engineering a BZD binding site into one of the prokaryotic channels poses several problems. Firstly, both GLIC and ELIC are homopentameric receptors. Though it is possible to insert mutations onto both sides of a single subunit so it orients into an engineered binding site, this would create a receptor with five such binding sites. Additionally, mutating in a BZD binding site to ELIC would engineer out the agonist binding site. ELIC has been shown to be activated by primary amines that bind at the subunit interface in the ECD, under loop C (Zimmermann and Dutzler, 2011, Gonzalez-Gutierrez et al., 2012). It is possible to overcome this by constructing concatameric receptors, some subunit interfaces with the

native binding site, some with engineered BZD sites. Additionally, injection or transfection of both WT and mutant RNA or DNA may allow mixed receptors to assemble with both binding sites. In GLIC, the agonist binding site is unknown. However, GLIC is activated by protons and it is unlikely that proton binding is isolated to a single location in the receptor or that this binding would easily be occluded.

There are caveats to these type of experiments including the large amount of mutagenesis involved which may affect expression or trafficking of the receptor or may alter the receptor so heavily as to not be a good representation of a BZD binding site. However, these chimeric types of receptors would be very useful in attaining an atomic level structure of BZDs bound with in a $GABA_A$ receptor type binding site. Information about ligand-amino acid interactions and ligand orientation could be used in future small molecule design. Additionally this type of chimeric receptor could be helpful in studying hypotheses from this thesis about the effect of ligand orientation on BZD efficacy and modulator type. For example, specific mutations have been shown to change the type of modulation a BZD ligand elicits compared to the WT receptor. At WT receptors, ESZ is a potent positive modulator, data from chapter 3 indicates that in the presence of αF99C containing receptors, ESZ is a negative modulator. Crystal structures of prokaryotic chimeras containing the "WT" vs the F99C binding site would indicate ligand orientation and provide clues as to the effects of orientation on modulator type. This information could be a basis for design of drug structures that would find an intended orientation within the binding site to exert specific modulatory effects. Crystal structures of GPCRs have been utilized to indicate the importance of ligand orientation as well as for drug screens to optimize chemical compounds for a binding site (Shoichet and Kobilka, 2012).

Similarly, it is possible to use what is known about the structure of the BZD binding for drug screening. A recent study used homology models of the $GABA_A$ receptor and *in silico* docking algorithms to model diazepam in the BZD binding site and used this dock as the basis for structure based drug screens (Richter et al., 2012). This screen accurately identified known BZD site ligands and identified a potential new class of BZD site ligands, the 3-hydroxyoxindoles, that were verified by radioligand binding and electrophysiology experiments. Utilizing similar methods and information provided in this thesis, similar work could be conducted to dock structurally diverse BZD ligands and employ this as a starting point for additional drugs screens. Also, this approach could be useful in screening compounds that would be selective for different $GABA_A$ receptor subunit interface. Modeling could utilize the $\alpha_{1,2,3}$ and α_5 subunits with the γ_2 subunit, but also other interfaces that are not commonly thought of as BZD sensitive. It is known that α_4 and α_6 subunits can bind beta-carbolines and imidazobenzodiazpines (Ito et al., 1994, Derry et al., 2004). Additionally, the α_6 subunit can be covalently modified by diazepam analogs if it contains an R100C mutation. This diazepam "binding" confers positive modulation of I_{GABA} (Baur et al., 2008), suggesting that ligands that could bind to the native site could have BZD like effects at α_6 receptors. Additionally, work utilizing concatameric subunits limited an α_1H101C mutation (or the analogous mutations in other α subunits) to a single α subunit at the $\alpha-\beta$ interface in receptors containing a diazepam insensitive α_6 subunit at the $\alpha-\gamma$ interface. Covalently linking a diazepam analog to the α_xH101C$\beta_2\alpha_6\gamma_2\beta_2$ receptors at the $\alpha-\beta$ interface indicates BZDs may bind at this site (Baur et al., 2008). Further evidence for BZD actions at an $\alpha-\beta$ interface comes from a

screen of BZD ligands at $\alpha_1\beta_3$ receptors (containing no γ subunit) that found a low affinity for several drugs (Ramerstorfer et al., 2011, Sieghart et al., 2011).

Both atomic level structures of a chimeric BZD binding site and *in silico* docking studies would provide information about ligand orientation within the binding site. This would expand upon and verify data from my thesis. Ultimately, this type of information could be used to evaluate the hypothesis that ligand orientation, and thus interaction with specific amino acid residues within the binding site contribute to the efficacy of BZDs. This may provide information about what dictates BZD modulator type (agonist, antagonist, or inverse agonist). Data provided in this thesis expands our understanding of the local structures within the BZD binding site that contribute to the mechanisms by which BZDs bind and assert their affects. Further studies suggested in this chapter will utilize this data for methods that could lead to a focused approach to drug discovery.

APPENDIX 1: The β_2 subunit Loop 9 Region Is Involved in $GABA_A$ Receptor Activation

A1.1 Contributions

This work was a continuation of work completed by Jose Mercado. Dr. Mercado constructed the mutant containing subunits and performed the MTS reaction and general mutant characterization experiments. I performed experiments with double mutant containing receptors assessing ability to form intersubunit disulfide bridges. I contributed to data analysis, figure preparation and writing of the chapter.

A1.2 Abstract

Protein movements underlying Cys-loop ligand-gated ion channel (LGIC) gating are poorly understood. Molecular simulations of homo-oligomeric receptors and the acetylcholine binding protein (AChBP) indicate that neurotransmitter binding triggers movement of Loop 9. In hetero-oligomeric $GABA_A$ receptors ($GABA_A$Rs), Loop 9 is located at both agonist binding site and non-binding site subunit interfaces. This raises the question of whether Loop 9 movements at non-binding site interfaces are important for coupling agonist binding to channel gating. Loop 9 is comprised of a stretch of approximately 18-22 residues that spans from the Loop B binding site region to the C-terminal end of β-strand 9 that lies near the transmembrane domain. Therefore, β_2 Loop 9 is in an ideal position to transduce binding site movements from the Loop B region of the β_2 subunit to gating movements in the coupling interface and channel domain. Loop 9

residues in the β_2 subunit (W168-Q185; non-binding site interface) were mutated to cysteine, expressed with wild-type α_2 and γ_2 subunits in *Xenopus laevis* oocytes and the effects on $GABA_AR$ function examined using two-electrode voltage clamp. Mutations at 8 of 17 positions altered GABA EC_{50} indicating that cysteine substitutions at these positions altered GABA activation. The MTSEA-biotin rate of modification of W168C, V175C and Q185C varied in the presence of agonists and antagonists, indicating that GABA-induced channel gating and antagonist binding induce localized structural rearrangements. Additionally, disulfide trapping β_2 loop 9 to either the adjacent α or γ subunits' M2-M3 loop significantly decreased currents activated by GABA and etomidate indication that channel opening depends on conformational rearrangements at non-binding site interfaces.

A1.3 Introduction

Gamma-aminobutyric acid type A ($GABA_AR$), nicotinic acetylcholine (nAChR), $5HT_3$ serotonin and glycine receptors are members of the cys-loop superfamily of ligand-gated ion channels (LGIC) and mediate fast synaptic transmission throughout the nervous system (Karlin, 2002). Our understanding about the structure of these receptors has been advanced from the recent 4-Å resolution model of the nAChR (Unwin, 2005), the crystal structure of the related acetylcholine binding protein (AChBP) (Brejc et al., 2001, Celie et al., 2004b) and more recently the structures of homologous prokaryotic channels (Brejc et al., 2001, Hilf and Dutzler, 2008) and eukaryotic homolog, GluCl (Hibbs and Gouaux, 2011). Receptors in this superfamily are formed by five homologous or identical subunits assembled around a central ion-conducting pore. In each subunit, the N-terminal

~210 residues form an extracellular domain consisting predominately of β-strands that contains the neurotransmitter binding site. The principal subunit provides residues from Loops A, B, and C, whereas residues within Loops D, E, and F come from the complementary subunit (Galzi et al., 1990, Akabas, 2004). The extracellular domain (ECD) of each subunit is connected to a transmembrane domain (TMD) comprised of four α helices (M1-M4) where the "gate" of the ion channel is located (Fig. A1.1).

The GABA binding site lies some distance (~50 Å) from the channel gate located in the transmembrane domain, a key question in the field is focused on elucidating the structural rearrangements associated with coupling GABA binding to channel gating. Insights into the structural changes associated with neurotransmitter binding and gating have been gained from photolabeling studies (Leite et al., 2003) and molecular simulations (Nury et al., Gao et al., 2005b, Henchman et al., 2005) of homo-oligomeric receptors as well as the related AChBP (Brejc et al., 2001, Celie et al., 2004b). More recently, comparing the crystal structure of prokaryotic LGICs in an assumed open and presumed closed state have led to hypotheses about the structural rearrangements involved in channel gating (Hilf and Dutzler, 2008, Bocquet et al., 2009). These studies suggest that ligand binding induces conformational rearrangements of Loop 9 as well as Loop C in the binding site. Loop 9 is comprised of a stretch of approximately 18-22 residues that link β-strand 8 and β-strand 9 in the extracellular domain of each subunit (Fig. A1.1). In hetero-oligomeric $\alpha_1\beta_2\gamma_2$ $GABA_A$Rs, Loop 9 is located on: 1) α_1 subunits where it forms part of the agonist binding site with the neighboring β_2 subunit, 2) the γ_2 subunit where it forms part of the benzodiazepine binding site with the neighboring α_1 subunit, and 3) β_2 subunits where it forms a non-binding interface with

either an α_1 or $\gamma_2$subunit (Fig. A1.1). This raises the question of whether Loop 9 movements in the β_2 subunits at non-binding site interfaces are important for coupling agonist binding to channel gating.

Loop 9 in the β_2 subunit of the $GABA_AR$ (W168-Q185) spans from the Loop B binding site region to the C-terminal end of β-strand 9 that lies near the TMD (Fig. A1.1). Thus, β_2 Loop 9 is in an ideal position to transduce binding site movements from Loop B to gating movements in the coupling interface and TMD. Here, we used the substituted cysteine accessibility method (SCAM) to examine the structure, solvent accessibility and dynamics of the β_2 Loop 9 W168-Q185 region of the $GABA_AR$. In additiona, we used disulfide linking of engineered cysteines to assess the mobility of loop 9 and its proximity to the TMD of the neighboring α or γ subunits. Previous work in the Jenkins laboratory focused on this region, examining the effects on $GABA_AR$ activation in receptors containing alanine mutations of residues from G170-Q185 (Williams et al., 2009). They posit that Q185 in its native state helps to stabilize the closed state of the receptor our Q185C data support this conclusion.

Our data indicate that structural perturbation of the region alters GABA induced gating of the receptor. Moreover, we demonstrate that this region is solvent accessible and undergoes structural rearrangements during GABA and pentobarbitol (PB) gating of the channel consistent with this region acting as a dynamic element during channel gating transitions. Additionally, tethering the Q185C at the tip of loop 9 to the adjacent α or γ subunits inhibits I_{GABA} and $I_{etomidate}$ suggesting that mobility in this area is critical for channel gating and suggests a possible locale for translating ECD binding movments to gating transitions in the TMD.

A1.4 Materials and Methods

A1.4.1 Mutagenesis

Rat cDNAs encoding α_1 and β_2 $GABA_AR$ subunits were used for all molecular cloning and functional studies, γ_{2L} was used in receptors subjected to DTT and H_2O_2 to assay for crosslinking, all other studies used receptors containing γ_{2s}. Cysteine mutants were made using the QuickChange Site-Directed Mutagenesis Kit (Stratagene, La Jolla, CA). Mutagenic oligonucleotides were synthesized to introduce the desired mutation and a silent restriction site was used to screen for the desired mutations. All mutant cDNA was verified by double stranded cDNA sequencing to confirm that the desired point mutation was present and that the cDNA was free of additional mutations.

A1.4.2 Expression in *Xenopus laevis* Oocytes.

Oocytes were prepared as previously described (Boileau et al., 1998). Capped cRNAs encoding the α_1, β_2, γ_{2s}, β_2W168C, β_2R169C, β_2G170C, β_2D171C, β_2D172C, β_2N173C, β_2A174C, β_2V175C, β_2T176C, β_2G177C, β_2V178C, β_2T179C, β_2K180C, β_2I181C, β_2E182C, β_2L183C, β_2P184C and β_2Q185C subunits in the vector pUNI (Venkatachalan et al., 2007) were transcribed *in vitro* using the mMessage mMachine T7 kit (Ambion, Austin, TX). Single oocytes were injected within 24 hr with 27nL of cRNA (10ng/μL for α and β subunits, 100ng/μL per γ subunit) (Boileau et al., 1998). Oocytes were incubated at 18°C in ND96 (in mM: 96 NaCl, 2 KCl, 1 $MgCl_2$, 1.8 $CaCl_2$, and 5 HEPES, pH 7.2) supplemented with 100μg/mL gentamycin and 100μg/mL BSA for 2-14 days before use.

A1.4.3 Two-electrode Voltage Clamp.

Oocytes were continuously perfused at a rate of 5mL/min with ND96 while being held under two-electrode voltage clamp at -80 mV. The bath volume was ~200 μL. Stock solutions of GABA (Sigma-Aldrich, St. Louis, MO), SR-95531 (Sigma-Aldrich, St. Louis, MO) and pentobarbital (Research Biochemicals, Natick, MA) were prepared fresh in ND96. Borosilicate electrodes (Warner Instruments, Hamden, CT) were filled with 3M KCl and had resistances between 0.7 to 2 MΩ. Electrophysiological data were acquired with a GeneClamp 500 (Axon Instruments, Foster City, CA) interfaced to a computer with an ITC16 analog-to-digital device (Instrutech, Great Neck, NY) and recorded using Whole Cell Program 3.2.9 (kindly provided by J. Demspter; University of Strathclyde, Glasgow, Scotland).

A1.4.4 Concentration-Response Analysis.

Concentration-response experiments were performed as described previously (Boileau and Czajkowski, 1999). In brief, GABA concentration-responses were scaled to a low, nondesensitizing concentration of GABA (EC_2-EC_{10}) applied just before the test concentration to correct for any slow drift in GABA-induced current (I_{GABA}) responsiveness over the course of the experiment. Currents elicited by each test concentration were normalized to the corresponding low concentration current before curve fitting. GraphPad Prism 4 software (San Diego, CA) was utilized for data analysis and fitting. Concentration-response data were fit to the following equation: $I = I_{max}/(1 + (EC_{50}/[A])^n)$, where I is the peak response to a given concentration of GABA; I_{max} is the maximum amplitude of current; EC_{50} is the concentration of GABA that evokes half-maximal response; [A] is the agonist concentration; and n is the Hill coefficient. For concentration response before and after DTT exposure, full concentration response

curves were performed before or after a 2 minute exposure to DTT. Stability of reduced disulphide bridges in the absence of H_2O_2 was assayed with pulses of GABA EC_{50}. EC_{50} I_{GABA} did not vary in double mutants (<5% change) after 2 minute exposure to DTT for the duration of the concentration-response analysis.

Etomidate concentration-response was performed as with GABA and fit with the same equation. 50mM stock solutions of etomidate (Tocris Bioscience, Ellisville, MO) were made in DMSO and diluted to working concentrations in ND96 (final DMSO concentration ≤ 2%).

To measure the sensitivity to SR-95531, GABA (EC_{50}) was applied via gravity perfusion followed by a brief (1 min) washout period before co-application of GABA (EC_{50}) and increasing concentrations of SR-95531. The response to the application of SR-95531 and GABA was normalized to the response elicited by the agonist alone. Concentration-inhibition curves were generated for each recombinant receptor, and the data were fit by non-linear regression analysis using GraphPad Prism software. Data were fit to the following equation: $1 - 1/(1 + (IC_{50}/[Ant])^n)$, where IC_{50} is the concentration of antagonist ([Ant]) that reduces the amplitude of the GABA-evoked current by 50% and *n* is the Hill coefficient. K_I values were calculated using the Cheng-Prussof correction: $K_I = IC_{50}/(1 + ([A]/EC_{50}))$, where [A] is the concentration of GABA used in each experiment and EC_{50} is the concentration of GABA that elicits a half-maximal response for each receptor (Cheng and Prusoff, 1973).

BZD potentiation of I_{GABA} was recorded at GABA (EC_5). Potentiation is defined as $(I_{GABA + DRUG}/I_{GABA}) - 1)$, where $I_{GABA + DRUG}$ is the current response in the presence of 3 μM flurazepam, and I_{GABA} is the control GABA-induced current.

A1.4.5 Modification of Introduced Cysteine Residues by MTSEA-biotin.

MTSEA-biotin (Biotium, Hayward, CA) was the sulfhydryl-specific reagent used in this study. It is a relatively impermeant compound with dimensions of 14.5Å unreacted moiety and 11.2Å reacted moiety. Stocks solutions (100mM) were made in DMSO, aliquoted into microcentrifuge tubes and rapidly frozen on ice before storage at -20°C. For each application of MTSEA-biotin, a new aliquot was thawed, diluted in ND96 to the working concentration and used immediately to avoid hydrolysis of the MTS compound. The final DMSO concentrations were ≤ 2%. These solvent concentrations did not affect $GABA_AR$ functional responses.

MTSEA-biotin modifications of the engineered cysteines were assayed by measuring changes in GABA evoked current (I_{GABA}). The effects of MTSEA-biotin were studied using the following protocol: GABA (EC_{40-60}) current responses (10-30 sec) were measured from oocytes expressing wild type ($\alpha_1\beta_2\gamma_2$) or mutant receptors and stabilized. Stability was defined as < 5% variance of peak current responses to GABA on two consecutive applications. After stabilization, the MTSEA-biotin (2mM) was bath-applied for 2 min, followed by a 5- to 7-min wash, and then I_{GABA} was measured at the same concentration as before the MTSEA-biotin treatment. The effect of the MTSEA-biotin application was calculated as: $[((I_{after}/I_{initial}) -1) \times 100]$, where I_{after} is the peak GABA current elicited after the MTSEA-biotin and $I_{initial}$ is the peak current before MTSEA-biotin.

A1.4.6 Rate of MTSEA-biotin Modification.

The rates at which the MTSEA-biotin modified the engineered cysteines were determined by measuring the effect of sequential applications of low concentrations of MTSEA-

biotin on I_{GABA} as described previously (Holden and Czajkowski, 2002). The protocol is described as follows: EC_{40-60} GABA was applied for 10 sec every 3- to 5-min until I_{GABA} stabilized (< 3% variance). After a 40 s ND96 washout, a low concentration of MTSEA-biotin was applied for 5- to 20-s and the cell was then washed for an additional 2.5- to 4.5-min. The MTSEA-biotin application was repeated until I_{GABA} no longer changed indicating that the reaction had proceeded to completion. Concentration of MTSEA-biotin and time of application varied as follows: β_2W168C, 500μM, 10s; β_2V175C, 5μM, 10s; β_2Q185C, 25μM, 10s. The effects of GABA (agonists), SR-95531 (antagonists) and pentobarbital (PB; allosteric modulator) on the rate of MTSEA-biotin modification was assayed by co-applying GABA (EC_{80-90}), 10μM SR-95531 (saturating concentrations), or PB (EC_{50}) with the MTSEA-biotin. PB concentrations used for β_2W168C (600μM), β_2V175C (500μM), and β_2Q185C (200μM) were estimated by determining EC_{50} (μM)/10 mM PB current ratio. For the rates of MTSEA-biotin modification, I_{GABA} was stabilized as follows: EC_{40-60} GABA was applied for 10s, oocyte washed for 40s, the test drug was applied for 5-20 s and the oocyte washed for 5-12min. The procedure was repeated until I_{GABA} from EC_{40-60} GABA was < 3% of the previous I_{GABA} peak. This ensured complete wash-out of the different test drugs during the protocol and ensured that any alteration in the current amplitudes following MTS treatment in the presence of drug was the result of MTS modification and not the result of inadequate washout of the drug. Concentrations of MTSEA-biotin and times of applications in the presence of GABA (EC_{80-90}) were as follows: β_2W168C, 500μM, 10s; β_2V175C, 10μM, 20s; β_2Q185C, 70μM, 10s. In the presence of PB (200-600μM): β_2V175C, 25μM, 20s; β_2Q185C, 50μM, 10s. In the

presence of 10μM SR-95531: β_2W168C, 500μM, 20s; β_2V175C, 25μM, 10s; β_2Q185C, 25μM, 10s.

For all rate experiments, the decrease or increase in I_{GABA} was plotted versus cumulative time of MTSEA-biotin exposure. Peak current at each time point was normalized to the initial peak current (t=0), and fit to a single exponential function using GraphPad Prism software. A pseudo-first order rate constant (k_1) was determined and a second order rate constant (k_2) was calculated by dividing k_1 by the concentration of the MTSEA-biotin used (Pascual and Karlin, 1998).

A1.4.7 Disulfide crosslinking.

Treatment with dithiothreitol (DTT) and H_2O_2 were performed as described previously (Hanson and Czajkowski, 2011). Dithiothreitol (Fisher) was dissolved in water to make a 1 M stock solution and stored at −20°C. DTT and hydrogen peroxide (H_2O_2) (3%; Fisher) were diluted in ND96 buffer to final concentrations of 10 mM and 0.3%, respectively, before each experiment. Before application of DTT or H_2O_2, oocytes were stabilized by applying GABA or etomidate (EC_{50}) at 3 min intervals until the I_{GABA} or $I_{etomidate}$ peak current amplitude varied by <5% (generally 2–3 pulses). After achieving current stability, 10mM DTT was applied for 2 min, followed by a 2 min wash period. GABA or etomidate (EC_{50}) was applied again. In each case, current amplitude remained stable with multiple GABA or etomdiate applications. Oocytes were then treated with 0.3% H_2O_2 for 2 min (or 10 min, where indicated), followed by a 2 min wash and GABA or etomidate (EC_{50}) test pulses. A second treatment of 10 mM DTT for 2 min, followed by GABA (EC_{50}) application was used to assess the reversibility of the H_2O_2 effect. Percent change in I_{GABA} or $I_{etomidate}$ calculated as (($I_{GABAafterDTT}$/ $I_{GABAbefore}$)-1) x 100 and (($I_{GABAafterH2O2}$/

$I_{GABAbefore}$)-1) x 100 or (($I_{etomidate,afterDTT}$/ $I_{etomidate,before}$)-1) x 100 and (($I_{etomdiate,afterH2O2}$/ $I_{etomidate,before}$)-1) x 100 where $I_{GABAafterDTT}$ or $I_{etomidate,afterDTT}$ refers to the current after a treatment in DTT, $I_{GABAbefore}$ and $I_{etomidate,before}$ refer to an initial current elicited by GABA or etomidate before any application of DTT or H_2O_2, and $I_{GABAafterH2O2}$ and $I_{etomidate,afterH2O2}$ refer to the current after treatment in H_2O_2.

A1.4.8 Statistical analysis.

Log k_I values and second order (k_2) rates were analyzed using a one-way analysis of variance, followed by a post-hoc Dunnett's test to determine the level of significance between wild-type and mutant receptors. Alterations in GABA EC_{50} for β_2W168C resulting from MTS treatment in the absence and presence of PB were analyzed using a Student's two-tailed unpaired *t* test. Log (EC_{50}) values, flurazepam potentiation and changes in GABA EC_{50} after MTSEA-biotin modification were analyzed using the false discovery rate (FDR) method (Benjamini and Hochberg, 1995) due to the large number of mutations being compared to wild type. Percent changes in I_{GABA} or $I_{etomidate}$ from mutant containing receptors before and after exposure to DTT or H_2O_2 were compared to WT under the same condition by one-way ANOVA with a Dunnett's post hoc test. Statistical comparisions among conditions for the same receptor type were compared with a Student's two-tailed unpaired *t* test.

A1.4.9 Structural Modeling. A model of the entire $GABA_A$ receptor was built as previously described (Mercado and Czajkowski, 2006). Other homology models of the $GABA_AR$ shown in Fig. A.11 are based on the torpedo nAChR structure (Unwin, 1995, Miyazawa et al., 2003) (PDB:1OED) GLIC (Bocquet et al., 2009) (PDB: 3EAM) and ELIC (Hilf and Dutzler, 2008) (PDB: 2VLO).

A1.5 Results

A1.5.1 Functional Characterization of β_2 Loop 9 Cysteine Mutants

Eighteen residues (W168, R169, G170, D171C, D172, N173C, A174, V175, T176, G177, V178, T179, K180, I181, E182, L183, P184 and Q185) in the Loop 9 region of the $GABA_AR$ β_2 subunit were individually mutated to cysteine (Fig. A.1) and co-expressed with wild-type α_1 and γ_2 subunits in *X. laevis* oocytes. All mutant subunits formed GABA-activated channels indicating that the cysteine substitutions were tolerated and yielded functional receptors. Maximal GABA current amplitudes ranged from 1 to 20 μA and did not differ significantly from maximal currents elicited from oocytes expressing wild-type $\alpha_1\beta_2\gamma_2$ receptors. Seven of eighteen mutations significantly altered GABA EC_{50} values compared with wild-type receptors (EC_{50} = 18.3 ± 1.9 μM, n_H = 1.4 ± 0.04, Fig. A.2 and Table A.1) suggesting that structural perturbation of this region affects GABA activation of the receptor. The largest increase in GABA EC_{50} was observed for $\alpha_1\beta_2$A174Cγ_2 receptors (33-fold). Receptors containing β_2W168C, β_2G170C, β_2D171C, β_2T176C and β_2G177C significantly increased GABA EC_{50} values between 3- and 11-fold. Cysteine substitution of β_2Q185 significantly decreased GABA EC_{50} by 4-fold. The Hill coefficients for GABA activation of β_2D171C, β_2A174C, β_2T176C, β_2G177C and β_2Q185C-containing receptors were significantly lower than wild type (Table 1). Of the seven cysteine substitutions that altered GABA EC_{50}, only two, β_2D171C and β_2A174C, significantly altered the k_I for the competitive antagonist SR-95531, and these changes were ≤ 3-fold (Fig. A1.3 and Table A1.2). Interestingly, cysteine mutations in

the β subunit loop F region has much larger effects than cysteine substitutions in the α or γ subunits (Fig A1.2D).

Except for β_2L183C, the mutations did not alter flurazepam (3 μM) potentiation of GABA responses and while potentiation of β_2L183C was reduced 1.8-fold, it was not completely obliterated (Fig. A1.4). The mutations had no effect on pentobarbital (200-600 μM) activation of the receptor (data not shown) compared with wild-type receptors. Taken together these data indicate that cysteine containing receptors express, assemble and are functional.

A1.5.2 Modification of Introduced Cysteine Residues by MTSEA-biotin

To define the solvent accessibility of the β_2 subunit W168C-Q185C segment, wild type and mutant receptors were exposed to MTSEA-biotin (2mM) for 2 min (Fig. A1.5). MTSEA-biotin altered I_{GABA} on 9 of the 18 mutant containing receptors. MTSEA-biotin significantly reduced I_{GABA} at β_2V175C (83.2 ± 1%, n = 3), β_2L183C (38.5 ± 3.4%, n = 4) and β_2Q185C (90.7 ± 3.3%, n = 3) and significantly potentiated I_{GABA} at β_2W168C (50.8 ± 3.5%, n = 4), β_2G170C (13 ± 3%, n = 3), β_2D172C (18 ± 4%, n = 3), β_2V178C (18.7 ± 1.9%, n = 3), β_2E182 (20 ± 3.1%, n = 3) and β_2P184 (27.7 ± 1.7%, n = 3) (Fig. A1.5). MTSEA-biotin had no effect on wild-type $\alpha_1\beta_2\gamma_2$ receptors or those containing β_2R169C, β_2D171C, β_2N173C, β_2A174C, β_2T176C, β_2G177C, β_2T179C, β_2K180C and β_2I181C (Fig. A1.5). The pattern of accessibility suggest a β-strand (i.e. every other residue) extending from W168 to D172, an α-helical structure (i.e. every third or fourth residue) extending from N173 to E182 and a loop/random coil from E182 to Q185. It is important to note, however, that the structure of this region cannot be absolutely assigned since a

lack of effect may indicate that the thiol group was not accessible to modification or that modification produced no detectable functional effect.

A1.5.3 MTSEA-biotin reaction rates

The rate at which MTSEA-biotin covalently modifies an accessible introduced cysteine depends on several factors, including the ionization of the sulfhydryl group, local steric restriction, the electrostatic potential near the cysteine, and the access route to the engineered cysteine. Methanethiosulfonate reagents react 10^9 to 10^{10} times faster with the ionized thiolate (RS-) form of cysteine than they do with the protonated form, and ionization is more likely in an aqueous environment (Roberts et al., 1986, Stauffer and Karlin, 1994). Second-order rate constants therefore provide information about the local environment of a substituted cysteine. To gain insight into the physico-chemical environment of the β_2 Loop 9 region in the resting, closed state of the receptor, we measured the second-order rate constants for MTSEA-biotin modification of introduced cysteines located in the middle (V175C) and either end (W168C and Q185C) of β_2 Loop 9 in the absence of ligands (Fig. A1.6). The second-order rate constant for β_2W168C was slow ($130 \pm 20 M^{-1}sec^{-1}$), suggesting that the thiol group is not well ionized and/or that the introduced cysteine residue is in a restricted buried environment (Fig. A1.6 and Table A1.3). The relatively fast second-order rate constants for MTSEA-biotin modification of β_2V175C ($11{,}285 \pm 923 M^{-1}sec^{-1}$) and β_2Q185C ($3465 \pm 923 M^{-1}sec^{-1}$) indicate that both residues are found in an open, aqueous environment (Table A1.3). The rates measured indicate that V175C and Q185C are solvent accessible, whereas W168C is less accessible, which is consistent with the predicted positions of these residues based on modelling. However, the rates also depend on the local electrostatic potentials near the

sulfhydryl groups, which are probably different at each position and contribute to the range of reaction rates measured.

A1.5.4 Effects of GABA, SR-95531 and PB on MTSEA-biotin second-order rate constants

To determine if the β_2 Loop 9 region undergoes structural rearrangements during channel gating (open/desensitized states), we measured the rates of MTS modification of β_2V175C, β_2Q185C and β_2W168C in the presence of the agonist GABA. If the rate of reaction of β_2V175C, β_2Q185C and β_2W168C changes when GABA is present, it indicates that the environment around the introduced cysteine has changed due to movements at, or near, the introduced residue. In the presence of GABA (~EC_{90}), the rates of modification of β_2V175C and β_2Q185C were significantly slowed by ~3 fold and modification of β_2W168 unchanged (Fig. A1.6 and Table A1.3), indicating that GABA binding/gating of the receptor triggers movements in or near the Loop 9 region of the β_2 subunits.

Changes in the rates of modification induced by GABA, can be due to ligand binding and/or gating of the channel. To determine whether movements in and near β_2 Loop 9 can occur by occupying the GABA binding site without gating the channel, we measured the rates of modification in the presence of the competitive antagonist, SR-95531. SR-95531 significantly slowed the rates of modification of β_2W168C and β_2V175C by 2 and 3 fold, respectively and had no effect on the modification of β_2Q185C (Fig. A1.6 and Table A1.3).

Pentobarbital (PB) binds to a site that is distinct from the GABA binding pocket (Amin and Weiss, 1993) and, at high concentrations, directly activates the $GABA_AR$. The

mean single channel conductances elicited by GABA and PB are similar (Jackson et al., 1982), suggesting that in the vicinity of the channel the structure of the open states are alike. Moreover, the pore lining M2 helix undergoes similar changes upon activation by GABA or the anesthetics pentobarbitol, propofol and isoflurane (Rosen et al., 2007). We therefore used PB EC_{50} to assess whether PB would also elicit movements in the β_2 Loop 9 region. The rate of modification at β_2V175C was slowed 2 fold in the presence of PB, while PB had no effect on the second order rate constant for β_2Q185C (Fig. A1.6). Rates of modification in the presence of PB for β_2W168C could not be reliably measured because when PB was present during MTSEA-biotin treatment, it had variable effects on the magnitude of the subsequent GABA current ranging from 2.5 to 52% potentiation (Fig. A1.7). At this position, MTSEA-biotin reacted even for those experiments where treatment of MTSEA-biotin in the presence of PB resulted in < 25% potentiation of subsequent GABA current. This suggests that the reaction had proceeded to apparent completion. In the absence of drug, MTSEA-biotin potentiated subsequent GABA currents 52 ± 3.5 % while in the presence of the drug the potentiation averaged 24 ± 8 % (Fig. A1.7). Statistical analysis revealed significant differences ($p< 0.03$) between the effect of MTSEA-biotin alone and MTSEA-biotin in the presence of PB on the subsequent GABA current. The data suggest that PB changes the environment near β_2W168C.

A1.5.5 Disulfide trapping of βQ185C to adjacent α and γ subunits' Mr-M3 loop

We used crosslinking of engineered cysteines between the α or γ subunit M2-M3 linker (the loop region that connects TMD helices M2 and M3) and βQ185C to assess the proximity of this residue, at the end of loop 9, to the TMD of the adjacent subunits. To

form a disulfide bond the two β carbons of the cysteine residues must come within ~4.6Å. We assayed for crosslinking by measuring GABA current before and after treatment of a reducing agent DTT, then an oxidizing agent, H_2O_2 and a second treatment in DTT. Percent change in I_{GABA} after treatment with both DTT and H_2O_2 did not differ in WTαβγ and single mutant containing receptors (αA280Cβγ, αβQ185Cγ and αβγY292C) and did not differ significantly between treatments (WT: 7.6 ± 2.3% after DTT, -4.0 ± 3.2% after H_2O_2, -2.4 ± 3.6% After 2nd exposure to DTT, n = 13) (Fig. A1.8A, B, D, G). Whereas αA280CβQ185Cγ receptors differed in percent change of I_{GABA} between treatments (111 ± 16% after DTT, -5.7 ± 8.3% after H_2O_2, 103 ± 15% after a second exposure to DTT, n = 3). Also, percent change in I_{GABA} before and after the first and second treatment with DTT differed significantly from percent changes to the WT receptor after the same treatments (Fig. A1.8E). Similarly, αβQ185CγY292C receptors differed significantly in their percent change in I_{GABA} from WT receptors after a first and second exposure to DTT and after a 2 minute exposure to 0.3% H_2O_2 (657 ± 99% after DTT, 406 ± 71% after H_20_2, 705 ± 162% after 2nd exposure to DTT, n = 3) (Fig. A1.8H). After 10 minute incubation in 0.3% H_2O_2 I_{GABA} returned to levels similar to pre-DTT currents, the percent change was not significantly different from WT receptors and the percent change in I_{GABA} was statistically different from that after the 1st and 2nd treatment with DTT (374 ± 49% after DTT, 8.3 ± 32% after 10 minutes in H_2O_2, 444 ± 13% after second exposure to DTT) (Fig. A1.8K). The large increase in I_{GABA} after initial exposure to DTT suggests that a crosslink spontaneously forms across subunits from ECD to TMD and inhibits GABA activation, this effect is reversible after reforming a crosslink by incubation in H_2O_2 (10 minutes for αβQ185CγY292C). We performed full

GABA concentration-response experiments before and after exposure to DTT. There were no alteration in GABA EC_{50} in the presence and absence of a crosslink (αβQ185CγY292C before DTT: 37.1 ± 8.1μM, n=3, after DTT: 21.4 ± 5.8μM, n =4; αA280CβQ185Cγ before DTT: 17.3 ± 2.2μM, n=3, after DTT: 17.9 ± 1.6μM, n=3) (Fig. A1.9 and Table A1.4). Despite no difference in EC_{50} there were large increases in I_{max} after crosslink reduction (αβQ185CγY292C before DTT: 3883 ±1028nA , n=3, after DTT: 5830 ± 732nA, n =4; αA280CβQ185Cγ before DTT: 900 ± 198nA, n=3, after DTT: 3764 ± 1594nA, n=3) (Fig. A1.9 and Table A1.4).

To assay if this effect is specific to GABA activation, we examined the effects of the disulfide bonds on etomidate activation. Etomidate binds at the β-α interface, as does GABA, but unlike GABA etomidate binds within the TMD between the β M3 and α M1 helix (Li et al., 2006). As with GABA, effects on etomidate activation were assayed by pulses of etomidate EC_{50} before and after treatment with DTT and H_2O_2 (dose response curves: Fig. A1.10B). Crosslink effects on $I_{etomidate}$ were similar to that of GABA (WT: 20.8 ± 9.8% after DTT, -12.1 ± 13.1& after H_2O_2. -7.1 ± 8.6% after a second exposure to DTT, n= 3) (Fig. 9A), with αA280CβQ185Cγ experiencing significant differences in percent change in $I_{etomidate}$ between reducing and oxidizing agent treatment (89.2 ± 32.4% after DTT, -3.6 ± 3.7% after H_2O_2, 75.2 ± 39.1% after a second exposure to DTT, n = 3) (Fig. A1.10C, D). There was also an increase in EC_{50} $I_{etomidate}$ amplitude after initial DTT application as was seen with I_{GABA} but this increase did not reach significance. αβQ185CγY292C receptors responded similarly to etomidate activation as to GABA activation. They experienced significant increases in percent change in $I_{etomidate}$ after each treatment (465 ± 93% after DTT, 176 ± 43 after H_2O_2. 571 ± 133 after a second exposure

to DTT, n = 3) (Fig. A1.10E, F). The increase in $I_{etomidate}$ after DTT exposure was not fully reversible with a 2 minute incubation in H_2O_2, a 10 minute incubation was not tried in this case. The similar effects seen with both GABA and etomidate activation of the $GABA_AR$ is indicative of movement in β loop 9 relative to the M2-M3 linker of adjacent subunits occurring in channel activation irrespective of the activating agonist's binding site.

A1.6 Discussion

Experimental and computational studies have begun to provide molecular insights about the conformational changes leading to channel activation. In the structural model proposed by Unwin, only two of the five subunits in the nAChR move in response to ligand biding (Unwin et al., 2002). The conformational changes correspond to a 10-degree clockwise rotation of the extracellular inner beta strands and an eleven-degree outward tilt of the outer beta strands. The proposed movements in Unwin's structural model shows strong correlation with recent molecular dynamics simulations of the α_7 nAChR ligand-binding domain comparing the "open" state conformation with the "closed" state α-Cobratoxin-bound form (Yi M et al., 2008). In the $GABA_AR$, the β_2 subunit forms the principal side of the GABA-binding site (Fig. A1.1) and is the subunit that would undergo this movement. The β_2 subunit segment between W168 and Q185 (Loop 9) links β-strands 8 and 9 and is a transition point between inner and outer β-strands. Thus, if agonist binding triggers movements in the inner and outer β-strands of the β_2 subunits relative to each other, one would expect that mutations in the Loop 9

region would disrupt these movements and affect GABA-induced activation of the receptor.

Indeed, seven of eighteen cysteine substitutions in this region of the β_2 subunits significantly altered GABA EC_{50} values whereas mutations in homologous residues in the α and γ loop 9 regions have relatively little affect on GABA EC_{50} (Fig. A1.2). The changes in EC_{50} reflect changes in either microscopic GABA binding affinity and/or channel gating (Colquhoun, 1998). Two of the seven mutations that increase GABA EC_{50} (D171C and A174C) also significantly increased SR-95531 K_I (Fig. A1.3), suggesting that these mutations may alter ligand binding, because SR-95531 does not gate the channel (but see (Ueno et al., 1997). Hill coefficients for GABA activation were significantly reduced for $\alpha_1\beta_2$D171Cγ_2, $\alpha_1\beta_2$A174Cγ_2, $\alpha_1\beta_2$T176Cγ_2, $\alpha_1\beta_2$G177Cγ_2 and $\alpha_1\beta_2$Q185Cγ_2 receptors (Table 1) suggesting that these mutations may also alter gating efficacy (Colquhoun, 1998). Since the β_2 Loop 9 region spans from Loop B of the GABA binding site to regions near the TMD, changes in binding and gating might be expected for mutations in this region.

Consistent with our findings, a study using chimeric receptors comprised of AChBP fused to the transmembrane pore domain of the serotonin type-3A ($5HT_{3A}$) receptor demonstrated that functional coupling between binding and gating was only restored when Loops 2, 7, and 9 from AChBP were replaced with $5HT_{3A}$ receptor sequences (Grutter et al., 2005). In the $GABA_AR$, 4 of 9 alanine mutations in β loop 9 cause significant alterations in GABA EC_{50} (Williams et al., 2009). These indicate that Loop 9 is one of the critical structural elements involved in coupling the extracellular binding domain to the transmembrane channel gating domain. It should be noted,

however, that the Loop 9 region in the above chimeric receptor is present in both, binding and non-binding interfaces. Thus, the independent contribution of each Loop 9 region in the coupling mechanism could not be determined in the aforementioned study. However, in the γ subunit loop 9, intrasubunit crosslinks (to beta strand 9) and intersubunit crosslinks (to α loop 2) inhibit benzodiazepine potentiation of I_{GABA} suggesting that at this non GABA binding interface movements affecting I_{GABA} also occur (Hanson and Czajkowski, 2011). Here, we provide evidence that the β Loop 9 region at non-binding interfaces is important for $GABA_AR$ activation and therefore might play a role in the structural transitions involved in the transduction of binding to gating of the channel potentially through interactions with the M2-M3 loop of adjacent α and γ subunits.

While the 4-angstrom structure of the nicotinic acetylcholine receptor provides information about the path of the peptide backbone, residue side chain position is difficult to determine at this resolution especially in regions without secondary structure such as the Loop 9 region. Our data revealed two clusters of residues in the β_2 Loop 9 that are sensitive to cysteine substitutions. The first cluster of amino acids consists of W168-D171 (located at the top of the Loop 9) while the second cluster consists of A174-G177 (located at the middle) (Fig. A1.10). In addition, a single amino acid at the bottom end of the β_2 Loop 9 region (Q185) is sensitive to structural perturbations, this is consistent with work by the Jenkins group indicating mutation of this residue increases leak current and decreases GABA EC_{50} (Williams et al., 2009).

The GABA antagonist SR-95531, but not GABA, induces structural rearrangements at or near β_2W168C (Fig. A1.6 and Table A1.3). β_2W168C points towards β-strand 9 (Fig. A1.10) and is within 4 Å of β_2L193 and β_2T195 on β-strand 9,

which forms part of Loop C. Therefore, we predict that movements of Loop C, out and upward, upon antagonist binding (Hibbs et al., 2006) would change the environment of W168 in Loop 9 (Fig. A1.10). SR-95531 slows the MTSEA-biotin rate of modification of W168C (Fig. A1.6B) consistent with this region of Loop 9 and β-strand 9 moving closer to each other. Movements of Loop C inward to cap the binding site upon agonist binding will move β-strand 9 away from W168 in Loop 9 (Unwin et al., 2002, Celie et al., 2004b). The lack of effect on the MTSEA-biotin rate of β_2W168 in the presence of GABA suggest that Loop C capping movements upon agonist binding are not detected near the top of β_2 Loop 9. Thus, we postulate that the top of β_2 Loop 9 is "confomationally sensitive" to the binding of antagonist. In addition, PB binding/activation induces changes near β_2W168 indicating that the top of Loop 9 is sensitive to an allosteric modulator that does not bind at the GABA binding site and that PB and GABA trigger different movements in this region.

By using the structures of unliganded AChBP and AchBP bound with a variety of ligands (agonists and antagonists) to homology model homo-oligomeric $5HT_{3A}$ receptors, Thompson and colleagues (2006) proposed that ligand binding does not induce large movements in Loop 9 but induces local changes in residue side-chain rotation that is dependent upon the bound ligand and the location of the residue in the Loop 9. Comparing bound and unbound $5HT_{3A}$ receptors revealed a significant rotational movement of W195 (which aligns with $GABA_AR$ β_2W168). These movements were most pronounced for antagonist-bound models, which showed that the side chain of W195 rotates clockwise between 90º (small antagonist) and 180º (large antagonist). The

modeling is consistent with our data and supports our hypothesis that the top of the β_2 Loop 9 region (W168-D171) is conformationally sensitive to the binding of antagonist.

GABA and SR-95531 significantly slows MTSEA-biotin modification of β_2V175C (approximately threefold) (Fig. A1.7 and Table A1.3) indicating that this region undergoes conformational rearrangements during antagonist binding and GABA binding/gating. In addition, PB significantly slows modification of β_2V175 indicating that this residue is sensitive to channel gating by an allosteric modulator that does not bind at the GABA binding site (Fig. A1.7 and Table A1.3). Interestingly, the $5HT_3$ modeling study (Thompson et al., 2006) as well as recent molecular dynamics simulations of the α_7 nAChR ligand-binding domain of the apo and toxin bound forms (Yi et al., 2008) revealed changes in flexibility, orientation and positioning in response to ligand binding of Loop 9 residues corresponding to amino acids D172 to G177 of the $GABA_AR$ β_2 subunit. GABA significantly slowed the rate of MTSEA-biotin modification of β_2Q185C located at the bottom end of the β_2 Loop 9 region indicating that this region of Loop 9 also undergoes conformational rearrangements during receptor activation and/or desensitization. We postulate that the middle (A174-G177) and bottom (Q185) of β_2 Loop 9 undergo conformational changes during the transition from the resting state to the open state. Consistent with our hypothesis, photolabeling and electrophysiological studies on the nAChR identified a region on the α_1 subunit between residues S162 and E180 in Loop 9 that was photolabeled only in the open state (Leite et al., 2003). These residues are aligned with the residue(s) located at the middle and bottom of β_2 Loop 9 of the $GABA_AR$ (Fig. A1.1).

Since the β_2 Loop 9 of $GABA_AR$ is a transition point between inner and outer β-strands, the movements in this region likely reflect changes in the relative positions of the inner and outer β-strands upon agonist binding. Movements in Loop 9 may not only contribute to the inner and outer β-strands conformational rearrangements upon agonist binding but may also influence other closely located domains. Recently, the Jenkins group hypothesized that Q185 stabilizes the closed state of the receptor through hydrophilic interactions(Williams et al., 2009). Our data suggest that βQ185 is in close apposition to the M2-M3 loop of both the α and γ subunits. The cryo-EM strcuture of the nACHR suggest interactions from extracellular β-strands with the M2-M3 loop are involved in propogating extracellular protein movements into the TMD (Unwin, 2005). It has been shown previously that residues within the M2-M3 loop experience differences in cysteine accesibility to sulfhydryl modifying agents during channel activation (Bera et al., 2002). Our data indicate that a crosslink can spontaneously form between βQ185C and αA280C as well as γY292C indicating that these regions lie in cross proximity in the resting state. Both of these crosslinks inhibits I_{GABA} suggesting that movements at the non-binding, α-β and β-γ interfaces occur during channel activation. Interestingly, similar affects are seen with etomidate activation. Etomidate binds at the β-α interface within the α helices of the TMD (Li et al., 2006). Thus, conformational movements inhibited by this crosslink at the TMD/ECD interface are not specific to GABA activation. Furthermore, recent comparisons of prokaryotic channel crystal structures indicate a twisting motion of the ECD counter to the twising in the TMD (Hilf and Dutzler, 2008). Our data support this hypothesis, by joining the ECD and TMD by disulfide bond this opposing twisting movement is limited. When the disulfide is reduced

by DTT, the receptor is free to twist resulting in a large increase in I_{GABA} or $I_{etomidate}$ is seen.

Additionally, in comparing distances between α280 and β185 or β185 and γ292 beta carbons in structural homology models of the $GABA_AR$ based on crystal structures of homologous channels ELIC (Hilf and Dutzler, 2008), GLIC (Bocquet et al., 2009) and the nAChR (Unwin, 2005) our data indicate that the $GABA_AR$ more strongly resembles the prokaryotic channels in these regions (Fig. A1.11). In the nAChR based model, the distances between α280 and β185 (20.6 Å), and β185 and γ292 (14.7 Å) are far out of reach of a disulfide bond (approximately 4.6 Å). The distances for the ELIC based model between α280 and β185 (3.8 Å), and β185 and γ292 (9.2 Å) are much closer to the distance necessary to form a crosslink especially given in this model these residues fall in an unstructured region that presumably has more mobility and may flex to within the 4.6 Å range (Fig. A1.11). In the GLIC based model the distances between α280 and β185 (8.5 Å), and β185 and γ292 (11.0 Å) are, again, somewhat outside of the range where they would likely form a disulfide bond (Fig. A1.11). GLIC was crystallized in a presumed open state (Bocquet et al., 2009), our data is in keeping with this as it would suggest crosslinks are more likely to form in a closed receptor (more closely resembling the ELIC based model) and I_{GABA} is greatly increased after reduction of the crosslink, allowing these regions to spread as the channel opens (more closely resembling the GLIC based model).

Overall our data support the idea that Loop 9 at non-binding interfaces moves in response to agonist/antagonist binding as well as channel activation and limiting this mobility inhibits channel activation. The cluster of residues located at the top of the β_2

Loop 9 region (W168-D171) are conformationally sensitive to the binding of antagonist while the structural rearrangements near the residues located in the middle (A174-G177) and bottom (Q185) of the Loop 9 likely play an important role allowing movements between the inner and outer β-strands as well as simultaneously propagating these movements to the TMD potentially through interactions with the M2-M3 linker. Higher resolution structures of the closed and open states of the receptor are needed to support these hypotheses.

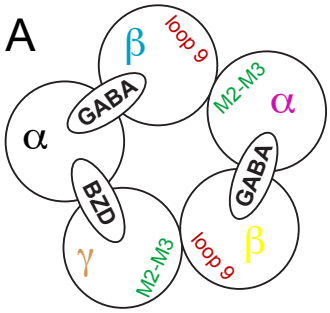

B

```
GABA α1  WTREPARSVVVAEDGS-RLNQ 189
GABA γ2  WKRS---SVEVGDTRSWRLYQ 199
GABA β2  WRGD---DNAVTGVTKIELPQ 185
GluCl    WDPS--TPVQLKPGVGSDLPN 189
GLIC     VDLE-----KVGKNDDVFLTG 159
ELIC     DIQVYTENIDNEEIDEWWIRK 164
AChBP    TDTDQVDLSSYYASSKYEILS 195
```

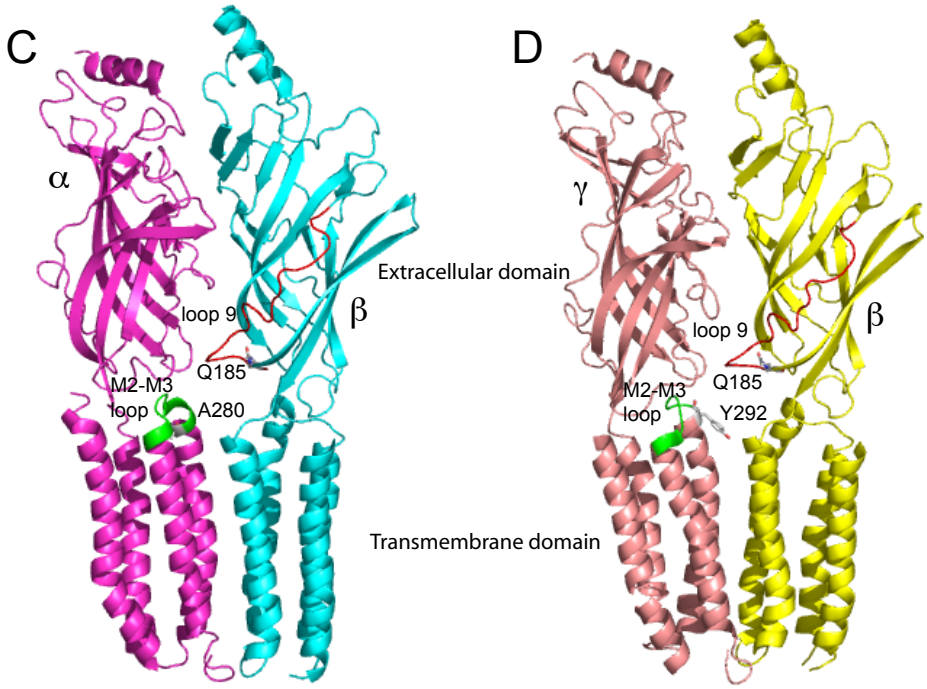

Figure A1.1. The β_2 Loop 9 region of the $GABA_AR$. (A) Schematic representation of a $GABA_AR$ showing subunit stoichiometry and arrangement, and the binding sites for GABA and BZD. Note that Loop 9 in the β_2 subunits is at a non-binding interface adjacent to the M2-M2 loop of either an α or γ subunit. (B) Alignment of the rat $GABA_AR$ β_2W168- β_2Q185 region with analogous regions of the rat $GABA_AR$ α_1 and γ_2 subunits, *Caenorhabditis elegans* GluCl channel, GLIC, ELIC and *Aplysia Californica* AChBP. The numbering corresponds to the position of the residues in the mature subunits. Homology model of the $GABA_A$ receptor α_1-β_2 interface (C) and of the γ_2-β_2 interface (D) based on the nAChR cryo-EM structure (Unwin, 2005). The β loop 9 region is indicated in red with Q185C at the c-terminal end of loop 9 indicated in sticks. The M2-M3 loop of the opposing α (C) or γ (D) subunit are highlighted in green, with residues of interest αA280 (C) and γY292 (D) shown in sticks.

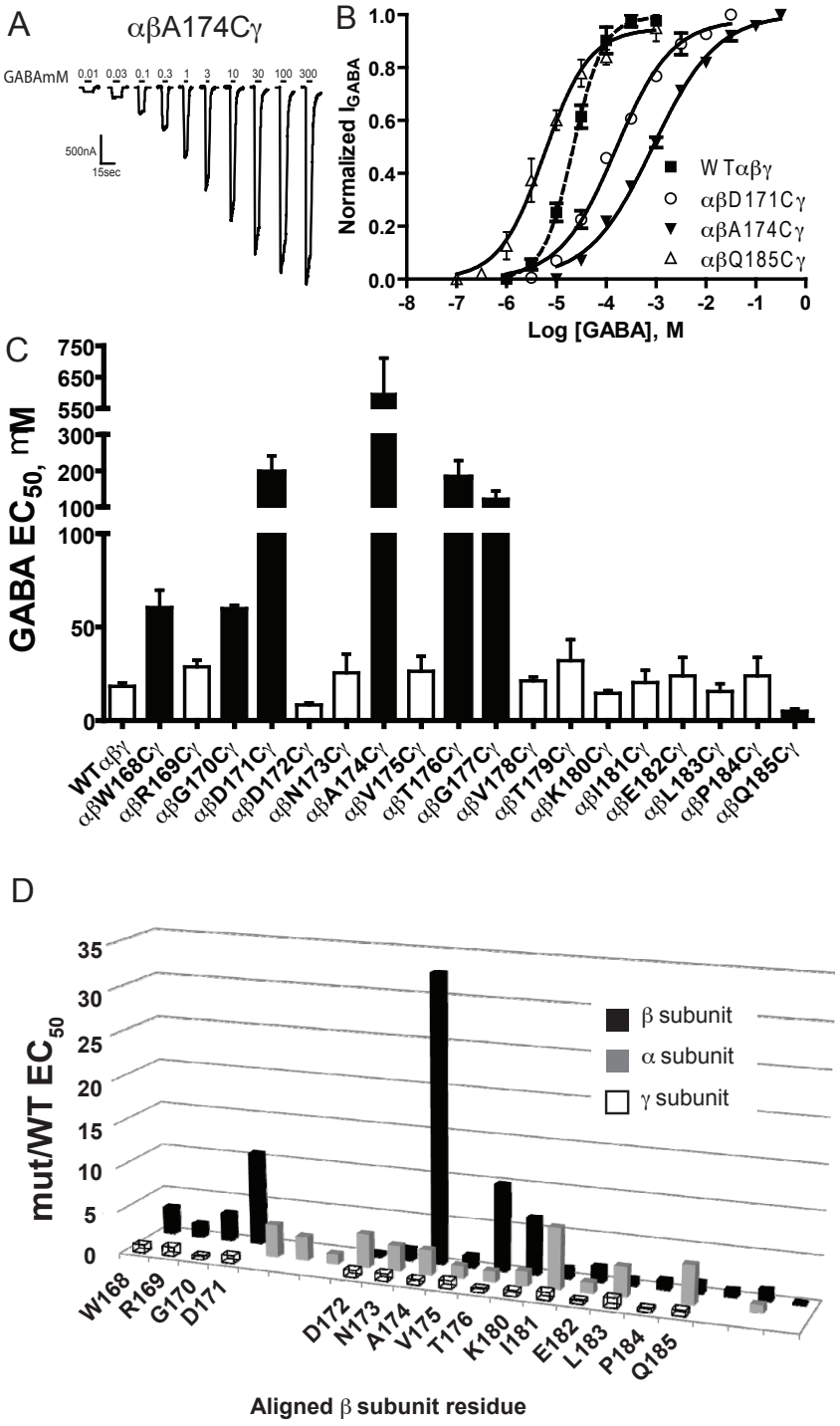
A
αβA174Cγ
GABAmM 0.01 0.03 0.1 0.3 1 3 10 30 100 300
500nA
15sec
B
Normalized I_GABA
1.0
0.8
0.6
0.4
0.2
0.0
-8 -7 -6 -5 -4 -3 -2 -1 0
Log [GABA], M
WTαβγ
αβD171Cγ
αβA174Cγ
αβQ185Cγ
C
GABA EC50, mM
750
650
550
300
200
100
100
50
0
WTαβγ
αβW168Cγ
αβR169Cγ
αβG170Cγ
αβD171Cγ
αβD172Cγ
αβN173Cγ
αβA174Cγ
αβV175Cγ
αβT176Cγ
αβG177Cγ
αβV178Cγ
αβT179Cγ
αβK180Cγ
αβI181Cγ
αβE182Cγ
αβL183Cγ
αβP184Cγ
αβQ185Cγ
D
mut/WT EC50
35
30
25
20
15
10
5
0
β subunit
α subunit
γ subunit
W168
R169
G170
D171
D172
N173
A174
V175
T176
K180
I181
E182
L183
P184
Q185
Aligned β subunit residue

Figure A1.2. GABA concentration responses of wild type $\alpha_1\beta_2\gamma_2$ and mutant $GABA_AR$. (A) Representative current responses from an oocyte expressing $\alpha_1\beta_2$A174Cγ_2 receptors elicited by increasing concentrations of GABA (mM). (B) GABA concentration response curves from oocytes expressing $\alpha_1\beta_2\gamma_2$ (■, dashed line), $\alpha_1\beta_2$D171Cγ_2 (○), $\alpha_1\beta_2$A174Cγ_2 (▼) and $\alpha_1\beta_2$Q185Cγ_2 (Δ) receptors. Data were fit by nonlinear regression analysis as described in Materials and Methods. (C) Summary of the effects on GABA EC_{50} of mutant $GABA_A$ receptors. Bars represent the mean ± SEM from 3 to 7 independent experiments. The solid black bars indicate values that were statistically different from wild-type values (p<0.002). GABA EC_{50} and n_H values are reported in Table 1. (D) Relative EC_{50}'s of α_1, β_2 and γ_2 subunit loop 9 regions. Bar graph indicates fold change from respective WT calculated as mutant EC_{50}/WT EC_{50}. Data from α subunit mutations are from αβ receptors and come from (Newell and Czajkowski, 2003). Data from γ subunit mutations are from Hanson et al. 2008 (Hanson and Czajkowski, 2008). X-axis is labeled with the aligned β subunit residues (refer to Fig. 1B).

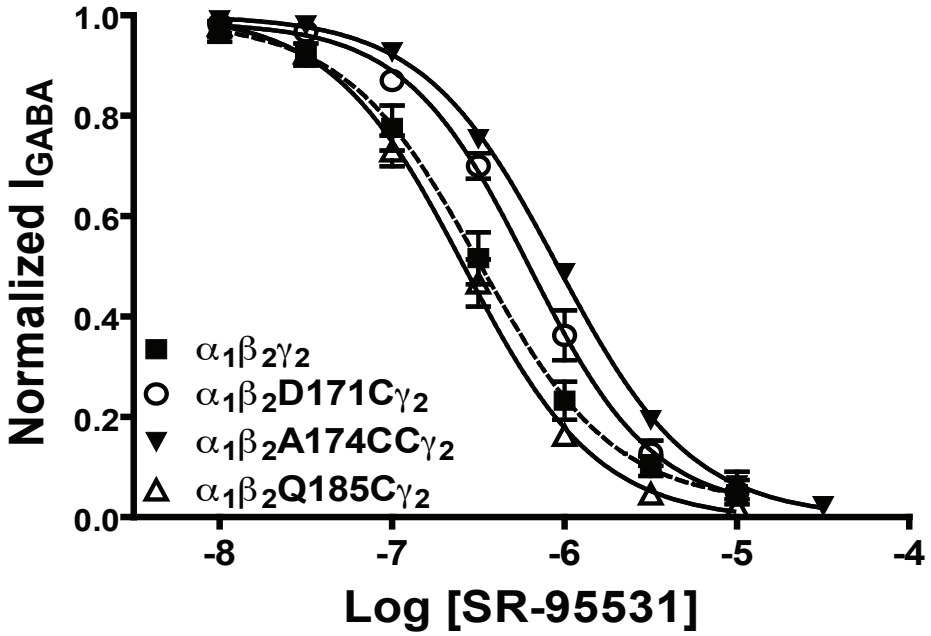
1.0
0.8
0.6
0.4
0.2
0.0
Normalized I_{GABA}
$\alpha_1\beta_2\gamma_2$
$\alpha_1\beta_2$D171Cγ_2
$\alpha_1\beta_2$A174CCγ_2
$\alpha_1\beta_2$Q185Cγ_2
-8
-7
-6
-5
-4
Log [SR-95531]

Figure A1.3. SR-95531 concentration response curves of wild type $\alpha_1\beta_2\gamma_2$ and mutant $GABA_A$Rs. Concentration-dependence of SR-95531-mediated reduction of I_{GABA} (EC_{50}) for wild-type (■, dashed line), $\alpha_1\beta_2$D171Cγ_2 (○), $\alpha_1\beta_2$A174Cγ_2 (▼) and $\alpha_1\beta_2$Q185Cγ_2 (Δ) receptors. Data represent the mean ± SEM of at least three independent experiments. The K_I values and calculated Hill coefficients are summarized in Table 2.

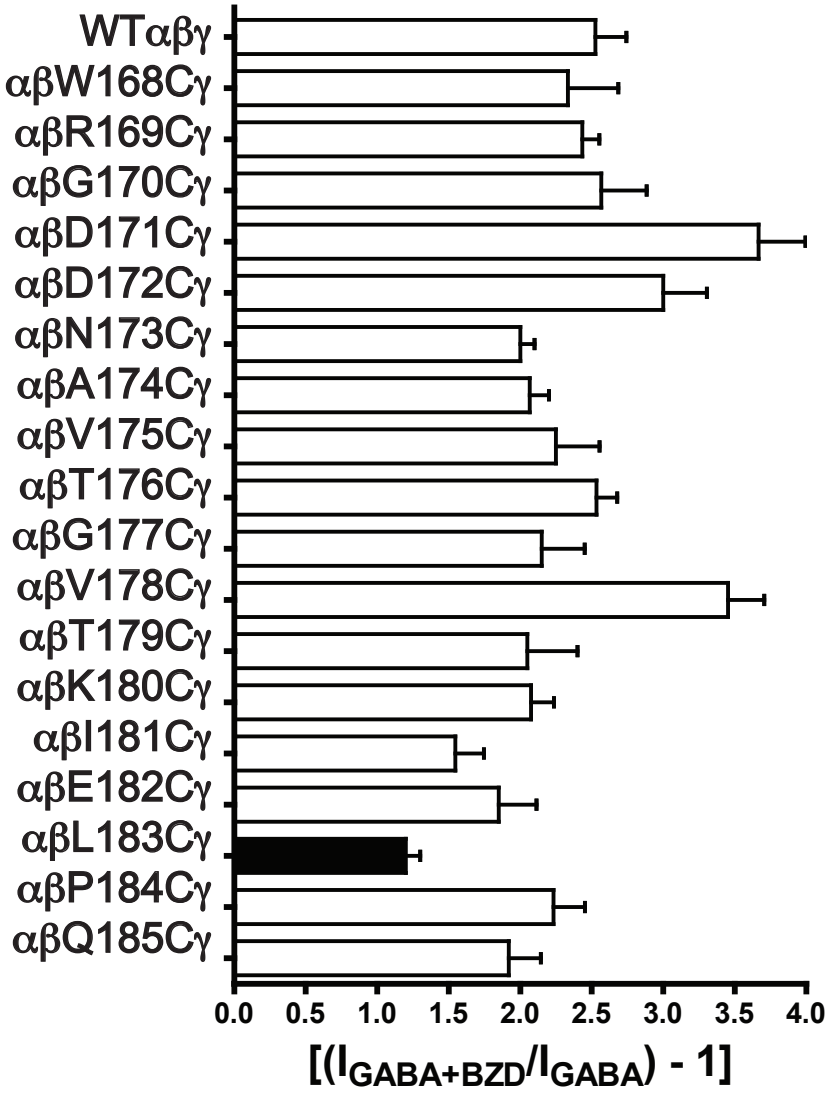
WTαβγ
αβW168Cγ
αβR169Cγ
αβG170Cγ
αβD171Cγ
αβD172Cγ
αβN173Cγ
αβA174Cγ
αβV175Cγ
αβT176Cγ
αβG177Cγ
αβV178Cγ
αβT179Cγ
αβK180Cγ
αβI181Cγ
αβE182Cγ
αβL183Cγ
αβP184Cγ
αβQ185Cγ
0.0 0.5 1.0 1.5 2.0 2.5 3.0 3.5 4.0
[(I GABA+BZD/I GABA) - 1]

Figure A1.4. Flurazepam potentiation of I_{GABA} for wild type $\alpha_1\beta_2\gamma_2$ and mutant $GABA_AR$. Oocytes expressing $\alpha_1\beta_2\gamma_2$ and mutant receptors were treated with GABA (EC_5) or GABA (EC_5) plus 3 μM flurazepam. Flurazepam potentiation response ratio was determined by dividing the peak current for $\alpha_1\beta_2\gamma_2$ and mutant receptors exposed to GABA (EC_5) plus flurazepam by the response to GABA (EC_5) alone: $[(I_{GABA+BZD}/I_{GABA}) - 1]$. Bars represent the mean ± SEM of at least three independent experiments and the solid black bar indicates a value that is significantly different from wild type ($p < 0.01$).

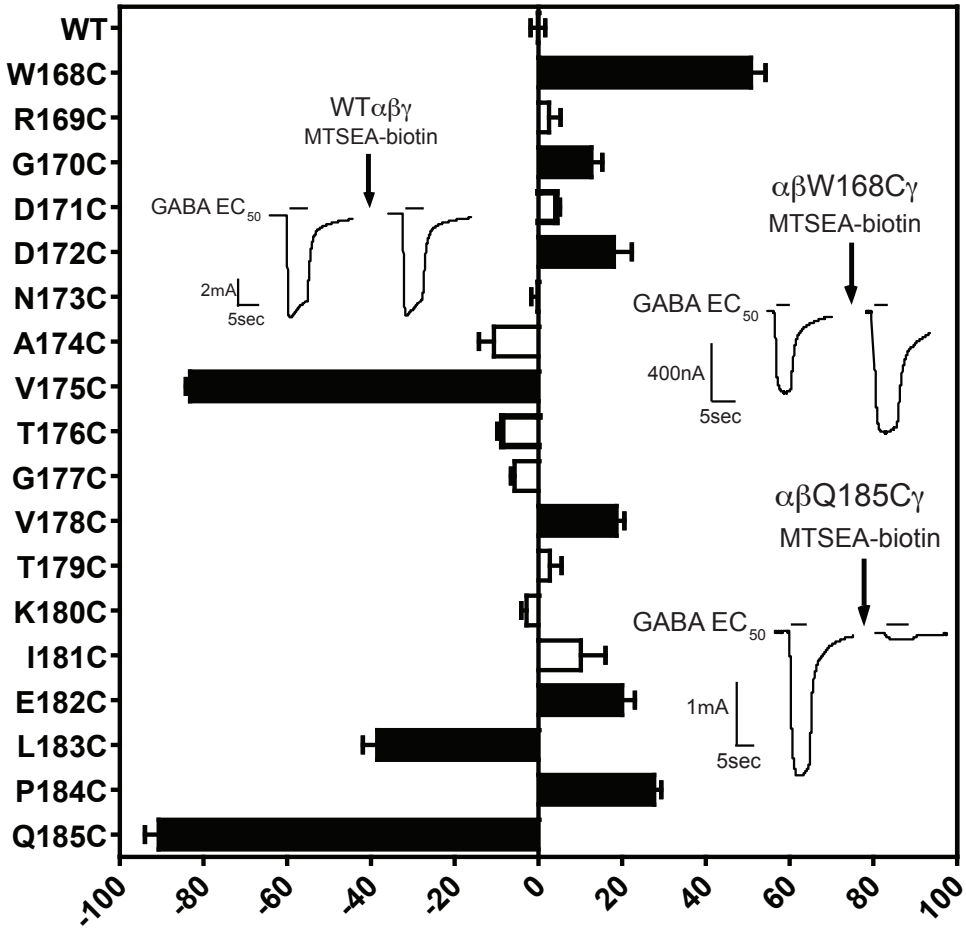
WT
W168C
R169C
G170C
D171C
D172C
N173C
A174C
V175C
T176C
G177C
V178C
T179C
K180C
I181C
E182C
L183C
P184C
Q185C
-100
-80
-60
-40
-20
0
20
40
60
80
100
WTαβγ
MTSEA-biotin
GABA EC50
2mA
5sec
αβW168Cγ
MTSEA-biotin
GABA EC50
400nA
5sec
αβQ185Cγ
MTSEA-biotin
GABA EC50
1mA
5sec

Figure A1.5. Effects of MTSEA-biotin on wild type and mutant $GABA_A$Rs.

Summary of the effects of a 2 min application of 2 mM MTSEA-biotin on wild type (WT) and mutant receptors. The percent change in I_{GABA} after MTSEA-biotin treatment is defined as: [(($I_{after}/I_{initial}$) -1) x 100]. Data represent the mean ± SEM from at least 3 independent experiments. The black solid bars indicate values that were statistically different from wild-type values ($p<0.002$). Inset are representative current traces demonstrating the effects of MTSEA-biotin (2mM, 2min) on GABA-mediated current (EC_{50}) on wild type, and W168C and Q185C containing receptors. The arrows represent MTSEA-biotin application, and the breaks in the current trace represent the subsequent wash (5 min).

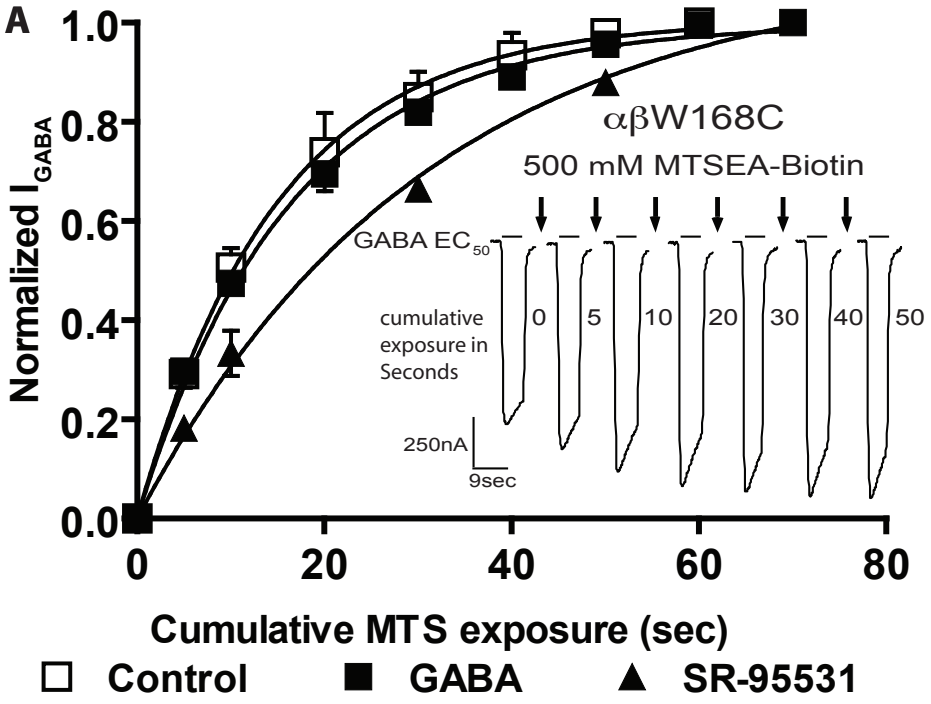
A
Normalized I_{GABA}
1.0
0.8
0.6
0.4
0.2
0.0
αβW168C
500 mM MTSEA-Biotin
GABA EC_{50}
cumulative exposure in Seconds
0
5
10
20
30
40
50
250nA
9sec
0
20
40
60
80
Cumulative MTS exposure (sec)
Control
GABA
SR-95531

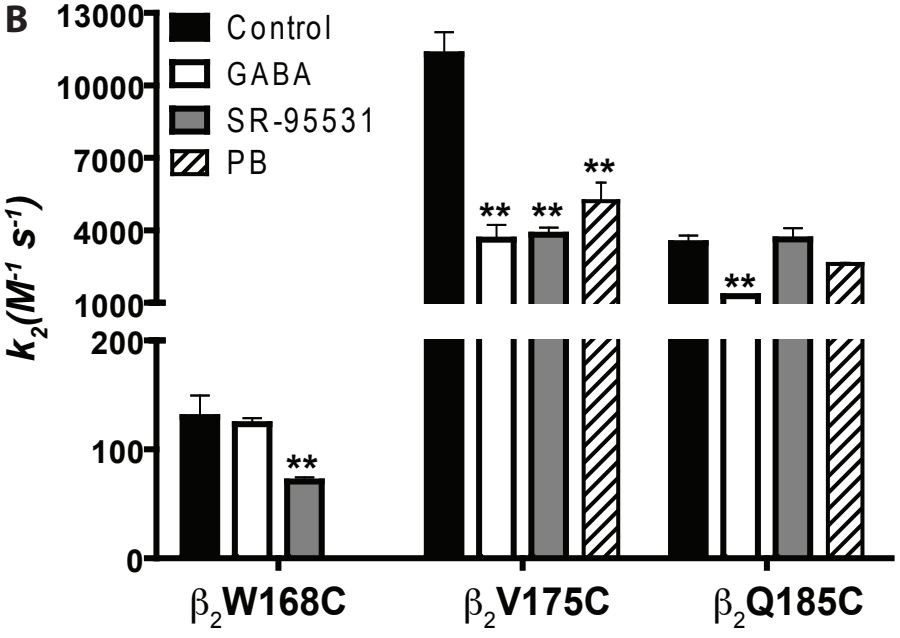
B
13000
10000
7000
4000
1000
200
100
0
$k_2(M^{-1} s^{-1})$
Control
GABA
SR-95531
PB
**
β_2W168C
β_2V175C
β_2Q185C

Figure A1.6. Rates of MTSEA-biotin modification. (A) Normalized GABA current responses from αβW168Cγ receptors were plotted versus cumulative time of MTSEA-biotin (□) and MTSEA-biotin coapplied with $EC_{80\text{-}90}$ GABA (■) or 10mM SR-95531 (▲) and fit with single exponential functions. Data were normalized to the maximal amount of potentiation of I_{GABA} for each experiment and represent mean ± SEM from at least 3 independent experiments. Inset are representative current traces recorded while applying MTSEA-biotin to αβW168Cγ receptors. GABA $EC_{40\text{-}60}$ current responses were recorded before and after successive applications (5-10sec) of MTSEA-biotin (arrows). (B) Summary of the second order rate constants (k_2) for reaction of MTSEA-biotin with mutant receptors in the absence (Control) and presence of GABA, SR-95531 or pentobarbital (PB). Second order rate constant (k_2) are reported in Table 3. ** Values significantly different than MTS alone (p <0.001).

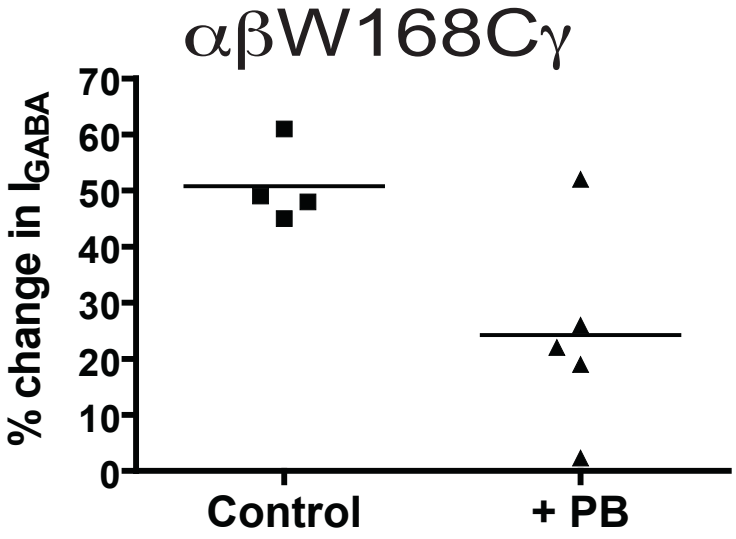
αβW168Cγ
% change in I_{GABA}
70
60
50
40
30
20
10
0
Control
+ PB

Figure A1.7. Effects of pentobarbital on MSTEA-biotin accessibility to αβW168Cγ receptors. Summary of the effects of a 2 min application of 2 mM MTSEA-biotin on β_2W168C in the absence (Control) and presence of 600 μM pentobarbital (PB). The percent change in I_{GABA} after MTSEA-biotin treatment is defined as: [(($I_{after}/I_{initial}$) -1) x 100]. Symbols represent data from individual experiments; line represents the mean for each data set.

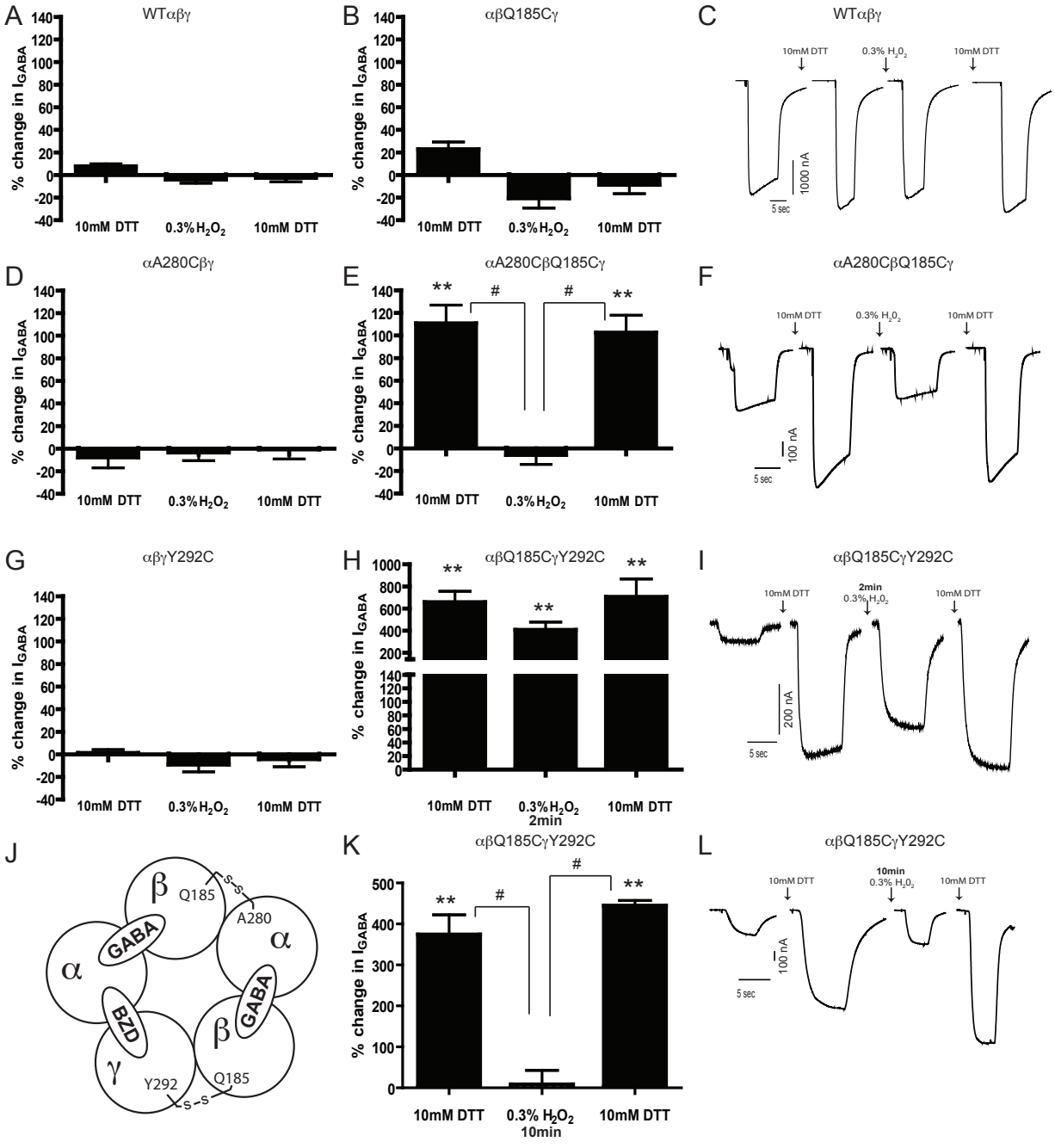
A
WTαβγ
% change in I_{GABA}
10mM DTT
0.3% H_2O_2
10mM DTT
B
αβQ185Cγ
C
WTαβγ
10mM DTT
0.3% H_2O_2
10mM DTT
1000 nA
5 sec
D
αA280Cβγ
E
αA280CβQ185Cγ
**
#
#
**
F
αA280CβQ185Cγ
100 nA
5 sec
G
αβγY292C
H
αβQ185CγY292C
I
αβQ185CγY292C
2min
200 nA
5 sec
J
β
Q185
A280
α
α
GABA
GABA
BZD
γ
Y292
β
Q185
S-S
K
αβQ185CγY292C
10min
L
αβQ185CγY292C
100 nA
5 sec

Figure A1.8. βQ185C forms an aparent crosslink to αA280C or γY292C located in the adjacent subunit's M2-M3 loop. WTαβγ (A) and single mutant receptors [αβQ185Cγ (B), αA280Cβγ (D), and αβγY292C (G)] experience minimal perecent change in I_{GABA} after exposure to a reducing agent (DTT) and oxidizing agent (H_2O_2). Whereas receptors with engineered cysteines in two subunits experience significant perecent increases in I_{GABA} after reduction of putative crosslinks by 10mM DTT [αA280CβQ185Cγ (E,F) and αβQ185CγY292C (H, J)]. This effect is reversible upon 2 min exposure to 0.3% H_2O_2 for αA280CβQ185Cγ (E), but not for αβQ185CγY292C, which requires a 10 minute incubation in H_2O_2 to restore I_{GABA} to WT levels (K). Panels C, F, I and L show representative current traces from WT and mutant containing receptors before and after exposure to DTT and H_2O_2. Panel J depicts a top down schematic of the $GABA_AR$ illustrating the location of putative crosslinks. All values come from three or more oocytes from at least two batches. Percent changes calculated as $((I_{GABAafterDTT}/ I_{GABAbefore})-1) \times 100$ and $((I_{GABAafterH2O2}/ I_{GABAbefore})-1) \times 100$. **indicates statistical difference from WT percent change in I_{GABA} under the same condition by one-way ANOVA, $p < 0.01$. $^{\#}$indicates statistical difference within treatments on the same receptor type by t-test, $p < 0.05$.

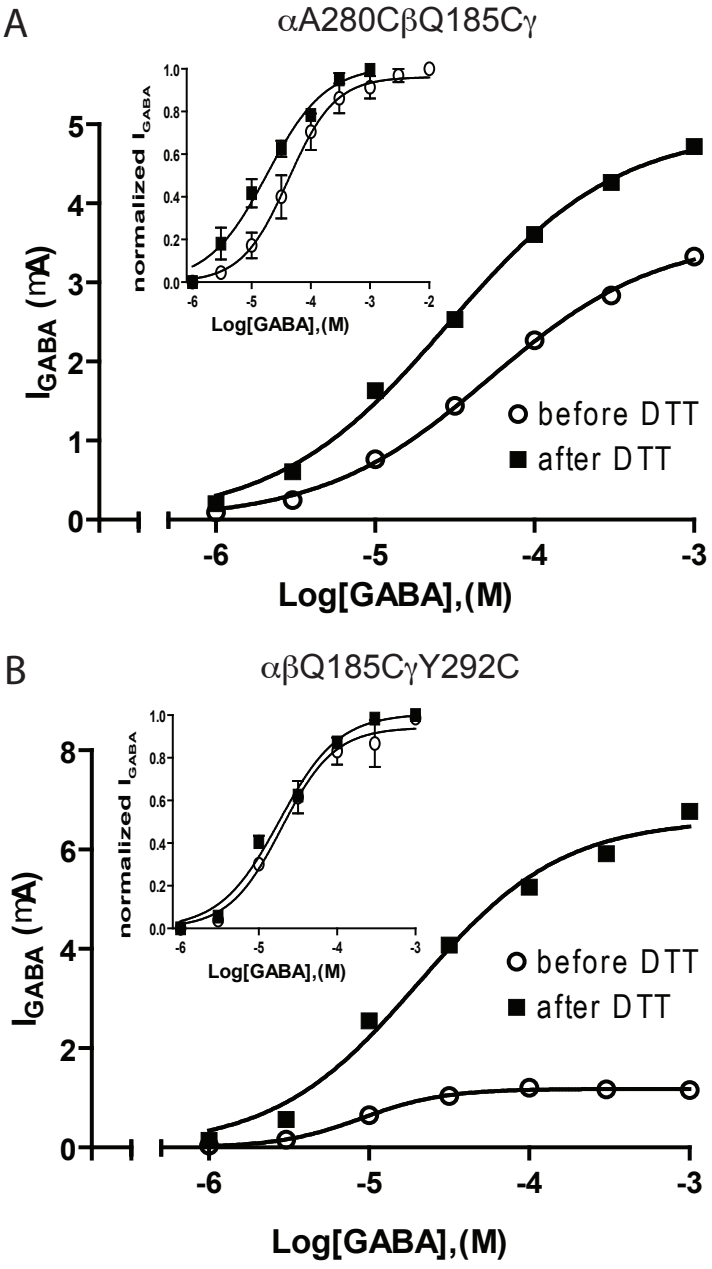
A
αA280CβQ185Cγ
normalized I_{GABA}
Log[GABA],(M)
I_{GABA} (mA)
before DTT
after DTT
Log[GABA],(M)
B
αβQ185CγY292C
normalized I_{GABA}
Log[GABA],(M)
I_{GABA} (mA)
before DTT
after DTT
Log[GABA],(M)

Figure A1.9. I_{GABA} is increased but EC_{50} is unchanged for αA280CβQ185Cγ and αβQ185CγY292C receptors after exposure to DTT. Representative GABA concentration-response curves before (○) and after (■) 2min exposure to 10mM DTT for αA280CβQ185Cγ (A) and αβQ185CγY292C (B) receptors. Inset panels show averaged curves for I_{GABA} normalized to max currents demonstrating similar EC_{50}s before and after DTT. Averaged curves are from at least three oocytes from two different batches.

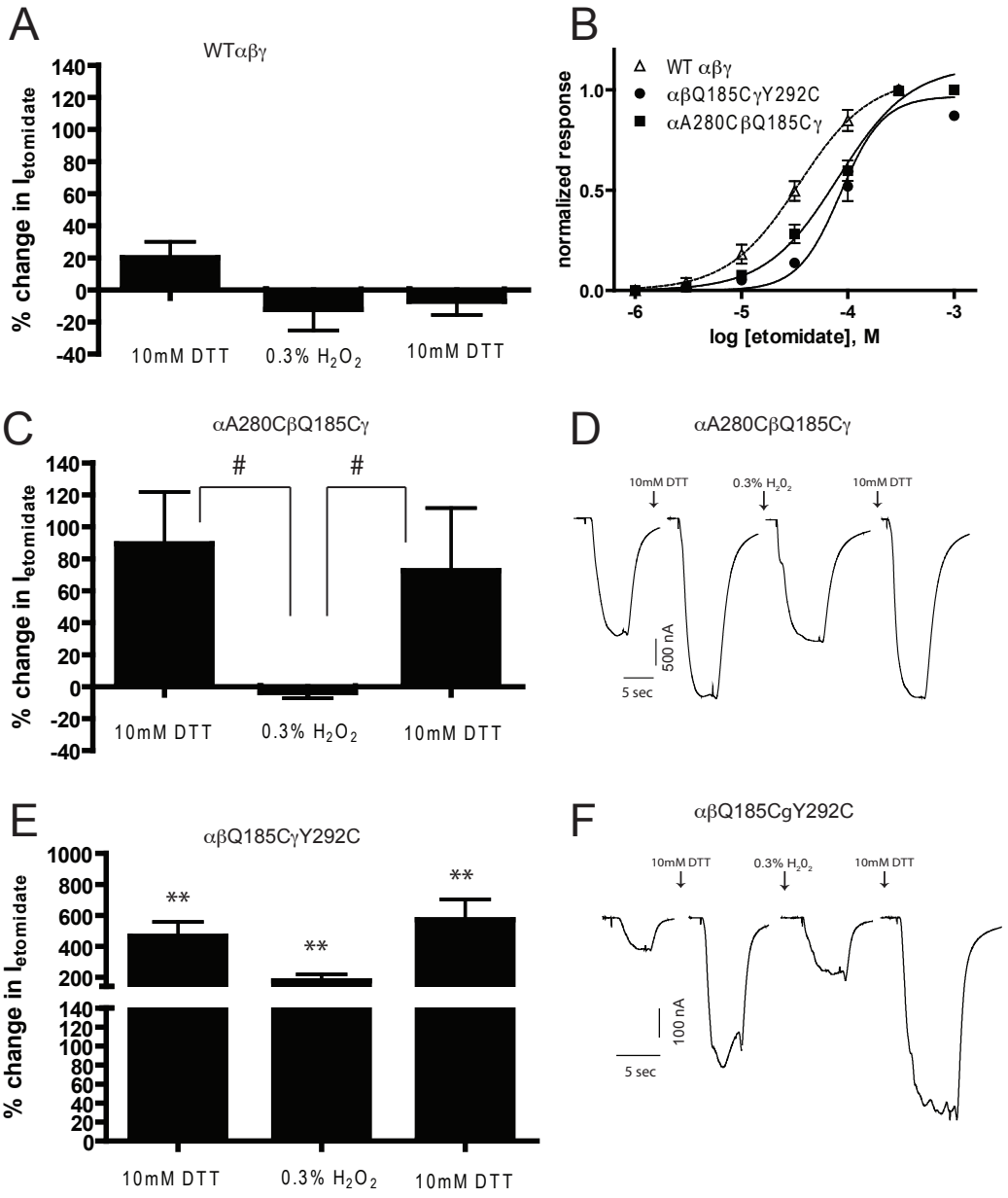
A
WTαβγ
% change in $I_{etomidate}$
10mM DTT
0.3% H_2O_2
10mM DTT
B
WT αβγ
αβQ185CγY292C
αA280CβQ185Cγ
normalized response
log [etomidate], M
C
αA280CβQ185Cγ
#
#
% change in $I_{etomidate}$
10mM DTT
0.3% H_2O_2
10mM DTT
D
αA280CβQ185Cγ
10mM DTT
0.3% H_2O_2
10mM DTT
500 nA
5 sec
E
αβQ185CγY292C
**
**
**
% change in $I_{etomidate}$
10mM DTT
0.3% H_2O_2
10mM DTT
F
αβQ185CgY292C
10mM DTT
0.3% H_2O_2
10mM DTT
100 nA
5 sec

Figure A1.10. Crosslinks at α-β and β-γ interface inhibit $I_{etomidate}$. (A) WTαβγ receptors experience little percent change in EC_{50} $I_{etomdiate}$ after exposure to 10mM DTT or 0.3% H_2O_2. (B) Etomidate concentration response was performed to determine etomidate EC_{50}. (C) αA280CβQ185Cγ receptors experience significant differences in percent change in $I_{etomidate}$ between treatments with DTT and H_2O_2. (E) For αβQ185CγY292C receptors percent change in $I_{etomidate}$ increased significantly after DTT exposure. Panels D and F show representative current traces from mutant containing receptors before and after exposure to DTT and H_2O_2. All values come from three or more oocytes from at least two batches. Percent changes calculated as (($I_{etomidate,afterDTT}$/ $I_{etomidate,before}$)-1) x 100 and (($I_{etomidate,afterH2O2}$/ $I_{etomidate,before}$)-1) x 100. **indicates statistical difference from WT percent change in I_{GABA} under the same condition by one-way ANOVA, $p < 0.01$. $^{\#}$indicates statistical difference within treatments on the same receptor type by t-test, $p < 0.05$.

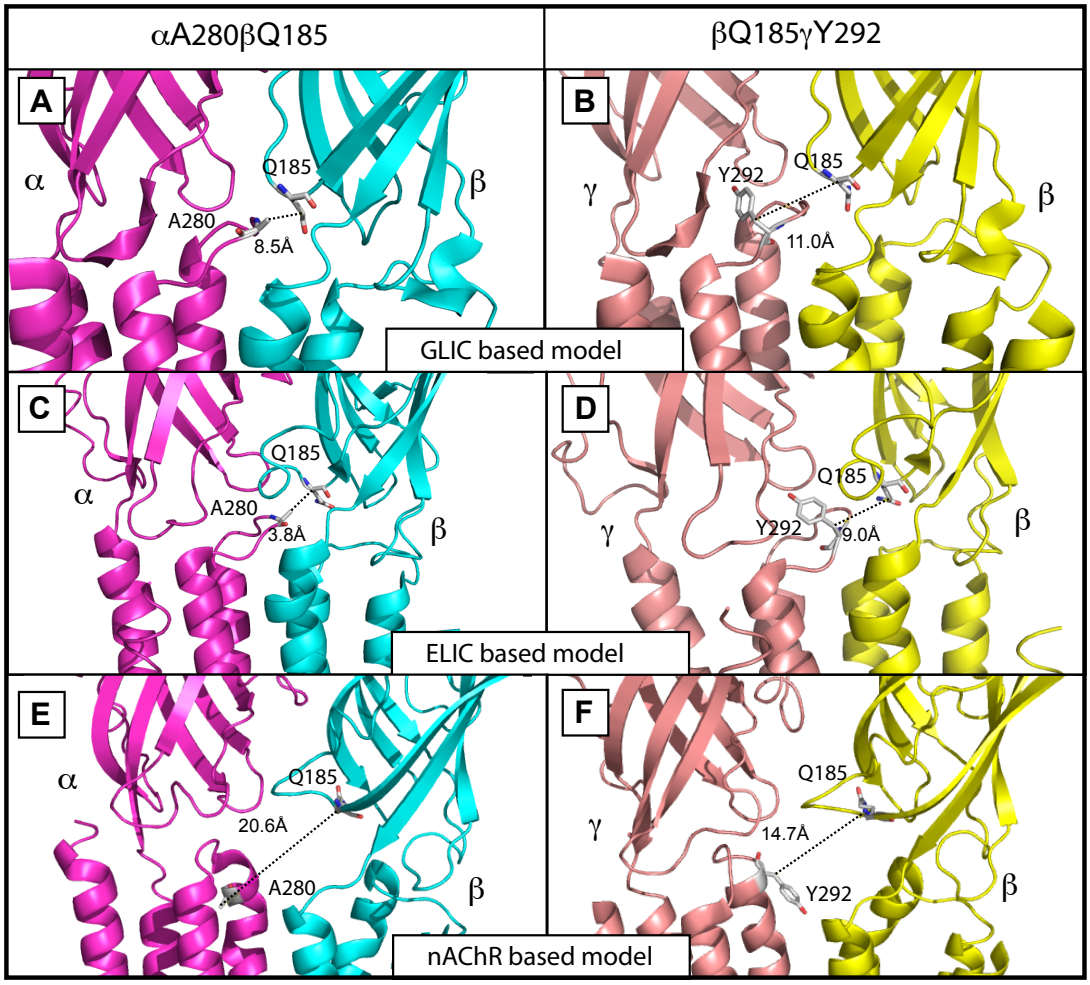
αA280βQ185
βQ185γY292
A
α
Q185
A280
8.5Å
β
B
γ
Y292
Q185
11.0Å
β
GLIC based model
C
α
Q185
A280
3.8Å
β
D
γ
Q185
Y292
9.0Å
β
ELIC based model
E
α
Q185
20.6Å
A280
β
F
γ
Q185
14.7Å
Y292
β
nAChR based model

Figure A1.11. GLIC and ELIC based homology model of the $GABA_A$ receptor are in keeping with crosslinking data. Homology models of a putative crosslink between αA280 and βQ185 (A,C, and E) and βQ185 and γY292 (B,D, and F) show variance in distances between the loop 9 and M2-M3 loop residues. (A, B) Homology models based on GLIC structure in a presumed closed state (PDB# 3EAM) indicate distances unlikely to form a disulfide bond. (C,D) Whereas, a model of the GABA receptor based on the assumed open state ELIC structure (PDB# 2VLO) indicate residues are closer in the open state and assuming some flexibility of unstructure regions could form crosslinks. (E,F) A model of the receptor based on the nAChR cryo-EM structure (PDB# 2BG9) would suggest residues in these regions are very distant and buried in structured regions unlikely to be flexible enough to form disulfide bonds.

Table A1.1. GABA EC_{50} and Hill coefficient values of wild type and mutant receptors.

Receptor	EC_{50}	n_H	n	mut/wt EC_{50}
	μM			
$\alpha_1\beta_2\gamma_2$	18.3 ± 1.9	1.4 ± 0.04	7	1
$\alpha_1\beta_2$(W168C)γ_2	60.4 ± 9.3*	1.7 ± 0.1	3	3.3
$\alpha_1\beta_2$(R169C)γ_2	28.7 ± 3.6	1.1 ± 0.1	4	1.6
$\alpha_1\beta_2$(G170C)γ_2	59.9 ± 1.7*	1.0 ± 0.1	3	3.3
$\alpha_1\beta_2$(D171C) γ_2	196.3 ± 45*	0.6 ± 0.02*	4	10.7
$\alpha_1\beta_2$(D172C) γ_2	8.3 ± 1.1	1.4 ± 0.1	3	0.45
$\alpha_1\beta_2$(N173C)γ_2	25.5 ± 10.1	1.2 ± 0.1	3	1.4
$\alpha_1\beta_2$(A174C)γ_2	597.7 ± 113.2*	0.5 ± 0.1*	3	32.7
$\alpha_1\beta_2$(V175C)γ_2	26.4 ± 8.1	1.4 ± 0.2	3	1.4
$\alpha_1\beta_2$(T176C)γ_2	182.3 ± 45.6*	0.6 ± 0.05*	5	10
$\alpha_1\beta_2$(G177C)γ_2	121.5 ± 22.8*	0.7 ± 0.1*	3	6.6
$\alpha_1\beta_2$(V178C)γ_2	21.2 ± 2.1	1.6 ± 0.1	3	1.2
$\alpha_1\beta_2$(T179C)γ_2	32.0 ± 11.2	1.1 ± 0.1	4	1.8
$\alpha_1\beta_2$(K180C)γ_2	14.6 ± 1.5	1.5 ± 0.1	3	0.8
$\alpha_1\beta_2$(I181C)γ_2	20.3 ± 6.6	1.6 ± 0.1	3	1.1
$\alpha_1\beta_2$(E182C)γ_2	23.9 ± 9.9	1.1 ± 0.2	3	1.3
$\alpha_1\beta_2$(L183C)γ_2	15.6 ± 4.0	1.0 ± 0.1	3	0.85
$\alpha_1\beta_2$(P184C)γ_2	23.9 ± 9.9	1.3 ± 0.03	3	1.3
$\alpha_1\beta_2$(Q185C)γ_2	5.0 ± 1.3*	0.8 ± 0.1*	3	0.27

EC_{50} and Hill coefficient values are expressed as mean ± SEM.
*p<0.002, significantly different from control.

Table A1.2. K_I and Hill coefficient values of wild type and mutant receptors.

Receptor	K_I	n_H	n	mut/wt
	μM			
$\alpha_1\beta_2\gamma_2$	0.21 ± 0.06	1.2 ± 0.03	5	1
$\alpha_1\beta_2$(W168C)γ_2	0.15 ± 0.04	1.3 ± 0.2	3	0.7
$\alpha_1\beta_2$(G170C)γ_2	0.18 ± 0.05	1.2 ± 0.02	3	0.9
$\alpha_1\beta_2$(D171C) γ_2	0.33 ± 0.04*	1.3 ± 0.2	4	1.6
$\alpha_1\beta_2$(A174C)γ_2	0.60 ± 0.1*	1.1 ± 0.0	2	3
$\alpha_1\beta_2$(T176C)γ_2	0.20 ± 0.03	1.2 ± 0.03	3	1
$\alpha_1\beta_2$(G177C)γ_2	0.27 ± 0.03	1.4 ± 0.1	4	1.3
$\alpha_1\beta_2$(Q185C)γ_2	0.13 ± 0.02	1.2 ± 0.1	3	0.6

K_I and Hill coefficient values are expressed as mean ± SEM.
*p<0.01, significantly different from control.

Table A1.3. Second-order rate constants (k_2) for reaction of MTSEA-biotin with mutant receptors in the absence (control) and presence of GABA, SR-95531 and PB.

	Control		GABA EC_{80-90}		SR95531 (10 μM)		Pentobarbital (500 μM)	
Receptor	k_2 ($M^{-1}s^{-1}$)	*n*	k_2 ($M^{-1}s^{-1}$)	*n*	k_2 ($M^{-1}s^{-1}$)	*n*	k_2 ($M^{-1}s^{-1}$)	*n*
$\alpha_1\beta_2$W168Cγ_2	130 ± 20	3	123 ± 6	3	71 ± 4*	3	N.M.	
$\alpha_1\beta_2$V175Cγ_2	11285 ± 923	3	3621± 600**	3	3818 ± 293**	3	5207 ± 768**	3
$\alpha_1\beta_2$Q185Cγ_2	3465 ± 315	3	1281 ± 13**	3	3627 ± 461	3	2607± 47	3

MTSEA-biotin concentrations used were different depending on the mutant and are reported in "Material and Methods".
N.M. indicate not measured.
Values are the mean ± SEM.
* and ** indicate values significantly different from control with $p<0.05$ and $p<0.01$.

Table A1.4 GABA EC_{50} before and after exposure to reducing agent DTT.

Receptor	GABA EC_{50} (μM)	n_H	I_{max} (nA)	n
α_1A280Cβ_2Q185Cγ_2 before DTT	37.1±8.1	1.02±0.11	3883±1028	3
α_1A280Cβ_2Q185Cγ_2 after DTT	21.4±5.8	0.82±0.03	5830±732	4
$\alpha_1\beta_2$Q185Cγ_2Y292C before DTT	17.3±2.2	1.37±0.13	900±198[§]	3
$\alpha_1\beta_2$Q185Cγ_2Y292C after DTT	17.9±1.6	1.12±0.03	3764±1594[§]	3

Values expressed as mean ± SEM.

[§]significantly different from each other by Students t-test.

REFERENCES

Achermann G, Ballard TM, Blasco F, Broutin PE, Buttelmann B, Fischer H, Graf M, Hernandez MC, Hilty P, Knoflach F, Koblet A, Knust H, Kurt A, Martin JR, Masciadri R, Porter RH, Stadler H, Thomas AW, Trube G, Wichmann J (2009) Discovery of the imidazo[1,5-a][1,2,4]-triazolo[1,5-d][1,4]benzodiazepine scaffold as a novel, potent and selective GABA(A) alpha5 inverse agonist series. Bioorganic & medicinal chemistry letters 19:5746-5752.

Akabas MH (2004) GABAA receptor structure-function studies: a reexamination in light of new acetylcholine receptor structures. Int Rev Neurobiol 62:1-43.

Akinci MK, Schofield PR (1999) Widespread expression of GABA(A) receptor subunits in peripheral tissues. Neuroscience research 35:145-153.

Alqazzaz M, Thompson AJ, Price KL, Breitinger HG, Lummis SC (2011) Cys-loop receptor channel blockers also block GLIC. Biophys J 101:2912-2918.

Amin J, Brooks-Kayal A, Weiss DS (1997) Two tyrosine residues on the alpha subunit are crucial for benzodiazepine binding and allosteric modulation of gamma-aminobutyric acidA receptors. Mol Pharmacol 51:833-841.

Amin J, Weiss DS (1993) GABAA receptor needs two homologous domains of the beta-subunit for activation by GABA but not by pentobarbital [see comments]. Nature 366:565-569.

Amin J, Weiss DS (1994) Homomeric rho 1 GABA channels: activation properties and domains. Receptors Channels 2:227-236.

Atack JR (2010) Preclinical and clinical pharmacology of the GABAA receptor alpha5 subtype-selective inverse agonist alpha5IA. Pharmacol Ther 125:11-26.

Avoli M, de Curtis M (2011) GABAergic synchronization in the limbic system and its role in the generation of epileptiform activity. Prog Neurobiol 95:104-132.

Ballard TM, Knoflach F, Prinssen E, Borroni E, Vivian JA, Basile J, Gasser R, Moreau JL, Wettstein JG, Buettelmann B, Knust H, Thomas AW, Trube G, Hernandez MC (2009) RO4938581, a novel cognitive enhancer acting at GABAA alpha5 subunit-containing receptors. Psychopharmacology 202:207-223.

Balter MB, Uhlenhuth EH (1992) New epidemiologic findings about insomnia and its treatment. J Clin Psychiatry 53 Suppl:34-42.

Barberis A, Mozrzymas JW, Ortinski PI, Vicini S (2007) Desensitization and binding properties determine distinct alpha1beta2gamma2 and alpha3beta2gamma2 GABA(A) receptor-channel kinetic behavior. The European journal of neuroscience 25:2726-2740.

Baulac S, Huberfeld G, Gourfinkel-An I, Mitropoulou G, Beranger A, Prud'homme JF, Baulac M, Brice A, Bruzzone R, LeGuern E (2001) First genetic evidence of GABA(A) receptor dysfunction in epilepsy: a mutation in the gamma2-subunit gene. Nat Genet 28:46-48.

Baumann SW, Baur R, Sigel E (2001) Subunit arrangement of gamma-aminobutyric acid type A receptors. J Biol Chem 276:36275-36280.

Baumann SW, Baur R, Sigel E (2002) Forced subunit assembly in alpha1beta2gamma2 GABAA receptors. Insight into the absolute arrangement. J Biol Chem 277:46020-46025.

Baur R, Tan KR, Luscher BP, Gonthier A, Goeldner M, Sigel E (2008) Covalent modification of GABAA receptor isoforms by a diazepam analogue provides evidence for a novel benzodiazepine binding site that prevents modulation by these drugs. J Neurochem 106:2353-2363.

Belelli D, Casula A, Ling A, Lambert JJ (2002) The influence of subunit composition on the interaction of neurosteroids with GABA(A) receptors. Neuropharmacology 43:651-661.

Belelli D, Harrison NL, Maguire J, Macdonald RL, Walker MC, Cope DW (2009) Extrasynaptic GABAA receptors: form, pharmacology, and function. J Neurosci 29:12757-12763.

Benavides J, Peny B, Durand A, Arbilla S, Scatton B (1992) Comparative in vivo and in vitro regional selectivity of central omega (benzodiazepine) site ligands in inhibiting [3H]flumazenil binding in the rat central nervous system. J Pharmacol Exp Ther 263:884-896.

Benes FM, Berretta S (2001) GABAergic interneurons: implications for understanding schizophrenia and bipolar disorder. Neuropsychopharmacology : official publication of the American College of Neuropsychopharmacology 25:1-27.

Benjamini Y, Hochberg Y (1995) Controlling the false discovery rate: a practical and powerful approach to multiple testing. J Royal Stat Soc B 57:289-300.

Benke D, Mertens S, Trzeciak A, Gillessen D, Mohler H (1991) GABAA receptors display association of gamma 2-subunit with alpha 1- and beta 2/3-subunits. J Biol Chem 266:4478-4483.

Benson JA, Low K, Keist R, Mohler H, Rudolph U (1998) Pharmacology of recombinant gamma-aminobutyric acidA receptors rendered diazepam-insensitive by point-mutated alpha-subunits. FEBS Lett 431:400-404.

Bera AK, Chatav M, Akabas MH (2002) GABA(A) receptor M2-M3 loop secondary structure and changes in accessibility during channel gating. J Biol Chem 277:43002-43010.

Berezhnoy D, Nyfeler Y, Gonthier A, Schwob H, Goeldner M, Sigel E (2004) On the benzodiazepine binding pocket in GABAA receptors. J Biol Chem 279:3160-3168.

Bianchi MT, Botzolakis EJ, Haas KF, Fisher JL, Macdonald RL (2007) Microscopic kinetic determinants of macroscopic currents: insights from coupling and uncoupling of GABAA receptor desensitization and deactivation. J Physiol 584:769-787.

Bianchi MT, Botzolakis EJ, Lagrange AH, Macdonald RL (2009) Benzodiazepine modulation of GABA(A) receptor opening frequency depends on activation context: a patch clamp and simulation study. Epilepsy Res 85:212-220.

Bianchi MT, Haas KF, Macdonald RL (2001) Structural determinants of fast desensitization and desensitization-deactivation coupling in GABAa receptors. J Neurosci 21:1127-1136.

Bianchi MT, Haas KF, Macdonald RL (2002a) Alpha1 and alpha6 subunits specify distinct desensitization, deactivation and neurosteroid modulation of GABA(A) receptors containing the delta subunit. Neuropharmacology 43:492-502.

Bianchi MT, Song L, Zhang H, Macdonald RL (2002b) Two different mechanisms of disinhibition produced by GABAA receptor mutations linked to epilepsy in humans. J Neurosci 22:5321-5327.

Bocquet N, Nury H, Baaden M, Le Poupon C, Changeux JP, Delarue M, Corringer PJ (2009) X-ray structure of a pentameric ligand-gated ion channel in an apparently open conformation. Nature 457:111-114.

Boileau AJ, Baur R, Sharkey LM, Sigel E, Czajkowski C (2002a) The relative amount of cRNA coding for gamma2 subunits affects stimulation by benzodiazepines in GABA(A) receptors expressed in Xenopus oocytes. Neuropharmacology 43:695-700.

Boileau AJ, Czajkowski C (1999) Identification of transduction elements for benzodiazepine modulation of the GABA(A) receptor: three residues are required for allosteric coupling. J Neurosci 19:10213-10220.

Boileau AJ, Evers AR, Davis AF, Czajkowski C (1999) Mapping the agonist binding site of the GABAA receptor: evidence for a beta-strand. J Neurosci 19:4847-4854.

Boileau AJ, Kucken AM, Evers AR, Czajkowski C (1998) Molecular dissection of benzodiazepine binding and allosteric coupling using chimeric gamma-aminobutyric acidA receptor subunits. Mol Pharmacol 53:295-303.

Boileau AJ, Li T, Benkwitz C, Czajkowski C, Pearce RA (2003) Effects of gamma2S subunit incorporation on GABAA receptor macroscopic kinetics. Neuropharmacology 44:1003-1012.

Boileau AJ, Newell JG, Czajkowski C (2002b) GABA(A) receptor beta 2 Tyr97 and Leu99 line the GABA-binding site. Insights into mechanisms of agonist and antagonist actions. J Biol Chem 277:2931-2937.

Boileau AJ, Pearce RA, Czajkowski C (2005) Tandem subunits effectively constrain GABAA receptor stoichiometry and recapitulate receptor kinetics but are insensitive to GABAA receptor-associated protein. J Neurosci 25:11219-11230.

Bormann JH, O.; Sakmann, B. (1987) Mechanism of anion permeation through channels gates by glycine and gamma-amino butryic acid in mouse culture spinale neurones. J Physiol 385: 243-86.

Brejc K, van Dijk WJ, Klaassen RV, Schuurmans M, van Der Oost J, Smit AB, Sixma TK (2001) Crystal structure of an ACh-binding protein reveals the ligand-binding domain of nicotinic receptors. Nature 411:269-276.

Brickley SG, Mody I (2012) Extrasynaptic GABA(A) receptors: their function in the CNS and implications for disease. Neuron 73:23-34.

Brooks-Kayal AR, Shumate MD, Jin H, Rikhter TY, Coulter DA (1998) Selective changes in single cell GABA(A) receptor subunit expression and function in temporal lobe epilepsy. Nat Med 4:1166-1172.

Buhr A, Baur R, Malherbe P, Sigel E (1996) Point mutations of the alpha 1 beta 2 gamma 2 gamma-aminobutyric acid(A) receptor affecting modulation of the

channel by ligands of the benzodiazepine binding site. Mol Pharmacol 49:1080-1084.
Buhr A, Baur R, Sigel E (1997a) Subtle changes in residue 77 of the gamma subunit of alpha1beta2gamma2 GABAA receptors drastically alter the affinity for ligands of the benzodiazepine binding site. J Biol Chem 272:11799-11804.
Buhr A, Schaerer MT, Baur R, Sigel E (1997b) Residues at positions 206 and 209 of the alpha1 subunit of gamma-aminobutyric AcidA receptors influence affinities for benzodiazepine binding site ligands. Mol Pharmacol 52:676-682.
Buhr A, Sigel E (1997) A point mutation in the gamma2 subunit of gamma-aminobutyric acid type A receptors results in altered benzodiazepine binding site specificity. Proc Natl Acad Sci U S A 94:8824-8829.
Burkat PM, Yang J, Gingrich KJ (2001) Dominant gating governing transient GABA(A) receptor activity: a first latency and Po/o analysis. J Neurosci 21:7026-7036.
Burzomato V, Beato M, Groot-Kormelink PJ, Colquhoun D, Sivilotti LG (2004) Single-channel behavior of heteromeric alpha1beta glycine receptors: an attempt to detect a conformational change before the channel opens. J Neurosci 24:10924-10940.
Campo-Soria C, Chang Y, Weiss DS (2006) Mechanism of action of benzodiazepines on GABAA receptors. Br J Pharmacol 148:984-990.
Caraiscos VB, Elliott EM, You-Ten KE, Cheng VY, Belelli D, Newell JG, Jackson MF, Lambert JJ, Rosahl TW, Wafford KA, MacDonald JF, Orser BA (2004) Tonic inhibition in mouse hippocampal CA1 pyramidal neurons is mediated by alpha5 subunit-containing gamma-aminobutyric acid type A receptors. Proc Natl Acad Sci U S A 101:3662-3667.
Casalotti SO, Stephenson FA, Barnard EA (1986) Separate subunits for agonist and benzodiazepine binding in the gamma-aminobutyric acidA receptor oligomer. J Biol Chem 261:15013-15016.
Celentano JJ, Wong RK (1994) Multiphasic desensitization of the GABAA receptor in outside-out patches. Biophys J 66:1039-1050.
Celie PH, Kasheverov IE, Mordvintsev DY, Hogg RC, van Nierop P, van Elk R, van Rossum-Fikkert SE, Zhmak MN, Bertrand D, Tsetlin V, Sixma TK, Smit AB (2005a) Crystal structure of nicotinic acetylcholine receptor homolog AChBP in complex with an alpha-conotoxin PnIA variant. Nat Struct Mol Biol 12:582-588.
Celie PH, Klaassen RV, van Rossum-Fikkert SE, van Elk R, van Nierop P, Smit AB, Sixma TK (2005b) Crystal structure of acetylcholine-binding protein from Bulinus truncatus reveals the conserved structural scaffold and sites of variation in nicotinic acetylcholine receptors. J Biol Chem 280:26457-26466.
Celie PH, van Rossum-Fikkert SE, van Dijk WJ, Brejc K, Smit AB, Sixma TK (2004a) Nicotine and carbamylcholine binding to nicotinic acetylcholine receptors as studied in AChBP crystal structures. Neuron 41:907-914.
Celie PH, van Rossum-Fikkert SE, van Dijk WJ, Brejc K, Smit AB, Sixma TK (2004b) Nicotine and carbamylcholine binding to nicotinic acetylcholine receptors as studied in AChBP crystal structures. Neuron 41:907-914.

Chang Y, Wang R, Barot S, Weiss DS (1996) Stoichiometry of a recombinant GABAA receptor. J Neurosci 16:5415-5424.
Changeux JP (2011) Allostery and the Monod-Wyman-Changeux Model After 50 Years. Annual review of biophysics 41:103-33.
Cheng X, Wang H, Grant B, Sine SM, McCammon JA (2006) Targeted molecular dynamics study of C-loop closure and channel gating in nicotinic receptors. PLoS computational biology 96 (9):3582-90.
Cheng Y, Prusoff WH (1973) Relationship between the inhibition constant (K1) and the concentration of inhibitor which causes 50 per cent inhibition (I50) of an enzymatic reaction. Biochem Pharmacol 22:3099-3108.
Clayton T, Chen JL, Ernst M, Richter L, Cromer BA, Morton CJ, Ng H, Kaczorowski CC, Helmstetter FJ, Furtmuller R, Ecker G, Parker MW, Sieghart W, Cook JM (2007) An updated unified pharmacophore model of the benzodiazepine binding site on gamma-aminobutyric acid(a) receptors: correlation with comparative models. Curr Med Chem 14:2755-2775.
Codding PW, Muir AK (1985) Molecular structure of Ro15-1788 and a model for the binding of benzodiazepine receptor ligands. Structural identification of common features in antagonists. Mol Pharmacol 28:178-184.
Cole BJ, Hillmann M, Seidelmann D, Klewer M, Jones GH (1995) Effects of benzodiazepine receptor partial inverse agonists in the elevated plus maze test of anxiety in the rat. Psychopharmacology 121:118-126.
Colquhoun D (1998) Binding, gating, affinity and efficacy: the interpretation of structure-activity relationships for agonists and of the effects of mutating receptors. Br J Pharmacol 125:924-947.
Colquhoun D, Hawkes AG (1995) Desensitization of N-methyl-D-aspartate receptors: a problem of interpretation. Proc Natl Acad Sci U S A 92:10327-10329.
Corradi J, Gumilar F, Bouzat C (2009) Single-channel kinetic analysis for activation and desensitization of homomeric 5-HT(3)A receptors. Biophys J 97:1335-1345.
Corringer PJ, Baaden M, Bocquet N, Delarue M, Dufresne V, Nury H, Prevost M, Van Renterghem C (2010) Atomic structure and dynamics of pentameric ligand-gated ion channels: new insight from bacterial homologues. J Physiol 588:565-572.
Crestani F, Keist R, Fritschy JM, Benke D, Vogt K, Prut L, Bluthmann H, Mohler H, Rudolph U (2002) Trace fear conditioning involves hippocampal alpha5 GABA(A) receptors. Proc Natl Acad Sci U S A 99:8980-8985.
Cromer BA, Morton CJ, Parker MW (2002) Anxiety over GABA(A) receptor structure relieved by AChBP. Trends Biochem Sci 27:280-287.
Dalziel JE, Cox GB, Gage PW, Birnir B (1999) Mutant human alpha(1)beta(1)(T262Q) GABA(A) receptors are directly activated but not modulated by pentobarbital. Eur J Pharmacol 385:283-286.
Darcourt G, Pringuey D, Salliere D, Lavoisy J (1999) The safety and tolerability of zolpidem--an update. J Psychopharmacol 13:81-93.

Davies M, Bateson AN, Dunn SM (1998) Structural requirements for ligand interactions at the benzodiazepine recognition site of the GABA(A) receptor. J Neurochem 70:2188-2194.

Davies M, Martin IL, Bateson AN, Hadingham KL, Whiting PJ, Dunn SM (1996) Identification of domains in human recombinant GABAA receptors that are photoaffinity labelled by [3H]flunitrazepam and [3H]Ro15-4513. Neuropharmacology 35:1199-1208.

Davies M, Newell JG, Derry JM, Martin IL, Dunn SM (2000) Characterization of the interaction of zopiclone with gamma-aminobutyric acid type A receptors. Mol Pharmacol 58:756-762.

Del Castillo J, Katz B (1957) Interaction at end-plate receptors between different choline derivatives. Proc R Soc Lond B Biol Sci 146:369-381.

Dellisanti CD, Hanson SM, Chen L, Czajkowski C (2011) Packing of the extracellular domain hydrophobic core has evolved to facilitate pentameric ligand-gated ion channel function. J Biol Chem 286:3658-3670.

Dellisanti CD, Yao Y, Stroud JC, Wang ZZ, Chen L (2007) Crystal structure of the extracellular domain of nAChR alpha1 bound to alpha-bungarotoxin at 1.94 A resolution. Nat Neurosci 10:953-962.

Derry JM, Dunn SM, Davies M (2004) Identification of a residue in the gamma-aminobutyric acid type A receptor alpha subunit that differentially affects diazepam-sensitive and -insensitive benzodiazepine site binding. J Neurochem 88:1431-1438.

Dhir A, Rogawski MA (2012) Role of neurosteroids in the anticonvulsant activity of midazolam. Br J Pharmacol 165:2684-2691.

Dibbens LM, Harkin LA, Richards M, Hodgson BL, Clarke AL, Petrou S, Scheffer IE, Berkovic SF, Mulley JC (2009) The role of neuronal GABA(A) receptor subunit mutations in idiopathic generalized epilepsies. Neurosci Lett 453:162-165.

Dominguez-Perrot C, Feltz P, Poulter MO (1996) Recombinant GABAA receptor desensitization: the role of the gamma 2 subunit and its physiological significance. J Physiol 497 (Pt 1):145-159.

Downing SS, Lee YT, Farb DH, Gibbs TT (2005) Benzodiazepine modulation of partial agonist efficacy and spontaneously active GABA(A) receptors supports an allosteric model of modulation. Br J Pharmacol 145:894-906.

Duncalfe LL, Carpenter MR, Smillie LB, Martin IL, Dunn SM (1996) The major site of photoaffinity labeling of the gamma-aminobutyric acid type A receptor by [3H]flunitrazepam is histidine 102 of the alpha subunit. J Biol Chem 271:9209-9214.

Duncalfe LL, Dunn SM (1996) Mapping of GABAA receptor sites that are photoaffinity-labelled by [3H]flunitrazepam and [3H]Ro 15-4513. Eur J Pharmacol 298:313-319.

Duret G, Van Renterghem C, Weng Y, Prevost M, Moraga-Cid G, Huon C, Sonner JM, Corringer PJ (2011) Functional prokaryotic-eukaryotic chimera from the pentameric ligand-gated ion channel family. Proc Natl Acad Sci U S A 108:12143-12148.

Edwards FA, Konnerth A, Sakmann B (1990) Quantal analysis of inhibitory synaptic transmission in the dentate gyrus of rat hippocampal slices: a patch-clamp study. J Physiol 430:213-249.

Ericksen SS, Boileau AJ (2007) Tandem couture: Cys-loop receptor concatamer insights and caveats. Mol Neurobiol 35:113-128.

Eyre MD, Renzi M, Farrant M, Nusser Z (2012) Setting the Time Course of Inhibitory Synaptic Currents by Mixing Multiple GABAA Receptor alpha Subunit Isoforms. J Neurosci 32:5853-5867.

Farrant M, Nusser Z (2005) Variations on an inhibitory theme: phasic and tonic activation of GABA(A) receptors. Nature reviews Neuroscience 6:215-229.

Farrar SJ, Whiting PJ, Bonnert TP, McKernan RM (1999) Stoichiometry of a ligand-gated ion channel determined by fluorescence energy transfer. J Biol Chem 274:10100-10104.

Feng HJ, Macdonald RL (2004) Proton modulation of alpha 1 beta 3 delta GABAA receptor channel gating and desensitization. J Neurophysiol 92:1577-1585.

Fisher JL, Macdonald RL (1997) Single channel properties of recombinant GABAA receptors containing gamma 2 or delta subtypes expressed with alpha 1 and beta 3 subtypes in mouse L929 cells. J Physiol 505 (Pt 2):283-297.

Fritschy JM, Benke D, Mertens S, Oertel WH, Bachi T, Mohler H (1992) Five subtypes of type A gamma-aminobutyric acid receptors identified in neurons by double and triple immunofluorescence staining with subunit-specific antibodies. Proc Natl Acad Sci U S A 89:6726-6730.

Gabriella G, Giovanna C (2010) gamma-Aminobutyric acid type A (GABA(A)) receptor subtype inverse agonists as therapeutic agents in cognition. Methods in enzymology 485:197-211.

Galzi JL, Revah F, Black D, Goeldner M, Hirth C, Changeux JP (1990) Identification of a novel amino acid alpha-tyrosine 93 within the cholinergic ligands-binding sites of the acetylcholine receptor by photoaffinity labeling. Additional evidence for a three-loop model of the cholinergic ligands-binding sites. J Biol Chem 265:10430-10437.

Gao F, Bren N, Burghardt TP, Hansen S, Henchman RH, Taylor P, McCammon JA, Sine SM (2005a) Agonist-mediated conformational changes in acetylcholine-binding protein revealed by simulation and intrinsic tryptophan fluorescence. J Biol Chem 280:8443-8451.

Gao F, Bren N, Burghardt TP, Hansen S, Henchman RH, Taylor P, McCammon JA, Sine SM (2005b) Agonist-mediated conformational changes in acetylcholine-binding protein revealed by simulation and intrinsic tryptophan fluorescence. J Biol Chem 280:8443-8451.

Ghanouni P, Gryczynski Z, Steenhuis JJ, Lee TW, Farrens DL, Lakowicz JR, Kobilka BK (2001) Functionally different agonists induce distinct conformations in the G protein coupling domain of the beta 2 adrenergic receptor. J Biol Chem 276:24433-24436.

Gielen MC, Lumb MJ, Smart TG (2012) Benzodiazepines Modulate GABAA Receptors by Regulating the Preactivation Step after GABA Binding. J Neurosci 32:5707-5715.

Goldschen-Ohm MP, Wagner DA, Petrou S, Jones MV (2010) An epilepsy-related region in the GABA(A) receptor mediates long-distance effects on GABA and benzodiazepine binding sites. Mol Pharmacol 77:35-45.

Gonzalez-Gutierrez G, Lukk T, Agarwal V, Papke D, Nair SK, Grosman C (2012) Mutations that stabilize the open state of the Erwinia chrisanthemi ligand-gated ion channel fail to change the conformation of the pore domain in crystals. Proc Natl Acad Sci U S A 109:6331-6336.

Graham D, Faure C, Besnard F, Langer SZ (1996) Pharmacological profile of benzodiazepine site ligands with recombinant GABAA receptor subtypes. Eur Neuropsychopharmacol 6:119-125.

Graham FL, van der Eb AJ (1973) Transformation of rat cells by DNA of human adenovirus 5. Virology 54:536-539.

Greenfield LJ, Jr., Zaman SH, Sutherland ML, Lummis SC, Niemeyer MI, Barnard EA, Macdonald RL (2002) Mutation of the GABAA receptor M1 transmembrane proline increases GABA affinity and reduces barbiturate enhancement. Neuropharmacology 42:502-521.

Grutter T, Prado de Carvalho L, Virginie D, Taly A, Fischer M, Changeux JP (2005) A chimera encoding the fusion of an acetylcholine-binding protein to an ion channel is stabilized in a state close to the desensitized form of ligand-gated ion channels. C R Biol 328:223-234.

Haas KF, Macdonald RL (1999) GABAA receptor subunit gamma2 and delta subtypes confer unique kinetic properties on recombinant GABAA receptor currents in mouse fibroblasts. J Physiol 514 (Pt 1):27-45.

Hales TG, Lambert JJ (1991) The actions of propofol on inhibitory amino acid receptors of bovine adrenomedullary chromaffin cells and rodent central neurones. Br J Pharmacol 104:619-628.

Hansen SB, Sulzenbacher G, Huxford T, Marchot P, Taylor P, Bourne Y (2005) Structures of Aplysia AChBP complexes with nicotinic agonists and antagonists reveal distinctive binding interfaces and conformations. Embo J 24:3635-3646.

Hanson SM, Czajkowski C (2008) Structural mechanisms underlying benzodiazepine modulation of the GABA(A) receptor. J Neurosci 28:3490-3499.

Hanson SM, Czajkowski C (2011) Disulphide trapping of the GABA(A) receptor reveals the importance of the coupling interface in the action of benzodiazepines. Br J Pharmacol 162:673-687.

Hanson SM, Morlock EV, Satyshur KA, Czajkowski C (2008) Structural requirements for eszopiclone and zolpidem binding to the gamma-aminobutyric acid type-A (GABAA) receptor are different. J Med Chem 51:7243-7252.

Harkin LA, Bowser DN, Dibbens LM, Singh R, Phillips F, Wallace RH, Richards MC, Williams DA, Mulley JC, Berkovic SF, Scheffer IE, Petrou S (2002) Truncation of the GABA(A)-receptor gamma2 subunit in a family with generalized epilepsy with febrile seizures plus. Am J Hum Genet 70:530-536.

Henchman RH, Wang HL, Sine SM, Taylor P, McCammon JA (2005) Ligand-induced conformational change in the alpha7 nicotinic receptor ligand binding domain. Biophys J 88:2564-2576.

Herb A, Wisden W, Luddens H, Puia G, Vicini S, Seeburg PH (1992) The third gamma subunit of the gamma-aminobutyric acid type A receptor family. Proc Natl Acad Sci U S A 89:1433-1437.

Hevers W, Luddens H (1998) The diversity of GABAA receptors. Pharmacological and electrophysiological properties of GABAA channel subtypes. Mol Neurobiol 18:35-86.

Hibbs RE, Gouaux E (2011) Principles of activation and permeation in an anion-selective Cys-loop receptor. Nature 474:54-60.

Hibbs RE, Radic Z, Taylor P, Johnson DA (2006) Influence of agonists and antagonists on the segmental motion of residues near the agonist binding pocket of the acetylcholine-binding protein. J Biol Chem 281:39708-39718.

Hilf RJ, Bertozzi C, Zimmermann I, Reiter A, Trauner D, Dutzler R (2010) Structural basis of open channel block in a prokaryotic pentameric ligand-gated ion channel. Nat Struct Mol Biol 17:1330-1336.

Hilf RJ, Dutzler R (2008) X-ray structure of a prokaryotic pentameric ligand-gated ion channel. Nature 452:375-379.

Hinkle DJ, Macdonald RL (2003) Beta subunit phosphorylation selectively increases fast desensitization and prolongs deactivation of alpha1beta1gamma2L and alpha1beta3gamma2L GABA(A) receptor currents. J Neurosci 23:11698-11710.

Holden JH, Czajkowski C (2002) Different residues in the GABA(A) receptor alpha 1T60-alpha 1K70 region mediate GABA and SR-95531 actions. J Biol Chem 277:18785-18792.

Hosie AM, Dunne EL, Harvey RJ, Smart TG (2003) Zinc-mediated inhibition of GABA(A) receptors: discrete binding sites underlie subtype specificity. Nat Neurosci 6:362-369.

Huey R, Morris GM, Olson AJ, Goodsell DS (2007) A semiempirical free energy force field with charge-based desolvation. J Comput Chem 28:1145-1152.

IMS (2011) The Use of Medicines in the United States: Review of 2010. Institute of Healthcare informatics.

Isaacson JS, Scanziani M (2011) How inhibition shapes cortical activity. Neuron 72:231-243.

Ito Y, Abiko E, Mitani K, Fukuda H (1994) Characterization of diazepam-insensitive [3H]Ro 15-4513 binding in rodent brain and cultured cerebellar neuronal cells. Neurochemical research 19:289-295.

Jackson MB, Lecar H, Mathers DA, Barker JL (1982) Single channel currents activated by gamma-aminobutyric acid, muscimol, and (-)-pentobarbital in cultured mouse spinal neurons. J Neurosci 2:889-894.

Jenkins A, Greenblatt EP, Faulkner HJ, Bertaccini E, Light A, Lin A, Andreasen A, Viner A, Trudell JR, Harrison NL (2001) Evidence for a common binding cavity for three general anesthetics within the GABAA receptor. J Neurosci 21:RC136.

Jia F, Pignataro L, Schofield CM, Yue M, Harrison NL, Goldstein PA (2005) An extrasynaptic GABAA receptor mediates tonic inhibition in thalamic VB neurons. J Neurophysiol 94:4491-4501.

Jones MV, Sahara Y, Dzubay JA, Westbrook GL (1998) Defining affinity with the GABAA receptor. J Neurosci 18:8590-8604.
Jones MV, Westbrook GL (1995) Desensitized states prolong GABAA channel responses to brief agonist pulses. Neuron 15:181-191.
Jones MV, Westbrook GL (1996) The impact of receptor desensitization on fast synaptic transmission. Trends Neurosci 19:96-101.
Jones MV, Westbrook GL (1997) Shaping of IPSCs by endogenous calcineurin activity. J Neurosci 17:7626-7633.
Karlin A (2002) Emerging structure of the nicotinic acetylcholine receptors. Nat Rev Neurosci 3:102-114.
Klausberger T (2009) GABAergic interneurons targeting dendrites of pyramidal cells in the CA1 area of the hippocampus. The European journal of neuroscience 30:947-957.
Kleingoor C, Wieland HA, Korpi ER, Seeburg PH, Kettenmann H (1993) Current potentiation by diazepam but not GABA sensitivity is determined by a single histidine residue. Neuroreport 4:187-190.
Kleinle J, Vogt K, Luscher HR, Muller L, Senn W, Wyler K, Streit J (1996) Transmitter concentration profiles in the synaptic cleft: an analytical model of release and diffusion. Biophys J 71:2413-2426.
Kloda JH, Czajkowski C (2007) Agonist-, antagonist-, and benzodiazepine-induced structural changes in the alpha1 Met113-Leu132 region of the GABAA receptor. Mol Pharmacol 71:483-493.
Krystal AD, Walsh JK, Laska E, Caron J, Amato DA, Wessel TC, Roth T (2003) Sustained efficacy of eszopiclone over 6 months of nightly treatment: results of a randomized, double-blind, placebo-controlled study in adults with chronic insomnia. Sleep 26:793-799.
Kucken AM, Teissere JA, Seffinga-Clark J, Wagner DA, Czajkowski C (2003) Structural requirements for imidazobenzodiazepine binding to GABA(A) receptors. Mol Pharmacol 63:289-296.
Kucken AM, Wagner DA, Ward PR, Teissere JA, Boileau AJ, Czajkowski C (2000) Identification of benzodiazepine binding site residues in the gamma2 subunit of the gamma-aminobutyric acid(A) receptor. Mol Pharmacol 57:932-939.
Kumar S, Nussinov R (1999) Salt bridge stability in monomeric proteins. J Mol Biol 293:1241-1255.
Lagrange AH, Botzolakis EJ, Macdonald RL (2007) Enhanced macroscopic desensitization shapes the response of alpha4 subtype-containing GABAA receptors to synaptic and extrasynaptic GABA. J Physiol 578:655-676.
Laha KT, Wagner DA (2011) A State-Dependent Salt-Bridge Interaction Exists across the {beta}/{alpha} Intersubunit Interface of the GABAA Receptor. Mol Pharmacol 79:662-671.
Lanctot KL, Herrmann N, Mazzotta P, Khan LR, Ingber N (2004) GABAergic function in Alzheimer's disease: evidence for dysfunction and potential as a therapeutic target for the treatment of behavioural and psychological symptoms of dementia. Can J Psychiatry 49:439-453.
Lape R, Colquhoun D, Sivilotti LG (2008) On the nature of partial agonism in the nicotinic receptor superfamily. Nature 454:722-727.

Lape R, Plested AJ, Moroni M, Colquhoun D, Sivilotti LG (2012) The alpha1K276E startle disease mutation reveals multiple intermediate states in the gating of glycine receptors. J Neurosci 32:1336-1352.
Lavoie AM, Twyman RE (1996) Direct Evidence For Diazepam Modulation of GABAA Receptor Microscopic Affinity. Neuropharmacology 35:1383-1392.
Leeb-Lundberg F, Snowman A, Olsen RW (1980) Barbiturate receptor sites are coupled to benzodiazepine receptors. Proc Natl Acad Sci U S A 77:7468-7472.
Leeb-Lundberg F, Snowman A, Olsen RW (1981a) Interaction of anticonvulsants with the barbiturate-benzodiazepine-GABA receptor complex. Eur J Pharmacol 72:125-129.
Leeb-Lundberg F, Snowman A, Olsen RW (1981b) Perturbation of benzodiazepine receptor binding by pyrazolopyridines involves picrotoxinin/barbiturate receptor sites. J Neurosci 1:471-477.
Leite JF, Blanton MP, Shahgholi M, Dougherty DA, Lester HA (2003) Conformation-dependent hydrophobic photolabeling of the nicotinic receptor: electrophysiology-coordinated photochemistry and mass spectrometry. Proc Natl Acad Sci U S A 100:13054-13059.
Leonard RJ, Labarca CG, Charnet P, Davidson N, Lester HA (1988) Evidence that the M2 membrane-spanning region lines the ion channel pore of the nicotinic receptor. Science 242:1578-1581.
Levitt P, Eagleson KL, Powell EM (2004) Regulation of neocortical interneuron development and the implications for neurodevelopmental disorders. Trends Neurosci 27:400-406.
Lewis DA, Hashimoto T, Volk DW (2005) Cortical inhibitory neurons and schizophrenia. Nature reviews Neuroscience 6:312-324.
Li GD, Chiara DC, Sawyer GW, Husain SS, Olsen RW, Cohen JB (2006) Identification of a GABAA receptor anesthetic binding site at subunit interfaces by photolabeling with an etomidate analog. J Neurosci 26:11599-11605.
Li SX, Huang S, Bren N, Noridomi K, Dellisanti CD, Sine SM, Chen L (2011) Ligand-binding domain of an alpha7-nicotinic receptor chimera and its complex with agonist. Nat Neurosci 14:1253-1259.
Low K, Crestani F, Keist R, Benke D, Brunig I, Benson JA, Fritschy JM, Rulicke T, Bluethmann H, Mohler H, Rudolph U (2000) Molecular and neuronal substrate for the selective attenuation of anxiety. Science 290:131-134.
Lowe SL, Francis PT, Procter AW, Palmer AM, Davison AN, Bowen DM (1988) Gamma-aminobutyric acid concentration in brain tissue at two stages of Alzheimer's disease. Brain : a journal of neurology 111 (Pt 4):785-799.
MacDonald RL, Rogers CJ, Twyman RE (1989) Barbiturate regulation of kinetic properties of the GABAA receptor channel of mouse spinal neurones in culture. J Physiol 417:483-500.
Macdonald RL, Young AB (1981) Pharmacology of GABA-mediated inhibition of spinal cord neurons in vivo and in primary dissociated cell culture. Molecular and cellular biochemistry 38 Spec No:147-162.
Majewska MD, Harrison NL, Schwartz RD, Barker JL, Paul SM (1986) Steroid hormone metabolites are barbiturate-like modulators of the GABA receptor. Science 232:1004-1007.

Marini C, Harkin LA, Wallace RH, Mulley JC, Scheffer IE, Berkovic SF (2003) Childhood absence epilepsy and febrile seizures: a family with a GABA(A) receptor mutation. Brain : a journal of neurology 126:230-240.

McCracken ML, Borghese CM, Trudell JR, Harris RA (2010) A transmembrane amino acid in the GABAA receptor beta2 subunit critical for the actions of alcohols and anesthetics. J Pharmacol Exp Ther 335:600-606.

McKernan RM, Rosahl TW, Reynolds DS, Sur C, Wafford KA, Atack JR, Farrar S, Myers J, Cook G, Ferris P, Garrett L, Bristow L, Marshall G, Macaulay A, Brown N, Howell O, Moore KW, Carling RW, Street LJ, Castro JL, Ragan CI, Dawson GR, Whiting PJ (2000) Sedative but not anxiolytic properties of benzodiazepines are mediated by the GABA(A) receptor alpha1 subtype. Nat Neurosci 3:587-592.

McKernan RM, Whiting PJ (1996) Which GABAA-receptor subtypes really occur in the brain? Trends Neurosci 19:139-143.

Mellor JR, Randall AD (1997) Frequency-dependent actions of benzodiazepines on GABAA receptors in cultured murine cerebellar granule cells. J Physiol 503 (Pt 2):353-369.

Mendez P, Bacci A (2011) Assortment of GABAergic plasticity in the cortical interneuron melting pot. Neural plasticity 2011:976856.

Mercado J, Czajkowski C (2006) Charged residues in the alpha1 and beta2 pre-M1 regions involved in GABAA receptor activation. J Neurosci 26:2031-2040.

Mihic SJ, Whiting PJ, Klein RL, Wafford KA, Harris RA (1994) A single amino acid of the human gamma-aminobutyric acid type A receptor gamma 2 subunit determines benzodiazepine efficacy. J Biol Chem 269:32768-32773.

Mihic SJ, Ye Q, Wick MJ, Koltchine VV, Krasowski MD, Finn SE, Mascia MP, Valenzuela CF, Hanson KK, Greenblatt EP, Harris RA, Harrison NL (1997) Sites of alcohol and volatile anaesthetic action on GABA(A) and glycine receptors. Nature 389:385-389.

Miyazawa A, Fujiyoshi Y, Unwin N (2003) Structure and gating mechanism of the acetylcholine receptor pore. Nature 423:949-955.

Mohler H (2007) Molecular regulation of cognitive functions and developmental plasticity: impact of GABAA receptors. J Neurochem 102:1-12.

Mohler H, Fritschy JM, Rudolph U (2002) A new benzodiazepine pharmacology. J Pharmacol Exp Ther 300:2-8.

Monod J, Wyman J, Changeux JP (1965) On the Nature of Allosteric Transitions: A Plausible Model. J Mol Biol 12:88-118.

Morlock EV, Czajkowski C (2011) Different residues in the GABAA receptor benzodiazepine binding pocket mediate benzodiazepine efficacy and binding. Mol Pharmacol 80:14-22.

Morris GM, Goodsell DS, Halliday RS, Huey R, Hart WE, Belew RK, Olson AJ (1998) Automated Docking Using a Lamarckian Genetic Algorithm and an Empirical Binding Free Energy Function. J Comput Chem 19:1639-1662.

Mortensen M, Ebert B, Wafford K, Smart TG (2010) Distinct activities of GABA agonists at synaptic- and extrasynaptic-type GABAA receptors. J Physiol 588:1251-1268.

Mortensen MP, B.; Smart, T. (2012) GABA Potency at GABAA receptors found in synaptic and extrasynaptic zones. Frontiers in cellular neuroscience 6.
Mozrzymas JW, Wójtowicz T, Piast M, Lebida K, Wyrembek P, Mercik K (2007) GABA transient sets the susceptibility of mIPSCs to modulation by benzodiazepine receptor agonists in rat hippocampal neurons. J Physiol 585:29-46.
Mukhtasimova N, Lee WY, Wang HL, Sine SM (2009) Detection and trapping of intermediate states priming nicotinic receptor channel opening. Nature 459:451-454.
Newell JG, Czajkowski C (2003) The GABAA receptor alpha 1 subunit Pro174-Asp191 segment is involved in GABA binding and channel gating. J Biol Chem 278:13166-13172.
Nury H, Bocquet N, Le Poupon C, Raynal B, Haouz A, Corringer PJ, Delarue M (2010) Crystal structure of the extracellular domain of a bacterial ligand-gated ion channel. J Mol Biol 395:1114-1127.
Nury H, Poitevin F, Van Renterghem C, Changeux JP, Corringer PJ, Delarue M, Baaden M One-microsecond molecular dynamics simulation of channel gating in a nicotinic receptor homologue. Proc Natl Acad Sci U S A 107:6275-6280.
Nury H, Van Renterghem C, Weng Y, Tran A, Baaden M, Dufresne V, Changeux JP, Sonner JM, Delarue M, Corringer PJ (2011) X-ray structures of general anaesthetics bound to a pentameric ligand-gated ion channel. Nature 469:428-431.
Nusser Z, Sieghart W, Mody I (1999) Differential regulation of synaptic GABAA receptors by cAMP-dependent protein kinase in mouse cerebellar and olfactory bulb neurones. J Physiol 521 Pt 2:421-435.
Nusser Z, Sieghart W, Somogyi P (1998) Segregation of different GABAA receptors to synaptic and extrasynaptic membranes of cerebellar granule cells. J Neurosci 18:1693-1703.
Ohayon MM (2002) Epidemiology of insomnia: what we know and what we still need to learn. Sleep Med Rev 6:97-111.
Olsen RW, Sieghart W (2009) GABA A receptors: subtypes provide diversity of function and pharmacology. Neuropharmacology 56:141-148.
Olsen RW, Snowman AM (1982) Chloride-dependent enhancement by barbiturates of gamma-aminobutyric acid receptor binding. J Neurosci 2:1812-1823.
Olsen RW, Yang J, King RG, Dilber A, Stauber GB, Ransom RW (1986) Barbiturate and benzodiazepine modulation of GABA receptor binding and function. Life sciences 39:1969-1976.
Ortells MO, Lunt GG (1995) Evolutionary history of the ligand-gated ion-channel superfamily of receptors. Trends Neurosci 18:121-127.
Pan J, Chen Q, Willenbring D, Yoshida K, Tillman T, Kashlan OB, Cohen A, Kong XP, Xu Y, Tang P (2012) Structure of the pentameric ligand-gated ion channel ELIC cocrystallized with its competitive antagonist acetylcholine. Nature communications 3:714.
Pascual JM, Karlin A (1998) State-dependent accessibility and electrostatic potential in the channel of the acetylcholine receptor. Inferences from rates of reaction of thiosulfonates with substituted cysteines in the M2 segment of the alpha subunit. J Gen Physiol 111:717-739.

Persohn E, Malherbe P, Richards JG (1992) Comparative molecular neuroanatomy of cloned GABAA receptor subunits in the rat CNS. The Journal of comparative neurology 326:193-216.

Petrini EM, Nieus T, Ravasenga T, Succol F, Guazzi S, Benfenati F, Barberis A (2011) Influence of GABAAR monoliganded states on GABAergic responses. J Neurosci 31:1752-1761.

Pirker S, Schwarzer C, Wieselthaler A, Sieghart W, Sperk G (2000) GABA(A) receptors: immunocytochemical distribution of 13 subunits in the adult rat brain. Neuroscience 101:815-850.

Pritchett DB, Seeburg PH (1990) Gamma-aminobutyric acidA receptor alpha 5-subunit creates novel type II benzodiazepine receptor pharmacology. J Neurochem 54:1802-1804.

Pritchett DB, Seeburg PH (1991) gamma-Aminobutyric acid type A receptor point mutation increases the affinity of compounds for the benzodiazepine site. Proc Natl Acad Sci U S A 88:1421-1425.

Puia G, Costa E, Vicini S (1994) Functional diversity of GABA-activated Cl- currents in Purkinje versus granule neurons in rat cerebellar slices. Neuron 12:117-126.

Puia G, Vicini S, Seeburg PH, Costa E (1991) Influence of recombinant gamma-aminobutyric acid-A receptor subunit composition on the action of allosteric modulators of gamma-aminobutyric acid-gated Cl- currents. Mol Pharmacol 39:691-696.

Ramakrishnan K, Scheid DC (2007) Treatment options for insomnia. Am Fam Physician 76:517-526.

Ramerstorfer J, Furtmuller R, Sarto-Jackson I, Varagic Z, Sieghart W, Ernst M The GABAA receptor alpha+beta- interface: a novel target for subtype selective drugs. J Neurosci 31:870-877.

Ramerstorfer J, Furtmuller R, Sarto-Jackson I, Varagic Z, Sieghart W, Ernst M (2011) The GABAA receptor alpha+beta- interface: a novel target for subtype selective drugs. J Neurosci 31:870-877.

Redrobe JP, Elster L, Frederiksen K, Bundgaard C, de Jong IE, Smith GP, Bruun AT, Larsen PH, Didriksen M (2011) Negative modulation of GABA(A) alpha5 receptors by RO4938581 attenuates discrete sub-chronic and early postnatal phencyclidine (PCP)-induced cognitive deficits in rats. Psychopharmacology.

Reinikainen KJ, Paljarvi L, Huuskonen M, Soininen H, Laakso M, Riekkinen PJ (1988) A post-mortem study of noradrenergic, serotonergic and GABAergic neurons in Alzheimer's disease. Journal of the neurological sciences 84:101-116.

Renard S, Olivier A, Granger P, Avenet P, Graham D, Sevrin M, George P, Besnard F (1999) Structural elements of the gamma-aminobutyric acid type A receptor conferring subtype selectivity for benzodiazepine site ligands. J Biol Chem 274:13370-13374.

Reynolds DS, Rosahl TW, Cirone J, O'Meara GF, Haythornthwaite A, Newman RJ, Myers J, Sur C, Howell O, Rutter AR, Atack J, Macaulay AJ, Hadingham KL, Hutson PH, Belelli D, Lambert JJ, Dawson GR, McKernan R, Whiting PJ, Wafford KA (2003) Sedation and anesthesia mediated by distinct GABA(A) receptor isoforms. J Neurosci 23:8608-8617.

Richter L, de Graaf C, Sieghart W, Varagic Z, Morzinger M, de Esch IJ, Ecker GF, Ernst M (2012) Diazepam-bound GABA(A) receptor models identify new benzodiazepine binding-site ligands. Nature chemical biology 8:455-464.

Rissman RA, Mobley WC (2011) Implications for treatment: GABAA receptors in aging, Down syndrome and Alzheimer's disease. J Neurochem 117:613-622.

Roberts DD, Lewis SD, Ballou DP, Olson ST, Shafer JA (1986) Reactivity of small thiolate anions and cysteine-25 in papain toward methyl methanethiosulfonate. Biochemistry 25:5595-5601.

Rogers CJ, Twyman RE, Macdonald RL (1994a) Benzodiazepine and beta-carboline regulation of single GABAA receptor channels of mouse spinal neurones in culture. J Physiol 475:69-82.

Rogers CJ, Twyman RE, Macdonald RL (1994b) Benzodiazepine and beta-carboline regulation of single GABAA receptor channels of mouse spinal neurones in culture. J Physiol (Lond) 475:69-82.

Rosen A, Bali M, Horenstein J, Akabas MH (2007) Channel opening by anesthetics and GABA induces similar changes in the GABAA receptor M2 segment. Biophys J 92:3130-3139.

Rossi DJ, Hamann M (1998) Spillover-mediated transmission at inhibitory synapses promoted by high affinity alpha6 subunit GABA(A) receptors and glomerular geometry. Neuron 20:783-795.

Roth FC, Draguhn A (2012) GABA Metabolism and Transport: Effects on Synaptic Efficacy. Neural plasticity 2012:805830.

Rowlett JK, Platt DM, Lelas S, Atack JR, Dawson GR (2005) Different GABAA receptor subtypes mediate the anxiolytic, abuse-related, and motor effects of benzodiazepine-like drugs in primates. Proc Natl Acad Sci U S A 102:915-920.

Rowley NM, Madsen KK, Schousboe A, Steve White H (2012) Glutamate and GABA synthesis, release, transport and metabolism as targets for seizure control. Neurochem Int.

Rudolph U, Crestani F, Benke D, Brünig I, Benson JA, Fritschy JM, Martin JR, Bluethmann H, Möhler H (1999) Benzodiazepine actions mediated by specific gamma-aminobutyric acid(A) receptor subtypes. Nature 401:796-800.

Rudolph U, Knoflach F (2011) Beyond classical benzodiazepines: novel therapeutic potential of GABAA receptor subtypes. Nature reviews Drug discovery 10:685-697.

Rudolph U, Mohler H (2006) GABA-based therapeutic approaches: GABAA receptor subtype functions. Curr Opin Pharmacol 6:18-23.

Rusch D, Forman SA (2005) Classic benzodiazepines modulate the open-close equilibrium in alpha1beta2gamma2L gamma-aminobutyric acid type A receptors. Anesthesiology 102:783-792.

Sancar F, Czajkowski C (2011) Allosteric modulators induce distinct movements at the GABA-binding site interface of the GABA-A receptor. Neuropharmacology 60:520-528.

Sancar F, Ericksen SS, Kucken AM, Teissere JA, Czajkowski C (2007) Structural determinants for high-affinity zolpidem binding to GABA-A receptors. Mol Pharmacol 71:38-46.

Sanger DJ (2004) The pharmacology and mechanisms of action of new generation, non-benzodiazepine hypnotic agents. CNS Drugs 18 Suppl 1:9-15; discussion 41, 43-15.

Sawyer GW, Chiara DC, Olsen RW, Cohen JB (2002) Identification of the bovine gamma-aminobutyric acid type A receptor alpha subunit residues photolabeled by the imidazobenzodiazepine [3H]Ro15-4513. J Biol Chem 277:50036-50045.

Saxena NC, Macdonald RL (1994) Assembly of GABAA receptor subunits: role of the delta subunit. J Neurosci 14:7077-7086.

Schaerer MT, Buhr A, Baur R, Sigel E (1998) Amino acid residue 200 on the alpha1 subunit of GABA(A) receptors affects the interaction with selected benzodiazepine binding site ligands. Eur J Pharmacol 354:283-287.

Scharf MB, Roth T, Vogel GW, Walsh JK (1994) A multicenter, placebo-controlled study evaluating zolpidem in the treatment of chronic insomnia. J Clin Psychiatry 55:192-199.

Schofield PR (1989) The GABAA receptor: molecular biology reveals a complex picture. Trends Pharmacol Sci 10:476-478.

Schreiber G, Fersht AR (1995) Energetics of protein-protein interactions: analysis of the barnase-barstar interface by single mutations and double mutant cycles. J Mol Biol 248:478-486.

Schwarzer C, Tsunashima K, Wanzenbock C, Fuchs K, Sieghart W, Sperk G (1997) GABA(A) receptor subunits in the rat hippocampus II: altered distribution in kainic acid-induced temporal lobe epilepsy. Neuroscience 80:1001-1017.

Scimemi A, Andersson A, Heeroma JH, Strandberg J, Rydenhag B, McEvoy AW, Thom M, Asztely F, Walker MC (2006) Tonic GABA(A) receptor-mediated currents in human brain. The European journal of neuroscience 24:1157-1160.

Semyanov A, Walker MC, Kullmann DM, Silver RA (2004) Tonically active GABA A receptors: modulating gain and maintaining the tone. Trends Neurosci 27:262-269.

Shames JL, Ring H (2008) Transient reversal of anoxic brain injury-related minimally conscious state after zolpidem administration: a case report. Archives of physical medicine and rehabilitation 89:386-388.

Sharkey LM, Czajkowski C (2008a) Individually monitoring ligand-induced changes in the structure of the GABAA receptor at benzodiazepine binding site and non-binding site interfaces. Mol Pharmacol 74:203-212.

Sharkey LM, Czajkowski C (2008b) Individually monitoring ligand-induced changes in the structure of the GABAA receptor at benzodiazepine binding site and non-binding-site interfaces. Mol Pharmacol 74:203-212.

Shoichet BK, Kobilka BK (2012) Structure-based drug screening for G-protein-coupled receptors. Trends Pharmacol Sci 33:268-272.

Sieghart W (2006) Structure, pharmacology, and function of GABAA receptor subtypes. Adv Pharmacol 54:231-263.

Sieghart W, Fuchs K, Tretter V, Ebert V, Jechlinger M, Hoger H, Adamiker D (1999) Structure and subunit composition of GABA(A) receptors. Neurochem Int 34:379-385.

Sieghart W, Ramerstorfer J, Sarto-Jackson I, Varagic Z, Ernst M (2011) A novel GABA(A) receptor pharmacology: drugs interacting with the alpha+beta- interface. Br J Pharmacol.

Sieghart W, Ramerstorfer J, Sarto-Jackson I, Varagic Z, Ernst M (2012) A novel GABA(A) receptor pharmacology: drugs interacting with the alpha(+) beta(-) interface. Br J Pharmacol 166:476-485.

Sieghart W, Sperk G (2002) Subunit composition, distribution and function of GABA(A) receptor subtypes. Curr Top Med Chem 2:795-816.

Sigel E (2002) Mapping of the benzodiazepine recognition site on GABA(A) receptors. Curr Top Med Chem 2:833-839.

Sigel E, Baur R, Kellenberger S, Malherbe P (1992) Point mutations affecting antagonist affinity and agonist dependent gating of GABAA receptor channels. Embo J 11:2017-2023.

Sigel E, Buhr A (1997) The benzodiazepine binding site of GABAA receptors. Trends Pharmacol Sci 18:425-429.

Sigel E, Schaerer MT, Buhr A, Baur R (1998) The benzodiazepine binding pocket of recombinant alpha1beta2gamma2 gamma-aminobutyric acidA receptors: relative orientation of ligands and amino acid side chains. Mol Pharmacol 54:1097-1105.

Sigworth FJ (1980) The variance of sodium current fluctuations at the node of Ranvier. J Physiol 307:97-129.

Simon J, Wakimoto H, Fujita N, Lalande M, Barnard EA (2004) Analysis of the set of GABA(A) receptor genes in the human genome. J Biol Chem 279:41422-41435.

Sivilotti LG (2010) What single-channel analysis tells us of the activation mechanism of ligand-gated channels: the case of the glycine receptor. J Physiol 588:45-58.

Smith GB, Olsen RW (1994) Identification of a [3H]muscimol photoaffinity substrate in the bovine gamma-aminobutyric acidA receptor alpha subunit. J Biol Chem 269:20380-20387.

Sohal VS, Keist R, Rudolph U, Huguenard JR (2003) Dynamic GABA(A) receptor subtype-specific modulation of the synchrony and duration of thalamic oscillations. J Neurosci 23:3649-3657.

Sperk G, Schwarzer C, Tsunashima K, Kandlhofer S (1998) Expression of GABA(A) receptor subunits in the hippocampus of the rat after kainic acid-induced seizures. Epilepsy Res 32:129-139.

Stauffer DA, Karlin A (1994) Electrostatic potential of the acetylcholine binding sites in the nicotinic receptor probed by reactions of binding-site cysteines with charged methanethiosulfonates. Biochemistry 33:6840-6849.

Strakhova MI, Harvey SC, Cook CM, Cook JM, Skolnick P (2000) A single amino acid residue on the alpha(5) subunit (Ile215) is essential for ligand selectivity at alpha(5)beta(3)gamma(2) gamma-aminobutyric acid(A) receptors. Mol Pharmacol 58:1434-1440.

Strecker GJ, Park WK, Dudek FE (1999) Zinc and flunitrazepam modulation of GABA-mediated currents in rat suprachiasmatic neurons. J Neurophysiol 81:184-191.

Stuhmer W (1998) Electrophysiologic recordings from Xenopus oocytes. Methods in enzymology 293:280-300.
Sullivan P (2005) Inventor of Valium, Once the Most Often Prescribed Drug, Dies. The Washington Post October 1.
Swaminath G, Deupi X, Lee TW, Zhu W, Thian FS, Kobilka TS, Kobilka B (2005) Probing the beta2 adrenoceptor binding site with catechol reveals differences in binding and activation by agonists and partial agonists. J Biol Chem 280:22165-22171.
Swaminath G, Xiang Y, Lee TW, Steenhuis J, Parnot C, Kobilka BK (2004) Sequential binding of agonists to the beta2 adrenoceptor. Kinetic evidence for intermediate conformational states. J Biol Chem 279:686-691.
Tan KR, Baur R, Gonthier A, Goeldner M, Sigel E (2007a) Two neighboring residues of loop A of the alpha1 subunit point towards the benzodiazepine binding site of GABAA receptors. FEBS Lett 581:4718-4722.
Tan KR, Gonthier A, Baur R, Ernst M, Goeldner M, Sigel E (2007b) Proximity-accelerated chemical coupling reaction in the benzodiazepine-binding site of gamma-aminobutyric acid type A receptors: superposition of different allosteric modulators. J Biol Chem 282:26316-26325.
Tanelian DL, MacIver MB (1991) Differential excitatory and depressant anesthetic effects on mammalian A-delta and C fiber sensory afferents. Ann N Y Acad Sci 625:273-275.
Teissere JA, Czajkowski C (2001) A (beta)-strand in the (gamma)2 subunit lines the benzodiazepine binding site of the GABA A receptor: structural rearrangements detected during channel gating. J Neurosci 21:4977-4986.
Thompson SA, Smith MZ, Wingrove PB, Whiting PJ, Wafford KA (1999) Mutation at the putative GABA(A) ion-channel gate reveals changes in allosteric modulation. Br J Pharmacol 127:1349-1358.
Tia S, Wang JF, Kotchabhakdi N, Vicini S (1996) Distinct deactivation and desensitization kinetics of recombinant GABAA receptors. Neuropharmacology 35:1375-1382.
Traub RD, Jefferys JG, Whittington MA (1999) Functionally relevant and functionally disruptive (epileptic) synchronized oscillations in brain slices. Advances in neurology 79:709-724.
Twyman RE, Rogers CJ, Macdonald RL (1989) Differential regulation of gamma-aminobutyric acid receptor channels by diazepam and phenobarbital. Ann Neurol 25:213-220.
Ueno S, Bracamontes J, Zorumski C, Weiss DS, Steinbach JH (1997) Bicuculline and gabazine are allosteric inhibitors of channel opening of the GABAA receptor. J Neurosci 17:625-634.
Unwin N (1995) Acetylcholine receptor channel imaged in the open state. Nature 373:37-43.
Unwin N (2005) Refined structure of the nicotinic acetylcholine receptor at 4A resolution. J Mol Biol 346:967-989.
Unwin N, Miyazawa A, Li J, Fujiyoshi Y (2002) Activation of the nicotinic acetylcholine receptor involves a switch in conformation of the alpha subunits. J Mol Biol 319:1165-1176.

Uusi-Oukari M, Korpi ER (2010) Regulation of GABA(A) receptor subunit expression by pharmacological agents. Pharmacol Rev 62:97-135.

van Rijnsoever C, Tauber M, Choulli MK, Keist R, Rudolph U, Mohler H, Fritschy JM, Crestani F (2004) Requirement of alpha5-GABAA receptors for the development of tolerance to the sedative action of diazepam in mice. J Neurosci 24:6785-6790.

Velisetty P, Chakrapani S (2012) Desensitization mechanism in a Prokaryotic ligand-gated ion channel. J Biol Chem 22:18467-77.

Venkatachalan SP, Bushman JD, Mercado JL, Sancar F, Christopherson KR, Boileau AJ (2007) Optimized expression vector for ion channel studies in Xenopus oocytes and mammalian cells using alfalfa mosaic virus. Pflugers Arch 454:155-163.

Venkatachalan SP, Czajkowski C (2008) A conserved salt bridge critical for GABA(A) receptor function and loop C dynamics. Proc Natl Acad Sci U S A 105:13604-13609.

Wagner DA, Czajkowski C, Jones MV (2004) An arginine involved in GABA binding and unbinding but not gating of the GABA(A) receptor. J Neurosci 24:2733-2741.

Wallace RH, Marini C, Petrou S, Harkin LA, Bowser DN, Panchal RG, Williams DA, Sutherland GR, Mulley JC, Scheffer IE, Berkovic SF (2001) Mutant GABA(A) receptor gamma2-subunit in childhood absence epilepsy and febrile seizures. Nat Genet 28:49-52.

Weerts EM, Kaminski BJ, Griffiths RR (1998) Stable low-rate midazolam self-injection with concurrent physical dependence under conditions of long-term continuous availability in baboons. Psychopharmacology 135:70-81.

Wei W, Zhang N, Peng Z, Houser CR, Mody I (2003) Perisynaptic localization of delta subunit-containing GABA(A) receptors and their activation by GABA spillover in the mouse dentate gyrus. J Neurosci 23:10650-10661.

Whiting PJ, Bonnert TP, McKernan RM, Farrar S, Le Bourdelles B, Heavens RP, Smith DW, Hewson L, Rigby MR, Sirinathsinghji DJ, Thompson SA, Wafford KA (1999) Molecular and functional diversity of the expanding GABA-A receptor gene family. Ann N Y Acad Sci 868:645-653.

Whittington MA, Traub RD (2003) Interneuron diversity series: inhibitory interneurons and network oscillations in vitro. Trends Neurosci 26:676-682.

Whittington MA, Traub RD, Jefferys JG (1995) Synchronized oscillations in interneuron networks driven by metabotropic glutamate receptor activation. Nature 373:612-615.

Whittington MA, Traub RD, Kopell N, Ermentrout B, Buhl EH (2000) Inhibition-based rhythms: experimental and mathematical observations on network dynamics. International journal of psychophysiology : official journal of the International Organization of Psychophysiology 38:315-336.

WHO (2011) Essential Medicines: World Health Organization Model List. 17th Edition.

Whyte J, Myers R (2009) Incidence of clinically significant responses to zolpidem among patients with disorders of consciousness: a preliminary placebo

controlled trial. American journal of physical medicine & rehabilitation / Association of Academic Physiatrists 88:410-418.
Wieland HA, Luddens H (1994) Four amino acid exchanges convert a diazepam-insensitive, inverse agonist-preferring GABAA receptor into a diazepam-preferring GABAA receptor. J Med Chem 37:4576-4580.
Wieland HA, Luddens H, Seeburg PH (1992) A single histidine in GABAA receptors is essential for benzodiazepine agonist binding. J Biol Chem 267:1426-1429.
Williams CA, Bell SV, Jenkins A (2009) A residue in loop 9 of the beta2-subunit stabilizes the closed state of the GABAA receptor. J Biol Chem 285:7281-7287.
Williams CA, Bell SV, Jenkins A (2010) A residue in loop 9 of the beta2-subunit stabilizes the closed state of the GABAA receptor. J Biol Chem 285:7281-7287.
Williams DB, Akabas MH (2000) Benzodiazepines induce a conformational change in the region of the gamma-aminobutyric acid type A receptor alpha(1)-subunit M3 membrane-spanning segment. Mol Pharmacol 58:1129-1136.
Wingrove PB, Thompson SA, Wafford KA, Whiting PJ (1997) Key amino acids in the gamma subunit of the gamma-aminobutyric acidA receptor that determine ligand binding and modulation at the benzodiazepine site. Mol Pharmacol 52:874-881.
Winter C, Henschel A, Tuukkanen A, Schroeder M (2012) Protein interactions in 3D: From interface evolution to drug discovery. Journal of structural biology.
Wisden W, Laurie DJ, Monyer H, Seeburg PH (1992) The distribution of 13 GABAA receptor subunit mRNAs in the rat brain. I. Telencephalon, diencephalon, mesencephalon. J Neurosci 12:1040-1062.
Wong G, Skolnick P (1992) High affinity ligands for 'diazepam-insensitive' benzodiazepine receptors. Eur J Pharmacol 225:63-68.
Xu M, Akabas MH (1993) Amino acids lining the channel of the gamma-aminobutyric acid type A receptor identified by cysteine substitution. J Biol Chem 268:21505-21508.
Xu M, Akabas MH (1996) Identification of channel-lining residues in the M2 membrane-spanning segment of the GABA(A) receptor alpha1 subunit. J Gen Physiol 107:195-205.
Zhang H, Karlin A (1998) Contribution of the beta subunit M2 segment to the ion-conducting pathway of the acetylcholine receptor. Biochemistry 37:7952-7964.
Zhu L, Cheng P, Lei N, Yao J, Sheng C, Zhuang C, Guo W, Liu W, Zhang Y, Dong G, Wang S, Miao Z, Zhang W (2011) Synthesis and biological evaluation of novel homocamptothecins conjugating with dihydropyrimidine derivatives as potent topoisomerase I inhibitors. Archiv der Pharmazie 344:726-734.
Zhu WJ, Vicini S (1997) Neurosteroid prolongs GABAA channel deactivation by altering kinetics of desensitized states. J Neurosci 17:4022-4031.
Zimmermann I, Dutzler R (2011) Ligand activation of the prokaryotic pentameric ligand-gated ion channel ELIC. PLoS biology 9:e1001101.